Signaling gradients and self-organization during tetrapod digit pattern formation and evolution

Inauguraldissertation

Zur

Erlangung der Würde eines Doktors der Philosophie

vorgelegt der

Philosophisch-Naturwissenschaftlichen Fakultät

der Universität Basel

von

Emmanuelle Grall

2022

Genehmigt von der Philosophisch-Naturwissenschaftlichen Fakultät
auf Antrag von

Prof. Dr. Patrick Tschopp,
Prof. Dr. Dieter Ebert, und
Prof. Dr. Jérôme Gros

Basel, den 26.04.2022

Prof. Dr. Marcel Mayor
Dekan

This work was supported by the University of Basel.

ACKNOWLEDGEMENTS

I would like to thank Patrick Tschopp for having given me the opportunity to do this PhD thesis in his laboratory. Thanks for having guided me through this amazing project and motivated me when we were stuck in experimental research. I appreciate that he trusted me and let me drive this project.

I am grateful that Dieter Ebert and Jérôme Gros accepted to evaluate my work and be part of my PhD thesis committee and I am honored to get their expertise in the Evo-Devo field.

I would like to thank all the people, and especially Chris and Tom, who contributed to the production of this thesis work and without whom this project would not have taken this wonderful turn.

A great thank to Maëva, who was an amazing mental support for me and boosted me to never give up. Her smile and her humor have embellished the days of intensive work in the lab.

Thanks also to Sabrina for her support and her indispensable help when I was lost in the lab. She taught me a lot of techniques and without her we would never have managed to get these viruses.

I thank all the member of the Tschopp lab with a particular attention for Bianka, my “sister” of PhD studies. Thanks to all of them for this wonderful working atmosphere that they all contributed to.

Last, but not least, I thank all my family, my parents Isabelle and Christian, and my sisters Aurélia and Victoria for supporting me throughout all these years and giving me so much love.

Un grand merci à mon compagnon Geoffrey, pour son soutien à toute épreuve et pour le merveilleux Papa qu’il est. Et merci à ma fille Cléo pour tout l’amour qu’elle m’apporte, malgré les nuits blanches passées lors de l’écriture de cette thèse…

Et encore un grand merci à tous mes amis pour ces moments de détente et de rire qui m’ont permis de traverser certaines épreuves plus en douceur.

SUMMARY

Segmentation of digits into individual bones, the so-called phalanges, connected to each other *via* synovial joints, is a major step during tetrapod limb formation. Thanks to this modular architecture, highly distinct digit morphologies have emerged over the course of vertebrate evolution. During embryogenesis, at the tip of each growing digit, a delicate balance of cell proliferation and cell type specification in a group of progenitor cells, the phalanx-forming region (PFR), needs to be precisely controlled to ensure proper digit patterning. The TGF-beta superfamily, including signaling through Bone morphogenetic proteins (BMPs), has been implicated in this process. However, the exact molecular mechanisms underlying the specification and diversification of digit patterns remain unclear.

This PhD thesis aims to decipher how molecular cues are integrated and interpreted, to orchestrate cell fate decisions at the PFR into either joint or phalanx precursors, and to what extent these mechanisms can be modified on an evolutionary timescale, to generate novel digit morphologies.

For this, we are using the chicken foot as a model, in which all digits are morphologically different. To decipher the underlying patterning mechanisms, we produced morphological growth and signaling dynamics data over the course of chicken digit development. Moreover, by combining this quantitative data with mathematical modeling, we tried to approximate digit patterning *in silico*. Indeed, this allowed us to formulate a Turing-like model based on BMP signaling modulators interactions that can explain the emergence of a repetitive phalanx-joint pattern.

In addition, to understand how signals received by the PFR are interpreted to allow for cell fate decisions control of the joint and phalanx precursors shaping a digit, data describing the transcriptional dynamics of chicken digit patterning was produced and analyzed. To this aim, we used single-cell RNA-sequencing, pseudotime analyses and experimental embryology to define candidate regulators of phalanx *versus* joint cell fate decisions.

Collectively, the present work aims to contribute to our understanding of the mechanisms underlying tetrapod digit patterns specification and diversification.

TABLE OF CONTENT

LIST OF FIGURES

GENERAL INTRODUCTION

CHAPTER I. Growth and signaling dynamics during digit development: pattern formation and diversification

CHAPTER II. Patterning relevant cell fate decision during digit development: establishment of the joint *versus* phalanx cell identity

MATERIALS AND METHODS

GENERAL INTRODUCTION

I. Pattern formation and evolution of repetitive morphological structures

(Published as Grall, E., and Tschopp, P. (2020). A sense of place, many times over - pattern formation and evolution of repetitive morphological structures. Dev. Dyn. *249*, 313–327.)

Repetitive structures are plentiful throughout nature – be it the juxtaposed leaves on the branch of a tree, the body segments of an insect, or the individual bones that make up the vertebrate spine. From an evolutionary perspective, such repetitive patterns can be explained by the adaptive value the repetition of a certain anatomical unit can provide in itself. Moreover, repeatedly re-deploying and modifying a pre-existing developmental patterning module can enable morphological diversification. For example, in case of the vertebrate spinal column, individual vertebrae are attached to one another in a stable yet movable fashion. This repetitive vertebral architecture ensures the overall suppleness of the structure that is required for body movement, while also providing a solid protective encasement of the delicate spinal cord it encloses. At the same time, by exploiting the inherent developmental modularity of these spinal building blocks, the overall number of vertebrae can differ substantially between species, and each individual vertebra along the anterior-posterior axis can be modified in its morphology (Gomez and Pourquié, 2009; Mallo et al., 2010). The concept of modularity is thus central to our understanding of how repetitive patterns can arise on both developmental and evolutionary timescales (Esteve-Altava, 2017; Wagner, 2014; Young et al., 2015). How then, however, is a certain patterning module repeatedly specified during embryogenesis, in a reliable and robust manner, while at the same time allowing for slight deviations that eventually can be canalized into evolutionarily novel morphologies?

50 years ago, the theoretical biologist Lewis Wolpert introduced his concept of ‘positional information’ that, to this day, continues to influence the way we think about developmental pattern formation (Wolpert, 1969). He hypothesized that cells in an embryonic field have their relative position specified through a coordinate system based on three essential features: boundaries, that define the field and to which the relative position of a cell needs to be specified; a scalar to measure the distance from said boundaries; and polarity, emergent from the juxtaposition of differing scalar values, to confer directionality to this measurement. Both scalar and polarity of the system have come to be associated most often with a diffusible substance or ‘morphogen’, a term originally introduced by Alan Turing (Turing, 1952), even though Wolpert also alluded to other potential mechanisms (Wolpert, 1989). To illustrate the

concept of positional information, Wolpert first assumed a multicellular field with uniform progenitor identities. Through localized production and subsequent dispersal of a substance, i.e. a morphogen, cells in the embryonic field would be exposed to differing concentrations along a gradient, which in turn bestows upon them distinct 'positional values'. According to distinct 'thresholds' of morphogen concentration, this continuous distribution of positional values is then differentially interpreted by the cells in the field and translated into discretized cellular states (Figure 1A). Thus, over the course of development, an initial asymmetry in morphogen production would allow cells to acquire different, concentration-based positional values, categorize these values into a discontinuous distribution of changes in cell-intrinsic parameters, and ultimately result in spatially distinct cell fate decisions. This is famously illustrated in the so-called 'French Flag problem', in which Wolpert's model posits the sub-division of a homogeneous population of cells into three discrete 'cell type domains' as a result of threshold-based interpretation of a continuous morphogen gradient (Figure 1A). In the decades since its initial proposal, the concept of positional information has accumulated support from a range of experimental observations, beginning with classical embryology approaches (Nüsslein-Volhard et al., 1987; Tickle et al., 1975), and followed by investigations into the underlying cellular, molecular and biochemical mechanisms (Driever and Nüsslein-Volhard, 1988; Green and Smith, 1990; Riddle et al., 1993).

Despite its far-reaching implications and experimental validation, there remain certain common patterning motifs, as well as evolutionary variations therein, that Wolpert's initial theory alone cannot explain satisfactorily. These patterns include, as already Wolpert acknowledged himself, the ones underlying the formation of repetitive morphological structures (Figure 1B,C). He reasoned that for highly repetitive architectures the assumption of a pre-patterning mechanism would provide a more parsimonious explanation than a purely positional information-based system, given the increasingly high number of distinct thresholds that are to be defined in the latter (Wolpert, 1989).

In this review, we focus on the repeated deployment of developmental patterning modules, and how positional information might work alongside other mechanisms to assure proper pattern formation and evolution. After a brief overview of repetitive pattern formation in both two- and one-dimensional domains, we will shift our focus to systems where the polarity of the resulting repetitive pattern is inherently linked to the directionality of tissue growth. We will highlight the role of positional information in defining the temporal and spatial dynamics of such directed growth and discuss the challenges of establishing morphogen gradients in non-static embryonic fields with high cellular turnover. At the same time, positional information can define windows of 'patterning competency', for proliferating progenitors to respond to additional, often

self-organizing mechanisms, which eventually result in segmented architectures made of repetitive morphological structures. We emphasize the apparent ease with which evolutionary variations in segment repetitions can be achieved under such conditions – through modifications of positional information, growth parameters or the additional patterning modules – as evidenced by morphological extremes like the vertebral column of snakes or the number of digit bones in cetacean flippers. Finally, we will review experimental and theoretical approaches to study these processes *in vivo*, *ex vivo, in vitro* and *in silico*, and how results from such studies continue to contribute to our understanding of developmental pattern formation and evolutionary diversification.

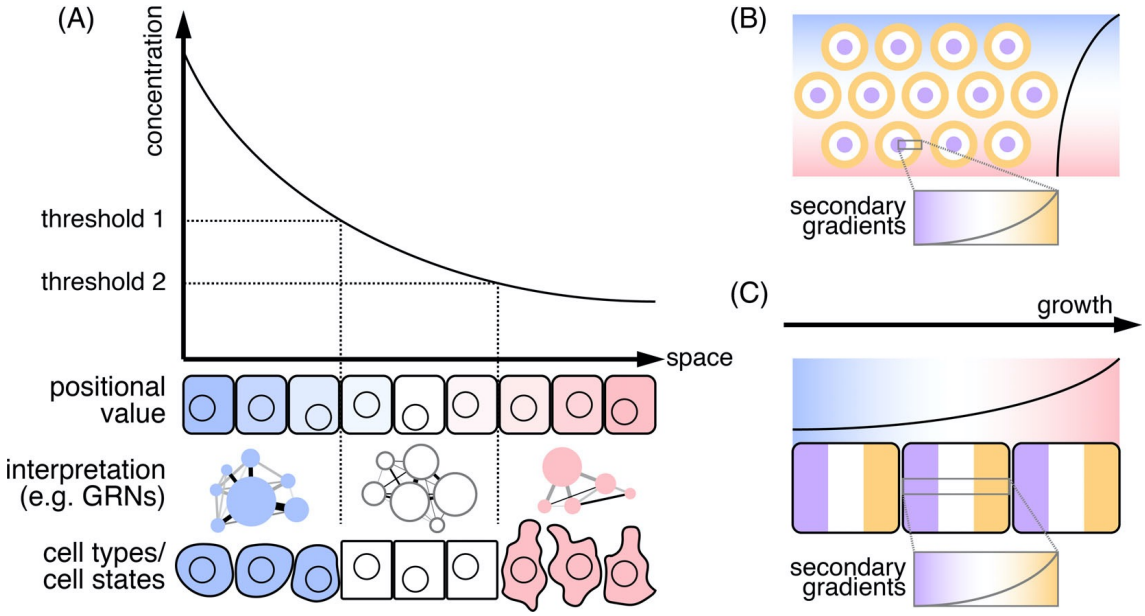

Figure 1. 'Positional information' and the emergence of repetitive patterns. (**A**) Wolpert's classic illustration of positional information and its relation to the 'French Flag problem'. A morphogen is locally produced, secreted, and dispersed to establish a molecular gradient over an embryonic field. Cells are exposed to different molecular concentrations along the gradient, endowing them with distinct 'positional values'. According to distinct 'thresholds', these positional values are differentially interpreted by the cells (e.g. rewiring of gene regulatory networks (GRNs)) and result in distinct cell fate decisions. (**B**) Positional information in two-dimensional, repetitive patterns. While the formation of many two-dimensional, repetitive patterns can be explained by self-organizing principles, their implementation is often constrained by additional, pre-existing positional information cues (blue to red gradient). Once initiated, repetitive elements may act as secondary morphogen sources and exert their effect on the surrounding tissue in a positional information-like manner (concentric patterns, purple to orange gradients). (**C**) Positional information in one-dimensional, repetitive patterns driven by directional growth. Growth dynamics and their underlying progenitor populations rely on morphogen gradients that determine a field of competency (blue to red gradient). Moreover, previously formed segments may inherit positional information-containing polarity and establish secondary morphogen gradients themselves, to modulate the formation of successive elements (purple to orange gradients).

1. The formation of repetitive patterns in nature – Positional information and self-organization

Pattern formation is an essential feature of multicellular organism development, and variations in patterning mechanisms are thought to contribute substantially to morphological diversification. Consequently, pattern formation has fascinated scientists for centuries and, owing to its amenability to abstraction, has stimulated collaborations between experimental and theoretical biologists (Glen et al., 2019; Multerer et al., 2018; Sharpe, 2017). Formation of periodic patterns, in particular, has attracted mathematicians and computational modelers alike (Hiscock and Megason, 2015). Two of the most prominent conceptual frameworks in the field of pattern formation are certainly Wolpert's theory on positional information, and Alan Turing's 'reaction-diffusion'-based mechanisms. Unlike positional information, Turing models do not explicitly require any polarized molecular asymmetries prior to pattern emergence. Rather, slight spatial imbalances in the initial distribution of a cross-regulatory pair of an 'activator' and an 'inhibitor' are accentuated over time, due to different diffusibilities of the two substances, and thereby give rise to essentially self-organizing patterns (Green and Sharpe, 2015; Turing, 1952; Wolpert, 1969). While positional information had found plenty of experimental support early on – owing in large part to the rise of molecular genetics that helped to elucidate the segmentation network in *Drosophila* or cell fate specification in the early frog embryo (see below) – Turing systems and other self-organizing models have recently gained renewed interest (Schweisguth and Corson, 2019). Examples include symmetry-breaking events that underlie the emergence of repetitive, two-dimensional patterns (Figure 1B), like the induction of ectodermal appendages in the amniote skin (Sick et al., 2006), spacing of stripe-color patterns in fish (Nakamasu et al., 2009), bristles placement on the fruit fly thorax (Corson et al., 2017), rugae formation in the mammalian palate (Economou et al., 2012), or the formation of digits in the tetrapod autopod (Sheth et al., 2012). Additionally, rather than focusing exclusively on the self-organizing properties of reaction-diffusion-type molecular systems, the role of cellular and/or mechanical mechanisms is increasingly being acknowledged (Ho et al., 2019; Mahalwar et al., 2014; Panousopoulou and Green, 2016; Shyer et al., 2017), as well as the potential to rely on the inherent periodicity of molecular oscillators to generate repetitive patterns (Oates et al., 2012). While the oscillatory nature of these latter systems can be an emergent property at the tissue level, and hence be referred to as self-organizing (Hubaud et al., 2017; Tsiairis and Aulehla, 2016), their impact on the formation of repetitive spatial patterns is less direct. Unlike Turing models, which can reach stable states inside static embryonic fields, the temporal dynamics of a molecular oscillator necessitate its

coupling to other variables, e.g. polarized growth, to translate wave-like gene activities into a defined spatial pattern (Figure 1C) (Richmond and Oates, 2012), Importantly, however, in most of the patterning scenarios investigated thus far, neither self-organizing principles nor positional information seem to function in an entirely isolated fashion. Rather, they frequently co-occur, in parallel or close temporal succession, and similar patterning principles might repeat themselves during the maturation of a particular morphological structure. For example, while the periodicity of a given two-dimensional pattern may rely on self-organizing properties, potential sub-types of the resulting units – e.g. different *Drosophila* sensory bristles or tetrapod digit homeotic identities – can be defined by pre-existing morphogen gradients (Figure 1B; blue to red) (Corson et al., 2017; Dahn and Fallon, 2000; Raspopovic et al., 2014). Once initiated, these repetitive structures have the potential to act as morphogen sources themselves, to refine the emerging pattern or instruct the fate of neighboring elements (Figure 1B,C; purple to orange) (Corson et al., 2017; Manukyan et al., 2017). Collectively, combining 'positional information' with growth and additional patterning modules alleviates many of the problems inherent to the establishment of highly repetitive structures, were they to be specified by 'positional information' only (e.g. setting up reliable long-range gradients or precisely defining multiple threshold values). Such combinatorial patterning modules can therefore contribute to increase patterning robustness as well as boost the potential for their evolutionary reshuffling (Dahn and Fallon, 2000; Gómez-Skarmeta et al., 2003; Haupaix et al., 2018). Hence, it appears that the strict dichotomy often attributed to the deployment of these two distinct patterning concepts during embryogenesis – i.e. 'positional information' or 'self-organization' – is likely artificial and, as previously suggested, a more realistic approximation of development would entail various combinations of the two (Figure 1B,C) (Green and Sharpe, 2015; Schweisguth and Corson, 2019; Wolpert, 1989).

2. Arthropod segmentation – Positional information and the specification of repetitive patterns in static and expanding domains

It can been argued that part of the tremendous evolutionary success of arthropods, both in terms of taxonomic diversity and sheer abundance, is attributable to their segmented, metameric body plan organization. Indeed, functional specializations of different body segments have enabled the exploitation of a wide variety of different ecological niches (Akam, 1995; Wainwright and Reilly, 1994). The study of insect embryogenesis and segment formation, in particular, has substantially contributed to our understanding of how positional information can instruct the formation of repetitive patterns. For one, unlike for the

aforementioned combinatorial patterning modes, during the early segmentation of the *Drosophila* embryo Wolpert's concept of positional information manifests itself most explicitly. Accordingly, anterior-posterior patterning in *Drosophila* was amongst the first experimental models to unequivocally prove some of Wolpert's key predictions. During *Drosophila* embryogenesis, all body segments are already contained within the length of the embryo's syncytial blastoderm. Fundamental to establishing positional information in this system, and by extension the specification of primary body axis segmentation and polarity, are two opposing gradients. Their presence had already been inferred from cytoplasmic constriction and transplantation experiments, and was predicted to rely on maternal gene products deposited on either end of the egg (Nüsslein-Volhard et al., 1987). With the identification of *bicoid*, the causative anterior determinant, and subsequently *Nanos*, its posterior counterpart, the first molecules emerged to validate Wolpert's claims (Driever and Nüsslein-Volhard, 1988; Wang and Lehmann, 1991). Downstream of *bicoid* and *Nanos*, a hierarchically organized gene regulatory network interprets the positional values of the two gradients, to sub-divide the anterior-posterior body axis, specify individual segments and establish segment polarity and identity (Jaeger, 2011). Hence, within the static domain of the *Drosophila* embryo, two opposing gradients, with cross-regulatory interactions for increased precision, and their differential cell-intrinsic interpretation suffice to reliably specify the positional values required for the formation of all body segments.

However, while the simultaneous specification of body segments is characteristic for long-germ band insects such as *Drosophila*, in short-germ band insects like the flour beetle *Tribolium casteneum* segments are formed sequentially, from anterior to posterior as the embryo elongates (Choe et al., 2006). This mode of segmentation thus intimately links growth-based axis elongation to periodic pattern formation and is, in fact, considered to be the ancestral condition for arthropods in general (Patel, 1994). The posterior region of short-germ band embryos contains a growth zone of proliferating progenitor cells that drives axis elongation. Positional information, based on a gradient of Wnt/β-catenin activity that delineates a posterior growth zone, and a molecular oscillator, involving the cyclic expression of 'Pair rule' genes, are required for axis extension and segmentation in short-germ band insects (Bolognesi et al., 2008; Choe et al., 2006; Nagy and Carroll, 1994; Sarrazin et al., 2012). Unlike in *Drosophila*, where Pair-rule genes are concomitantly expressed in a striped pattern demarcating the future segments, dynamic waves of cyclic Pair-rule gene expression propagate along the *Tribolium* growth zone, to sequentially segment the emerging primary body axis. Additionally, *Caudal*, *Dichaete* and *Odd-paired* expression in *Tribolium* form spatiotemporally dynamic wavefronts that travel along the anterior-posterior axis of the elongating embryo, while in *Drosophila* their

sequential activation acts as a timer of Pair-rule gene expression (Clark and Peel, 2018). Hence, although displaying drastically different growth modes for axis elongation, in both long-germ and short-germ insect segmentation similar sets of orthologous genes are essential in anterior-posterior pattern formation. The underlying genetic circuitries thus seem to contain an ability to compute and execute analogous patterning functions, both within static embryonic fields as well as along progressively elongating domains (Clark and Peel, 2018; Verd et al., 2018; Zhu et al., 2017). Disparities in their regulatory architectures, though, between long-germ and short-germ insects, emphasize the importance of properly integrating temporally dynamic gene expression programs with positional information in directionally growing domains (Clark and Peel, 2018; Peter and Davidson, 2011; Zhu et al., 2017). The fact that short-germ band insects do not seem to exploit their mode of axis elongation to increase overall segment number, like for example in the vertebral column of snakes (see below), may hint at an underlying developmental constraint, originating from molecular crosstalk between the two systems in insects (Choe et al., 2006; Schoppmeier and Schröder, 2005). Intriguingly, though, primary body axis patterning in other arthropod clades such as the *Myriapoda* clearly is more variable, with overall segment numbers in e.g. geophilomorph centipedes ranging from 27 to 191 (Chipman et al., 2004). Hence, how seemingly similar genetic cassettes are cross-regulated in both space and time, and integrated with a particular growth dynamic, is what ultimately appears to determine the resulting segmented pattern and its evolvability (Brena and Akam, 2013; Patel, 1994).

3. Positional information, directional growth, and the periodic specification of one-dimensional patterns

By explicitly decoupling the control of growth dynamics from a self-organizing mechanism, modular variations of periodic pattern formation – and hence segment numbers – can be achieved through evolutionary modifications altering either one or both of the two parameters. For the control of directional growth, morphogen-based positional information often delineates a pool of progenitor cells and, accordingly, gradient dynamics can define the spatial and temporal extent of proliferative axis elongation. Establishing accurate positional information within a directionally growing embryonic field, however, can present several challenges. Rather than cells being located statically within the field, and thus able to interpret a morphogen gradient both spatially and temporally, they dynamically traverse the domain to be patterned, as tissue elongation occurs. The history of positional cues that the cells experience thus directly relates to the directional growth dynamics they themselves help to establish.

There are numerous examples in nature where the creation of repetitive morphological structures depends on growth dynamics that can be approximated along a one-dimensional domain. While for much of the remainder of this review we focus on two iconic 1D-patterns in vertebrates – that of the somite-driven segmentation of the primary body axis and the individualization of phalangeal bones in tetrapod digits – it is worth mentioning that similar periodic patterns, some with striking similarities, have also arisen in the plant kingdom. Given the independent advent of multicellularity in the animal and plant kingdoms, the underlying mechanisms of these patterning systems must have evolved convergently. However, as previously argued by others, certain unifying design principles, as well as conserved molecular and/or cellular features implemented in these patterning systems, can emerge from such distant comparisons (Abley et al., 2013; Mentink and Tsiantis, 2015; Ten Tusscher, 2018).

a. Plant Shoot segmentation: repetitive patterns of phytomers

In most plants, above-ground growth relies on cell proliferation at the tip of the elongating shoot. This growth is sustained by a stem cell population that is located inside the so-called 'shoot apical meristem' (SAM) (Sussex, 1989). The basic structure of the SAM can be roughly subdivided into a central zone - the reservoir containing the stem cells - a rib zone which forms the bulk of the plant stem, and a peripheral zone from which lateral organs such as leaves develop (Bowman and Eshed, 2000). Importantly, shoot elongation occurs in a segmented fashion, through the successive addition of repetitive structures known as 'phytomers'. Each phytomer is composed of a node carrying a leaf, an internode region and an axillary bud that allows for branching (Figure 2A).

Inside the SAM, stem cell proliferation *versus* differentiation needs to be tightly balanced. Genetic analyses in *Arabidopsis,* as well as comparative studies across species, have revealed the presence of multi-faceted regulatory cascades centered on the CLAVATA-WUSCHEL axis that maintain the undifferentiated state of the SAM stem cells (Lee and Clark, 2013; Somssich et al., 2016). SAM stem cells provide the cellular building blocks to the different components of the phytomer, including the axillary buds. Axillary buds can act as meristems, just like the SAM, and give rise to secondary shoots that are either vegetative (e.g. lateral branches) or reproductive (i.e. flowers) in nature. They can thus be considered as several secondary 1D-growing fields connected to one major 1D-growing domain whose directionality is determined by the location of the SAM. By extension, spatiotemporal modulation of the patterning and positioning of these axillary buds along the apical-basal axis

of the main shoot allows plants to diversify their overall architectures (Teichmann and Muhr, 2015).

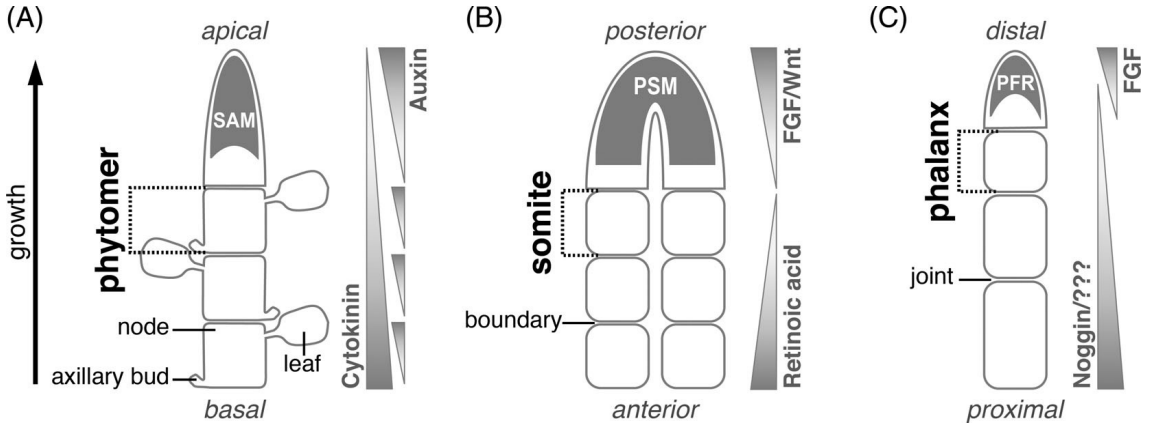

Figure 2. Formation of repetitive morphological structures across kingdoms. (**A**) In plants, apical-basal growth depends on a proliferative zone at the apex of the shoot called the 'shoot apical meristem' (SAM). The elongating shoot is segmented into repetitive structures known as 'phytomers', which are composed of a node carrying the leaf, an internode region and an axillary bud. The integration of two opposing gradient systems of phytohormones - auxin, mainly synthetized in the meristems, and cytokinin, mainly synthetized in roots - provides positional information along the apical-basal axis, and helps to define a balance of proliferation and differentiation. (**B**) Vertebrate axial elongation depends on the successive formation of 'somites', which originate from progenitors within the presomitic mesoderm (PSM). Posterior-to-anterior gradients of FGF and Wnt and an anterior-to-posterior gradient of Retinoic acid (RA) provide positional information along the primary body axis. These gradients delineate a 'determination front', at which progenitors respond to molecular oscillators to initiate segmentation. (**C**) Tetrapod digits grow proximal-distally due to progenitor proliferation within the phalanx forming region (PFR), which relies on a distal FGFs. Once progenitors leave the PFR, cell fate decision into either joint- or cartilage-forming cells instruct the digit segmentation pattern into individual 'phalanges', potentially modulated by BMP inhibitors released from previously formed elements.

Inside the main shoot, the repetitive deployment of the segmental phytomers depends on 'phyllotaxis', the process of periodic placement of plant lateral organs in regular intervals both around the central and apical-basal axes of the shoot (Bhatia and Heisler, 2018). Subsequent elongation of the phytomer then leads to the species-specific spacing patterns observed between the individual segments. For the radial patterns circumscribing the shoot, lateral organ placement can occur in whorled, distichous (alternate), decussate (opposite) as well as spiral arrangements – the latter invoking the famous Fibonacci sequence (Callos and Medford, 1994; Douady and Couder, 1992; Gola and Banasiak, 2016). Auxin, a phytohormone produced in the SAM, has been shown to have a central role in lateral organ formation and thus phyllotaxis. Indeed, micro-manipulations of auxin concentration reveal that when auxin levels decrease, stem cells start to differentiate (Reinhardt et al., 2000; Smith et al., 2006). Thus, gradients of

auxin concentration provide positional information along the apical-basal axis, and critically contribute to control the balance between cell proliferation and differentiation (Figure 2A) (Reinhardt et al., 2000). During phyllotaxis, PIN proteins, a family of membrane bound efflux carriers, control the generation of new auxin maxima and polar transport of auxin by PIN proteins allows for periodic pattern formation of organ initiation on the plant shoot (Benková et al., 2003; Kuhlemeier, 2017; Reinhardt et al., 2000). Several studies have suggested the presence of additional feedback mechanisms to ensure proper organ placement, both at the level of auxin transport or *via* inhibition from previously formed organ primordia (Bhatia et al., 2016; Domagalska and Leyser, 2011). In parallel to these mostly auxin-based inhibitory functions, cytokinin, another phytohormone, plays important roles in phyllotactic patterning (Vanstraelen and Benková, 2012). Cytokinin is mainly produced in roots and is transported up the shoot, thus forming a basal-to-apical gradient of cytokinin and, in association with auxin, defining robust positional information along the shoot (Figure 2A). Cross-regulatory effects between the two hormones, at the level of their respective syntheses or transport modes, as well as intercellular movement of additional inhibitors seem to define this interaction at a molecular and cellular level (Besnard et al., 2014; Domagalska and Leyser, 2011; Müller and Leyser, 2011). Moreover, the fact that the eventual basal-to-apical 1D-pattern of the shoot involves - in its inception - a two-dimensional component, namely the circumferential positioning of lateral branches, has led to the consideration of different self-organizing properties involved in the process. For example, inhibitory fields of leaf primordia have been proposed to affect spacing during phyllotactic patterning (Douady and Couder, 1992), and already Turing himself, and others, have argued that activator-inhibitor pairs might underlie the patterning phenomenon of phyllotaxis (Bhatia and Heisler, 2018; Meinhardt et al., 1998; Swinton et al., 2016; Turing, 1952). How exactly such interplay of positional information and self-organizing principles is realized, however, and in which way the rate of apical-basal growth as determined by the SAM affects this balance, is an area of active investigation using both theoretical and experimental approaches (Bhatia and Heisler, 2018; Smith et al., 2006; Yonekura et al., 2019).

b. Vertebrate primary body axis segmentation: repetitive patterns of somites

During vertebrate embryogenesis, the paraxial mesoderm, localized on both sides of the developing neural tube, is segmented into a series of repetitive structures that are known as ‘somites’. Cells inside these somites give rise to a variety of tissues in the adult body, such as

e.g. muscle, dermis, tendons or the progenitors of the axial skeleton (Pourquié, 2018). Most somite-derived tissues lose their segmented appearance as they mature. Notably, although somite number determines vertebral count, even the separation into individual vertebrae is secondary to the original somite boundaries. Vertebrae form from the repeated fusion of the caudal and rostral halves of two consecutive somites, with additional patterning cues emanating from the notochord (Goldstein and Kalcheim, 1992; Remak, 1855; Wopat et al., 2018). From an evolutionary perspective, overall somite number, and by extension vertebral count, can vary substantially between different vertebrate species (Gomez and Pourquié, 2009). Moreover, these skeletal somite derivatives appear highly regionalized along the anterior-posterior axis, with characteristic vertebral morphologies that reflect their distinct functions along the spine (Jones et al., 2018; Wellik, 2009).

Somitogenesis initiates anteriorly, adjacent to the head mesoderm, and progresses along the primary body axis as the embryo elongates at its posterior end. Segmentation occurs periodically, with a species-specific temporal rhythm, with somites progressively forming from the paraxial mesoderm with a remarkably regular rate of segmentation (Oates et al., 2012). The maintenance of this process critically depends on a posterior progenitor population, which in its unsegmented state is known as the 'presomitic mesoderm' (PSM) and acts as a unidirectional growth zone (Figure 2B) (Dubrulle and Pourquié, 2004a). As these mesenchymal cells approach the anterior margin of the PSM, an epithelium surrounding a mesenchymal core begins to form, thereby defining the individual somites. Hence, by controlling the elongation rate inside the PSM, as well as the temporal rhythmicity with which new boundaries are initiated, the basic pattern of somitogenesis is controlled (Mallo, 2016). Several models have been suggested to conceptualize the temporal and spatial aspects of this somitogenic process, most notably the 'clock and wavefront' model (Cooke and Zeeman, 1976). This model proposes two distinct mechanisms that, in combination, provide an explanation for the sequential formation of somites. First, a molecular oscillator, or 'segmentation clock', instructs the temporal periodicity with which new somites are formed. And second, a hypothetical gradient provides positional information in form of a 'wavefront', to define an anterior-posterior position inside the PSM where cells become responsive to the segmentation signals of the clock. This particular location is often referred to as the 'determination front'. Indeed, the clock and wavefront model has been supported by numerous experimental observations. For example, cyclic expression of *Notch* target genes was reported in the PSM of chick embryos (Aulehla and Johnson, 1999; Palmeirim et al., 1997). Moreover, mutations therein, as well as experimental perturbations in *Notch* modulators, were shown to affect the molecular clock and somitogenesis in various vertebrate species (Dale et al., 2003;

Liao et al., 2016; Morimoto et al., 2005). Following studies have revealed a substantially expanded oscillatory regime inside the PSM. Besides the *Notch* pathway, this includes members of the *Wnt* and *Fgf* signaling cascades (Aulehla et al., 2003; Dequéant et al., 2006), both of which have also been implicated in the second major constituent of the model, the 'wavefront' (see below). Intriguingly, while the overall pathways of the oscillator seem conserved amongst vertebrates, the actual gene members that show cyclic behavior can vary considerably between species (Krol et al., 2011). This argues for substantial stability when determining the net output of the respective signaling network, potentially conferred by multiple feedback loops, which in turn can explain the apparent drift in the developmental system at the molecular level (Maroto et al., 2012; True and Haag, 2001). The second major prediction in the model of Cooke and Zeeman is the presence of a wavefront at the anterior margin of the PSM, which acts as a traveling frontier of somite formation competency that moves posteriorly as the embryo elongates (Cooke and Zeeman, 1976). It was suggested that positional information by morphogen signaling gradients emanating from the PSM instructs the positioning of the wavefront. Indeed, posterior-to-anterior gradients of FGF and Wnt as well as an anterior-to-posterior gradient of Retinoic acid (RA) have been reported (Figure 2B). FGF signaling has been shown to determine wavefront position along the axis of the PSM and to be involved in the onset of the segmentation program (Dubrulle et al., 2001). High levels of FGF activity maintain an undifferentiated state and confer elevated levels of mobility in posterior cells (Bénazéraf et al., 2010). As FGF production is restricted to the posterior end of the PSM, FGF levels decrease as the cells travel along to the PSM, allowing anteriorly located progenitors to start their segmentation program while at the same time contributing to axis elongation (Dubrulle and Pourquié, 2004b; Naiche et al., 2011). Additionally, graded *Wnt* activity contributes to the positioning of the wavefront, as well as providing a molecular link to the segmentation clock itself and the proliferative control of axial progenitors (Aulehla et al., 2003, 2008; Bajard et al., 2014; Dunty et al., 2008). From the anterior end, a gradient of RA refines this boundary, while at the same time buffering for left-right asymmetries in the formation of somites on either side of the neural tube (Kumar and Duester, 2014; Moreno and Kintner, 2004; Vermot and Pourquié, 2005). Hence, integrating the spatial and temporal dynamics of these gradients with the oscillations of a molecular clock, determines overall elongation and segmentation rate of the PSM, and provides a conceptual framework to contextualize somite size control (Aulehla and Pourquié, 2010; Mallo, 2016).

The development of models that are able to approximate important aspects of somite segmentation *ex vivo*, *in vitro* and/or *in silico* have empowered experimental and theoretical approaches to study the process at a more quantitative level. Many of them focus on some of

the apparent self-organizing properties of the process, in particular for size scaling and the emergence of the molecular oscillator (Hubaud et al., 2017; Ishimatsu et al., 2018; Lauschke et al., 2013; Murray et al., 2011; Sonnen et al., 2018; Tsiairis and Aulehla, 2016). Some iterations abandon the notion of the importance of global positional information *via* gradients altogether, in favor of an oscillatory reaction-diffusion mechanism (Cotterell et al., 2015). Importantly, however, only by explicitly including termination of elongation and patterning in these models will the true evolutionary diversity in vertebral formulas be accounted for (Jörg et al., 2016). This would further entail the control to balance segmentation speed and progenitor pool size (Gomez et al., 2008), as well as incorporating the temporal and spatial effects of an axial *Hox* code on progenitor proliferation and somite identity (Aires et al., 2019; Carapuço et al., 2005; Iimura and Pourquié, 2006; Tschopp and Duboule, 2011). Intriguingly, either modulations in the speed of the segmentation clock or, alternatively, changing the duration of progenitor pool persistence have been shown to alter the eventual number of segments in the vertebral column of different species (Aires et al., 2019; Gomez et al., 2008).

c. Tetrapod digit segmentation: repetitive patterns of phalanges

Another striking example of repetitive pattern formation along a single axis of embryonic growth is the development of tetrapod digits. Tetrapod digits are segmented into individual digit bones called phalanges, which in adult hands and feet are connected to each other by synovial joints. Analogous to the somite-derived vertebral column, different numbers of phalanges per digit occur, both within and between species. According to the fossil record, early tetrapods already showed differences in phalanges count in their digits (Clack, 2002). Once the pentadactyl 'ground state' of the autopod had been established, the ancestral phalanx numbers per digit are believed to be 2-3-4-5-3, for digits I to V (Wagner, 2014; Xu and Mackem, 2013). However, these numbers have changed considerably in different tetrapod clades. For example, the majority of mammalian autopods display a 2-3-3-3-3 phalanx formula for their five digits (Wagner, 2014; Xu and Mackem, 2013), while certain cetacean species have drastically increased the overall number of bones per digit. This resulted in an extreme variation of the ancestral phalanges pattern known as 'hyperphalangy' (Cooper et al., 2007). Moreover, phalanges in a given digit vary not only in number, but also differ markedly in individual size, both length- and girth-wise. As a consequence, within a given species, the number, size and shape of the phalanges are reflective of each digit's homeotic identity (Dahn and Fallon, 2000; Wagner, 2014).

At the onset of digit development the autopod plate is composed of alternating interdigit areas

and digital rays, as previously specified by a Turing-like patterning mechanism (Hiscock et al., 2017; Raspopovic et al., 2014; Sheth et al., 2012). While in the more proximal parts the metacarpals and metatarsals already start to condense, at the very distal tip of the autopod the actual outgrowth of the digits starts. Interestingly, the underlying molecular mechanisms for building these distal autopod elements are likely distinct from the more proximal ones, as demonstrated by the loss of phalange development in *Bmpr1b* knockout mice while metacarpals remain relatively unaffected (Yi et al., 2000). Proliferation of a distal progenitor population, known as the 'phalanx-forming region' (PFR), or 'digital cresent' (DC) (Montero et al., 2008; Suzuki et al., 2008; Witte et al., 2010), allows for the growth of the digit to occur unidirectionally along its proximal-distal axis (Figure 2C). The PFR itself is thought to originate from the distal mesenchyme, localized just beneath a specialized epithelial structure called the apical ectodermal ridge (AER). Epithelial cells inside the AER are known to mediate overall limb growth, by secreting FGF signals that promote proliferation in the underlying mesenchyme (Mariani et al., 2017). Consequently, a FGF gradient specifies a distal domain of growth competency, which is translated into digit elongation at the PFR (Figure 2C) (Feregrino et al., 2019; Hiscock et al., 2017; Montero et al., 2008; Suzuki et al., 2008). FGF signaling from the AER seems to have a role not only in the control of digit length, but also phalanx numbers. By examining *Fgf8* expression in the developing chicken foot - in which each digit is morphologically different, both length- and phalanx number-wise - a correlation of the duration of *Fgf8* expression at the digit tip and the resulting number of phalanges was observed (Sanz-Ezquerro and Tickle, 2003b). Experimentally prolonging *Fgf8* expression at the digit tip induces the formation of an additional phalanx, while use of an FGF receptor inhibitor prevents formation of the most distal phalanx (Sanz-Ezquerro and Tickle, 2003b). Temporal variations in AER persistence, and by extension duration of FGF signaling, have therefore the potential to explain even extreme deviations from an ancestral phalanx formula, such as for example seen in the hyperphalangy of cetacean flippers (Richardson and Oelschläger, 2002). However, while the effect of FGF on cell proliferation suggests an obvious mechanism to control digit length, how can the segmentation into individual phalanges occur at the cellular and molecular level?

It is also within the PFR population that distinct cell fate decisions are thought to occur during digit elongation, instructing digit segmentation along its proximal-distal axis. In contrast to somite formation, where a change of tissue organization (i.e. mesenchymal-to-epithelial) drives segmentation, the partitioning of digits into individual phalanges involves the specification of two distinct cell types. Once proliferation of the PFR progenitor cells has displaced the source of the FGF gradient distally, the proximally located cells lose their

progenitor state and undergo a divergent cell type specification. They differentiate accordingly into either chondrocytes - the cellular building blocks of the phalanges themselves - or prospective interzone cells that eventually form the synovial joints to connect the digit bones (Hiscock et al., 2017; Shwartz et al., 2016). Hence, by controlling the temporal aspects of this divergent cell fate decision with respect to the overall growth rate, the digit segmentation pattern into individual phalanges can be determined. To faithfully execute this process, the PFR assimilates various signaling inputs that confer positional information and modulate additional, possibly self-organizing mechanisms, to result in correct digit segmentation patterns and thus homeotic identity. Most notably, it has been demonstrated in chicken embryos that the forming digits have their segmentation pattern specified by the interdigit mesenchyme that is located immediately posterior to them (Dahn and Fallon, 2000). Interdigit mesenchyme “cut-and-swap” experiments result in homeotic transformations that corroborate the idea that the interdigit mesenchyme is involved in digit identity specification. Multiple lines of evidence implicate gradients of BMP signaling, originating from the interdigit tissue, to establish this positional information system at the molecular level. For example, implantation of a bead soaked with the BMP antagonist NOGGIN within the interdigit induces an anteriorization of digit identity (Dahn and Fallon, 2000). Moreover, the PFRs of different digits were found to carry distinct levels of SMAD1/5/8 activity that correlate well with the eventual differences in their segmentation patterns (Suzuki et al., 2008).

While the role of BMP signaling in determining phalanx numbers in each digit is well accepted, there is mounting evidence that it could also influence phalanx size. Within each digit the phalanges sizes do not vary randomly, but rather seem to change as an integral developmental module, separate from the rest of the autopod (Hiscock et al., 2017; Kavanagh et al., 2013). Capitalizing on a broad phylogenetic sampling covering multiple vertebrate clades, it was demonstrated that the ratios of measured areas of successive phalanges change in a predictable manner. Namely, the size of a proximally located phalanx is prognostic for the size of more distal phalanges, with the largest phalanges usually found at the proximal end of the digit (Kavanagh et al., 2013). Thus, despite the complexity and diversity of phalangeal morphology across digits and species, there appear certain remarkably conserved relationships amongst the distinct elements that point to the presence of conserved developmental modules. Moreover, the periodicity of the eventual pattern may hint at an underlying self-organizing property of the process, potentially Turing-like in nature, that acts concomitantly as digit elongation occurs. Indeed, individualized phalanges sizes are not merely the result of post-patterning events like, e.g., growth plate-mediated long bone elongation. Rather, they represent an integral part of the patterning process itself, as size differences are

already apparent at early stages of phalanx specification. This corresponds to a timepoint when synovial joint interzones separating the successive phalanges are being initiated (Huang et al., 2016; Kavanagh et al., 2013). Barrier insertion and viral overexpression experiments in chicken, as well as genetic manipulations in mice, suggest that one or more diffusible cues from the previously formed phalanx and/or interzone may be instrumental in this process (Huang et al., 2016; Kavanagh et al., 2013). Several experimental observations also imply the presence of additional, partially self-organizing principles that may help to refine digit pattern periodicity (Hiscock et al., 2017). For example, the ectopic induction of an interzone using retroviral overexpression of *Wnt9a* has been shown to inhibit formation of subsequent joint sites at a distance (Hartmann and Tabin, 2001). Likewise, insertion of a barrier into a proximal phalanx leads to an increased segment sizes in subsequently forming phalanges (Kavanagh et al., 2013). Based on its expression in maturing phalanges, as well as the lack of phalangeal joint formation in mutant embryos, *Noggin* has been proposed as the putative diffusible cue underlying these effects (Figure 2C) (Brunet et al., 1998). A progressive build-up of NOGGIN protein, caused by the increasing phalanx expression domain, could instruct subsequent joint specification, once a critical threshold of BMP inhibition has been reached (Huang et al., 2016). Using an allelic series in mice, NOGGIN-modulated BMP activity itself has been shown to lie downstream of a 5'Hoxd-Gli3 antagonism. Since both 5'Hoxd genes and Gli3 show quantitative differences in their expression levels along the pinky-to-thumb axis of the developing autopod, this model provides an elegant explanation of how anterior-posterior positional information could be translated into distinct digit identities (Huang et al., 2016; Sanz-Ezquerro and Tickle, 2003b). However, based on the apparent dynamics of BMP signaling in the forming phalanges, across both space and time, additional modulators might be involved in the exact determination of digit-specific phalanx-joint patterns (Grall and Tschopp, unpublished observations).

4. Conclusions and future directions

As highlighted in the examples above, the three key components of a positional information-based coordinate system – boundaries, scalar, and polarity – face distinct challenges when we consider their implementation in a directionally growing domain. As for the non-expanding condition proposed in Wolpert's original model, morphogen gradients play an essential role in determining all three parameters. How they are established, however, can be quite different from their static counterparts. For phytomers, somites and phalanges, the position of a proliferating progenitor population defines one of the boundaries of the field to be patterned, as well as the directionality of tissue growth (Figure 2A-C). Localized production of a

morphogen within (SAM, PSM) or nearby (AER) this progenitor population provides the source for establishing a molecular gradient. The time required for a cell to traverse the resulting gradient field, i.e. the interval a cell is displaced from the gradient's range of influence by the proliferation of more distally located cells, thus becomes central to the temporal integration of the signal (Harfe et al., 2004; Wolpert, 1989). Moreover, the distal production of the morphogen in phytomer and somite progenitors themselves, and the control of its polarized transport or stability, as the cells journey through the field, are essential to define the scalar of the gradient (Dubrulle and Pourquié, 2004b; Smith et al., 2006). For the PFR, responsiveness to the FGF signals emanating from the overlaying AER alters proliferation rates and, by extension, the time the progenitors spend inside the gradient. The unidirectional nature of the growth, resulting from the distal location of the proliferating progenitor populations, inherently defines the polarity of these gradients. To ensure robustness in establishing and interpreting all of these primary gradients, secondary and opposing gradients act in conjunction (Figure 2A-C). In case of cytokinins (phytomers) and retinoic acid (somites), they function by directly counteracting the distal gradients (Moreno and Kintner, 2004; Vanstraelen and Benková, 2012), whereas *Noggin* (phalanges) has been suggested to spatially modulate the induction of the following segments (Brunet et al., 1998; Huang et al., 2016). These proximally located gradients are also key to control secondary patterning events in the prospective segments, be it for a graded size control of the forming phalangeal segments (Kavanagh et al., 2013), to balance left-right asymmetries in somites (Vermot and Pourquié, 2005), or to control the spacing and orientation of subsequently forming secondary organs in plant shoots (Besnard et al., 2014; Müller and Leyser, 2011). Importantly, in all three cases the production of these secondary gradients initiates in an already formed segment, i.e in cells that have been removed from the embryonic field to be patterned. As such, they help to determine and refine the proximal boundaries of the field, while at the same time contribute to segment size control (Aulehla and Pourquié, 2010; Müller and Leyser, 2011; Young et al., 2015).

Combining growth-driven displacement of molecular gradients, to establish positional information, with a secondary, self-organizing patterning module appears to be a common design principle in the establishment of periodic patterns (Richmond and Oates, 2012). In somitogenesis, the location of segment boundary formation famously depends on the combination of a gradient-dependent, moving 'determination front' and cell-intrinsic molecular oscillators (Oates et al., 2012; Tsiairis and Aulehla, 2016). Likewise, for root growth in plants – which relies on a SAM-like arrangement of its proliferating progenitors, the root apical meristem (RAM) – oscillating gene expression networks have been reported to control the periodicity of lateral branching (Moreno-Risueno et al., 2010). Above ground, however,

phyllotaxis has been successfully approximated *in silico* by activator/inhibitor- and transport-based models (Jönsson et al., 2006; Meinhardt et al., 1998; Smith et al., 2006). While molecular similarities to the oscillator-based segmentation of the primary body axis have been proposed for overall tetrapod limb patterning (Sheeba et al., 2016), self-organizing mechanisms in general await further experimental validation and quantitative data, in particular for the patterning of individual phalanges in the distal limb (Hiscock et al., 2017; Huang et al., 2016). Clearly, however, it appears that the combination of positional information-based directional growth with additional patterning modules, often self-organizing in nature, might generally underlie the periodicity of repetitive morphological structures (see e.g. palate growth and Turing mechanisms during mammalian rugae formation (Economou et al., 2012)).

Indeed, by combining Wolpert's positional information with further patterning systems, either temporally or spatially, the overall robustness of the system might increase, and could thus be buffered against slight developmental deviations that eventually might transition into evolutionary novel patterns (Payne and Wagner, 2019; True and Haag, 2001). While variations in segment numbers are easily explained by alterations in the size or the temporal persistence of the progenitor pool, results from morphological extremes, like vertebral count in snakes or cetacean phalanges, suggest that different sub-modules of the system - for example the speed of an oscillator or proliferation-dependent feedback into the segmentation module - can be affected as well (Gomez et al., 2008; Richardson and Oelschläger, 2002). Moreover, size control between individual elements might be internally constrained by the molecular and/or cellular architecture of the ancestral segmentation process, thus restricting the exploration of the entire theoretically available morphospace (Young et al., 2015). And lastly, post-patterning processes, like discretized growth control of individual segments, may provide an additional layer of evolutionary diversification (Sears et al., 2006; Thompson, 1992). Importantly, all of these observations highlight the fact that rarely, if ever, a certain patterning module might function in a truly isolated fashion. It is therefore more likely that these tight interconnections, between positional information and additional systems hint at the existence of largely context-dependent patterning outputs.

While providing patterning robustness and evolvability, such combinatorial systems can render the acquisition of quantitative data cumbersome, as well as severely impede the design of clearly interpretable experimental perturbations in order to test certain hypotheses. Here, the development of dedicated *ex vivo* and/or *in vitro* models might prove invaluable to study a given patterning module in true isolation. This has already successfully been realized for important aspects of somitogenesis, or in different organoid systems (Hubaud et al., 2017; Lauschke et al., 2013; Rossi et al., 2018; Turner et al., 2016). In combination with microfluidic

or optogenetic approaches controlling morphogen signaling, such *ex vivo*/*in vitro* methods are likely to contribute to a more quantitative understanding of the underlying molecular and cellular processes (Huang et al., 2016; Manfrin et al., 2019; Sako et al., 2016). Furthermore, emerging techniques to measure and perturb various intrinsic parameters with cellular resolution will help to disentangle how virtually homogenous, extracellular positional information can be interpreted differentially cell-intrinsically, to result in discretized cellular states (Feregrino et al., 2019; Li and Elowitz, 2019). Quantitative data from these newly available technologies should in turn result in the continuing refinement of mathematical and computational models, to approximate periodic patterning of repetitive morphological structures *in silico* (Hiscock and Megason, 2015; Schweisguth and Corson, 2019).

Finally, implementing these experimental and theoretical methods within the context of an evolutionary-comparative framework might turn out to be mutually beneficial. For example, *in silico* models may help to predict the causative parameter alterations that can transform one species-specific pattern into another, whereas contrasting repetitive pattern formation over different evolutionary timescales can instruct the design of improved models and experimental approaches alike. Here, studies at the micro-evolutionary level will reveal the degree of plasticity associated with a certain patterning process, while macro-evolutionary comparisons can inform us about potential development constraint. Indeed, embracing the power of comparative approaches may bring us full circle with Wolpert's initial proposition of 'positional information', where he discusses the problem in the context of species as diverse as hydra, *Drosophila* or chicken (Wolpert, 1969). Such efforts have certainly contributed to our appreciation of two of the major underlying design principles in the patterning systems of highly repetitive structures: the fact that positional information seems to work preferentially in conjunction with additional, often self-organizing patterning modules, and that a decoupling of growth and segmentation control allows for modular alterations in segment numbers.

II. Vertebrate limb development – Repetitive patterns of skeletal elements

The vertebrate limb has proven to be a great model to study different examples of repetitive pattern formation. The distal part of tetrapod limb in particular, the so-called autopod, is composed of alternating interdigit areas and digital rays, resulting in the repetition and species-specific number of digits in the adult limb. Additionally, those digits are themselves segmented into a repetition of individual digit bones, the so-called phalanges, which in adult hands and feet are connected to each other by synovial joints. In this chapter, I will introduce basic concepts of limb development, the specification and patterning of digits in the tetrapod autopod along the antero-posterior axis, as well as the segmentation process of individual digits, into phalanges connected to one another *via* synovial joints.

1. Outgrowth and patterning of the limb bud

During development, the limb originates from the lateral plate mesoderm and is developing as a mass of proliferating mesenchymal cells, covered by the ectoderm forming a bud on the lateral side of the embryo (Gros and Tabin, 2014; Zeller et al., 2009). Elongation of the limb occurs along the proximal-distal axis and mesenchymal cells condense to form the different skeletal elements of the limb: one long bone in the proximal part giving the rise to the stylopod, two long bones in the middle part of the limb corresponding to the zeugopod, and smaller bones in the distal part forming the autopod. The autopod, giving rise to the future hand and foot, is composed of digital rays separated by interdigits, and connects *via* carpal and tarsal bones to the zeugopod. This basic pattern in three parts, along the proximal-distal axis is conserved over the course of tetrapod evolution. Thus, limb progenitor cells need to proliferate and be properly patterned to determine their position and prospective cellular identities, to result in the final structures of the limb (Figure 3) (McQueen and Towers, 2020; Zeller et al., 2009). To this end, the limb bud needs positional information, which will induce patterning along the three axes: the anterior-posterior, the dorsal-ventral and the proximal-distal axis.

The apical ectodermal ridge (AER) is a specialized part of the ectoderm that covers the distal margin of the limb bud (Figure 3). Limb bud outgrowth occurs in response to signals emanating from the AER. A series of embryological experiments in chicken limb buds established a functional role of the AER in limb outgrowth. Removal of the AER results in a truncated chicken

limb skeleton, caused by developmental arrest (Saunders, 1948). Moreover, removing the AER at different stages results in truncations of the limb skeleton at different levels along the proximodistal axis (Saunders, 1948). This suggest that the time spend by mesenchymal cells under the AER influence is linked with their subsequent specification along the proximodistal axis. Indeed, this zone was identified as a “progress zone”, and the longer the cells will stay in this zone, the more distal they will end up in the final limb structure (Summerbell et al., 1973; Tabin and Wolpert, 2007). Additionally, grafting AER tissue to another part of the limb bud results in ectopic outgrowth, supporting the role of the AER in directing limb growth (Fallon et al., 1983). FGF signaling was shown to be the molecular cue involved in this process. Indeed, it was shown that applying FGFs beads after AER ablation can stimulate outgrowth and patterning of the limb bud along the proximo-distal axis (Fallon et al., 1994; Niswander et al., 1993). These signals are also involved in maintaining the limb bud progenitors in an undifferentiated and proliferative state (Cooper et al., 2011; Roselló-Díez et al., 2011). Altogether, these experiments demonstrate the importance of AER-FGF signaling for limb bud outgrowth and patterning along the proximo-distal axis.

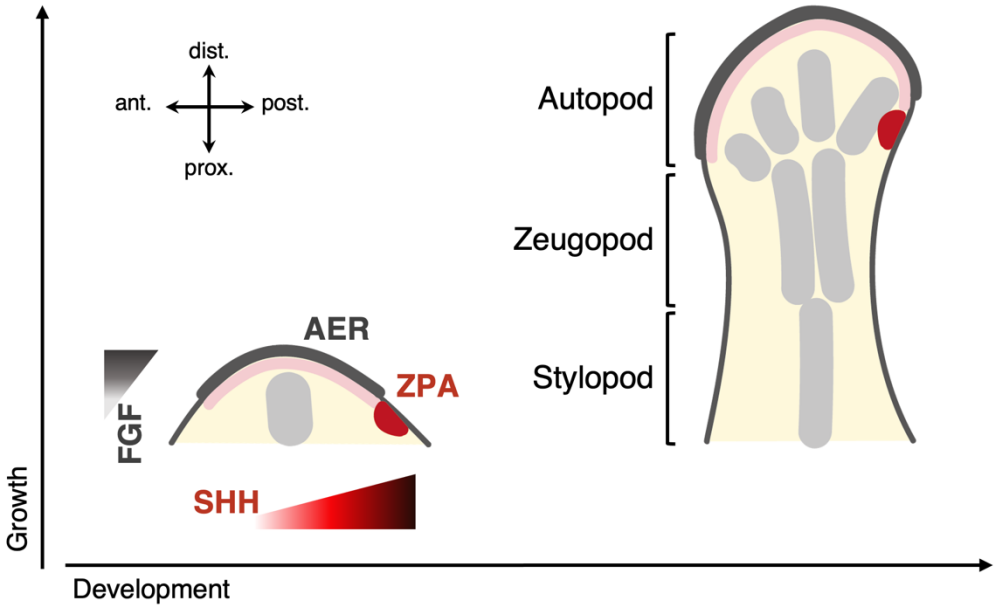

Figure 3. Patterning and outgrowth of the limb bud. In the limb bud, a FGF gradient coming from the AER allows the limb outgrowth distally, keeping the distal mesenchyme proliferative and undifferentiated. This signal also helps to define the proximo-distal axis, along which is specified the 3 skeletal parts of the limb: one long bone in the proximal part giving the stylopod, two long bones in the middle part of the limb corresponding to the zeugopod, and smaller bones in the distal part forming the autopod, giving rise to the future hand and foot. A SHH gradient coming from the ZPA defines the antero-posterior axis, with specification in the zeugopod domain of the radius anteriorly and ulna posteriorly and in the autopod domain of the different digits.

The anterior–posterior axis is specified by another organizing center, the zone of polarizing activity (ZPA) (Figure 3). Transplant experiments of this posterior region of the limb bud mesenchyme to the anterior margin of chicken wings bud result in mirror image duplications of the digits within the autopod (Saunders and Gasseling, 1968; Tickle et al., 1975). The ZPA specifies positional information in the limb bud by secreting a diffusible molecule (Wolpert, 1969). Sonic Hedgehog (SHH) was identify being the molecular cue produced by the ZPA (Riddle et al., 1993). For the specification of the dorso-ventral axis, expression of *Wnt7a* in the dorsal ectoderm, and ventral ectoderm expresses of *engrailed1* (Loomis et al., 1998) provides the necessary molecular cues. Additionally, interlinked feedback loops, between the different signaling center, were shown to coordinate limb bud axis specification, growth and patterning (Zeller et al., 2009).

Collectively, to achieve proper limb development, interconnection of different signaling centers provides the positional information needed for outgrowth and patterning of the limb bud along the three major axes.

2. Periodic pattern of digits – Alternating digital rays and interdigit along the antero-posterior axis

Early during development, the distal part of vertebrate limb, the autopod, is composed of alternating interdigit areas and digital rays, resulting into the repetitive pattern of digits in the adult limb. This alternation of digital rays and interdigit is set along the antero-posterior axis, specified by SHH signaling. The digital rays will undergo chondrogenesis whereas interdigit tissue will undergo apoptosis, which is required to separate digits. Formation of the digital rays has been shown to occur asynchronously (Zhu et al., 2008), and starts out as regularly spaced spots that extend distally, as the autopod grows out (Hiscock et al., 2017).

The emergence of the periodic pattern of these digital rays was proposed to be specified by a Turing patterning mechanism (Raspopovic et al., 2014; Sheth et al., 2012). Decreasing progressively distal Hox genes level (*Hoxa13* and *Hoxd11-Hoxd13*) in a Gli3-null mutant background results in progressively more densely packed digits (Sheth et al., 2012). Combining this observation with *in silico* modeling, a Turing-type model was proposed in which the level of distal Hox genes modulates the spacing between digits, and thus the wavelength of the periodic pattern of digital rays and interdigits (Sheth et al., 2012). A study proposed that the Turing-like mechanism of periodic pattern of digit relies on a molecular network involving *Sox9*, and the BMP and WNT signaling pathways (Raspopovic et al., 2014). BMP signaling was proposed to be active in regions of the digital rays, to promote chondrogenesis and thus

the expression of the early chondrogenic marker *Sox9*. WNT signaling was proposed to be active in regions of interdigits, to inhibit chondrogenesis and thus of *Sox9* expression. In this SOX9-BMP-WNT-based Turing mechanism, BMP pathway signaling acts as the inducer of digits identity, and WNT pathway signaling as the inhibitor of digits. Both pathways interact in concert with *Sox9,* to periodically specify its expression that precedes the formation of digital rays.

To sum up, distal Hox genes are proposed to modulate the wavelength of the periodic pattern of digits, which relies on a SOX9-BMP-WNT-based Turing mechanism resulting in alternating digital rays and interdigit along the antero-posterior axis (Figure 4) (Lopez-Rios, 2016). However, whether this mechanism is important for specifying the digit-interdigit wavelength throughout the outgrowth process, or only at its initiation, is still a matter of debate (Hiscock et al., 2017).

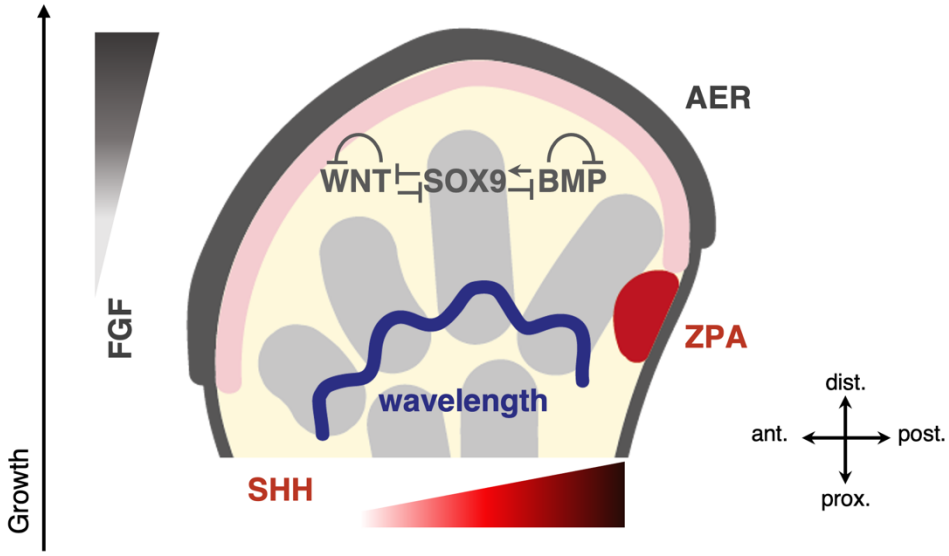

Figure 4. Periodic pattern of digits. Periodic patterns of digits (grey) and interdigit (yellow) is simultaneously controlled by distal Hox genes expression, which modulates the wavelength of the pattern, and by a SOX9-BMP-WNT-based Turing mechanism resulting in alternating digital rays and interdigit along the antero-posterior axis (Adapted from Lopez-Rios, 2016).

3. Digit specification – Determination of the digit identities

Once that the location of digital rays, and hence the origins of the digit are defined, their identities need to be specified. Morphologically, digit identity is defined by the number, size, and shape of the phalanges (digits bones), connected to each other by synovial joints (Young et al., 2011). The gradient of SHH emanating from the ZPA, and which established the antero-posterior axis of the limb bud, was shown to be involved in the specification of the identity of

these digital rays (Harfe et al., 2004; Hu and He, 2008; Zhu et al., 2008). Indeed, deleting *Shh* gene in mouse at different times using conditional mutant results in progressive loss of digits (Zhu et al., 2008). Moreover, digit identity specification of digit 2 to 5 in the mouse is determined by the dose of SHH received by the digital ray (Harfe et al., 2004). In addition, Hox genes were also shown to regulate digit identity (Pérez-Gómez et al., 2018), and in mouse, digit 1, formed by two phalanges, possesses a unique Hox code (Montavon et al., 2008). Moreover, alteration of this Hox code along with shift in digit identity was observed in the chicken limb, when SHH signaling was decreased using pharmacological inhibition by Cyclopamine (Vargas and Wagner, 2009).

Besides SHH and Hox genes, it has been demonstrated in chicken embryos that the forming digits have their identity specified by the interdigit mesenchyme that is located immediately posterior to them (Figure 5) (Dahn and Fallon, 2000; Suzuki and Fallon, 2021). Interdigit mesenchyme "cut-and-swap" experiments result in homeotic transformations that corroborate the idea that the interdigit mesenchyme is involved in digit identity specification. Indeed, these

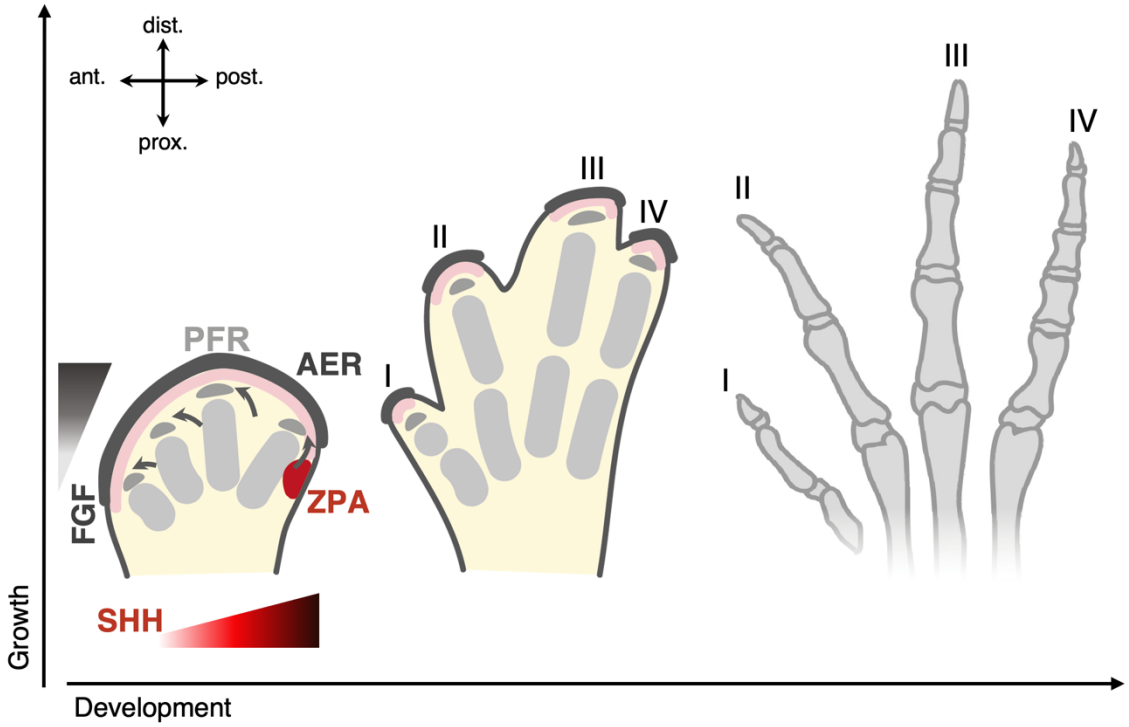

Figure 5. Determination of the digit identities. A gradient of SHH emanating from the ZPA is involved in the specification of the identity of these digital rays. In addition, progenitors of the phalanx forming region (PFR) at the tip of digital rays received positional information form the posterior interdigit to determine the definitive digit identity. Digital rays then elongate distally during development to give final structure of digits which possess their own identity defined by the number, size and shape of the phalanges (digits bones) connected to each other by synovial joints.

experiments reveal that the removal of interdigit 2 induces the transformation of digit 2 to digit 1, and removal of interdigit 3 induces the transformation of digit 3 to digit 2.

Overall, digit identity is specified early by the dose of SHH received across the autopod, and later determined by additional BMP pathway signals coming from the immediately posteriorly located interdigit mesenchyme.

All in all, during early limb development, different signaling centers, like the AER-FGF and the ZPA-SHH, provide positional information needed for outgrowth and patterning of the limb bud along the major embryonic axes. Periodic patterns of digits within the distal part of the developing limb, the autopod, occurs along the antero-posterior axis and relies on a SOX9-BMP-WNT-based Turing mechanism, whose wavelength is modulated by distal Hox genes. Identities of these digital rays are specified early by SHH, and later determined by BMP signals coming from posterior interdigit. As a result, distinct digit morphologies are being specified, distinguished by their number and the length of the individual digits bones, the phalanges, and their connections *via* synovial joints. Much of the cellular and molecular dynamics necessary for the specification of these repetitive patterns has been reviewed before, in part I of this general introduction, under “Tetrapod digit segmentation: Repetitive patterns of phalanges”.

4. Tetrapod digit evolution – Emergence of morphologically distinct digit patterns

Digits are sophisticated, movable skeletal structures, allowing tetrapod to display fine motor tasks, like digging, grabbing, or even writing and playing music. Thanks to their modular architecture, of phalanges and joints, highly distinct digit morphologies have emerged over the course of vertebrate evolution. Indeed, the autopod, localized most distally from the trunk is subject to more extensive modifications compared to the rest of the limb, and thus show the highest degree of diversity (Cooper et al., 2018; Fedak and Hall, 2004; Sears et al., 2006).

The fin-to-limb transition, resulting from the transitioning of aquatic vertebrates onto land, is at the origin of the appearance of digits (Stewart et al., 2020). This transformation was suggested to be either an adaptation of a preexisting regulatory mechanism, or the emergence of a novel regulatory mechanism resulting in the specific structure of digits (de Bakker et al., 2021; Stewart et al., 2017). Across tetrapods, a remarkable diversity of digit morphologies is observed. For example, in bats, elongated digits are supporting a wing membrane allowing this mammalian species to fly. Rather an increased in the number of phalanges to have elongated digits, their digits are composed of elongated phalanges (Sears et al., 2006). In cetaceans flippers, on the other hand, prolonged AER activity let to emergence of so-called

hyperphalangeal digits (Richardson et al., 2009). Among birds, a great variability in digit morphologies is observed and in the hindlimb of some birds, the penultimate phalanx is elongated (de Bakker et al., 2013, 2021; Kavanagh et al., 2013).

Overall, tetrapods thus exhibit highly variable digit morphologies. To generate these different digit identities, embryonic digit patterning needs to be modified (see Figure 6, and above, General Introduction - part I). Importantly, however, the eventual digit patterns are made of the same cell and tissue types, for all the different tetrapod digit morphologies.

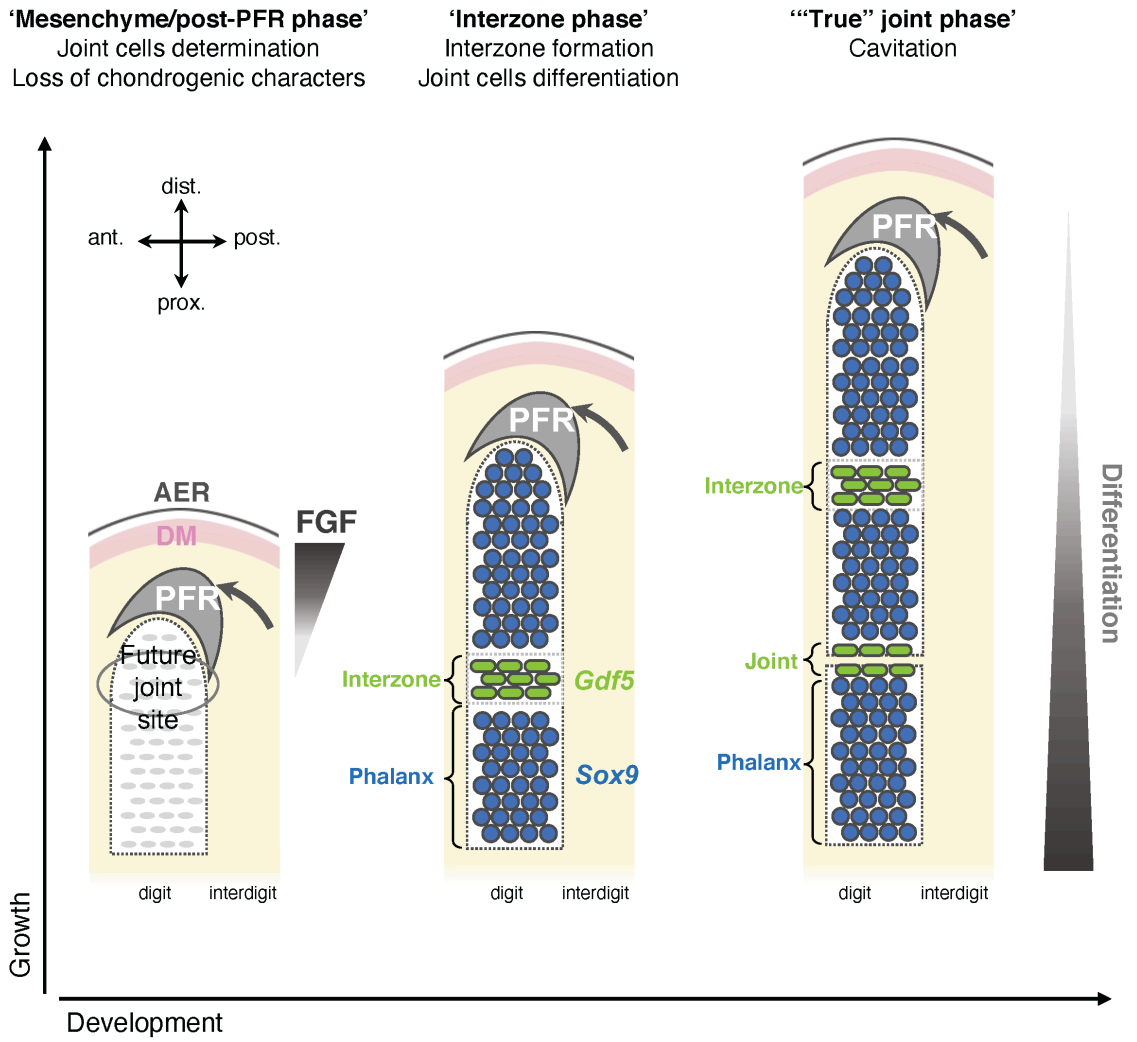

Figure 6. Tetrapod digit patterning and development. Tetrapod digits grow proximal-distally due to progenitor proliferation within the phalanx forming region (PFR), relying on distal FGF gradient coming from the AER. PFR progenitors receive positional information, in part from the posterior interdigit, to make cell fate decisions into either joint or phalanx progenitor cells during digit elongation. Joint formation begins with the initiation of a group of cells known as an 'interzone', molecularly characterized by the expression of specific marker genes like *Gdf5*, and absence or down-regulation of expression of chondrocyte-specific genes like *Sox9.* These cells then differentiate to give the different cell type of a synovial joint which makes the connection between phalanges in a digit-specific pattern.

5. Phalanx and joint development – Digit cell type differentiation and maturation

Once that joint and phalanx progenitor cells have been specified at their correct relative locations, they can undergo differentiation into the different mature cell types that compose the tissues, forming the phalanges bones connected by synovial joints (Lefebvre and Bhattaram, 2010). The bones forming the phalanges are long bones formed by endochondral ossification. The skeletal development of a phalanx starts with the condensation of mesenchymal cells of the digital rays that will become chondrocytes, marked by expression of *Sox9* (Bi et al., 1999; Healy et al., 1999). Elongation of this cartilage template is driven by adding cells distally, through progenitor specification at the PFR (Suzuki et al.,2008 and General Introduction - part I, above). These formed chondrocytes will proliferate, to additionally induce longitudinal growth at so-called growth plate structures (Kozhemyakina et al., 2015). Moreover, they will start to express collagen genes like *Col9a1* and *Col2a1*, which are structural proteins of the early cartilage (Genzer and Bridgewater, 2007; Lefebvre et al., 1997). Chondrocytes located towards the middle of the future phalanx, below the growth plates, will become pre-hypertrophic chondrocytes, expressing *Ihh* (Vortkamp et al., 1996), whereas chondrocytes at the periphery of the forming skeletal element will form the perichondrium (Bandyopadhyay et al., 2008). Then, pre-hypertrophic chondrocytes mature into hypertrophic chondrocytes, which express *Col10a1* (Gu et al., 2014). Finally, hypertrophic chondrocytes are replaced by bone marrow and bone, and the perichondrium by the periosteum (Deng et al., 2008). This process relies on the induction of so-called ossification centers, formed by osteoblast precursors, and is followed by the invasion of blood vessels (Kozhemyakina et al., 2015). Chondrocyte maturation was shown to be regulated by transcription factors *Runx2* and *Runx3* (Lefebvre and Bhattaram, 2010). Additionally, FGF signaling induced hypertrophic differentiation of chondrocytes (Minina et al., 2005). TGF-beta and BMP signaling were shown to be important for osteoblast differentiation and bone formation (Chen et al., 2012).

Synovial joints are composed of articular cartilage covering the distal tip of the bones, i.e. the surface of the epiphysis, ligaments and a fibrous capsule, which keeps the bones together, and forms the synovial cavity filled with synovial fluid (Decker et al., 2014). During development, joint progenitors forming the interzone are the first sign of the joint formation. Besides the histologically visible cell flattening, joint progenitors of this interzone are characterized by a loss of expression of chondrocyte-specific genes, like *Sox9 and Col2a1,* and the onset of joint marker genes expression like *Gdf5*, *Wnt4*, and *Wnt9a* (Guo et al., 2004; Hartmann and Tabin, 2001; Später et al., 2006; Storm et al., 1994). Later on, within the

interzone, a cavity is formed, and subsequently filled with fluid. This joint cavitation process is accompanied by the differentiation of the joint progenitors into articular chondrocytes, giving rise to the formation of articular cartilage. Several crucial factors involved in joint and articular cartilage development and maturation have been identified (Chijimatsu and Saito, 2019; Pacifici et al., 2005). Hedgehog signaling was shown to regulate joint development and morphogenesis (Rockel et al., 2016). Moreover, it was shown that articular cartilage differentiation needs a precise and ongoing spatial restriction of BMP signaling *via Noggin* (Ray et al., 2015), as well as continuing embryo movement (Singh et al., 2018).
While several signaling pathways have been identified to be required for differentiation and maturation of joint and phalanx cells, the detailed mechanism remain unknown.

6. Digit malformations – Digit segmentation disorders

Perturbations during digit development can results in digit segmentation disorders. Human digit malformations with digit segmentation disorders occur relatively frequent in the general population and the phenotypes of these malformations can be highly diverse.
One major class of congenital disorders is known as brachydactylies, corresponding to a shortening of hands or feet due to hypoplasia and/or aplasia (shortening or absence) of phalanges (Mundlos, 2009; Stricker and Mundlos, 2011). There are different types of brachydactyly, depending on which phalanges are affected. Indeed, the hypoplasia/aplasia can affect the middle phalanges or the terminal phalanges, within some or all digits. Moreover, brachydactylies are often associated with abnormal development of joints, which results in a condition called symphalangism, corresponding to a fusion of phalanges with or without shortening of digits (Stricker and Mundlos, 2011). Another well-known digit malformation observed in humans is the triphalangeal thumb, which correspond to a hyperphalangy (formation of additional phalanges) in the digit I, corresponding to the thumb (Potuijt et al., 2019). Genetic disorders affecting the ZPA regulatory sequence, known as the ZRS, were linked to triphalangeal thumb malformations (Potuijt et al., 2019). Many of the brachydactylies were shown to be linked to members of the BMP pathway, which plays an important role during digit development (Mundlos, 2009; Stricker and Mundlos, 2011). For example, genetic defects like *GDF5* or *BMPR1B* loss-of-function mutations were shown to induce brachydactylies. Likewise, *NOGGIN* loss-of-function mutations or *GDF5* gain-of-function mutations can cause symphalangism. Additionally, animal models were used to understand the pathogenic mechanisms of these mutations, to phenocopy human digit malformations and to confirm the

importance of precise BMP signaling regulation for proper digit development in mammals (Mundlos, 2009; Stricker and Mundlos, 2011).

Overall, several digit malformations are observed in humans, with varying degrees of severity and/or digits affected. Likely genetic factors for most of these malformations have been identified. However, the underlying developmental etiology still remains unclear in many cases. Nevertheless, understanding the pathogenic mechanisms of these human digit malformations may shed light on important aspects of the molecular and cellular mechanisms involved in digit development, as well as in evolutionary digit pattern diversification.

AIM OF THE THESIS

AIM OF THE THESIS

Formation of repetitive structures is highly regulated and reproducible, yet shows the tendency for modular evolutionary diversification. During embryonic development, it needs the precise implementation of patterning, cell fate specification and morphogenetic mechanisms, in order to give rise to the final intended repetitive shape. Evolutionary modulations of these processes can result in morphological diversity.

In the general introduction above, I reviewed the mechanisms of pattern formation of repetitive morphological structures, with a special focus on the specification and diversification of the repetitive patterns in the tetrapod digit. Digit growth and patterning depends on the proliferation and signaling integration in a pool of progenitor cells, the phalanx forming region (PFR), that will undergo cell fate decisions into either phalanx or synovial joint progenitor cells. Members of TGF-beta superfamily, including the Bone morphogenetic proteins (BMP), have been implicated in the digit segmentation process. However, the precise molecular and cellular mechanisms of digit morphological specification and evolutionary diversification have not yet been fully elucidated.

This thesis work thus aims at investigating how growth and cell fate decisions are differentially regulated during tetrapod digit development, and to what extent these mechanisms can be modified on an evolutionary timescale, to generate novel digit morphologies.

The first part of this thesis work studies how molecular cues are integrated at the PFR, to control digit emergence. For this purpose, quantitative morphological and signaling dynamics data of chicken digit patterning have been produced, to describe the molecular and cellular parameters of digit patterning at high spatiotemporal resolution. Moreover, single-cell RNA-sequencing pseudotime analyses in combination with mathematical modeling was used to approximate digit patterning *in silico*, to eventually screen extended parameter spaces and identify putative cellular and molecular changes underlying digit pattern diversification.

In the second part of this thesis, I intend to understand how signals received by the PFR are interpreted to allow for the controlled bifurcating cell fate decisions into either joint or phalanx precursors shaping a digit. To this aim, single-cell RNA-sequencing, pseudotime analyses and experimental embryology with viral mis-expression were used to identify candidate regulator genes of cell fate decisions, and assess their function *in vivo*.

Collectively, this work aims to contribute to our understanding of the cellular and molecular mechanisms underlying tetrapod digit patterns specification and diversification.

Chapter I

Growth and signaling dynamics during digit development: pattern formation and diversification

Abstract

Throughout nature, repetitive morphological structures are plentiful to be found. For example, tetrapod digits are composed of a series of individual digit bones, the so-called phalanges, connected to each other *via* synovial joints. Thanks to this modular architecture, morphologically highly distinct digit patterns have emerged over the course of vertebrate evolution. During embryogenesis, at the tip of each growing digit, a delicate balance of cell proliferation and cell type specification in a group of progenitor cells, the phalanx forming region (PFR), needs to be precisely controlled to ensure proper phalanx patterning. A gradient of FGF activity from the overlaying apical ectodermal ridge influences digit outgrowth, while genes of the TGF-beta superfamily have been implicated in controlling digit segmentation. How then are these molecular cues integrated to orchestrate cell fate decisions at the PFR, and to what extent can these mechanisms be modified on an evolutionary timescale, to generate novel digit morphologies? By producing quantitative *in vivo* data and combining it with mathematical modeling, we aim to decipher the underlying dynamics of digit pattern formation and diversification. Using the chicken foot as a model, in which all digits are morphologically different, we produce quantitative *in vivo* growth time series and signaling dynamics data of digit development. We then formulate a mathematical model, based on a BMP signaling-based Turing mechanism, to try to approximate digit patterning *in silico*. This model can recapitulate important aspects of digit patterning *in silico*, and, thus, can help to approximate pattern transitions from one digit formula into another. Collectively, studying pattern formation in vertebrate digits will help us to identify the molecular mechanisms underlying the modular architecture of a repetitive pattern of high morphological variability.

Introduction

Digits are sophisticated movable skeletal structures allowing tetrapod to display fine motor tasks, like digging, grabbing, or even writing and playing music. Digits are segmented into individual digit bones called phalanges, which in adult hands and feet are connected to each other by synovial joints. Thanks to this modular architecture, highly distinct digit morphologies have emerged over the course of vertebrate evolution. The fin-to-limb transition, resulting from invasion of aquatic vertebrates onto land, is the origin of appearance of digits (Stewart et al., 2020). According to the fossil record, the ancestral phalanx numbers per digit are believed to be 2-3-4-5-3, for digits I to V (Wagner, 2014; Xu and Mackem, 2013). However, these numbers have changed considerably in different tetrapod clades, like for example in mammals, where the majority of autopods display a 2-3-3-3-3 phalanx formula for their five digits (Wagner, 2014; Xu and Mackem, 2013). Certain cetacean species, however, have drastically increased the overall number of bones per digit, known as 'hyperphalangy' (Cooper et al., 2007). Moreover, phalanges in a given digit vary not only in number, but also differ markedly in individual size, both length- and girth-wise. Rather than an increasing in the number of phalanges to have elongated digits, bat digits are composed of individual elongated phalanges, to support a wing membrane allowing this mammalian species to fly (Sears et al., 2006). Among birds, a great variability in digit morphology is observed, and in the hindlimb of some birds, like for example raptors, the penultimate phalanx is elongated (Kavanagh et al., 2013).

During development, the distal part of vertebrate limb, the autopod, is composed of alternating interdigit areas and digital rays, whose periodic digit-interdigit pattern was proposed to rely on a Turing-like mechanism (Raspopovic et al., 2014). Formation of the digital rays was shown to occur asynchronously (Zhu et al., 2008), and starts as regularly spaced spots of mesenchymal condensation, giving rise to chondrogenic cells that will proliferate and elongate into digit rays as the limb bud grows (Hiscock et al., 2017). The digital rays are the first sign of digit formation. Members of the TGF-beta signaling were shown to be required for the induction of the mesenchymal condensation, through induction of cell surface adhesion and extracellular matrix proteins expression (Chimal-Monroy and Díaz de León, 1999; Lorda-Diez et al., 2022). At the tip of each digital ray, a group of progenitor cells, called the phalanx forming region (PFR), will proliferate to be added distally into the digital ray to allow its elongation (Montero et al., 2008; Suzuki et al., 2008). A FGF gradient, coming from specialized epithelial structure called the apical ectodermal ridge (AER), specifies a distal domain of growth competency, which is translated into digit elongation at the PFR (Sanz-Ezquerro and Tickle, 2003b).

It is also within this PFR population that distinct cell fate decisions are thought to occur during digit elongation, to drive digit segmentation into the individual phalanges. The progenitors of the PFR proliferate to allow the digit to grow. Thereafter, they are specified to differentiate into chondrocytes, corresponding to phalanx progenitors, or interzone cells, corresponding to the joint progenitors, to result in the sequential phalanx-joint modules shaping a digit. Once that both phalanx and joint progenitors are specified at the right location, they differentiate into the different cell types composing the phalanges and the joints. The phalanges are long bones formed by endochondral ossification and the joints connecting them are synovial joints, composed of articular cartilage covering the distal tip of the bones, ligaments and fibrous capsule, which keeps the bones together, and forms the synovial cavity filled with synovium (Decker et al., 2014).

In order to make the correct cell fate decisions giving rise to these chondrocytes and joint progenitors, and produce the correct digit segmentation pattern, each PFR needs to assimilate various signaling inputs. As a result, each digit has an individual 'homeotic identity', determined by the number and size of the eventual digit bones (Wagner, 2014). It has been demonstrated that digit identity is specified by positional information received from the posterior distal interdigit (Dahn and Fallon, 2000). Interdigit mesenchyme "cut-and-swap" experiments suggest that the interdigit mesenchyme is involved in digit patterning specification, and gradients of BMP signaling, originating from the interdigit tissue were suggested to be involved (Dahn and Fallon, 2000; Suzuki et al., 2008). Recently, each PFR was shown to respond only to positional information from the interdigits located immediately posterior to it (Suzuki and Fallon, 2021).

During digit outgrowth, cell fate decisions within the PFR need to be properly controlled in both space and time. Members of the TGF-beta superfamily, including the Bone Morphogenetic Proteins (BMP), have been shown to be essential for the determination of phalanx-joint patterning (Lorda-Diez et al., 2022). Several human digit malformation syndromes are caused by mutations in genes involved in BMP pathway (Stricker and Mundlos, 2011). For example, mutations in *GDF5,* a BMP pathway ligand belonging to the growth and differentiation factors sub-family, result in digit malformations like brachydactylies or symphalangism. Additionally, dominant negative mutations in the BMP receptor BMPR1B, which GDF5 preferentially binds to (Antebi et al., 2017), also result in brachydactylies. Analysis of a mouse mutant model has shown that *Gdf5*, which is the earliest marker of developing joints, stimulates phalange development and inhibits joints development (Storm and Kingsley, 1999). In addition, *Bmpr1b* was shown to have a role in chondrogenesis of phalanges (Yi et al., 2000). Indeed, loss of phalange development is observed in *Bmpr1b* knockout mice, while the more proximal

metacarpals of the autopod remain relatively unaffected. Additionally, NOGGIN, a BMP pathway inhibitor, was suggested to bind GDF5, to block its action *in vivo* (Brunet et al., 1998; Merino et al., 1999a). Indeed, *Noggin* mouse mutants fail to develop joints (Brunet et al., 1998). In addition, NOGGIN bead implantations at the tip of the developing chicken digit induce digit truncations (Merino et al., 1999a). BMP pathway activity modulation by NOGGIN, lying downstream of a 5'Hoxd-Gli3 antagonism from the interdigit, was suggested to induce specification of joint progenitors at the digit tip (Huang et al., 2016). In addition, 5'Hoxd genes and Gli3 show quantitative differences in their expression levels along the antero-posterior axis of the developing autopod, which could explain the distinct digit identities along this axis (Huang et al., 2016; Sanz-Ezquerro and Tickle, 2003a). Overall, these observations suggest that a precise regulation of BMP signaling is needed for proper digit development, and that both activating and inhibitory signals are involved.

From regulatory point of view, that is how these activating and inhibitory signals interact, the periodicity of the phalanges pattern and its apparent modularity indicated that it may rely on a self-organizing process (Hiscock et al., 2017; Kavanagh et al., 2013). Indeed, during self-organization processes, a homogenous tissue breaks symmetry spontaneously, to form periodic patterns of repetitive structures. To do so, a reaction-diffusion system involving local interaction and long-range inhibition, between activator and inhibitor diffusible molecules, will result in a stable state of alternating spatial domains of activator and inhibitor activity. This self-organization process was first theorized by Alan Turing (Turing, 1952). Several experimental observations have suggested the presence of a self-organizing, potentially Turing-like process during digit development. For example, measures of the ratio of successive phalanges areas within a digit reveal that proximal phalanx size influences the size of more distal phalanges, with the largest phalanges usually found at the proximal end of the digit (Kavanagh et al., 2013). Additionally, experimental perturbation of digit formation, by blocking diffusible signals with a foil barrier from the previously formed phalanx, perturbs distal joint positioning, and the size of distal phalanges (Kavanagh et al., 2013). Furthermore, genetic manipulations in mice suggest that one or more diffusible cues from the previously formed phalanx and/or interzone may be involved in this process (Huang et al., 2016). Finally, ectopic induction of a joint, using *Wnt9a* overexpression, inhibits the formation of subsequent joints at a distance, suggesting the presence of long-range inhibition between joints (Hartmann and Tabin, 2001). Thus, several experimental observations support the role of BMP signaling in digit patterning, and that the periodic phalanx-joint pattern could rely on a self-organizing process. *Noggin*, a BMP pathway inhibitor, was proposed as a candidate diffusible cue acting in this process (Brunet et al., 1998; Huang et al., 2016; Sanz-Ezquerro and Tickle, 2003b). However, the exact role of

the different BMP pathway players, and their regulatory relationship between each other to form a potentially self-organizing process producing a periodic phalanx-joint pattern, remains unknown.

In this work, we aim to elucidate how molecular cues are integrated at the PFR, to regulate growth and cell fate decisions during tetrapod digit development, and to give rise to distinct digit morphologies. To do so, we use the chicken foot as a model system, in which all digits are morphologically different. Indeed, in its four digits, the chicken foot displays a 2-3-4-5 phalanx formula. We first produced quantitative *in vivo* growth time series data and looked at the transcriptional dynamics during the PFR-to-joint or -phalanx cell fate decisions using single-cell RNA-sequencing and pseudotime analyses. Focusing on the BMP pathway, we produced quantitative signaling dynamics data of digit development in the chicken foot. Based on the observed dynamics, we then formulated a mathematical model, inspired by a Turing mechanism and centered on BMP signaling pathway interactions, to try to approximate digit patterning *in silico*. This model can explain different wild type digit patterns, as well as phenotypes observed in BMP pathway mutants and/or experimental perturbations. Collectively, these results provide new insights into the molecular and cellular regulation of phalanx-joint patterning during digit development, and provide an experimental and theoretical approach to understand the evolution of distinct digit morphologies.

Results

1. Morphological dynamic of chicken digit patterning

Digits are growing unidirectionally along the proximal-distal axis of the limb, thanks to the proliferation of progenitors in the PFR (Montero et al., 2008; Suzuki et al., 2008; Witte et al., 2010). The PFR originates from the distal mesenchyme, localized just beneath the AER, and an FGF gradient, coming from the AER, specifies a distal domain of growth competency, which is translated into digit elongation at the PFR (Feregrino et al., 2019; Hiscock et al., 2017; Montero et al., 2008; Suzuki et al., 2008). However, the precise timing/dynamics of phalanges formation and joint appearance, i.e. digit segmentation, has not been described so far. Moreover, chicken digits have different identities, defined by different phalanges numbers, shapes, and sizes. Therefore, we first aimed to describe the morphological dynamics of chicken digit patterning, to investigate the underlying growth and patterning differences. We focused our analysis on digit II, III and IV of the chicken (Figure 1A). To analyze growth

dynamics of those digits over the course of development, we produced a time series of phalanx growth and joint specification. To do so, chicken autopods were collected at different time points of development (128 to 336 h of development, or Hamburger-Hamilton stages HH27 to HH40). Digits were dissected, embedded sidewise and sectioned longitudinally. *In situ* hybridization for the joint marker *Gdf5* was performed on cryosections of digits to visualize the appearance of joints and, hence, individual phalanges. Pictures of those staining were taken and measurements of phalanx length were done for each time point, by drawing a line going from the middle of a joint to the middle of the following joint or from the most distal joint, the last joint, to the AER (Figure 1B). Plots of the total length of each digit shows that overall growth

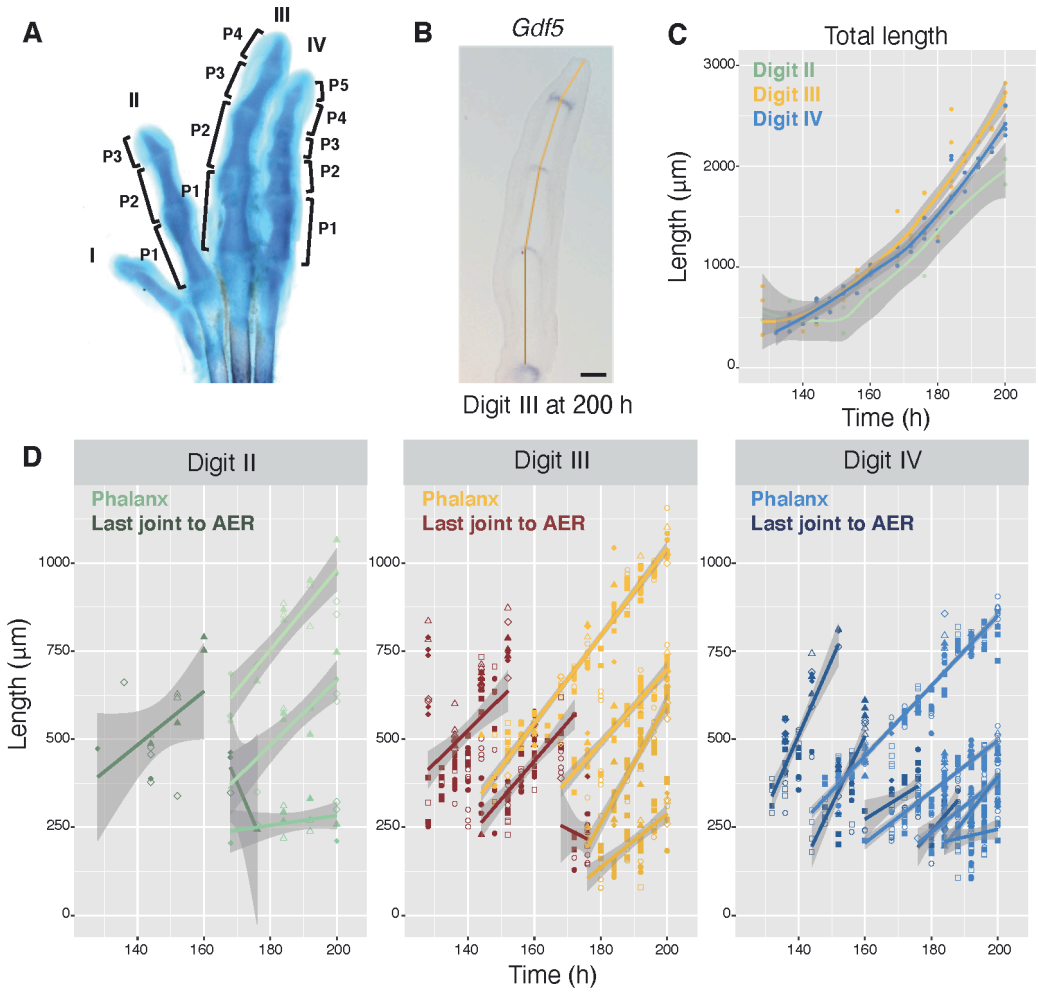

Figure 1. Growth and segmentation data in chicken developing digit. (**A**) Skeletal preparation of a chicken foot at day 11 of development (Courtesy of Patrick Tschopp). (**B**) Measurements of the different elements for digit 3 taken on the image of a RNA *in situ* hybridization of *Gdf5* in a longitudinal section of a digit at 200 h of development. Scale bar = 100 µm. (**C**) Total lengths for digits II, III and IV in function of the developmental time. (**D**) Lengths of the different elements for digits II, III and IV in function of the developmental time. Point shapes: biological replicates ; Full shape: right limb ; Empty shape: left limb ; Shaded area: SEM.

rates are quite similar early on, between digits (Figure 1C). However, after 160 h, digit III grows slightly faster than the other digits (Figure 1C and S1). These differences are probably linked to post-patterning events, like e.g. long bone elongation. Indeed, phalanges are long bones formed by endochondral ossification, and chondrocytes are proliferating in the growth plates to allow for further long bone elongation (Lefebvre and Bhattaram, 2010).

In order to see if there are phalanx growth rate variations within each digit, we plotted the length of each individual element. First, we observed that joints appear sequentially, and occurs simultaneously with digit elongation (Figure 1D). For example, in digit III, the first interphalangeal joint appears around 144h, the second around 168h and the third around 176h. Additionally, within a digit, growth rates are different between the phalanges. Interestingly, in all digits, the second to last phalanx seems to show an increase in growth rate, compared to the other phalanges. We also observed that overall phalanges growth rates are slightly different between digits. Indeed, phalanges in digit IV appear to grow slower than digit III phalanges, and slower than digit II phalanges. However, looking at the last joint to AER length, digit IV tip seems to grow faster than the tip of digit III.

Next, to see if there are cellular differences of growth at the digit tip between the different digits, we assessed cell proliferation using BrdU incorporation (Gratzner, 1982). To do so, BrdU solution was injected into the amniotic cavity of chicken embryos at 6 days of development (= 144 h) and embryos were collected 3 h after BrdU application (Zou et al., 1997). Digits were dissected, embedded and cryosectionned longitudinally. Immunohistochemistry for BrdU and for pSmad1,5,9, present in the PFR, reveal that at the digit tip, cells are positive for BrdU, except in the PFR, where there is a decrease of cells positive for BrdU (Figure 2A-B''). This observation was already reported by Montero et al. (Montero et al., 2008). However, between tip of digit III and digit IV, no striking differences in cell proliferation are observed. Further replicates and quantifications would be needed to be able to conclude on this. To investigate differences in putative regulators of proliferation, between digit III and IV, we looked at the *Sprty2* gene, which was suggested to be a negative regulator of FGF signaling and thus inhibit limb outgrowth (Impagnatiello et al., 2001). Fluorescent RNA *in situ* hybridization for *Sprty2* was performed in combination with immunohistochemistry for pSmad1,5,9 on digit tip sections (Figure 2C-D''). Results reveal the presence of gene transcripts just below the AER, distal to the PFR, and *Sprty2* seems to be slightly more expressed at the tip of digit IV compared with the tip of digit III. Again, further replicates and quantifications would be required to assess the significance of this observation.

Collectively, in the chicken autopod, growth rate differences are observed both between and within digits. Digits segmentation occurs simultaneously with digit outgrowth, through induction of joint interzones at digit-specific frequencies and timepoints of development.

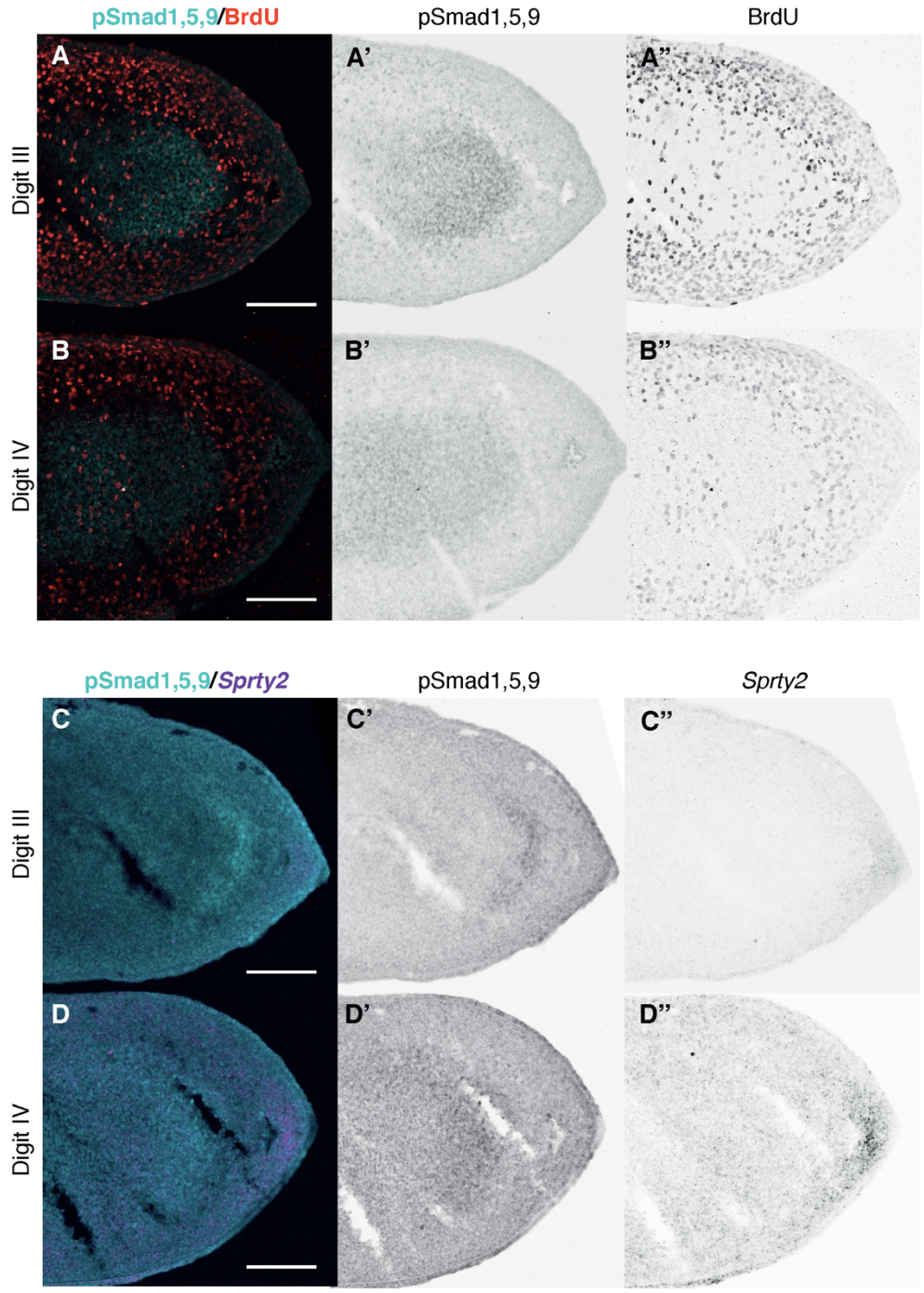

Figure 2. Cell proliferation at the developing digit tip in chicken. (**A-B''**) Immunohistochemistry for BrdU incorporation and pSmad1,5,9 in longitudinal section at the tip of digit III and IV at D6 of the development. (**C-D''**) Fluorescent RNA *in situ* hybridization for *Sprty2* combined with immunohistochemistry for pSmad1,5,9 in longitudinal section at the tip of digit III and IV at day 6 (= 144 h) of the development. Scale bars = 100 µm.

2. Signaling dynamics of chicken digit patterning

The frequency of phalanx-joint patterning within digits relies on the spatiotemporal control of cell fate decisions at the PFR, into either phalanx or joint progenitors. In order to better understand how these cell fate decisions are regulated during digit development, we need to know the underlying molecular dynamics.

To study the molecular dynamics of cell fate decisions at the PFR, we used pseudotime analysis on autopod single-cell RNA sequencing data (the entire process of pseudotime calculation and validation is explained in more detail in Chapter II). Given the genetic evidence for the importance of the TGF-beta superfamily, we specifically focused on its gene members, at the pseudotime divergence point of the joint and phalanx progenitor trajectories. Hierarchical clustering of differential expression signatures along the branches revealed six top differentially expressed genes, with three phalanx- and three joint-enriched gene signatures (Figure 3). Amongst them are candidates known from previous molecular genetic studies (Huang et al., 2016; Lorda-Diez et al., 2022; Ray et al., 2015). *Inhba*, an Activin protein family encoding gene expressed in the PFR, was proposed to induce digit morphogenesis (Lorda-Diez et al., 2022). In our pseudotime reconstruction, *Inhba* is expressed in the part shared by the two trajectories, corresponding to the mesenchymal progenitors that differentiate into the chondrocyte progenitors of the PFR. In addition, *Inhba* expression is maintained in the joint progenitors pseudotime trajectory. Expression of *Gdf5*, known to be a joint marker and a BMP pathway activator (Seemann et al., 2005; Storm and Kingsley, 1996), is restricted to the joint progenitors pseudotime trajectory. *Bmpr1b*, a BMP pathway receptor that GDF5 preferentially binds to (Antebi et al., 2017), and which is known to be expressed in the PFR (Suzuki et al., 2008), is expressed along the phalanx progenitors pseudotime trajectory and in the part shared by the two trajectories. *Noggin*, a BMP pathway inhibitor (Brunet et al., 1998; Merino et al., 1999a), is expressed in the phalanx progenitors pseudotime trajectory. *Chrdl1* and *Chrdl2*, paralog genes belonging to the Chordin protein family, were suggested to be BMP pathway inhibitors (Nakayama et al., 2001, 2004). *Chrdl1* is expressed along the phalanx progenitors pseudotime trajectory, whereas expression of *Chrdl2* is restricted to the joint progenitors pseudotime trajectory. Moreover, *Chrdl1* is expressed in the part shared by the two trajectories, supposed to contain the PFR progenitors. Additionally, outside of top 6 genes, dynamic expression of other interesting candidates was observed. *Tgfbl*, also known as *βig-h3* (Lorda-Diez et al., 2013a), is expressed in the mesenchymal progenitors of the pseudotime reconstruction. *Tgfbl* was reported to be expressed in the growing digit tip and was suggested to have a role in the differentiation of connective tissue (Lorda-Diez et al., 2013a). Its expression is downregulated

when expression of *Inhba* is starting, which suggests that *Tgfbl* is expressed earlier in the digit progenitor lineage than *Inhba*. Most of these genes have been shown to be involved in digit patterning (see Introduction). Nevertheless, their exact roles in digit patterning and the dynamics of cell fate decisions at the PFR have not been established yet.

With this pseudotime analysis, we recapitulated expression dynamics of several gene members of the TGF-beta superfamily along the two pseudotime trajectories. The expression of the top differently expressed genes observed along the joint and phalanx progenitors pseudotime trajectories suggests a potential role in the regulation of the phalanx-joint cell fate decision of the PFR progenitors. However, spatial dynamics are lost in single-cell RNA

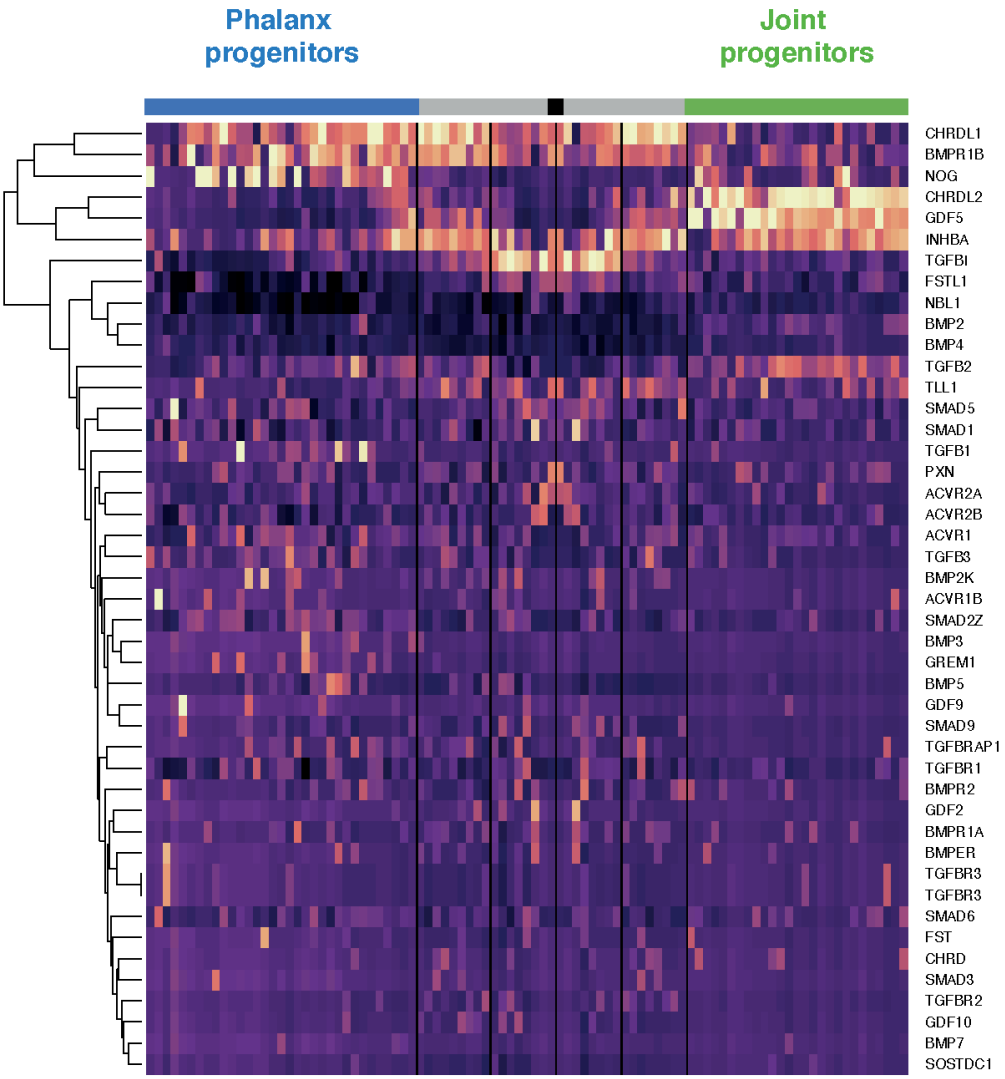

Figure 3. Phalanx-joint pseudotime analyses of chick HH29 hindlimb single-cell RNA sequencing data. Pseudotime heatmap of gene members of the TGF-beta superfamily, differentially expressed between the phalanx (blue) and joint progenitors trajectories (green). The black zone corresponds to the starting point of the pseudotime. The grey zone corresponds to the part shared by the two trajectories. Orange: high scaled expression; Purple: low scaled expression.

sequencing and further experiments are thus required to look at their *in situ* expression dynamics during digit patterning. Accordingly, we next analyzed the spatiotemporal expression patterns of BMP pathway members *Gdf5*, *Noggin* and *Bmpr1b in vivo*. Additionally, we assessed BMP pathway activity, by measuring pSmad1,5,9 presence, i.e. the phosphorylated version of Smad1,5,9.

We first analyzed the BMP pathway spatial dynamics *in vivo* by staining chicken digit III sections, at a developmental time point when the two proximal phalanges are already formed and when the joint separating the third and the last phalanges is forming. To do so, immunohistochemistry for pSmad1,5,9, was performed on longitudinal digit cryosections in combination with fluorescent *in situ* hybridization for *Gdf5*, marking the joint. Results were imaged with confocal microscopy and fluorescence profiles were obtained by analyzing the distribution of the pSmad1,5,9 fluorescence intensity and *Gdf5* transcripts along the digit

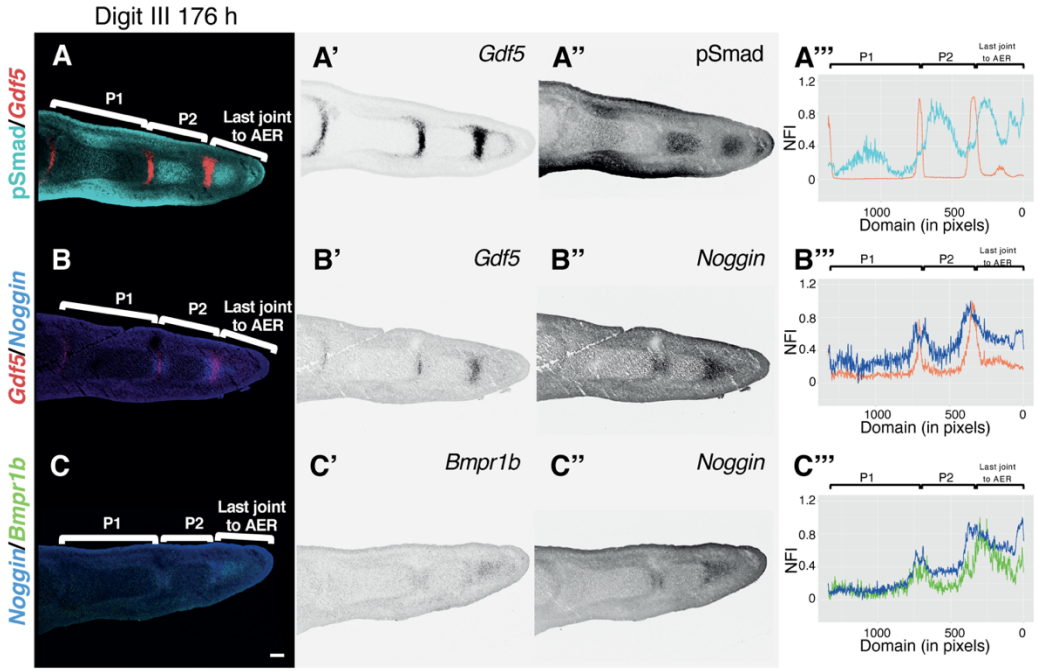

Figure 4. *In vivo* expression data for *Gdf5*, *Noggin* and *Bmpr1b* in chicken developing digit. (**A-A''**) Fluorescent RNA *in situ* hybridization for *Gdf5* combined with immunohistochemistry for pSmad1,5,9 in longitudinal section of digit III at 176 h of development. (**A'''**) Plot of normalized fluorescence intensity (NFI) of pSmad1,5,9 (Cyan) and *Gdf5* (Red) in function of digit domain elements for digit III at 176 h of development. (**B-B''**) Multiple fluorescent RNA *in situ* hybridization for *Gdf5* and *Noggin* in longitudinal section of digit III at 176 h of development. (**B'''**) Plot of normalized fluorescence intensity (NFI) of *Gdf5* (Red) and *Noggin* (Blue) in function of digit domain elements for digit III at 176 h of development. (**C-C''**) Multiple fluorescent RNA *in situ* hybridization for *Noggin* and *Bmpr1b* in longitudinal section of digit III at 176 h of development. (**C'''**) Plot of normalized fluorescence intensity (NFI) of *Noggin* (Blue) and *Bmpr1b* (Green) in function of digit domain elements for digit III at 176 h of development. **A**, **B** and **C** are serial cryosections separated by 18 µm. Scale bar = 100 µm. 1 pixel = 1,243 µm.

domain. We observed that the pSmad fluorescence intensity is highest at the level of the PFR ("croissant" shape), localized just underneath the AER (Figure 4A-A'''). In phalanges, pSmad fluorescence is present as a near-central dot in the newly formed phalanges. In more proximal phalanges, this dot is tilted towards the proximal end of the phalanx. Moreover, the intensity of pSmad fluorescence within phalanges is higher in newly formed phalanges than in more proximal phalanges. Importantly, joint regions are depleted for pSmad fluorescence, wherever *Gdf5* is expressed, and the two signals appear to be 'out of phase'. Indeed, our results reveal that *Gdf5* is expressed in a narrow intense stripe in the previously formed joints. Moreover, *Gdf5* appears to be expressed in a wider band of low intensity in a newly forming joint, which appears at the digit tip, exactly in the region proximal to the PFR and co-occurring with a dip in pSmad fluorescence (Figure 4A''', 'Last joint to AER'). *Noggin*, a BMP pathway inhibitor, is expressed in regions flanking the *Gdf5* band in the already formed joints and is absent/downregulated in the central part of the already formed phalanges (Figure 4B-B'''), where pSmad was detected on adjacent section (Figure 4A-A'''). Overall, however, *Noggin* expression dynamics appear to be 'in phase' with *Gdf5* expression. In the 'Last joint to the AER' region, *Noggin* is expressed throughout the currently forming phalanx 3, but decreasing its intensity towards the PFR. In this region, *Noggin* is co-expressed with *Gdf5* in the joint ('the last joint' before the AER), separating the phalanx 2 and the currently forming phalanx 3. In addition, at the tip of the currently forming phalanx 3, where *Gdf5* starts to be expressed in a new band, *Noggin* is also co-expressed with *Gdf5*. In the newly forming phalanx, *Noggin* expression is downregulated where pSmad1,5,9 is present (Figure S2). Similar to *Noggin, Bmpr1b*, a BMP pathway receptor, is expressed in regions flanking the already formed joints and is absent/downregulated in the central part of the already formed phalanges (Figure 4C-C'''). In the 'Last joint to the AER' region, *Bmpr1b* is expressed throughout the currently forming phalanx 3, and, contrary to *Noggin*, is not co-expressed with *Gdf5* in the joint separating the phalanx 2 and the currently forming phalanx 3. Indeed, *Bmpr1b* expression is excluded from the forming joint. In addition, *Bmpr1b* seems to be expressed in a graded fashion, with high expression within the PFR and expression getting progressively lower in the distal forming phalanx (Figure S3A-B'').

Overall, we provide evidence for a repetitive pattern of *Noggin* and *Gdf5* expression which is in phase with the forming joint regions, and alternating with Smad1,5,9 phosphorylation which is out of phase. This pattern is obvious in the proximal, already formed phalanx-joint segment. However, at the distal tip, in the newly forming phalanx-joint, the pattern appears to be more dynamic, with the presence of broader expression domains. Thus, two distinct temporal phases are observed: a late proximal phase, where the alternating patterns are well-

established, and an early distal and more dynamic phase. To further investigate these two phases, we produced temporal expression time series data for those genes.

First, we focused on the spatiotemporal dynamics of pSmad1,5,9, the BMP pathway read-out, and *Gdf5*, the joint marker, at different time points of development. We performed fluorescent RNA *in situ* hybridization for *Gdf5* combined with immunohistochemistry against pSmad1,5,9, on digit III longitudinal sections of embryos covering the developmental stages of the last joint formation, i.e. from 176 h to 192 h (Figure 5). We found that in newly forming joints, *Gdf5* starts to be expressed in a wide band, in a region proximal to the PFR, together with a drop of pSmad (Figure 5A-A''). Then, over time, *Gdf5* expression gets stronger and its expression domain narrows (Figure 5B-C''). In addition, pSmad dots gradually appear distal to the newly forming joint, and, over time, the intensity of pSmad fluorescence within phalanges gets lower and tilted towards the proximal *Gdf5* band (Figure 5B-C''). Counterintuitively, the expression of *Gdf5* – a BMP pathway activator – and pSmad are 'out of phase'. These apparent dynamics of BMP

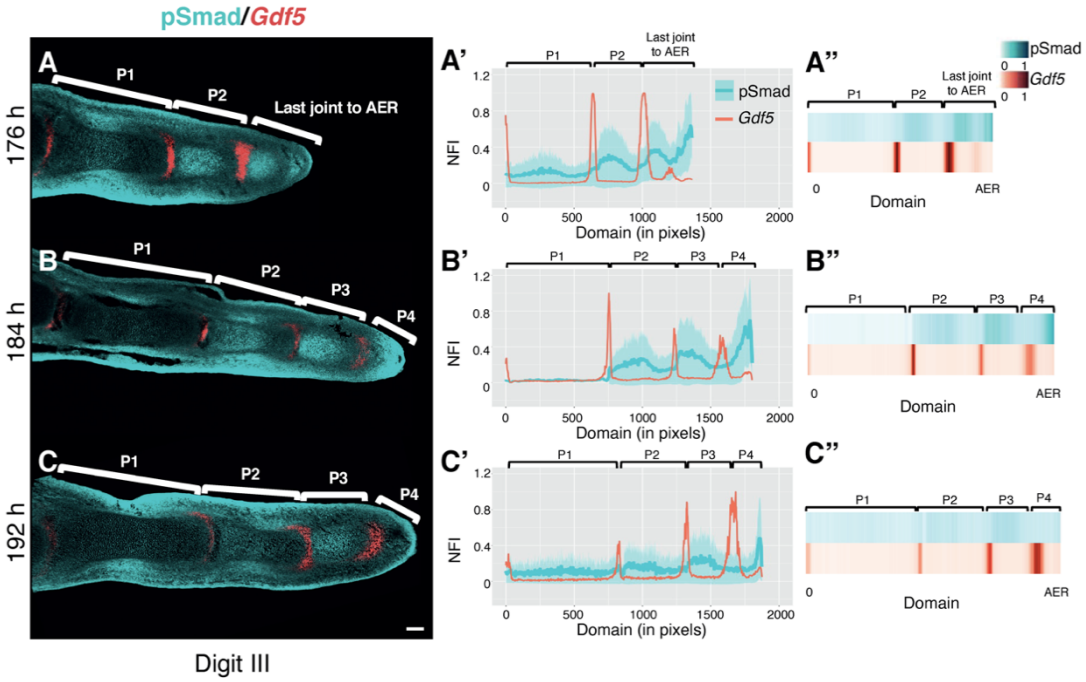

Figure 5. Spatiotemporal *in vivo* data for *Gdf5* gene expression and BMP signaling activity in chicken developing digit. (**A, B and C**) Fluorescent RNA *in situ* hybridization for *Gdf5* combined with immunohistochemistry for pSmad1,5,9 in longitudinal section of digit III at 176, 184 and 192 h of development. Scale bar = 100 µm. (**A', B' and C'**) Plot of normalized fluorescence intensity (NFI) of pSmad1,5,9 (Cyan) and *Gdf5* (Red) in function of digit domain elements for digit III at 176, 184 and 192 h of development. For pSmad1,5,9, the NFI correspond to the mean of 3 Z stacks. Shaded area: SEM. 1 pixel = 1,243 µm. (**A'', B'' and C''**) Heat map visualization of NFI of pSmad1,5,9 (Cyan) and *Gdf5* (Red) in function of digit domain elements for digit III at 176, 184 and 192 h of development.

signaling during digit development thus suggest that additional BMP modulators might be involved in digit patterning, like for example the inhibitor *Noggin*.

Next, we aimed to investigate the spatiotemporal dynamics of BMP pathway activity in morphologically distinct digits – that is, digits II and IV – and compare it to digit III. For that, time series of stainings for pSmad1,5,9 and *Gdf5* were performed for digit II, III and IV, over a developmental time window covering the formation of the first phalanx until the formation of the last distal phalanx (Figure 6). We observed that in all three digits, expression of *Gdf5* and pSmad are 'out of phase'. However, differences are observed in the temporal appearance of newly formed *Gdf5* bands, and the associated drop of pSmad fluorescence intensity. Additionally, spatial differences are also observed in the repartition of pSmad, linked to the amount of *Gdf5* bands, and thus the number of joints per digit. Indeed, the wavelength of the patterns is different between the three digits, with short wavelengths associated with more joints and *vice versa*. Thus, the spatiotemporal distribution of BMP pathway activity is different between digits, depending on the resulting number of phalanx-joint modules in the final digit.

By summarizing our findings across different stages of joint development for pSmad, the BMP signaling activity read out, and for *Gdf5*, *Noggin* and *Bmpr1b*, BMP pathway gene members,

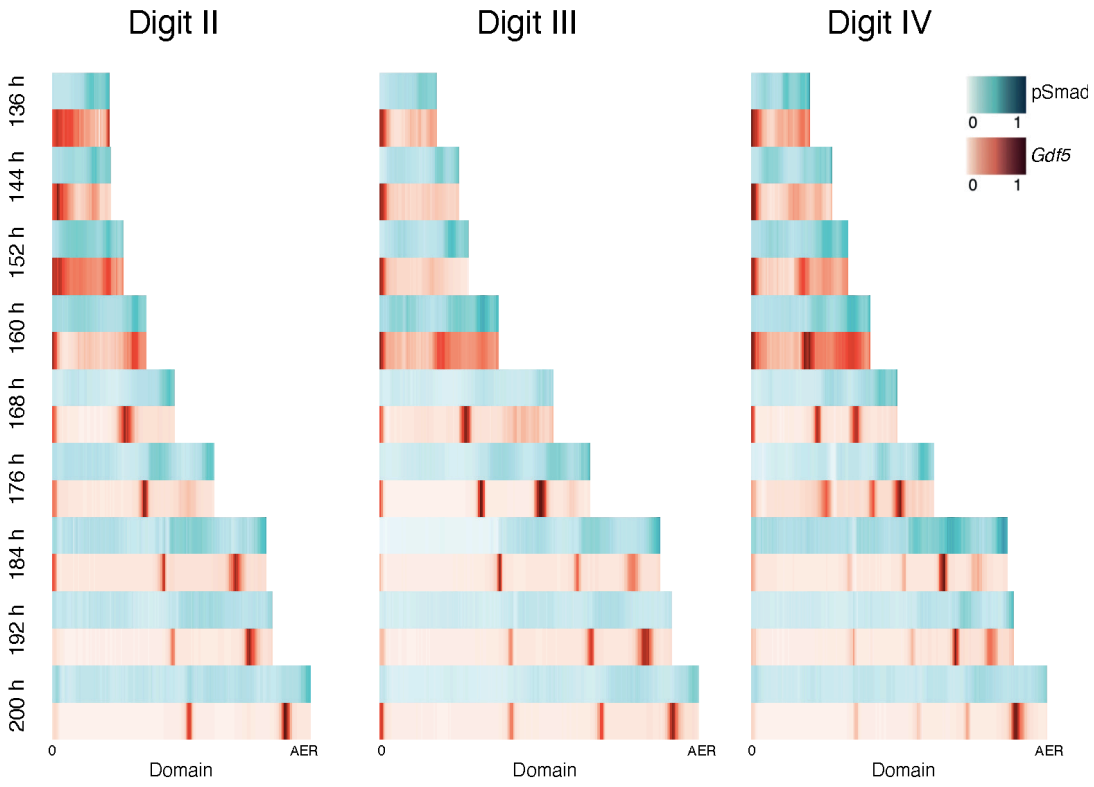

Figure 6. BMP signaling activity during development of chicken digit. Heat map visualization of normalized fluorescence intensity of pSmad1,5,9 (Cyan) and *Gdf5* (Red) in function of digit domain elements for digit II, III and IV at different time of the development.

we have good evidence for an alternating pattern between pSmad and *Noggin/Gdf5* (Figure 7). Indeed, *Gdf5* and *Noggin* are expressed near each other, and pSmad is 'out of phase' with them. A distal expression of *Noggin* appears where pSmad drops, proximally to the PFR. *Noggin* is co-expressed with *Gdf5*, for which the expression appears as a broad, weak band corresponding to the newly forming joint. Interestingly, *Bmpr1b* is expressed in a graded fashion in this zone where the joint cell fate determination is likely to occur. Then, over time, the *Gdf5* expression band narrows and *Noggin* expression decreases at the exact level of the *Gdf5* peak, but is maintained in regions flanking the band. In addition, pSmad dots gradually appear, 'out of phase' with the interzone and, over time, the intensity of pSmad fluorescence within phalanges gets lower and becomes tilted towards the proximal joint. Importantly, the spatiotemporal dynamics of *Noggin*, a known BMP pathway inhibitor, and *Gdf5*, known as a BMP pathway activator, suggest a potential role of those genes in a self-organizing, potentially Turing-like process at the origin of the periodic phalanx-joint pattern in the developing digit.

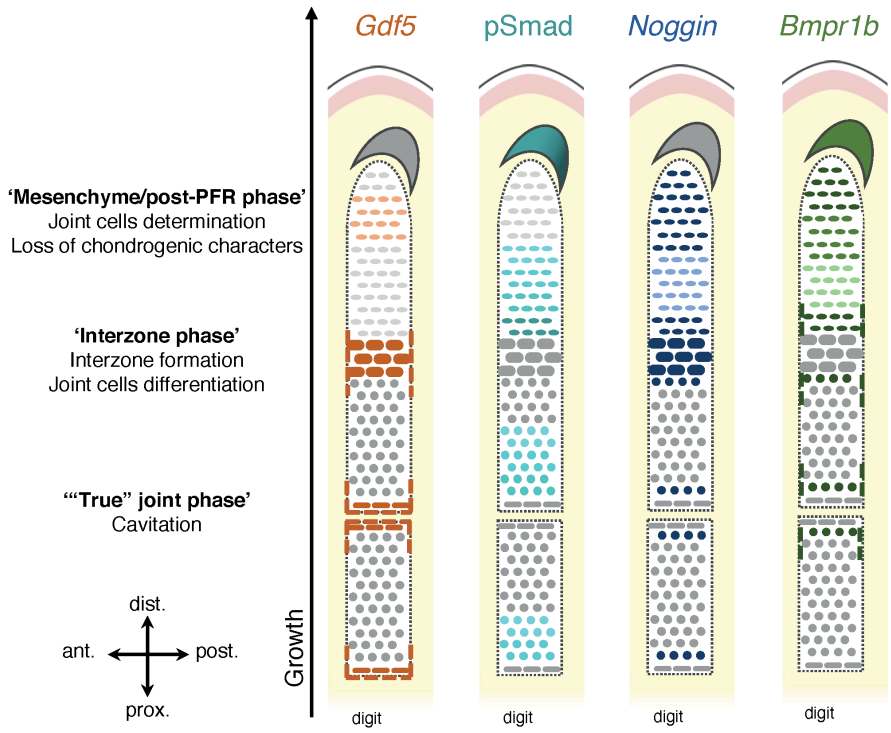

Figure 7. Summary of expression pattern of *Gdf5*, *Noggin* and *Bmpr1b* and Bmp signaling activity in the developing digit.

3. Mathematical modeling of digit patterning

Because of the repetitive nature of phalanx-joint pattern, and according to the signaling dynamics observed above, we were wondering if we can approximate this repetitive motif pattern *in silico*, with self-organizing, potentially Turing-like models. Indeed, we would like to

see if the candidates proposed above are potentially involved in a self-organizing process of digit pattern formation. Moreover, this would allow us to better understand the molecular control of cell fate decision dynamics during digit development, and how and which parameters can potentially change, to explain the apparent evolutionary flexibility in generating novel digit patterns.

We formulated a Turing model, based on the molecular interactions between three important BMP signaling molecules, which captures the symmetry-breaking events that underlie the emergence of repetitive patterns of joints and phalanges during digit development. Digit growth was simulated in this iteration of the model by incorporation of progenitor cells at the distal tip of the developing digit (Figure 8A). Molecular genetic studies has shown that *Gdf5* inhibit joints development (Storm and Kingsley, 1999) and that *Noggin* mouse mutant fail to develop joints in digits (Brunet et al., 1998). Moreover, analysis of the spatiotemporal expression dynamics of those genes, as described above, has shown that they are both out of phase with the BMP pathway activity readout pSmad. Accordingly, we propose that *Gdf5* and *Noggin* are part of a self-organizing process controlling the periodic pattern of phalanx-joint in the developing digit. Thus, the molecular players selected for our model were *Gdf5*, *Noggin* and pSmad (Figure 8B). In this model, *Gdf5* acts as the Turing inhibitor - i.e., it counterintuitively inhibits joint formation - and *Noggin* represents the Turing activator. Moreover, the model makes several assumptions about the roles and regulatory interactions of the different players. Firstly, both GDF5 and NOGGIN proteins can diffuse, yet GDF5 diffuses faster and possesses a long-range action. Secondly, GDF5 activates BMP signaling and thus inhibits the joint fate, through the phosphorylation of Smad. Thirdly, NOGGIN inhibits BMP signaling through the formation of a complex with GDF5. Indeed, NOGGIN was shown to interact with GDF5 (Nolan et al., 2016). Thus, NOGGIN activates joint fate indirectly, by the inhibition of pSmad through complex formation with GDF5. Finally, activation of BMP signaling inhibits both *Noggin* and *Gdf5* transcription, and thus represses joint fate. Indeed, pSmad was shown to be absent in joint progenitors (Huang et al., 2016) and ectopic activation of BMP signaling inhibits joint fate in the interzone (Ray et al., 2015). Accordingly, the proposed system forms a self-organizing feedback circuit that spontaneously assembles into periodic phalanx-joint digit patterns. The corresponding partial differential equations, to describe these molecular interactions, can be found in Figure S4. Importantly, this system is only supposed to be at work in the forming phalanx-joint segment. Once the relative locations of the interzones have been set, cell fates get “locked in”, and additional steps would have to be considered for pattern refinement (e.g. narrowing of *Gdf5* bands).

Simulations of the model players' expression and activity patterns were performed over the course of digit development (Figure 8C). Firstly, simulations revealed that the model can approximate the endogenous expression dynamics of *Gdf5* and *Noggin* observed *in vivo*. Indeed, in the simulation, both *Gdf5* and *Noggin* are expressed in the presumptive joint regions. Additionally, the model captures sequential appearance of *Gdf5* expression and thus the sequential formation of joints. Secondly, the model can also recapitulate the spatiotemporal dynamics of BMP signaling observed *in vivo*. In the simulation, pSmad is localized in the phalanges, between the flanking *Gdf5* joint regions. However, the model does not recapitulate the skewed signal distribution of pSmad that we observe in the phalanx *in vivo*. Thirdly, the model makes predictions for the distribution of NOGGIN and GDF5 proteins. Both NOGGIN and GDF5 proteins are produced near the presumptive joint regions. GDF5 protein shown in

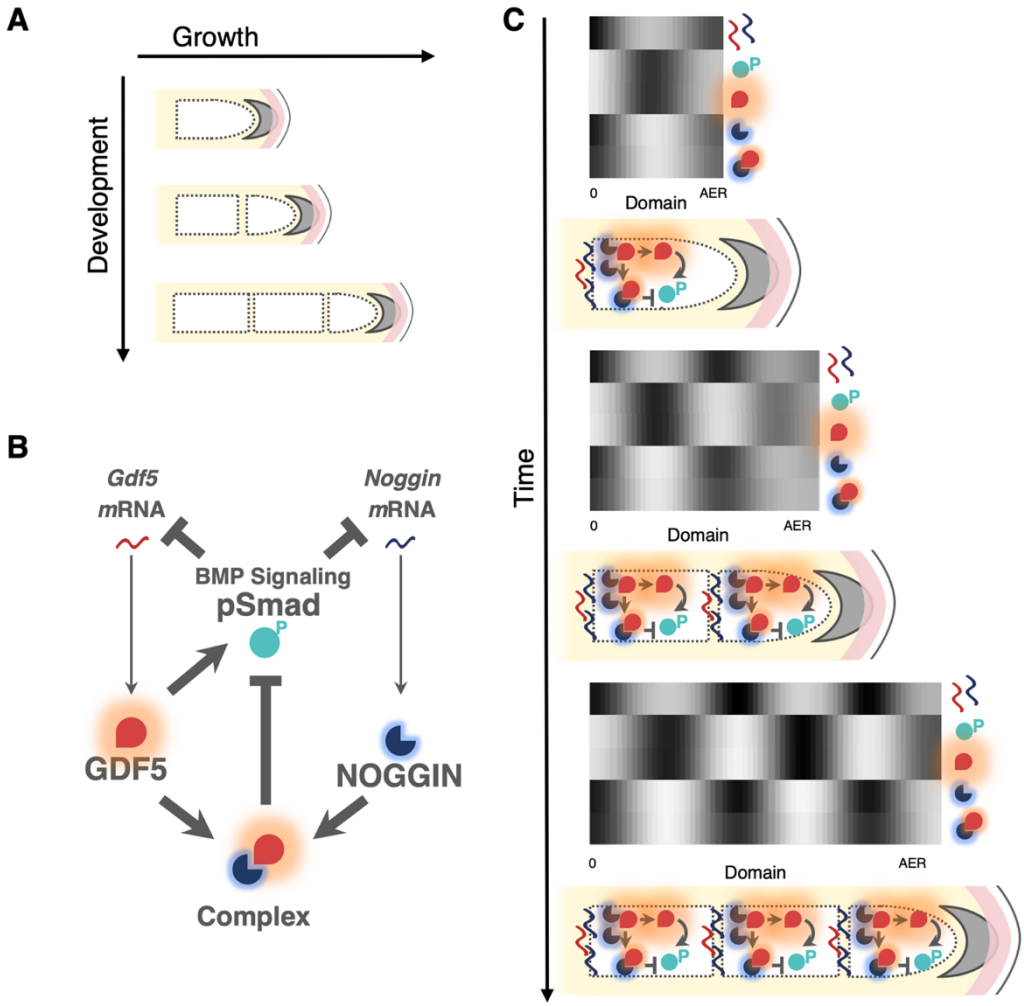

Figure 8. A BMP-based Turing model of digit patterning. (**A**) Schematic of digit patterning and growth over the development. (**B**) A Turing-like system that breaks symmetry to form phalanx-joint pattern. (**C**) Heat map visualization of model simulation snap-shots of normalized expression in function of digit domain at different time of development in parallel of scheme of *Gdf5* and *Noggin* mRNA and protein dynamics (diffusion and complex formation) within developing digit (Heat maps: courtesy of Tom Hiscock).

the simulation, however, only corresponds to the free fraction of GDF5 protein that is not currently bound by NOGGIN, to form the complex. If total GDF5 protein concentration would be displayed, it would be highest near the joint regions, where the *Gdf5* gene is expressed.
Together, these simulations suggest that NOGGIN protein, produced at the joint, prevents BMP signaling in the joint, which are devoid of pSmad. Moreover, this suggests that near the joint, there is an excess amount of NOGGIN protein which sequesters free GDF5 protein. Thanks to the differences in diffusion rates proposed by the model, between GDF5 and NOGGIN, GDF5 will diffuse faster than NOGGIN. Accordingly, it's only far away from the joint that GDF5 protein is free from NOGGIN inhibition and can activate BMP signaling in the phalanx center, where pSmad is found. Additionally, one possibility for the differences between NOGGIN and GDF5 ranges could be that NOGGIN protein is present at higher concentrations than the GDF5 protein, meaning that most of the GDF5 protein is bound to NOGGIN close to the forming joint sites.
To sum up, the BMP-based Turing model proposed here is able to approximate digit patterning *in silico* and to recapitulate the spatiotemporal molecular dynamics observed *in vivo*. This supports the importance of the model players, i.e. *Gdf5* and *Noggin*, in the formation of a periodic phalanx-joint pattern. Importantly, however, the model also makes predictions for protein distributions that were so far not reported *in vivo*. Moreover, mutations in the model players were reported to induce digit malformation with segmentation disorders, thereby providing us with known phenotypes to test the accuracy of our model (Brunet et al., 1998; Merino et al., 1999a; Storm and Kingsley, 1999; Stricker and Mundlos, 2011). Hence, in order to challenge the BMP-based Turing model proposed here, we set out to assess the *in silico* predicted protein distributions *in vivo*, as well as trying to phenocopy digit malformations induced by known mutations or embryological manipulations.

4. Challenging the *in silico* model of digit patterning

a. Validation of protein distribution predictions

First, because the model makes explicit predictions about the protein localizations of GDF5 and NOGGIN, we wanted to see their distribution within the digit *in vivo*. Chromogenic immunohistochemistry for GDF5 reveals that the protein seems to diffuse away from joint regions, towards phalanx center as it was predicted by the model simulation (Figure 9A-A'). This suggests that GDF5 activates BMP signaling in the phalanx and support the model assumption that *Gdf5* has a long-range action. Moreover, a strong signal of GDF5 appears to

locate to the perichondrium, again in the middle of the phalanx. Fluorescent immunohistochemistry for NOGGIN revealed that the protein is localized along the phalanx, and enriched towards its ends, flanking the joint (Figure 9B). When visualized at higher magnification, the sub-cellular distribution of NOGGIN protein seems to be different, between the proximal and distal ends of the phalanx (Figure 9C). Indeed, NOGGIN protein seems largely cytosolic and/or extracellular for cells of the distal phalanx end. At the proximal phalanx end, an increase in nuclear NOGGIN signal is observed (Figure 9D). All in all, these results are largely consistent with the protein distribution predicted by the model.

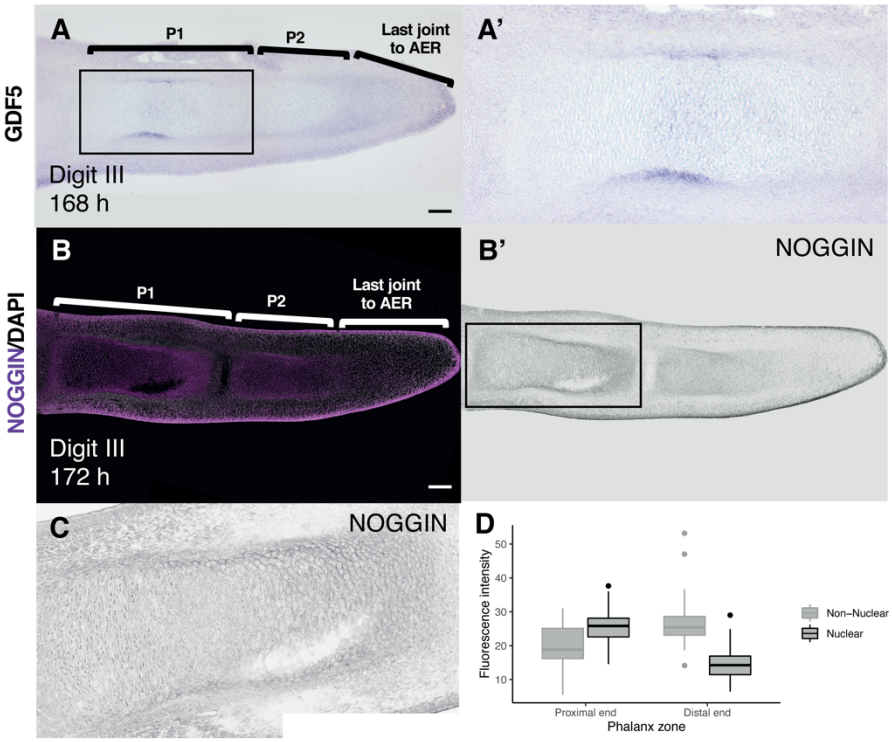

Figure 9. GDF5 and NOGGIN proteins localization in chicken developing digit. (**A**) Immunohistochemistry for GDF5 in longitudinal section of digit III at 168 h of development. (**A'**) Detailed view of the box in panel A. (**B-B'**) Immunohistochemistry for NOGGIN in longitudinal section of digit III at 172 h of development. (**C**) Detailed view of the box in panel B'. (**D**) Box plot of non-nuclear versus nuclear NOGGIN fluorescence intensity measured on cells in proximal end and distal end of the phalanx in panel D. Scale bars = 100 µm.

b. Prediction of digit malformations

Next, we aimed to test if our *in silico* model can recapitulate phenotypes induced by different mutations or embryological manipulations. To do so, we simulated perturbations in the BMP pathway, during the *in silico* patterning process. Based on published literature, covering both mouse and chicken experiments, different BMP pathway mutants or embryological

perturbations inducing digit malformation can be found (Figure 10, data part). In a wild type situation, *Gdf5* is expressed in joint progenitors as narrow stripes (Storm and Kingsley, 1999). Implantation of a GDF5 bead in wild type embryos, results in the local inhibition of *Gdf5* expression (Storm and Kingsley, 1999). *Gdf5* mutant mouse embryo have *Gdf5* expression throughout the digit ray (Storm and Kingsley, 1999). Similarly, in *Bmpr1b* mutant mice, an expanded domain of *Gdf5* expression is seen (Yi et al., 2000). Implantation of a GDF5-soaked bead in mouse embryo mutant for *Gdf5*, results in local inhibition of *Gdf5* expression (Storm and Kingsley, 1999). In *Noggin* mutant mouse embryo, *Gdf5* expression is absent (Brunet et al., 1998), whereas in the chick embryo, implantation of a NOGGIN-soaked bead at the tip of the developing digit induces a truncated digit with expanded *Gdf5* expression at the distal tip (Merino et al., 1999a).

To try to phenocopy these experimental interventions, *Gdf5* expression distribution, and thus an approximation of the pattern of future joints, was simulated *in silico*, for the same set of BMP pathway mutants or perturbations (Figure 10 simulation part). Simulation of a GDF5 bead implantation in wild type background results in *Gdf5* expression disruption, at the location

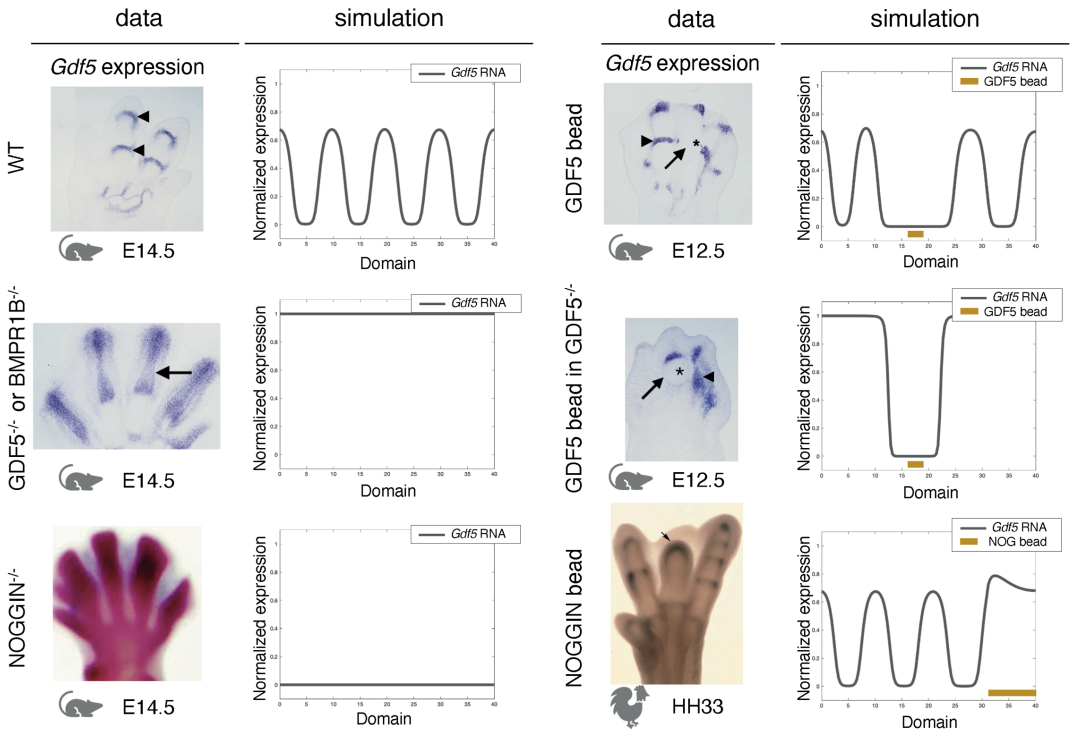

Figure 10. Model prediction of digit malformations. *In silico* simulations of *Gdf5* expression patterns to phenocopy digit malformations of BMP pathway mutants or perturbations. For all simulations, *Gdf5* normalized RNA expression is plotted along the digit domain, and ochre boxes highlight the location of the *in silico* implanted bead (data: images adapted from Storm and Kingsley, 1999 for wild type (WT), GDF5-/- and GDF5 beads, from Brunet et al., 1998 for NOG-/- and from Merino et al., 1999a for NOG bead; simulations: courtesy of Tom Hiscock).

where the bead is simulated. In addition, simulated loss of function of either GDF5 or BMPR1B results in high and homogenous *Gdf5* expression along the digit domain. Thus, the model predicts the same *Gdf5* expression dynamics throughout the digit ray, as were observed *in vivo* for *Gdf5* and *Bmpr1b* mutant embryos. Likewise, simulation of *Gdf5* bead implantation associated with a loss of function of GDF5 results in the local inhibition of *Gdf5* expression. The absence of *Gdf5* expression in *Noggin* mutant mice was also recapitulated by our model simulation of NOGGIN loss of function. Finally, simulation of NOGGIN bead implantation in a wild type background induces higher *Gdf5* expression at the distal tip. Thus, the model is able to mimic the molecular phenotype observed when NOGGIN bead is implanted at the digit distal tip of a chicken embryo.

Overall, our model was able to reproduce important patterning aspects of digit malformations observed in BMP pathway mutants or perturbations. Additionally, this shows that the model is able to reproduce different molecular signatures *in silico,* which eventually result in distinct digit morphologies. However, its ability to predict evolutionary transitions into novel digit patterns still needs to be further investigated.

c. Evolutionary conservation of BMP-based digit patterning and *in silico* prediction of digit malformations observed in a mouse model with increased BMP signaling

In contrast to chicken, where autopods have a 2-3-4-5 phalanx formula for their four digits, the majority of mammalian autopods display a 2-3-3-3-3 phalanx formula for their five digits (Wagner, 2014; Xu and Mackem, 2013). Moreover, genetic perturbations reveal a potential to 'revert' to an ancestral autopod type, which, according to fossil record, is believed to be a 2-3-4-5-3 formula, for digits I to V (Wagner, 2014; Xu and Mackem, 2013). Hence, the propensity for additional phalanges is still present in mammalian digits. Indeed, the DupC mutant mouse model, engineered by the group of Prof. Stefan Mundlos from the Max Planck Institute for Molecular Genetics, Berlin, shows an abnormal distal phalanx pattern (Figure 11A). These mice carry an engineered genomic duplication at the *Sox9* locus, which results in an ectopic expression of the neighboring gene *Kcnj2* in a *Sox9*-like expression pattern (Figure 11B) (Franke et al., 2016). *Kcnj2* is a gene encoding for a potassium inwardly rectifying channel, which was reported to be a BMP signaling modulator in *Drosophila* (Dahal et al., 2017). In this way, we first aimed to characterize the phenotype observed in the mouse, i.e. whether the segmented terminal phalanx indeed carries an additional joint, and secondly to investigate if BMP signaling activity is disturbed in DupC mice limbs.

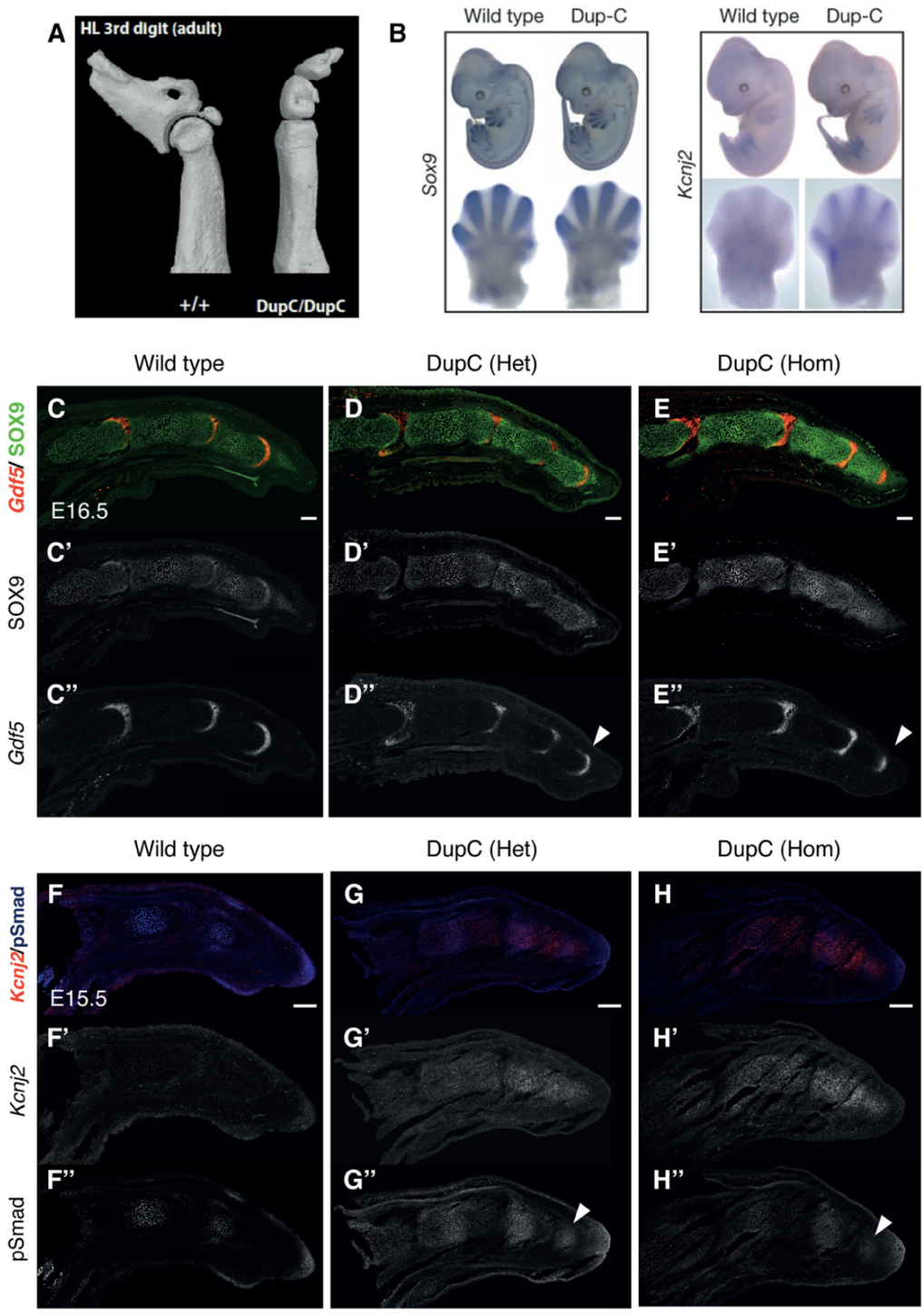

Figure 11. Impact of ectopic expression of *Kcnj2* on BMP signaling in a mouse model with extra-phalanx. (**A**) Micro-CT showing the digit skeletal morphology of DupC mutant compared to wild type mouse embryo (Scan courtesy of Daniel Ibrahim). (**B**) Whole mount *in situ* hybridization for *Sox9* and *Kcnj2* of DupC mutant limb compared to wild type mouse embryo limb at E12.5 (Image adapted from Franke et al., 2016). (**C-E''**) Fluorescent RNA *in situ* hybridization for *Gdf5* combined with immunohistochemistry for Sox9 in longitudinal section of digit IV at E16.5. Arrow indicates extra band of *Gdf5* expression. (**F-H''**) Fluorescent RNA *in situ* hybridization for *Kcnj2* combined with immunohistochemistry for pSmad1,5,9 in longitudinal section of digit IV at E15.5. Arrow indicates extra spot of pSmad1,5,9 (Images courtesy of Aline de Courten). Scale bars = 100 µm.

To further characterize the skeletal phenotype of the DupC mutant, we performed fluorescent RNA *in situ* hybridization for *Gdf5*, a joint progenitor marker, combined with immunohistochemistry for SOX9, a chondrocyte progenitor marker, on longitudinal section of DupC mouse digit at E16.5 (Figure 11C-E''). In DupC mouse mutant embryos, an extra band of *Gdf5* expression appears, compared to wild type littermates. Additionally, a SOX9-positive cell population is present distal to this extra band. The proximal digit structures, however, are morphologically indistinguishable between DupC mutant embryos and wild type littermates.

All together, these results suggest that in DupC mutant embryos, there is an aberrant patterning of the distal digit progenitors, which results in an additional phalanx-like structure separated by a joint-like structure. Interestingly, it also appears that this phenotype is observed more frequently in digit 3 and 4 (Daniel Ibrahim, personal communication), i.e. in digits that originally had the most phalanges in the ancestral condition (Xu and Mackem, 2013).

To characterize the impact of ectopic *Kcnj2* expression on BMP signaling in the DupC mouse, we performed fluorescent RNA *in situ* hybridization for *Kcnj2* combined with immunohistochemistry for pSmad1,5,9 on longitudinal sections of DupC mouse digits at E15.5 (Figure 11F-H''). In wild type mice, pSmad fluorescence intensity is high at the tip, directly below the AER, corresponding to the PFR. Additionally, joint regions are devoid of pSmad fluorescence compared to phalanges, in which fluorescence intensity is high in the center. Moreover, *Noggin*, the BMP pathway inhibitor, is expressed in regions flanking the *Gdf5* band in the joints and is absent/downregulated in the central part of the phalanges at E13.5, where pSmad is detected (Figure S5). Intriguingly, an extra spot of *Noggin* expression is detected at later stages (E14.5) in the middle of the proximal phalanges, where pSmad is also detected normally. However, this seems to be a relatively late event and thus probably not linked to the initial digit patterning. Next, looking to the BMP pathway activity in DupC mouse embryos, an ectopic spot of pSmad was detected at the level of the extra-phalangeal structure (Figure 11F-H''). This suggests a potential increase in BMP signaling pathway activity in DupC mouse mutants, distally in the forming digits, and probably linked to ectopic expression of *Kcnj2* in these mice. Moreover, *Msx2* and *Id1* genes, which are known downstream target genes of the BMP pathway, also seem to have a higher and broader expression at the digit tip in DupC mouse mutants, compared to wild type embryos (data not shown).

Given these molecular and morphological alterations, we next wanted to test whether overall elevated levels of BMP signal could cause changes in the pattern and/or frequency of *Gdf5* induction in DupC mutant mice. Using our previously established model, an increase of BMP signaling was simulated *in silico* to mimic the one observed *in vivo* in DupC mutants. Simulations resulted in the appearance of an additional peak of *Gdf5* expression when BMP

signaling activity was increased (Figure 12). Both *in vivo* and *in silico* data thus suggest a role for higher BMP signaling in the production of shorter wavelengths, which in turn results in more joint sites being induced.

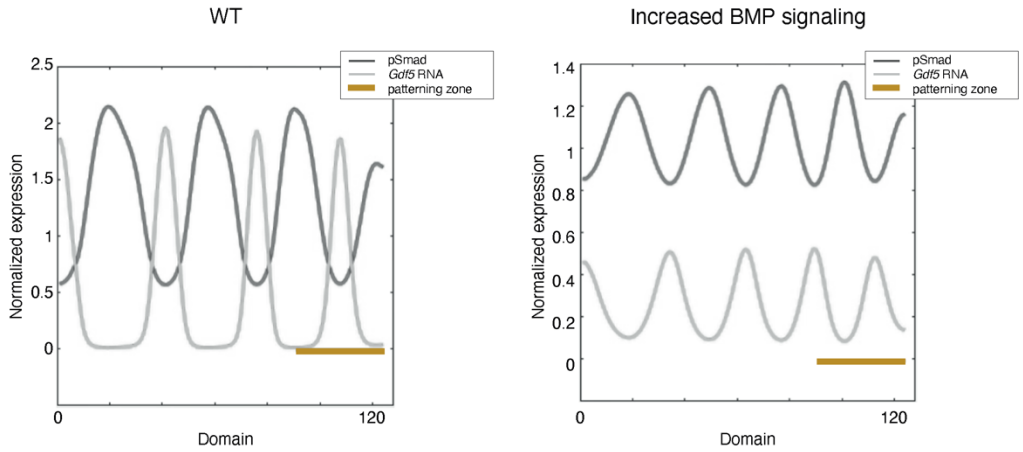

Figure 12. Model prediction of increased BMP signaling. Simulation of pSmad and *Gdf5* expression pattern in wild type developing digit or when BMP signaling is increased (Courtesy of Tom Hiscock).

Discussion

Highly distinct digit morphologies have emerged over the course of vertebrate evolution. Different numbers of phalanges per digit occur, both within and between species, ranging from a 2-3-4-5-3 phalanx formula in the putative ancestral condition, to a 2-3-4-5 phalanx formula in chicken or a 2-3-3-3-3 in mice (Wagner, 2014; Xu and Mackem, 2013). Members of the TGF-beta superfamily, including the Bone morphogenetic proteins (BMP), have been shown to be essential for digit patterning. Several human digit malformation syndromes are caused by mutations in these genes (Stricker and Mundlos, 2011). Moreover, studies in animal models have confirmed the importance of a precise regulation of BMP signaling for digit pattern formation, and led to a better molecular and cellular understanding of these human digit malformations (Mundlos, 2009; Stricker and Mundlos, 2011). However the exact roles of the different BMP pathway players, and their dynamic interactions during development are still not fully known.

In this study, we produced quantitative data for growth and signaling dynamics during digit development in the chicken foot and we combined them with *in silico* modelling, in order to understand digit pattern formation and diversification.

First, we produced data for growth dynamics during digit development in chicken, in which digits are morphologically different, to see if variations in growth and proliferation rates between digits could explain the different patterns. Our results revealed that within a digit,

growth rates are different between phalanges and suggest that there is difference in tip proliferation between digits. This difference in tip growth could explain differences in phalanges number. Indeed, prolongated *Fgf8* expression at the digit tip induces more phalanges (Sanz-Ezquerro and Tickle, 2003b). Moreover, prolongated growth due to AER persistence has been suggested as potential explanation for the hyperphalangy of whale flippers (Richardson and Oelschläger, 2002). Additionally, within a digit, phalange size differences could be explained by presence of an overall uniform digit growth, combined with tip growth, as was recently proposed with *in silico* simulations of digit patterning (Cornwall Scoones and Hiscock, 2020). Indeed, in the simulation digital rays undergo uniform growth while cells are still added at the distal tip. This results in variations of phalanx size along the digit, with proximal phalanges being longer than distal phalanges. *In vivo*, this could potentially be explained by differences in proliferation of the digit progenitor cells of the PFR at the distal tip, in combination with long bone elongation of the already formed phalanges along the digit. However, using BrdU incorporation, we were unable to find striking differences between morphologically different digits. To further investigate this hypothesis, additional and more global digit tip proliferation data would be required. For that, we plan to troubleshoot whole mount BrdU staining of embryonic chicken hindlimbs, followed by light sheet microscopy and finally by quantification. In addition to growth rate differences between digits, we also observed difference in growth rate of the individual phalanges within a digit. Interestingly, the second to last phalanx seems to show an overall increase in growth rate, compared to the other phalanges. This finding is of potential importance to explain the special digit morphology of raptors, or birds of prey, in which an elongation of the penultimate phalanx is observed (Kavanagh et al., 2013). This could be important in evolution of these birds, as it seems to be linked to the lifestyle and mode of hunting of these animals.

Furthermore, to evaluate the molecular dynamics of cell fate decisions at the PFR inducing the phalanx-joint pattern, we investigated the transcriptional and signaling dynamics of chicken digit development. To do so, we first performed pseudotime analysis on HH29 autopod single-cell RNA sequencing data. Differential dynamic expression analyses along the joint and phalanx progenitors pseudotime trajectories suggested the activities of BMP pathway members *Gdf5*, *Noggin* and *Bmpr1b* to be involved in the regulation of cell fate decisions of PFR progenitors. We then investigated the spatiotemporal expression pattern for these gene members of the BMP pathway, as well as BMP pathway activity during chicken digit patterning. We provide evidence for alternating patterns of bands of *Noggin* and *Gdf5,* which are in phase together, at the future joint region, and pSmad1,5,9, which is out of phase and located in the

presumptive phalanx bone. Additionally, we observed an evolving asymmetry of the pSmad profile, towards the proximally located joint site.

The spatiotemporal dynamics observed *in vivo* of *Noggin*, a BMP pathway inhibitor, and *Gdf5*, a BMP pathway activator, suggested to us a potential role of those genes in a putative self-organizing, Turing-like process driving the origin of the periodic phalanx-joint pattern in digit development. Accordingly, we formulated a BMP-based Turing mathematical model of digit patterning. This model is able to predict digit patterning *in silico* and reproduces important aspects of the spatiotemporal gene expression dynamics and BMP signaling activity observed *in vivo*. Additionally, it makes predictions on the expected protein distributions *in vivo*. We scrutinized these predictions using immunohistochemistry for GDF5 and NOGGIN proteins. GDF5 signal was predominately detected in the middle of the phalanx, where the model predicts its major mode of action on BMP activity. Unexpectedly, there is an absence of GDF5 antibody staining closer to the joints, i.e. where the gene is actually expressed. Whether or not this can be explained by epitope-obstruction *via* NOGGIN complex formation remains to be determined. NOGGIN protein is most strongly detected near the joint sites, in agreement with the model. Intriguingly, however, NOGGIN protein seems more cytosolic or extracellular in cells of the distal phalanx end, and more nuclear in cells of the proximal phalanx end. Potentially, this nuclear localization of NOGGIN could prevent it from binding to GDF5 more efficiently at the proximal phalanx end, and thereby explain the asymmetric distribution of the pSmad1,5,9 signal (see above).

Next, because different digit malformations are observed when BMP signaling is perturbed (Stricker and Mundlos, 2011), we were wondering if we can recapitulate the phenotypes induced by these mutations *in silico*. Simulations of BMP pathway perturbations mimicked *in silico* the phenotypes and molecular patterns observed *in vivo*. Thus, the model can approximate different digit morphologies *in silico*. This ability will be exploited in further investigations, to model and predict molecular parameter changes resulting in evolutionary distinct digit patterns. As a first test for such morphological transitions, we analyzed a mutant mouse model with an additional phalanx-like structure. This phenotype is observed more frequently in digits 3 and 4, i.e. in digits that originally had the most phalanges in the ancestral condition, revealing a potential to ‘revert’ to an ancestral autopod type. Molecular analyses of this mouse model showed that an increase in BMP signaling is inducing an extra-phalanx/joint phenotype. Additionally, our *in silico* model was able to reproduce the phenotype observed, by simulating an increase of BMP signaling. Thus, both *in vivo* and *in silico* data suggest a role for higher BMP signaling in production of shorter wavelengths, i.e. more joints. This is consistent with the gradient of BMP activity observed within the PFR, suggesting that high

BMP signaling activity will induce digit patterns with more phalanges/joints (Suzuki et al., 2008).

Based on prior experimental works, our quantitative molecular data and mathematical simulations, we propose a model of developmental digit patterning based on BMP signaling pathway activity, and divergent cell fate specifications into either joint or phalanx progenitors at the PFR (Figure 13). In this model, PFR cells receive positional information specifically from the interdigit located posterior to the PFR (Suzuki and Fallon, 2021). Expression dynamics data showed that *Bmpr1b* is expressed in a graded fashion. This graded expression of *Bmpr1b* suggests that it could control the zone where the phalanx *versus* joint cell fate choice is occurring. During the 'Mesenchyme/post-PFR phase', *Noggin* expression from the proximal condensations would induce a reduction of BMP signaling and thus pSmad in the PFR-adjacent cells, which in turn will start to express *Gdf5*. These PFR progenitor cells will thus be determined as joint cells, as long as GDF5 activity can be overridden by NOGGIN inhibition,

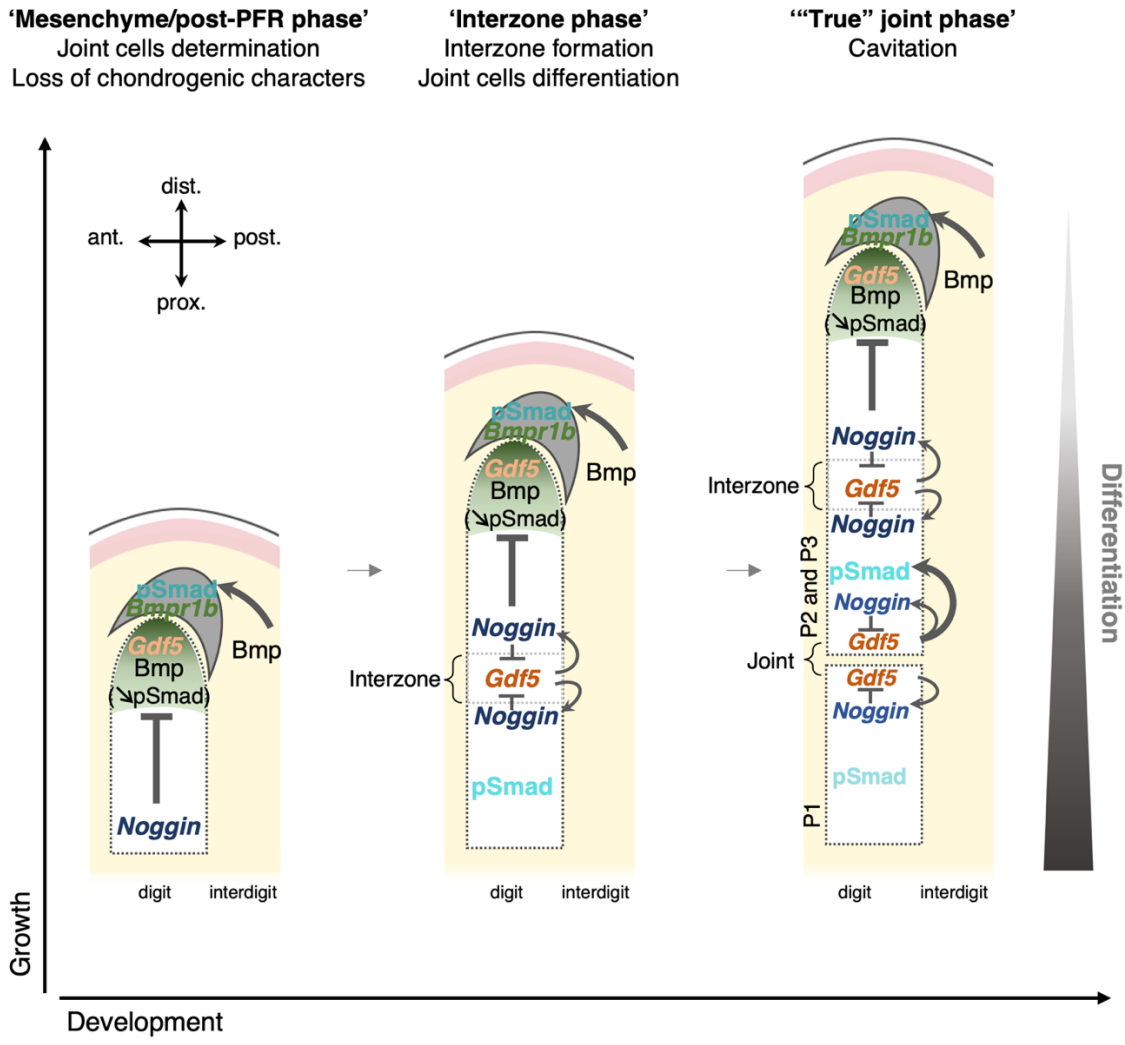

Figure 13. Model of digit patterning specification during development.

and will lose their chondrogenic characters. Then, during the 'interzone phase', *Gdf5* would limit the extend of the joint induction. Indeed, *Gdf5* would have a negative feedback on *Noggin*, through the activation of BMP pathway, which will inhibit *Noggin* transcription and thus limit the extend of the interzone. At the end of this phase, interzones are formed and joint cells start to differentiate. In the '"True" joint phase', *Noggin* expression near to the joint suggests that NOGGIN protein could sequester free GDF5 protein, and it's only far away from the joint that GDF5 is free from NOGGIN inhibition and can activate BMP signaling in the phalanx to induce chondrogenesis.

Despite the success of our BMP-based Turing model proposed in reproducing digit pattern formation and diversification, there are several points that require further attention. Indeed, the model proposed is approximating 1D components only, and 2D components, like for example the perichondrium, are not included. Indeed, Kavanagh et al., showed that the surface, and not the length of the proximal phalanx scales with the distal phalanx size, which suggest that the 'surface-like 2D' perichondrium could play a potential role (Kavanagh et al., 2013). Moreover, our data shows that *Gdf5* as well as *Bmpr1b* are expressed in the perichondrium surrounding the digit ray. Altogether, these observations indicate a potential role of the perichondrium in digit patterning. Furthermore, the model closely recapitulates the early spatiotemporal dynamics of signaling observed *in vivo*. However, it fails to recapitulate some subtle dynamics at later stages, like the progressive decrease of *Noggin* expression coinciding with the appearance of a new pSmad dot in the newly forming phalanx. A potential explanation for this subtle dynamic is that the patterning is relatively labile *in vivo*, and this variability is not modeled *in silico*. Indeed, the current model does not include a delay between a change in pSmad activity and *Noggin* expression levels. Finally, the model fails also to recapitulate the sharpening and intensifying of the *Gdf5* band. Thus, the model includes several simplifications, and makes assumptions on the roles and interaction of the different players, some of which still need to be validated. Indeed, experimental data demonstrating that BMP pathway activity inhibits *Noggin* transcription is lacking. We are currently investigating if *Noggin* mRNA is locally inhibited, when BMP signaling is ectopically activated. To do so, we are injecting the developing digit with cells infected with RCAS viruses for a constitutively active BMPR1B. Additionally, we are investigating the impact of ectopic GDF5 on *Noggin* expression. To do so, GDF5 overexpression with use of RCAS viruses is done in chicken developing digit. According to the model, we would expect an indirect downregulation of *Noggin* expression, *via* activation of BMP pathway signaling. In terms of pattern refinement, i.e. the sharpening of *Gdf5* expression and the split of the late *Noggin* domain, the complementary expression patterns of *Chrld1* and *Chrld2* (see Chapter II), provide interesting candidates for further investigations.

Collectively, in this study we provide insights into the molecular mechanisms underlying digit patterning. We show that a BMP-based Turing-like system can approximate digit segmentation *in silico*, in agreement with the observed transcriptional and molecular dynamics *in vivo*. Future investigations on the roles of the perichondrium and of cell proliferation at the digit tip will be required to complete our understanding of how growth and cell fate decision are differentially regulated during tetrapod digit development, and how they are modified to generate different digit morphologies. Moreover, as the proposed BMP-based Turing model can predict different digit morphologies, we speculate that it can be used as a tool to predict and investigate possible parameter modulations in this model to generate different digit morphologies seen across tetrapod evolution.

Contributions

This study was conceived and designed by the author, Tom Hiscock, Dagmar Iber and Patrick Tschopp. Experimental embryology (embryo collection and dissection), embryo processing (embedding and cryosectioning), cloning of probe templates, optimization of staining (*in situ* hybridization and immunohistochemistry) and confocal imaging were carried out by the author. Measurement to produce the growth and signaling dynamics data were performed by the author. Pseudotime analysis was conducted by Christian Feregrino and Patrick Tschopp. *In silico* model formulation and simulation was carried out by Tom Hiscock. DupC mouse embryo processing (embedding and cryosectioning), staining (*in situ* hybridization and immunohistochemistry) and confocal imaging were carried out by Aline De Courten and the author.

Supplementary figures

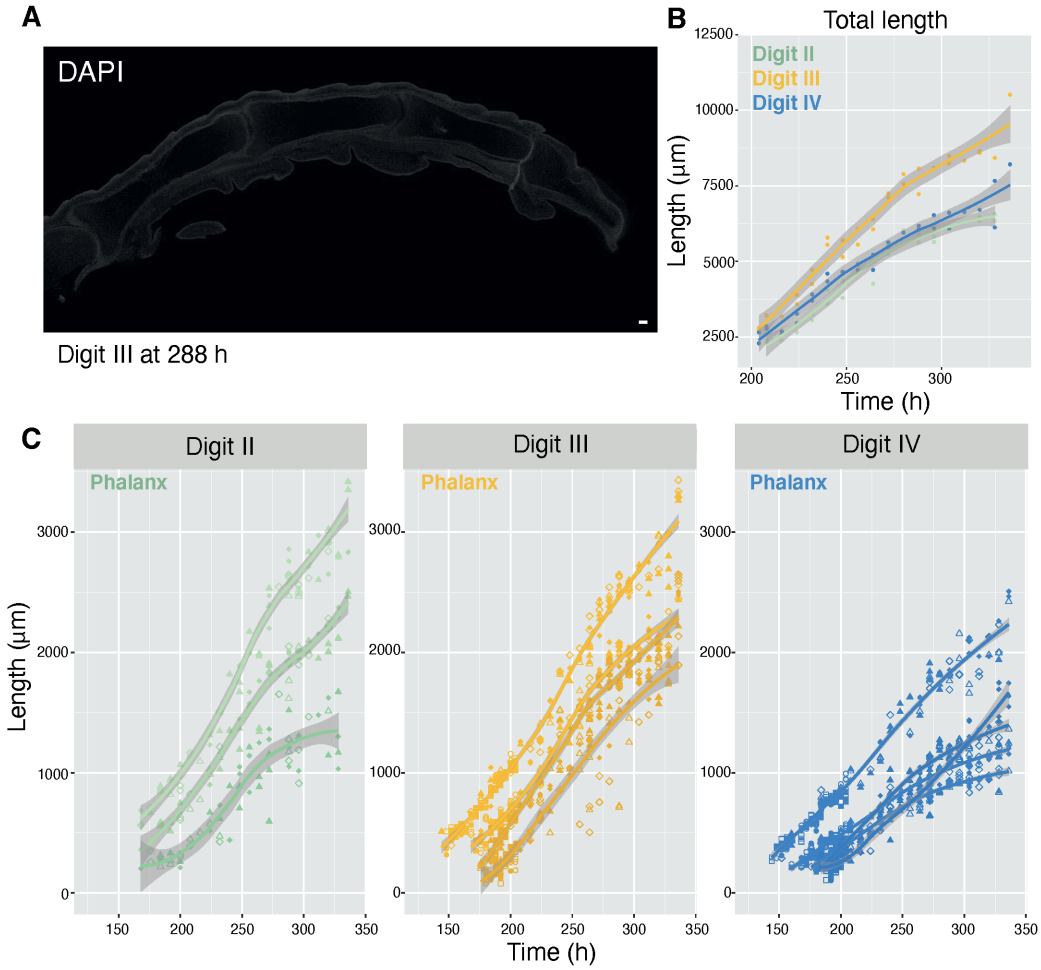

Figure S1. Growth data in chicken developing digit. (**A**) Example of image of a DAPI staining in a longitudinal section of a digit at 288 h of development used for measurement after 240 h of development. Scale bar = 100 µm. (**C**) Total lengths for digits II, III and IV in function of the developmental time. (**D**) Lengths of the different elements for digits II, III and IV in function of the developmental time. Point shapes: biological replicates ; Full shape: right limb ; Empty shape: left limb ; Shaded area: SEM.

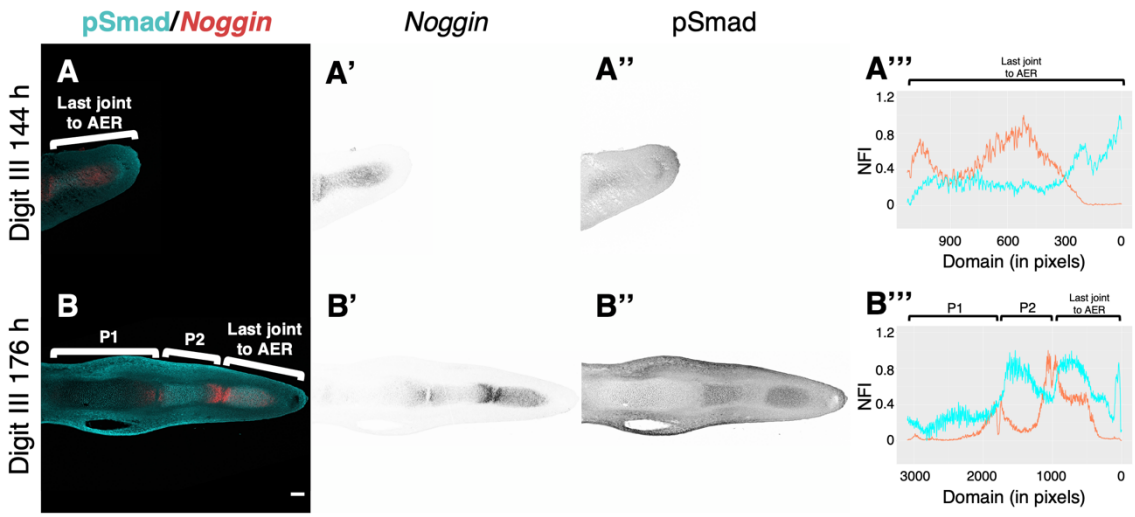

Figure S2. *Noggin* gene expression in chicken developing digit. (**A-B''**) Fluorescent RNA *in situ* hybridization for *Noggin* combined with immunohistochemistry for pSmad1,5,9 in longitudinal section of digit III at 144 and 176 h of development. Scale bar = 100 µm. (**A''' and B'''**) Plot of normalized fluorescence intensity (NFI) of pSmad1,5,9 (Cyan) and *Noggin* (Red) in function of digit domain elements for digit III at 144 and 176 h of development. 1 pixel = 1,243 µm.

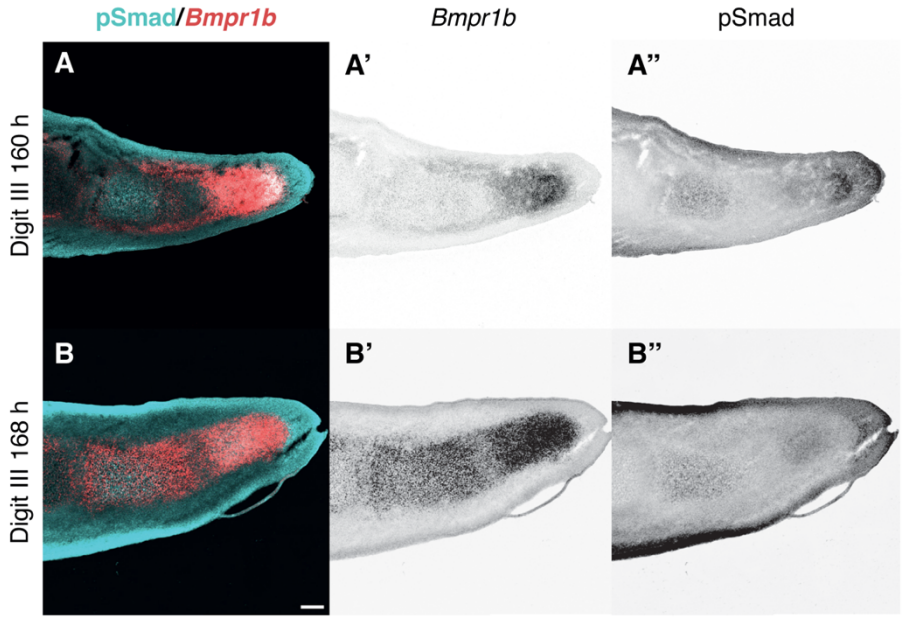

Figure S3. *Bmpr1b* gene expression in chicken developing digit. (**A-B''**) Fluorescent RNA *in situ* hybridization for *Bmpr1b* combined with immunohistochemistry for pSmad1,5,9 in longitudinal section of digit III at 160 and 168 h of development. Scale bar = 100 µm.

$$\frac{\partial[GDF5]}{\partial t} = \frac{k_4}{1+([PSMAD]/K)^n} - k_1[GDF5] + k_8[C] - k_7[GDF5][NOG] + D_{GDF5}\nabla^2[GDF5]$$

$$\frac{\partial[NOG]}{\partial t} = \frac{k_5}{1+([PSMAD]/K)^n} - k_2[NOG] + k_8[C] - k_7[GDF5][NOG] + D_{NOG}\nabla^2[NOG]$$

$$\frac{\partial[C]}{\partial t} = k_7[GDF5][NOG] - k_8[C] + D_C\nabla^2[C]$$

$$\frac{\partial[PSMAD]}{\partial t} = k_6[GDF5] - k_3[PSMAD]$$

Figure S4. Partial differential equations, to describe the molecular interactions of a BMP-based Turing model of digit patterning. (Courtesy of Tom Hiscock).

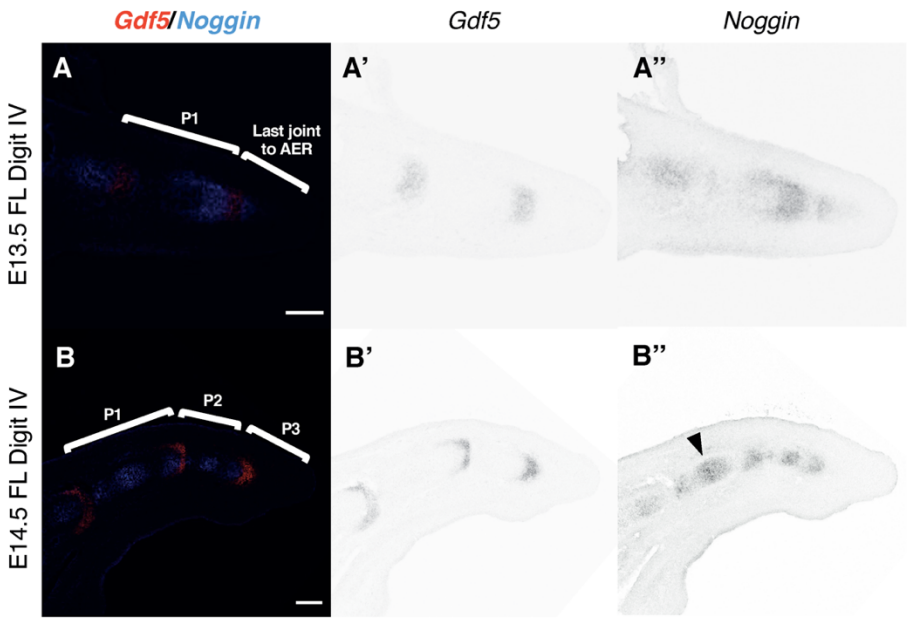

Figure S5. *Gdf5* and *Noggin* gene expression in mouse developing digit.
(**A-B''**) Multiple fluorescent RNA *in situ* hybridization for *Gdf5* and *Noggin* in longitudinal section of digit IV at E13.5 and E14.5. Arrow indicates extra spot of *Noggin* expression. Scale bars = 100 µm.

Chapter II

Patterning relevant cell fate decisions during digit development: establishment of the joint *versus* phalanx cell identity

Abstract

Digits are sophisticated, movable skeletal structures allowing tetrapods to display fine motor tasks in their hands and feet, like digging, grabbing, or even writing or playing music. Thanks to their modular architecture, highly distinct digit morphologies have emerged over the course of vertebrate evolution. Digits are shaped by individual bones, the so-called phalanges, connected to each other *via* synovial joints. Individual digit patterns are determined by the number and size of those structures. During development, digit progenitor cells originate form a distal pool of proliferative and undifferentiated cells: the phalanx forming region. These progenitor cells will proliferate, inducing digit elongation distally and, simultaneously, will be specified into either phalanx progenitor cells or joint progenitor cells that will eventually differentiate into the structures shaping a digit. However, the molecular mechanisms underlying this divergent cell fate decision, between joint and phalanx cell identity, remain unknown. Here, combining data of the transcriptional dynamics of digit patterning with viral overexpression in chicken embryos, we aim to elucidate how cell fate decisions at the phalanx forming region are controlled during digit development. To do so, we used bulk and single-cell RNA-sequencing data combined with pseudotime and *in situ* expression pattern analysis to identify candidate genes of cell fate decisions during digit development. We then used viral overexpression in the developing chicken limb to elucidate the function(s) of one of those candidate genes in digit cell type specification. Collectively, understanding the molecular mechanisms governing cell type specification of digit progenitors into phalanx or joint cell fates will help us to decipher the underlying mechanisms of digit morphological diversification.

Introduction

In tetrapod hands and feet, we find sophisticated, movable skeletal structures: the digits. Digits are involved in fine motor tasks, like digging, grabbing, or even writing or playing music. The diversity of these functions is linked to the emergence of highly distinct digit morphologies over the course of vertebrate evolution. Individual digit morphology is determined by the number, size and shape of digit bones, the so-called phalanges, connected to each other *via* synovial joints. Multiple cell types are involved in the formation of these phalanx and joint structures, and each of these cell types need to fulfil specific biomechanical properties that govern overall digit function (Decker, 2017; Koyama et al., 2008; Marín-Llera et al., 2019).

During development, the limb is developing as a mass of mesenchymal cells originating from the lateral plate mesoderm (Gros and Tabin, 2014; Pearse et al., 2007; Searls and Janners, 1971). The forming mesodermal bud on the lateral side of the embryo is encapsulated by an ectodermal layer, with important signaling interactions occurring between the two (Zuniga, 2015). Elongation of the limb occurs along the proximal-distal axis, and cells condense to form the different skeletal elements of the limb: one long bone in the proximal part giving the stylopod, two long bones in the middle part of the limb corresponding to the zeugopod, and smaller bones in the distal part forming the autopod (Roselló-Díez et al., 2011; Zeller et al., 2009). The autopod, giving rise to the future hand and foot, is composed of digital rays separated by interdigits (Dahn and Fallon, 2000). Digital ray formation starts under the distal edge of the limb bud with initiation of spot of mesenchymal condensation giving rise to chondrogenic cells (Hiscock et al., 2017). These cells will proliferate and elongate into digit rays as the limb bud grows. The digital rays are the first appreciable signs of digit formation. Members of the TGF-beta signaling were shown to be required for the induction of the mesenchymal condensation, through induction of cell surface adhesion and extracellular matrix proteins expression (Chimal-Monroy and Díaz de León, 1999; Lorda-Diez et al., 2022). In addition, ectopic formation of digit structures was observed after implantation of a bead soaked with ACTIVIN BETA A protein, encoded by *Inhba* gene, a member of the TGF-beta signaling into the distal margin of the interdigit (Gañan et al., 1996; Merino et al., 1999b). Thus, ACTIVIN protein was shown to be an early marker of these digital ray condensations and is responsible of digit condensation initiation. In addition, digit formation induction by ACTIVIN protein was shown to be mediated by BMP signaling pathway through the regulation of the BMP receptor *Bmpr1b* (Merino et al., 1999b).

At the tip of each digital ray, a group of progenitor cells, called the phalanx forming region (PFR), will proliferate to add distally to the growing digital ray, to allow for its elongation

(Montero et al., 2008; Suzuki et al., 2008). These PFR cells are expressing *Sox9*, attesting to the chondrogenic state of the PFR cells (Suzuki et al., 2008). In addition, within this cells, *Bmpr1b* expression is upregulated and BMP pathway is activated, indicated by a positive signal for phosphorylated Smad1,5,8 (Suzuki et al., 2008), in line with the role of the BMP pathway in promoting chondrogenesis *via* the induction of cell condensation (Barna and Niswander, 2007). BMP pathway inhibition with BMP antagonists, such as *Noggin* and *Gremlin*, results in digit truncation (Merino et al., 1999b). Similarly, loss of phalange development is observed in *Bmpr1b* knockout mice, while metacarpals remain relatively unaffected (Yi et al., 2000).

Besides the role of the PFR being a pool of progenitors supplying cells for digital ray elongation, this cell population is likely also the center where progenitor cells make cell fate decisions, to be specified into phalanx or joint progenitors that will differentiate into the different tissues types shaping a digit (Montero et al., 2008; Suzuki et al., 2008; Witte et al., 2010). The PFR originates from the distal mesenchyme, localized just beneath an epithelial structure called the apical ectodermal ridge (AER) (Montero et al., 2008; Suzuki et al., 2008; Witte et al., 2010). These distal mesenchyme cells are maintained in an undifferentiated state, due to the influence of an FGF gradient originating distally from the AER. Once digit progenitor cells are no longer under the influence of the AER, PFR cells can undergo cell type specification (Casanova and Sanz-Ezquerro, 2007). As development progresses, these initially undifferentiated cells differentiate either into chondrocytes, which are the progenitor cells for phalanges, or into interzone cells, which are the precursor population of the synovial joints connecting the digit bones (Hiscock et al., 2017; Shwartz et al., 2016). Thus, PFR cells will likely interpret signals according to their relative positions to the AER and the already formed digit segments, and the temporal dynamics of the repetitive phalanx-joint patterning process.

Phalanx progenitor cell fate specification starts with the upregulation of *Sox9* expression (Bi et al., 1999; Healy et al., 1999). *Sox9* expression is necessary for cartilage formation and its absence results in digit truncation (Akiyama et al., 2002; Bi et al., 1999). Upregulation of *Sox9* is followed by expression of chondrocytes specific genes like *Sox5*, *Sox6* (Akiyama et al., 2002; Chimal-Monroy et al., 2003) and genes of the BMP family like *Chrdl1* (Allen et al., 2013; Nakayama et al., 2001) and BMP receptors genes (Yoon et al., 2005; Zou et al., 1997). Additionally, *Sox9* induces the expression of collagen genes, like *Col9a1* and *Col2a1*, which are important structural components of the forming cartilage (Genzer and Bridgewater, 2007; Lefebvre et al., 1997). Several other genes essential for cartilage extracellular matrix formation, like e.g. *Acan* (Kiani et al., 2002), or osteoblast maturation genes like *Ihh* (Long et al., 2004) and *Runx2* (Shimoyama et al., 2007), start also to be expressed. Finally, cartilage

cells and the surrounding perichondrium will undergo maturation to give, rise to the final cell types composing the phalangeal bones (Lefebvre and Bhattaram, 2010).

Joint progenitor cell fate specification starts with initiation at the distal tip of the digital ray, close to the PFR. Histologically, joint progenitor cells appear as a non-cartilaginous region of flattened cells known as the interzone (Decker, 2017; Ray et al., 2015). Thus, the interzone is the region where joint progenitors are specified and removal of interzone cells was shown to induce joint loss accompanied by bone fusion (Holder, 1977). Molecularly, interzone cells are characterized by a loss of expression of chondrocyte-specific marker genes like *Sox9 and Col2a1,* and a transcriptional up-regulation of joint marker genes like *Gdf5*, *Wnt4*, and *Wnt9a* (Guo et al., 2004; Hartmann and Tabin, 2001; Später et al., 2006; Storm et al., 1994). These interzone cells are specified periodically, by molecular mechanisms which are still being fully elucidated (see Chapter I, this thesis).

Of the interzone markers identified so far, *Gdf5* is probably the best known. *Gdf5,* a BMP pathway ligand, is expressed early in the interzone cells and was shown to be implicated in joint specification (Storm and Kingsley, 1999). However, counterintuitively and contrary to role of BMP inhibitors like *Noggin, Gdf5* does not induce the joint fate but inhibit it (see also Chapter I, this thesis). Indeed, implantation of a GDF5-soaked bead in wild type embryos, results in local inhibition of *Gdf5* expression and *Gdf5* mutant mouse embryos have *Gdf5* expression throughout the digit ray (Storm and Kingsley, 1999). *Noggin*, on the other hand, an inhibitor of BMP signaling pathway, has been suggested to be involved in interzone formation (Huang et al., 2016). Indeed, *Noggin* starts to be expressed in future metacarpal/metatarsal (MC/MT) elements and in cells within the digital rays that might become interzone cells, thanks to suppression of BMP response in PFR adjacent cells by *Noggin*. Additionally, *Noggin* inactivation is followed by a complete absence of joint initiation (Brunet et al., 1998) and maturation and maintenance within the developing digit (Ray et al., 2015), which further supports the role of *Noggin* in joint formation. *Chordin*, another BMP antagonist, is expressed in the joint interzone, and reinforces the importance of BMP pathway repression in joint progenitor specification (Francis-West et al., 1999). Furthermore, Iroquois genes like *Irx1* were shown to promote joint formation, by maintaining chondrocytes in an immature state (Askary et al., 2015; Zülch et al., 2001).

Beside the role of BMP pathway in joint cell specification, Wnt signaling was shown to induce interzone formation. Indeed, overexpression of *Wnt9a* induces interzone formation (Hartmann and Tabin, 2001). Additionally, Wnt genes were shown to induce synovial joint formation through the beta-catenin signaling pathway, and activation of the Wnt/beta-catenin signaling pathway is sufficient and necessary for synovial joint initiation (Guo et al., 2004). It was also

shown that *c-Jun* induces expression within the interzone of Wnt genes like *Wnt9a,* to specify joint cell fates (Kan and Tabin, 2013). Moreover, expression of *Wnt9a* gene, as well as *Noggin* and *Gdf5* genes are regulated by *Tgfbr2,* and an absence of TGF-beta signaling induces a lack of interzones and consequently a failure of joint development (Spagnoli et al., 2007). Additionally, knockout or conditional inactivation of genes like *Wnt14*, *Tgfbr2* and *beta-catenin* in mice mutants induce severe joint defects (Hu and He, 2008).

Thus, TGF-beta signaling and Wnt/beta-catenin signaling act together to induce joint cell specification and differentiation of joint progenitor cells into the different cell types present in a synovial joint (articular cartilage, ligaments, synovium and fibrous capsule) (Decker et al., 2014). Several studies implicated different genes in digit cell specification, but many of the underlying molecular mechanisms at the origin of digit progenitor cell fate decision remain unknown, in particular for the distally located joints between digit phalanges.

In this work, our aim is to decipher how signals received by the PFR are interpreted to establish the phalanx *versus* joint cell fate decisions during digit development. To identify novel putative regulators of cell fate decisions, transcriptional dynamics data and experimental embryology were used to study transcriptional changes along the digit progenitor cells lineage. We first investigated the lineage of digit progenitor cells, to figure out the origin of joint and phalanx cells. We have good evidence that both cell types are coming from the PFR. Additionally, we report transcriptional signatures to identify the respective cell populations involved in digit development. We then use single-cell RNA-sequencing and pseudotime analyses to study the molecular dynamics of the process and provide a list of candidate genes for digit cell fate decision regulation. Expression patterns of those candidate genes were analyzed, and we then used viral overexpression to functionally test one of these candidates. Collectively, understanding the molecular mechanisms underlying cell type specification and differentiation during digit morphogenesis might help us to shed light on the mechanisms of pattern formation and diversification.

Results

1. Lineage tracing of digit progenitor cells

During development, the PFR is supposed to be the pool of progenitor cells for phalanges formation (Suzuki et al., 2008). It was proposed that the cells of this pool are coming from the distal mesenchyme, present directly under the AER, and that the progenitors are sequentially

determined in the different cell types shaping the developing digit (Figure 1A,B) (Suzuki et al., 2008). Additionally, the interzone cells were suggested to come from the de-differentiation of phalangeal chondrocytes, suggesting that the joint progenitors ultimately also originate from the PFR (Guo et al., 2004; Hartmann and Tabin, 2001; Später et al., 2006; Storm et al., 1994). To investigate which are the different cell types that the PFR gives rise to, i.e. to know their developmental history and whether both joint and phalanx cells share a common origin, we aimed to perform lineage tracing of PFR cells. We first trained to target the PFR with injection of DiI, a fluorescent lipophilic dye, that bind cell membrane and is commonly used to map cell fates in embryology (Vargesson et al., 1997). Here, we microinjected DiI *in ovo* at the tip of the digit III of the developing chicken foot, into the presumptive PFR, at stage HH29 of chicken embryogenesis (Figure 1C). Injected limbs were directly dissected after injection, and processed for histology and immunohistochemistry. We observed DiI localization at the tip of digit III (Figure 1D). Dissected digits were embedded and cryosectioned longitudinally, through

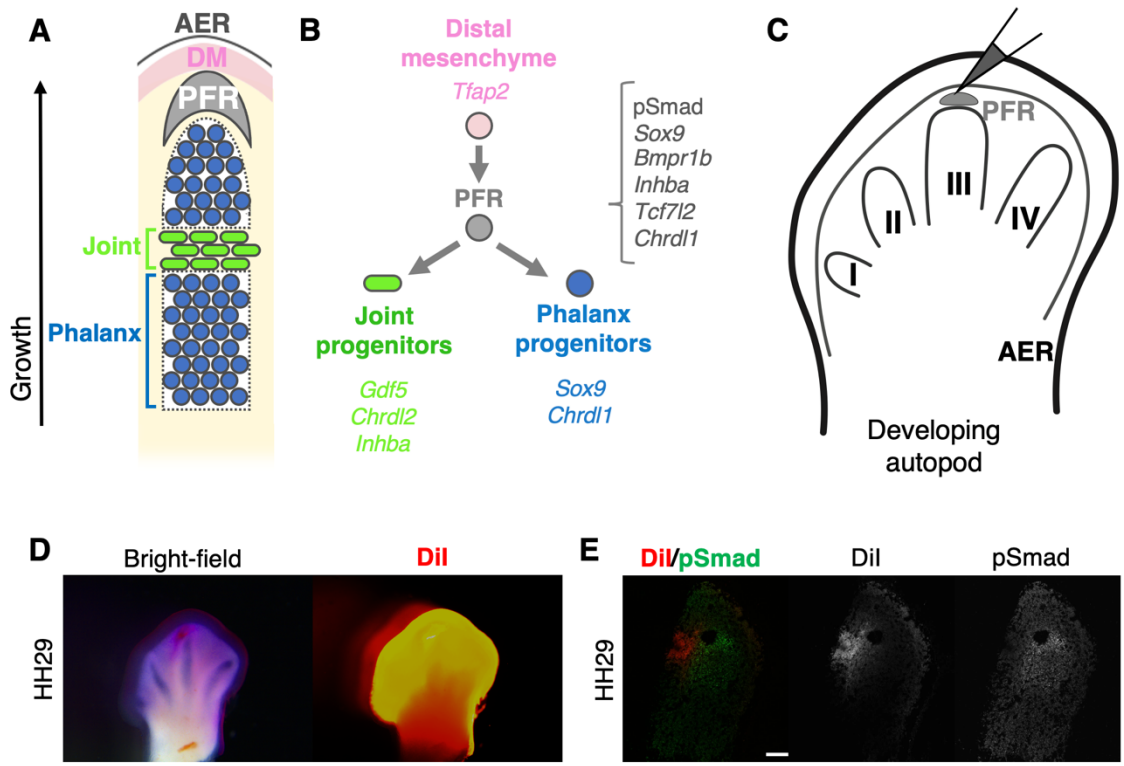

Figure 1. Lineage of digit progenitor cells during chicken development. (**A**) Schematic of the different cell populations present at the developing digit tip. AER: Apical ectodermal ridge. DM: Distal mesenchyme. PFR: Phalanx-forming region. (**B**) Schematic of the digit progenitor cells lineages, and marker genes for the different cell populations, as identified in this study and previous publications. (**C**) Schematic representing injection into PFR localized at the tip of the digital ray III in chick embryo. (**D**) Ventral view of DiI localization within limbs harvested directly after DiI injection into the PFR at stage HH29. (**E**) Immunohistochemistry for pSmad1,5,9 in longitudinal section at the tip of digit III directly after DiI injection into the PFR at stage HH29. Scale bar = 100 µm.

the digit tip. To see if we managed to inject DiI into the PFR, we performed immunohistochemistry against pSmad1,5,9, a marker of the PFR (Suzuki et al., 2008). Results showed that DiI colocalizes with the pSmad signal and thus the PFR (Figure 1E). Additionally, a hole left by the capillary used for the injection is visible in the PFR. Thus, we manage to successfully and with high precision target PFR with our DiI injections. Next, to trace the cell lineage of the PFR, we injected a lentivirus, driving ubiquitous expression of a fluorescent reporter in infected cells, into the PFR of digit III of chicken embryo *in ovo*. Eggs were let to incubate for an additional five days, and digits were collected and analyzed to trace the lineage of infected cells by the lentivirus. Preliminary results show only sparse presence of the fluorescent reporter, likely due to a low viral titer resulting in inefficient infections. However, labeled cells could be detected in both phalanx and joint progenitor cells (data not shown).
Collectively, combined with previous studies, we have evidence to suggest that both joint and phalanx progenitors originate from the same progenitor pool, the PFR. However, we will still need to reproduce lentiviral injection into PFR to confirm the observations we made on the lineage of digit progenitor cells during chicken development.

2. Spatiotemporal transcriptional dynamics of digit patterning

Next, to investigate the molecular mechanisms underlying cell fate decisions during digit development, we aimed to look for transcriptional changes along digit progenitor cell lineages. To begin our investigation of the transcriptional dynamics of digit patterning, we first wanted to describe the spatiotemporal expression patterns of marker genes of the different cell populations involved in digit development. Given the growth dynamics of the elongating digit, comparing the more proximal (~old) with more distal (~young) cells adds a temporal axis to these studies (Figure 1A, B). Data for expression of marker genes are available in the literature, but often in different species and at different time points of the digit development, or not in a combinatorial fashion. To know more on these marker genes expression along the digit progenitor cell lineage, we investigated their expression patterns during the chick digit development, at a stage where both the cell population of the PFR and the cell populations for the joint or phalanx progenitors are present.
We produced longitudinal cryosections of digits, going through the formed phalanges and joints as well as the digit tip. We performed fluorescent RNA *in situ* hybridization on these sections, for marker genes of the differentiating cell populations present in the developing digit, combined with immunohistochemistry against pSmad1,5,9, to mark the PFR (Suzuki et al., 2008) (Figure 2). We assessed *Sox9*, a well-known marker gene of chondrogenic cells

(chondrocyte progenitors and the PFR) (Healy et al., 1999; Suzuki et al., 2008), and *Gdf5*, a well-known marker gene of the joint progenitors (Storm and Kingsley, 1999) (Figure 2 A-A'''). These stainings allowed us to localize the major cell populations in involved in the forming phalanx-joint pattern, i.e. chondrocytes and interzone cells. Staining on adjacent sections revealed that in the developing chicken digit, *Bmpr1b*, *Inhba*, *Tcf7l2* and *Chrdl1*, colocalize with pSmad signal coming from the PFR. Expression of the BMP pathway receptor gene *Bmpr1b*, as well as expression of *Inhba*, the gene encoding for ACTIVIN BETA A protein, were already reported in the PFR (Merino et al., 1999b; Suzuki et al., 2008), as well as extending into the forming phalanges (Figure 2B''-B''' and D'-D'''). For *Inhba*, in addition to the known PFR signal, we find a broader expression and a late up-regulation in chicken (Figure 2B''-B''').

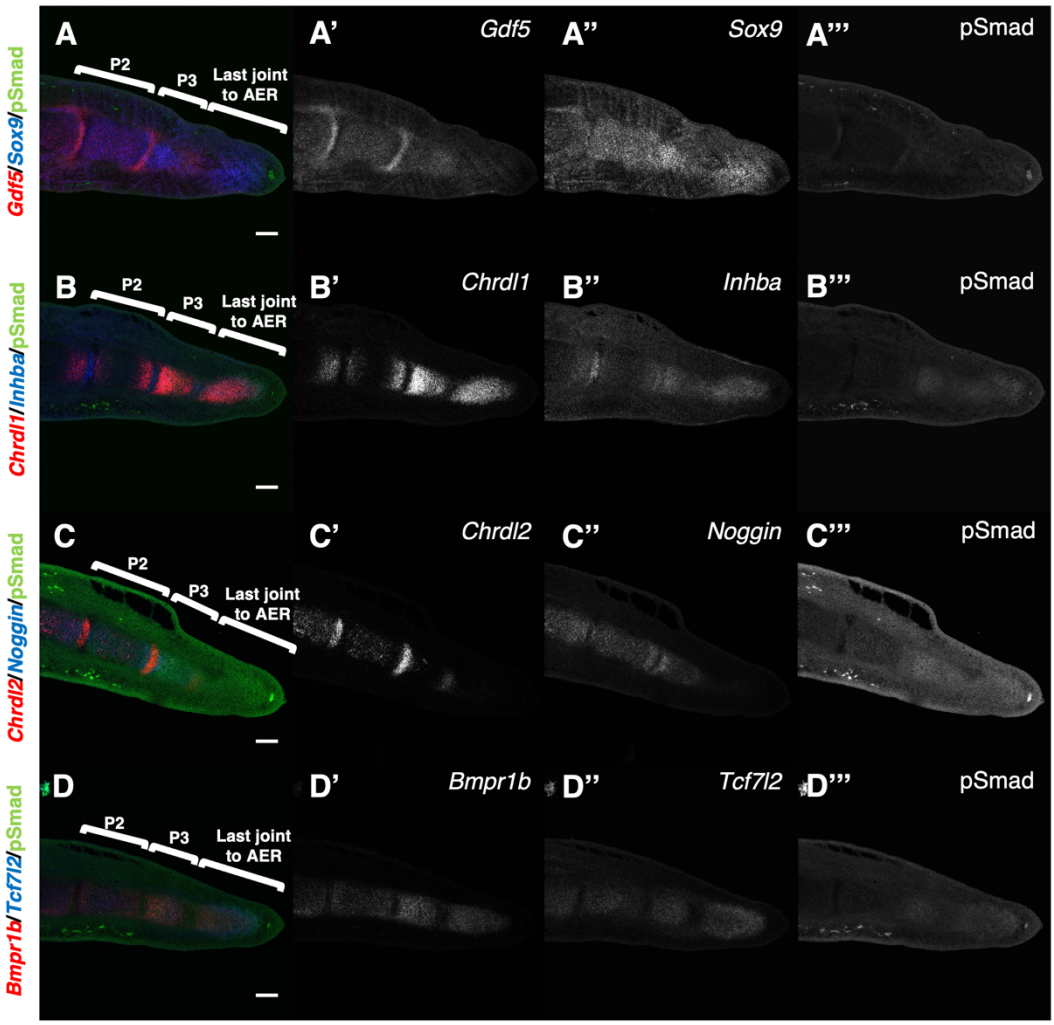

Figure 2. Expression pattern of marker genes of cell populations involved in chicken digit development. Multiple fluorescent RNA *in situ* hybridization for *Gdf5* and *Sox9* (**A-A'''**), or for *Chrdl1* and *Inhba* (**B-B'''**), or for *Chrdl2* and *Noggin* (**C-C'''**), or for *Bmpr1b* and *Tcf7l2* (**D-D'''**), combined with immunohistochemistry for pSmad1,5,9 in longitudinal section of digit IV at stage HH31. **A**, **B, C** and **D** are serial cryosections separated by 18 µm. Scale bars = 100 µm.

Concerning *Tcf7l2*, a gene belonging to the family of T-cell factor/lymphoid enhancer factors, which was shown to regulate chondrocyte maturation and proliferation (Mikasa et al., 2011), and its expression is excluded from the PFR in digits of the developing mouse embryo (Witte et al., 2010). However, in the chicken digit, we observe that *Tcf7l2* expression also colocalizes with the pSmad staining of the PFR (Figure 2 D''-D'''). Moreover, we observed colocalization of *Chrdl1*, a BMP pathway modulator (Nakayama et al., 2001), with pSmad staining in the PFR. In addition to the gene expression observed among the PFR cell population, we found that joint progenitors, marked by *Gdf5* expression, are expressing *Inhba* and *Chrdl2,* another putative BMP pathway modulator (Figure 2B'' and C'). These expression patterns have already been reported in the literature (Lorda-Diez et al., 2013b; Merino et al., 1999b; Nakayama et al., 2004). Concerning the phalanx progenitor cells population, marked by *Sox9* expression, expression of *Chrdl1*, *Noggin*, *Bmpr1b* and *Tcf7l2* were observed in the forming phalanges (Figure 2B', C'', D' and D''). Indeed, reported individual expression patterns of BMP family genes in phalanx progenitor cells like *Chrdl1* (Allen et al., 2013; Lorda-Diez et al., 2013b; Nakayama et al., 2001), *Noggin* (Brunet et al., 1998; Lorda-Diez et al., 2013b) and *Bmpr1b* (Lorda-Diez et al., 2013b; Yoon et al., 2005) are largely consistent with our findings. Additionally, *Tcf7l2* expression in chondrocytes was also reported (Mikasa et al., 2011).

In conclusion, according to the expression patterns we observed in the developing chicken digit, the PFR cell population can be characterized by the expression of *Sox9*, *Bmpr1b*, *Inhba*, *Tcf7l2* and *Chrdl1* together with a pSmad1,5,9 signal, the joint progenitor cell population by *Gdf5*, *Chrdl2* and *Inhba* expression and the phalanx progenitor cell population by *Sox9*, *Chrdl1*, *Noggin*, *Bmpr1b* and *Tcf7l2* (Figure 1B). Even if there is no marker gene exclusive to the chicken PFR, the combination of expression patterns of several of those genes constitutes a transcriptional signature to identify this essential cell population involved in digit development. In addition, this combinatorial, multi-FISH expression analysis sheds light on molecular players and their spatiotemporal relationship potentially involved in the cell fate decision during digit development.

3. Transcriptome-wide identification, temporal dynamics and evolutionary conservation of cell fate decision regulators during digit development

a. Single-cell RNA-sequencing data of the developing chicken digit

Next, we capitalized on these spatiotemporal expression patterns, to re-analyze single-cell RNA-sequencing data of the developing chicken digit. To do so, we used a previously

published single-cell RNA-sequencing dataset of the developing chicken autopod at HH29, a stage where the developing digit is composed of cells at different stages of differentiation (Figure 3A) (Feregrino et al., 2019). Using unsupervised graph-based clustering, 10 cell clusters were identified. tSNE visualization of cellular transcriptome similarities, combined with the projection of these cluster identities, revealed the presence of distinct cell populations. Based on the expression of known marker genes and gene ontology (GO)-term enrichment analyses, these cell populations were identified as follow: mesenchyme in red, muscle cells in black, skin in purple, blood cells in grey, interdigit mesenchyme in green, non-skeletal connective tissue (nsCT) in maroon, distal mesenchyme in yellow, endothelial cell of blood vessels in brown and smooth muscle of blood vessels in orange and finally, skeletal progenitors in blue (Figure 3B). This primary analysis allowed us to recover all the expected major cell types present during limb development. Then, using fine-scale unsupervised graph-based clustering, multiple sub-clusters were identified, with the goal to delineate distinct progenitor sub-types and cell states (Figure 3C) (Sacher et al., 2021). Amongst the skeletal progenitor population, 3 different sub-clusters were identified: sub-cluster 15, identified as early chondrocytes/progenitors, sub-cluster 3, identified as more mature chondrocytes and sub-cluster 17, identified as putative joint progenitors. This sub-clustering also allowed us to recover different cell states within the different cell type populations. Based on differential expression analysis done on these sub-clusters of mesenchymal cells (mesenchyme, distal mesenchyme, nsCT, interdigits and skeletal progenitors), we recovered the expression of the previously identified and assessed marker genes for the skeletal progenitor sub-populations (Figure 3D). Namely, pseudobulk expression analysis (Sacher et al., 2021) of early chondrocytes (sub-cluster 15) revealed high expression of *Tcf7l2*, *Sox9*, *Bmpr1b* and *Chrdl1* in that particular sub-cluster. Likewise, *Sox9*, *Chrdl1* and *Bmpr1b* showed continuing expression in the mature chondrocytes (sub-cluster 3) as well. As expected, high *Gdf5* expression was recovered from the sub-cluster of joint progenitors (sub-cluster 17). Moreover, testing for additional marker genes several genes with high, joint progenitors-specific expression were identified in sub-cluster 17: *Dusp1*, *Creb5*, *Inhba*, *Rcan1*, *Chrdl2*, and *Smoc1*. According to their differential expression amongst the joint progenitor population, but also to their expression patterns and phenotypes reported in literature, they are potential candidate genes for the establishment of joint cell identity.

Using chicken autpod single-cell RNA-sequencing data combined with marker gene analysis, we thus identified the patterning relevant cell populations and additional marker genes for the differentiation of cell types and states in the developing digit. Thereby, we provide the basis

for further temporal exploration of the data, as well as a list of candidate genes for the establishment of the joint cell identity.

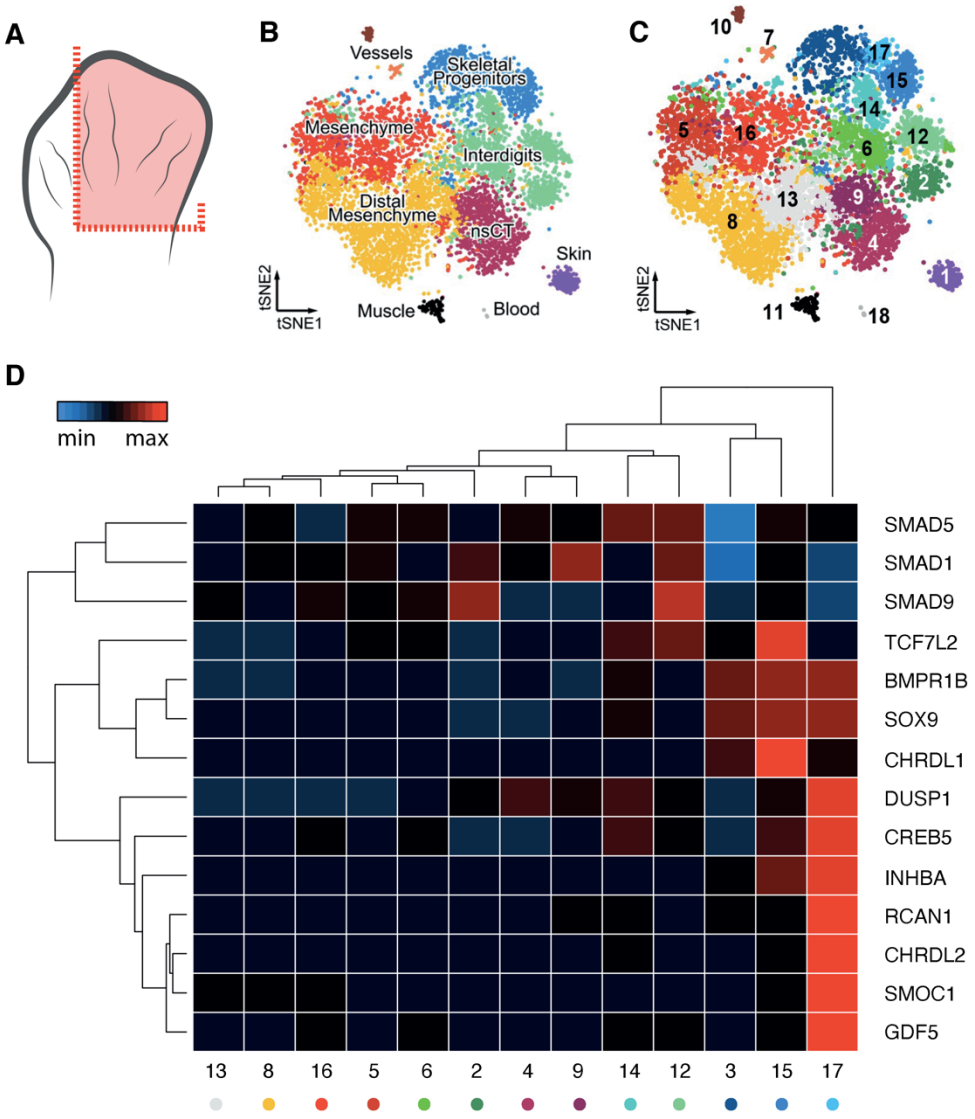

Figure 3. Analysis of chick HH29 hindlimb single-cell RNA-sequencing data. (**A**) Dissection strategy (highlighted in red) for sampling of chicken hindlimb stage HH29 (adapted from Feregrino et al., 2019). (**B**) tSNE visualization representing HH29 cells according to their transcriptome similarities. Unsupervised graph-based clustering is represented by the different colors (adapted from Feregrino et al., 2019). (**C**) tSNE plots representing fine-scale unsupervised graph-based clustering. For reference, sub-cluster numbers are added (adapted from Feregrino et al., 2019). (**D**) Heatmap visualization of marker genes and candidate genes pseudobulk expression across distinct mesenchymal cell sub-cluster in C, based on differential expression analyses done on the chick HH29 autopod single-cell RNA-sequencing data by Feregrino et al. 2019.

b. Single-cell pseudotemporal reconstruction of the chicken digit patterning

To get a better temporal resolution of the transcriptional dynamics during digit patterning, we focused on distinct sub-clusters of our HH29 single-cell RNA-sequencing data, to perform a so-called pseudotime analyses. The aim of a pseudotime analysis is to reconstruct the progression through a cellular differentiation process, based on transcriptional differences, and the likely transitions between them, of the individual cellular transcriptomes (Trapnell et al., 2014). Here, using Slingshot (Street et al., 2018), we calculate a pseudotemporal cell ordering of developing digit cells based on single cell gene expression profiles. Indeed, there is temporal variability of gene expression during cell differentiation and pseudotime analysis exploit this to order the cells according to their progress in the lineage. Along a growing digit, at a certain developmental stage, we can find cells at different stages of the differentiation, ordered proximal-distally according to their age of specification. Accordingly, we can recapitulate the molecular differentiation of digit progenitors occurring during development *in silico* using single-cell RNA-sequencing data from several, similarly staged embryos (Feregrino et al., 2019). Cells localized directly under the AER in the PFR start their differentiation while cells localized proximally are more mature. With our pseudotime analysis we thus aim to backtrace the differentiation trajectory to the point where the PFR trajectory splits into phalanx and joint progenitors, and to look for differentially expressed genes, to define potential cell-intrinsic regulators of this bifurcating cell fate decision. We used sub-clusters 3, 15 and 17, as identified previously in our single-cell RNA-sequencing data set presented above. Sub-cluster 15, was identified as ‘early chondrocytes’, sub-cluster 3 as ‘mature chondrocytes’ and sub-cluster 17, as potential ‘joint progenitors’. We used variable genes to calculate a diffusion map (Angerer et al., 2016), to visualize the relationships between the different chondrocytes sub-clusters cells we’ve selected (Figure 4A). We observe a transition and split of the early chondrocytes population into either a ‘mature chondrocytes’ trajectory or a ‘joint progenitors’ trajectory, thereby recapitulating the anticipated differentiation trajectories of the digit progenitor cells during development. Expression dynamics along the two trajectories, of genes known to be involved in the specification process of the phalanx or the joint cell identity, supported the notion that our pseudotime reconstruction indeed recapitulates the major, known transcriptional changes of the digit cell fate divergence *in silico* (data not shown). Then, using Slingshot (Street et al., 2018), we calculated pseudotime ordering of the cell to get the overall pseudotime along the trajectories, based on our diffusion map (Figure 4B). For that, the ‘early chondrocytes’ population was defined as the presumptive origin of the pseudotime, and

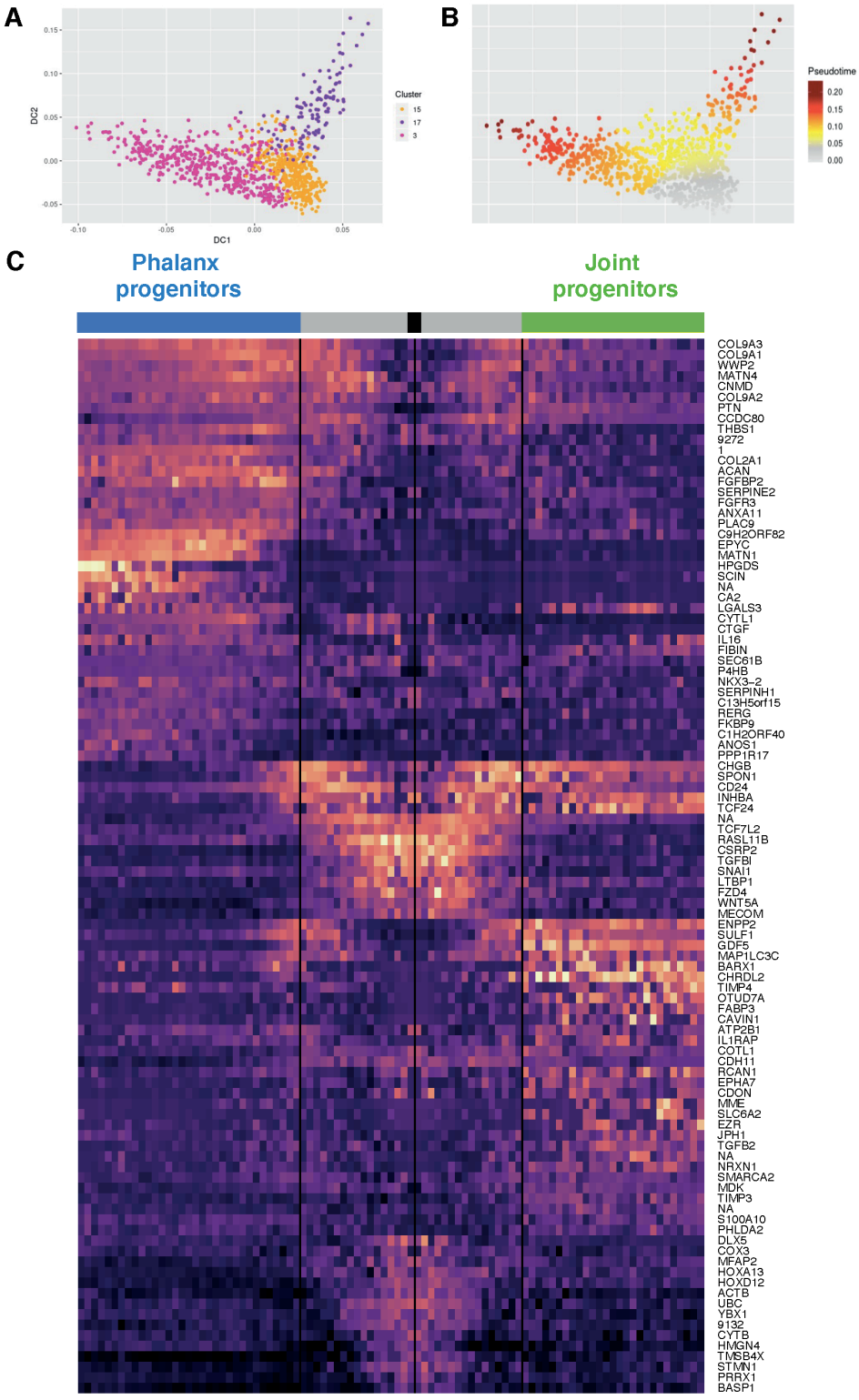

Figure 4. Single-cell pseudotemporal reconstruction of the chicken digit patterning process. (**A**) Diffusion map of the chondrocyte and joint sub-clusters recapitulating trajectories of the digit progenitor cell lineage (sub-clusters 3, 15 and 17 from Figure 3C). (**B**) Overall pseudotime progression along the two trajectories. (**C**) Pseudotime heatmap of differentially expressed genes between the phalanx progenitors trajectory (bleu) and joint progenitors trajectory (green). The black zone corresponds to the starting point of the pseudotime. The grey zone corresponds to the part shared by the two trajectories. Orange: high scaled expression; Purple: low scaled expression.

'mature chondrocytes' and the 'joint progenitors' as the end points. Finally, we performed differential expression analyses, along the respective branches of the pseudotime. Differentially expressed genes between the phalanx progenitor trajectory (blue) and joint progenitors trajectory (green) are visualized in a heatmap (Figure 4C). Expression dynamics of major genes known to be part of this divergence process are again recovered along the pseudotime trajectories. For example, along the chondrocyte progenitor trajectory, we recover the expression increase of several collagen genes needed for chondrocytes maturation (Genzer and Bridgewater, 2007). *Acan*, needed for cartilage extracellular matrix synthesis (Kiani et al., 2002), or also *Fgfr3*, a chondrocyte maturation inducer (Su et al., 2014) are likewise increasing their transcription. Along the joint progenitor trajectory, we recover the upregulation of the well-known joint marker *Gdf5* (Storm and Kingsley, 1999), as well as *Enpp2*, another marker of the joints also known as *Autotaxin* (Hartmann and Tabin, 2001). In addition, we recover joint-like expression dynamics of genes that were not previously shown to be involved in this cell fate decision, like *Chrdl2*, *Rcan1* and *Sulf1*. Apart from the transcription of *Inhba* (Montero et al., 2008), the PFR is usually identified by antibody stainings for pSmad1,5,9. However, we have indication that the PFR population as well as more naïve limb progenitors are represented transcriptionally, in our pseudotime reconstruction. As shown above (Figure 2), PFR cells are characterized by the expression of *Sox9*, *Bmpr1b*, *Inhba*, *Tcf7l2* and *Chrdl1*. In our differential expression pseudotime analysis, we recover *Inhba*, as well as *Tcf7l2* expression in the part shared by the two trajectories, which is supposed to contain the PFR population. Moreover, expression of *Tgfbl*, a marker for mesenchymal progenitors (Lorda-Diez et al., 2013a), as well as *Prrx1* (Logan et al., 2002; Nohno et al., 1993), is recovered at the starting point of the pseudotime, and is downregulated once expression of *Inhba* is starting. Additionally, expression of gene members of the TGF-beta superfamily, like *Bmpr1b* and *Chrdl1,* is also recovered in the part shared by the 2 trajectories (see Figure 3 Chapter I). Thus, we have good evidence that the PFR and potential PFR precursors mesenchymal are contained in our pseudotemporal reconstruction.

Overall, this pseudotime analysis thus allows us to look for transcriptional dynamics along the reconstructed phalanx and joint trajectories, thereby recapitulating digit progenitor cell fate divergence and helping us to identify potential regulators of that cell fate decision during digit development, whose role need to be investigated *in vivo*.

c. Evolutionary conservation

In order to know if there are conserved molecular signatures in these cell types across tetrapods, we next compared the single-cell RNA-sequencing data that we obtained from the chicken autopod with bulk RNA-sequencing data obtained in mouse. The mouse data had been generated previously, using transgenic reporter lines and FACS cell isolation. Briefly, mouse joint and chondrocyte cells were isolated at embryonic day E14.5, using Sox9-Cre and Gdf5-Cre mouse lines, respectively, crossed with a Rosa26-LoxP-tdTomato_STOP-LoxP-GFP reporter strain (Figure 5A) (Mori-Akiyama et al., 2003; Rountree et al., 2004). Embryos resulting from these crosses exhibit GFP (Green Fluorescent Protein) expression in either the joint cells, for Gdf5-Cre, or in chondrocytes, for Sox9-Cre. Fluorescent GFP+ samples were dissected, dissociated, and FACS-sorted to isolate proximal or distal *Gdf5*+ cells, and proximal or distal *Sox9*+ cells, knowing that the proximal cells are cells more advanced in their differentiation process than distal ones. Thus, proximal *Gdf5*+ cells correspond to late joint progenitor cells, distal *Gdf5*+ cells to early joint progenitor cells, proximal *Sox9*+ cells to late chondrocyte progenitor cells and distal *Sox9*+ cells to early chondrocyte progenitor cells. RNA was extracted, reverse transcribed and libraries were prepared for sequencing. Differential expression analyses were done to reveal genes that are specifically enriched in one or the other of these cell populations. PlotSmear visualization of differentially expressed genes, between joint and chondrocyte cells, show that known joint marker genes (Brown dots) are enriched in the *Gdf5*+ cells and known chondrocyte marker genes (Beige dots) are enriched in the *Sox9*+ cells (Figure 5B). Moreover, novel candidate genes *Chrdl2*, *Smoc1*, *Dusp1*, *Inhba*, *Rcan1*, *Gas1* and *Creb5* of the establishment of joint cell identity (Gold dots), as previously selected thanks to the differential expression analysis done on the chick HH29 autopod single-cell RNA-sequencing, are enriched in the *Gdf5*+ joint cells (Figure 5B). GO-term enrichment analyses show differentially expressed genes to be involved in the development of the limb skeleton, as for example extracellular matrix molecules, cartilage development or connective tissue development (Figure 5C). Heatmap visualization of differentially expressed genes in *Gdf5*+ and *Sox9*+ cell populations reveals that transcriptomes of the different cell population are clustering according to cell type (Figure 5D). We found that early and late *Gdf5*+ cells are transcriptionally similar as well as early and late *Sox9*+ cells. *Sox9*+ cells corresponding to chondrocyte progenitors show high expression of collagen genes like *Col9a1* and *Col2a1*, which are structural protein of the cartilage, genes for cartilage extracellular matrix formation like *Acan*, or of osteoblast maturation gene like *Ihh* and *Runx2.* *Gdf5*+ cells corresponding to joint progenitor cells are enriched for joint marker gene like *Irx1*.

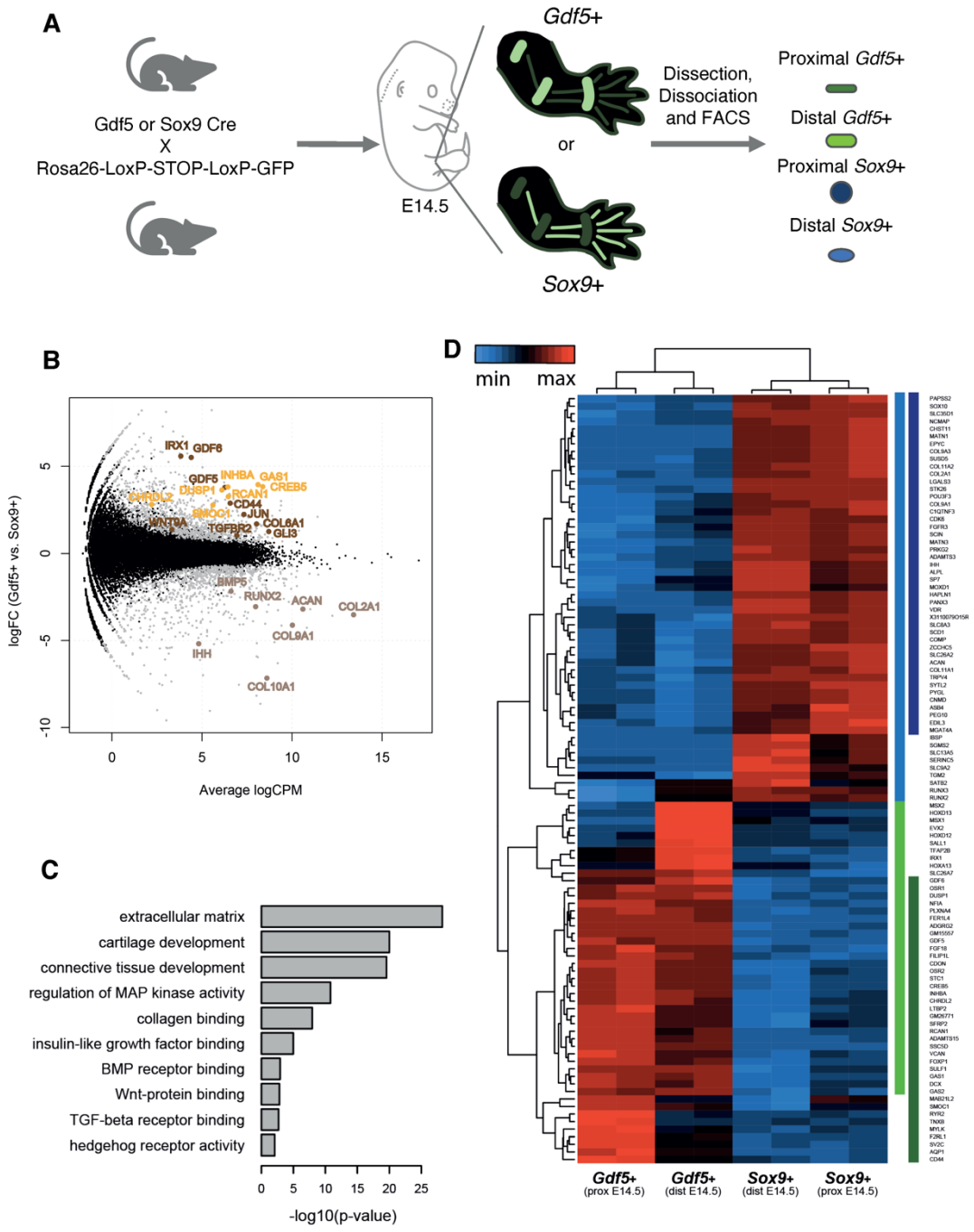

Figure 5. Analysis of mouse E14.5 joint and chondrocyte cells RNA sequencing data. (**A**) Dissection strategy for sampling of mouse E14.5 joint (*Gdf5*+) and chondrocyte (*Sox9*+) cells. (**B**) PlotSmear showing differentially expressed genes between joint and chondrocyte cells. Grey dots: significantly differentially expressed genes. Brown dots: joint marker genes. Beige dots: chondrocyte marker genes. Gold dots: candidate genes of the establishment of joint cell identity (Courtesy of Patrick Tschopp). (**C**) Select GO-terms, from analysis of the genes for all the cell populations (Courtesy of Patrick Tschopp). (**D**) Heatmap visualization of differentially expressed genes in joint (*Gdf5*+) and chondrocyte (*Sox9*+) cell populations, based on differential expression analysis done on mouse E14.5 joint and chondrocyte cells RNA sequencing data (Courtesy of Patrick Tschopp).

Additionally, the candidate gene *Chrdl2*, *Smoc1*, *Dusp1*, *Inhba*, *Rcan1*, *Gas1* and *Creb5* are enriched in the *Gdf5*+ cells. Similar patterns were found in chick HH29 pseudobulk data, when looking at the orthologous genes across the mesenchymal populations (Figure S1).

In conclusion, by comparing mouse bulk RNA-sequencing data to chicken HH29 single-cell RNA-sequencing data, we found conserved molecular markers in the two cell type populations, chondrocytes and joint progenitors. Additionally, expression patterns of novel, joint-specific genes seems to be conserved between chicken and mouse, making them interesting candidate regulators for the establishment of the joint cell identity. However, temporal and spatial variability of gene expression, present along the chondrocytes and joint cells lineages, can be lost with both bulk and single-cell RNA-seq, making and further experiments are needed to investigate this variability during digit progenitor cell differentiation.

4. Expression pattern of candidate genes for cell fate decision during digit development

To investigate a potential role in cell fate decisions of the candidate genes selected from our analysis of the transcriptional dynamics of digit patterning above, we first wanted to verify their expression pattern *in vivo*, to recover the spatial dynamics of their transcription lost with single-cell RNA-sequencing, and confirm their cell type specificity.

For this, we performed *in situ* hybridization, to visualize localization of gene transcripts in the developing limb structures. We first investigated gene expression pattern in the chicken limb, using either whole mount *in situ* hybridization of the entire autopod (Figure 6A-F) or in longitudinal sections of digits, through different stages of digit development (Figure 6G-N). We observe that candidate genes expression is generally restricted to the developing joints, with *Smoc1* and *Chrdl2* showing particularly strong expression in early joints. Then, to study the conservation of these expression patterns, we performed *in situ* hybridization on sections of digits of mouse at E15.5 (Figure 6O-U). Results showed that the candidate genes are also expressed in the developing mouse joints, demonstrating a conservation of expression patterns between chicken and mice. All in all, the expression patterns observed *in vivo* for the candidate genes selected from our transcriptional dynamic analysis support that those genes have a potential function in the joint cell fate decision.

Based on the observed transcriptional dynamics of TGF-beta superfamily members (see Chapter I, Figure 3) and results from the literature, we decided to focus on the candidate gene *Chrdl2*. *Chrdl2,* or *Chordin-like 2*, encodes a secreted protein shown to inhibit the action of BMP pathway members (Nakayama et al., 2004). According to the important role of the BMP

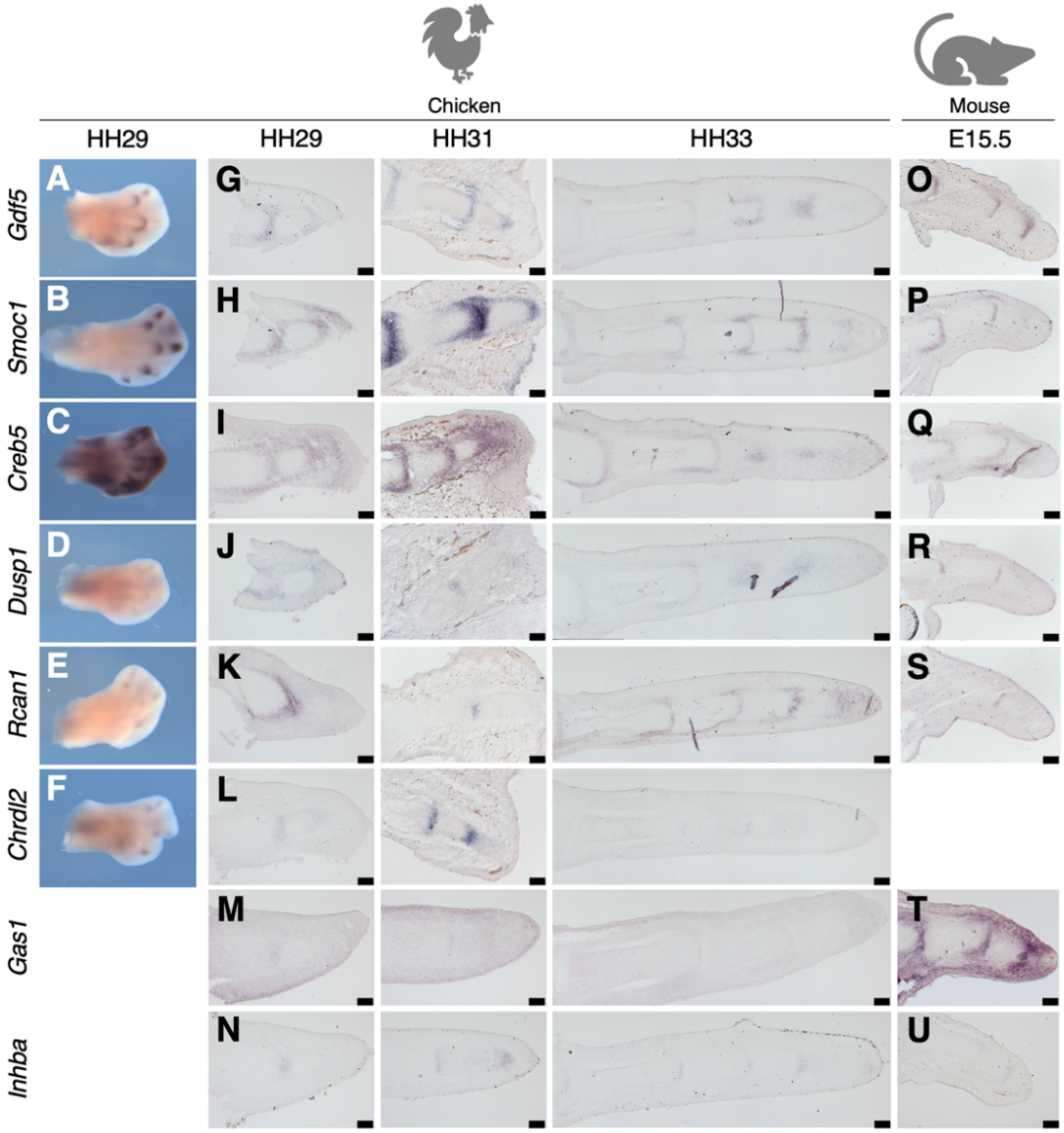

Figure 6. Expression pattern conservation of candidate genes for joint cell fate induction. (**A-F**) Whole mount *in situ* hybridization of candidate genes in chick autopods at HH29. (**G-N**) *In situ* hybridization of candidate genes in longitudinal sections of chick digits through stages of interzone formation and joint development (HH29, HH31 and HH33). (**O-U**) *In situ* hybridization of candidate genes in sections of mouse digits at E15.5. Scale bars: 100 µm.

signaling pathway in digit patterning and cell fate decision, as reported in the introduction, *Chrdl2* is thus a good candidate to investigate its role in cell fate decision, given its enrichment in joint cells and the upregulation along the joint-specific pseudotime branch (Figure 3D and 6L, see also Chapter I, Figure 3). Interestingly, these analyses also revealed that *Chrdl2* expression did not overlap with the expression pattern of its paralog, *Chrdl1*. Indeed, *in situ* hybridization in whole mount autopod or in longitudinal sections of digits show that *Chrdl2* is expressed in the developing joint, marked by *Gdf5* expression, and is not expressed in developing phalanges, where *Chrdl1* is expressed (Figure 7A-F). Additionally, to better

visualize the co-expression pattern of the two genes, we performed multi-fluorescent *in situ* hybridization for *Chrdl1* and *Chrdl2,* combined with immunohistochemistry for pSmad1,5,9 (Figure 7G-H'''). We observe complementary expression patterns of *Chrdl2* and *Chrdl1* in the developing digit, with presence of *Chrdl2* into the joint and absence/downregulation of *Chrdl1*

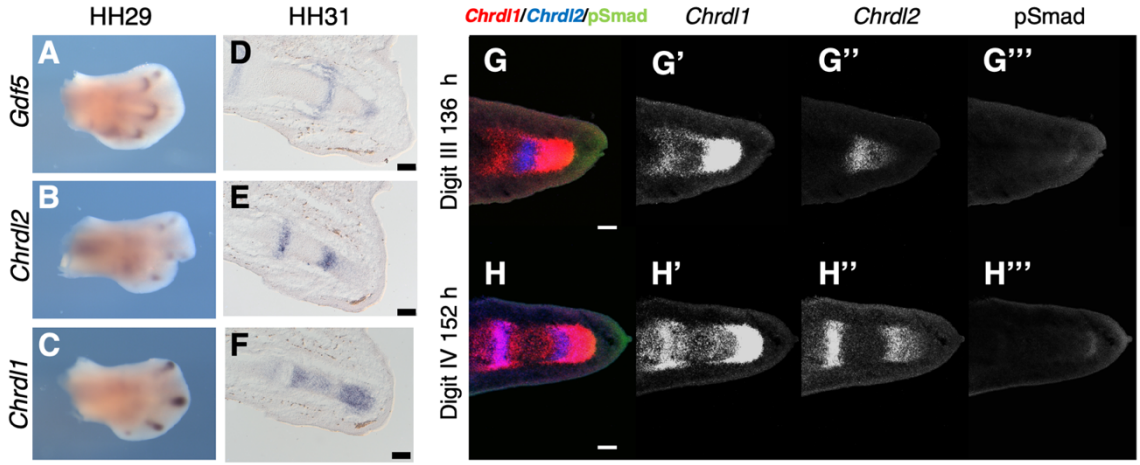

I

```
Chrd     MRTALLLLALLALPVRTARPKLALPIRPDSEPLPPGGAAGCAFGGRFYALEETWHPDLGEPFGVMRCVICHCETQRNRRGKPVGKVNCKNMKQDCPVPTCPRATLLPGHCCHTCPKALPG   120
Chrdl1   ------------------------------------------------------------------------------------------------------------------------   0
Chrdl2   ------------------------------------------------------------------------------------------------------------------------   0

Chrd     APEKSYKPPFDTFEYFQDKEDELDKPYNDRSYLSSEGSARDDARTEFVALLTSGPEPWHPTSSAVAKARFTLLRSYLLFSISYERLGRPSRVRFSDPEGTVLFEHPVQKSAAPEDGMLCG   240
Chrdl1   ------------------------------------------------------------------------------------------------------------------------   0
Chrdl2   ------------------------------------------------------------------------------------------------------------------------   0

Chrd     MWRTVSKANIQLLRAEQLRVSLITRAQPSGEVHGHILKHRALFAETFGAILTSSDPAHLGAGGMAMLTLSDTENNLHFILMARGLLEPGAEESPWVPLRVRILHQGQTLREAHANITMED   360
Chrdl1   ------------------------------------------------------------------------------------------------------------------------   0
Chrdl2   ------------------------------------------------------------------------------------------------------------------------   0

Chrd     PDFAEVLSDLSAHELQWLAQGQLRIVADTQGRHPRQLEGTITARRSCDTIQSVLCGADALQPTKTGAVGSAKLALHENGTLEYQVRVVGTASEVVGVTLETKPRRKNRRNVLFDMTPSYR   480
Chrdl1   ------------------------------------------------------------------------------------------------------------------------   0
Chrdl2   ------------------------------------------------------------------------------------------------------------------------   0

Chrd     AGMAQGVWHSPSARDVHMLLQNELFLNVATKDWAEGELRGQVISLPYSGLLARYTEMPVPLAGQLVSPPVSSGAGGHAWLSLDEHCHLHYEIVVAGLGRPADGTVSAQLHGVAELGEMGT   600
Chrdl1   ------------------------------------------------------------------------------------------------------------------------   0
Chrdl2   ------------------------------------------------MSGFLRSAVKSN---SSCTVLPADGWCQTEGAWLTAPVFLVLHQHHARNPQGRAASGGAFDR----SEANPDGH   67

Chrd     RPH--LHKRMLKGFYGTEAQGVVK---DLDAELLQH----------LAQG-----------------------TAFLQVSTKAHPRGEMRGWVHIPNRCQPGGARLSTGEAELSEGP   679
Chrdl1   ------------------------------------------------------------------------MRRKWRSE------DFHFVFFGVLCLL-LI   23
Chrdl2   RHHRDRHHRDLRGHRYRRAPAPLRPPPVIDTETSPSAGHHSPWVSPALTPGQPRAPAPGAAPGHRAATRQQPGCDTTAPTERRDRSSPGTDRRAAMLP------GAGPLAFLLRCLL-LL   180

Chrd     KGRNVEQLKKDFNSCFFEGQHHAHGTRWAPDYDK----KCSTCSCQK-RTVICDPILCQPLNCTRQVHPEELCCPICEEKKMEQEELKL----------ERARDSSEGTYFDGDKT   780
Chrdl1   DRGKLEQVKHSDTYCVFQDKKYRVGERWHPYLEPYGLVYCVNCLCSENGNVLCSRIRCPSLHCPSPVHVPQLCCPRCPEDSLFS----------VSSKITGKSCEYNGTTY   124
Chrdl2   FASESRARARPDMFCDFNGKKYSPGESWHPYLEPQGLMYCIRCSCSENGNTRCYRIQCPALQCASPVTDPQQCCPRCLGTGPSHGEGVAGAKGNFRTREPNSPSGLRAPVRSCQYNGTTY   300

Chrd     WRGSGTRWHPVVPPFGLIKCAICTCKGTTGEVHCEKVQCPRLTCANPVRVSPSDCCKQCPAPEKSIPELTD----------------------------------------------   851
Chrdl1   HHGEMFVAEGLFQNRQANQCAQCSC--SEGNVYCGLKTCPKLTCSFPVSVP-ESCCPVCKGDGELSWEQADGDIFRQPANREARHSYHRPHYE----LSPSSTRQVVNVPRFPSARSNRG   237
Chrdl2   QQGEMFTTSELFPSRQPNQCVQCSC--SEGQIYCGLVTCPELLCSNPLTVP-DSCCQVCKDGSYEKSAEEEP----LQLNRGVRHSQDQCLGEAMGRRPPGATASTM----LSSSLEFIP   409

Chrd     -----------------GMQADGFRACRFGRRWYLNNESWHPSVPPFGEMKCILCWCVSGETHCQRQECPPD-ACASPTRRDNPCCAKCRAPDAPSEKMYEATAEAWSR-----------   942
Chrdl1   VLPDPQQASGTIVQIVINNKHKHKHCRVCVSNGKTYSHGESWHPNLRAFGIVECVLCTCNITKQECKKIHCPEQYPCKYPQKVEGKCCKVCPEEVPSQS--FDNKDYFCGKETFPVYESIFT   355
Chrdl2   RSFKPKGGGGTTVKIVLK--EKHKKACVYNGKTYSHGEVWHPVFRLYGLLPCILCTCRDGVQDCQKITCPKEYPCDSPEKVDGKCCKICPETRVKPT--DEVITERCGKTPNHVLVYMFV   525

Chrd     ----------------------------------------------------------------------------------------------------------------------   942
Chrdl1   -----EEGETIRKIAVETEKPPQIEIHVWTIRKGILRHFYIEKMSKREFEE-LPYFKQITRTTSSQWKIFSEGEAQISQMCESRVCRTELEDLVKVLYLEKSEKGHC   456
Chrdl2   PPSSENSKEILRTVAIEKELAEEVEIYNWKLIKGIFHLIQTKKISKQEFKQEAQNYRLIARTNEGHWNIFQAQTSELRMTESP---EKETENL--------------   615
```

Figure 7. Expression pattern of *Chrdl1* versus *Chrdl2* during development of chick leg digit. (**A-C**) Whole mount *in situ* hybridization of *Gdf5*, *Chrdl2* and *Chrdl1* in chick autopods at HH29. (**D-F**) *In situ* hybridization of *Gdf5*, *Chrdl2* and *Chrdl1* in longitudinal sections of chick digits at HH31. Scale bars = 100 µm. (**G-H'''**) Multiple fluorescent RNA *in situ* hybridization for *Chrdl1* and *Chrdl2* combined with immunohistochemistry for pSmad1,5,9 in longitudinal section of digit III at 136 h of development (HH27) and digit IV at 152 h of development (HH29). Scale bars = 100 µm. (**I**) Alignment of amino acid sequences for CHORDIN (Chrd), CHRDL1 and CHRDL2 chicken proteins. The conservation is most prominent within ligand-binding domains (black boxes).

therein, and expression of *Chrdl1* in the developing phalanx with absence of *Chrdl2*. Moreover, *Chrdl1* is expressed in the PFR marked by pSmad signaling, but the PFR is devoid of *Chrdl2* expression.

Next, we compared the protein sequences of the two genes, to see if putative structural differences could support the hypothesis that they are responsible for distinct roles during digit development. To do so, we aligned the amino acid sequences for CHORDIN, CHRDL1 and CHRDL2 chicken proteins (Figure 7I). We observed that CHRDL1 and CHRDL2 proteins have overall different size (456 and 615 amino acids for CHRDL1 and for CHRDL2, respectively). However, we observed a conservation of the protein sequence within ligand-binding domains (black box). The BMP antagonist proteins contain cysteine-rich domain that allow them to bind to BMP ligand to inhibit the BMP pathway activity (Nakayama et al., 2001). By aligning the protein sequences of CHRDL1, CHRDL2 and CHORDIN proteins, we observed that the first ligand-binding domain in CHORDIN is absent in CHRDL1 and CHRDL2. However, with exception of the first box, the ligand-binding domains sequences seem to be conserved between all three proteins (Figure 7I). The first and the third ligand binding domains in both CHRDL1 and CHRDL2 were reported to be more homologous to the third domain of CHORDIN (Nakayama et al., 2004). Moreover, in CHORDIN, the first and the third ligand biding domains have the ability to bind to bind BMPs (Larraín et al., 2000; Troilo et al., 2014).

Overall, the two genes, *Chrdl2* and *Chrdl1*, show opposite expression patterns: *Chrdl2* is expressed in the developing joint and *Chrdl1* is expressed in the chondrogenic lineage and absent/downregulated in the developing joint, where *Chrdl2* is present. Despite the high overall amino acid sequence conservation, and the presence of three ligand binding domains, small amino acid and length differences do exist between the two proteins, encoded by *Chrdl2* and *Chrdl1*. These results thus suggest that they may have distinct, and potentially opposing roles during digit development, in the specification of phalanx and joint progenitor cells.

5. Functional characterization of a candidate gene of cell fate decision during digit development: *Chrdl2*

According to the observations made above, we were wondering if *Chrdl2* has a role in joint cell fate decision during digit development. To elucidate the function of *Chrdl2 in vivo*, and to see if modulation of its expression will perturb cell fate decisions and digit patterning during development, we aimed to ectopically express it in chicken embryos using the RCAS system. This system is based on the use of replication competent avian sarcoma virus, to deliver a gene of interest into cells of receptive chicken strains (Logan and Tabin, 1998). The technique

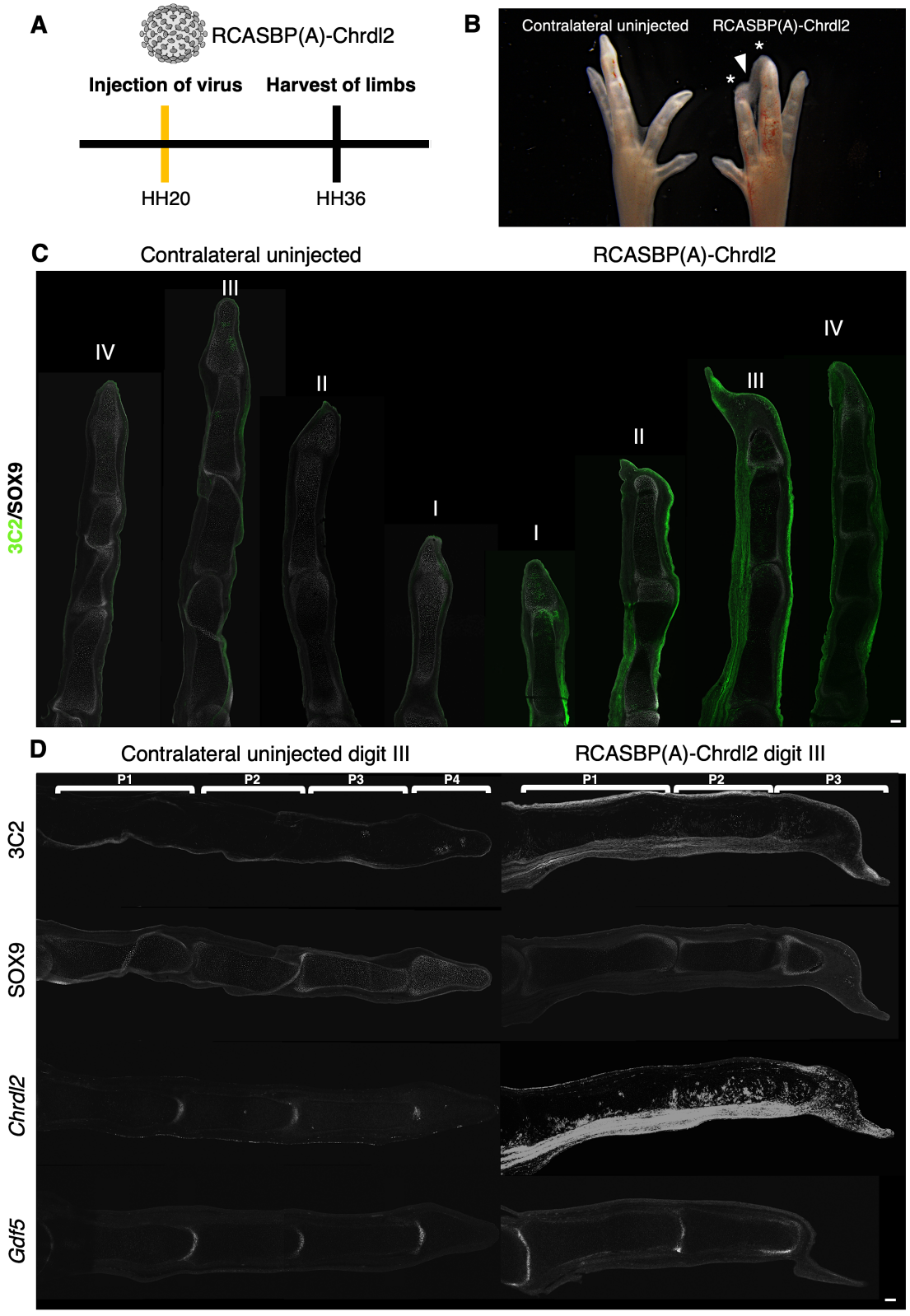

Figure 8. Effect of overexpression of *Chrdl2* on chick leg digit patterning. (**A**) Timeline of the experimental setup of RCASBP(A)-Chrdl2 microinjection into the limb bud. (**B**) RCASBP(A)-Chrdl2 infected limb at HH36 after injection into the limb bud right at HH20 and the contralateral uninjected limb. Note the truncation of digits 2 and 3 (asterisks), and the failure of interdigit mesenchyme regression (arrowhead) (**C**) Immunohistochemistry for 3C2 (viral protein) and SOX9 in longitudinal sections of digits from limbs in panel B. (**D**) Fluorescent RNA *in situ* hybridization for *Chrdl2* or *Gdf5* in adjacent longitudinal sections of digit III stained for 3C2/SOX9 in panel C. Scale bars = 100 µm.

consists of the insertion of the CDS of the gene of interest into a RCAS plasmid encoding for the virus. To produce the virus, the plasmid can be transfected into chicken fibroblasts, the cell line DF1. Viruses are released into the culture medium, which is harvested and concentrated for the virus using an ultracentrifuge (an optimization of the virus production procedures is described in the Materials and Methods section).

We started our investigation of *Chrdl2* function during digit development with the induction of ectopic expression in the limb bud, to try to get expression of *Chrdl2* in the whole limb. To do so, concentrated RCAS-Chrdl2 virus was injected into the middle margin of the chicken limb bud at stage HH20. Eggs were incubated up to stage HH36, 7 days after injection, to let the virus spread within the limb bud, and limbs were harvested for analysis (Figure 8A). Injections were performed always in the right limb bud, in order to use the contralateral, uninjected limb as a negative control. In addition, RCAS-GFP virus was injected in other embryos, as a control for the microinjection procedure and infection spread (Figure S2B-B''). Injection in the limb bud at stage HH20 with RCAS-GFP virus induced an infection throughout the limb at HH36, with infection visible within digits. As expected, RCAS-GFP did not induce morphological malformations in the limb. However, limbs injected with RCAS-Chrld2 virus exhibited varying degrees of malformations (Figure 8B and S3B). Indeed, some digits are truncated (Figure 8B) or even absent (Figure S3B), while in some limbs interdigit soft tissue failed to regress (Figure 8B), compared with contralateral uninjected limb in which digit are formed and separated from each other. Note that the stylopod and the zeugopod were not affected and indistinguishable from the corresponding structures of the contralateral limb. Then, to continue our investigation, digits of injected embryos were dissected and embedded to perform longitudinal sections. We performed immunohistochemistry for 3C2, a viral protein, to trace the viral infection, and for SOX9, the chondrocyte marker, to visualize the future skeletal elements (Figure 8C). We observed a reduction of phalanx numbers within some digits infected with RCAS-*Chrdl2*. Unexpectedly, a few infected cells were also observed within digit of the contralateral, uninjected limb. We suspect this could be linked to a transport of the virus within the blood circulation. However, these infected cells are very few compared to the injected limb, and did not result in any morphological alterations. To verify that injection of RCAS-Chrdl2 virus resulted in ectopic expression of *Chrdl2*, we performed fluorescent *in situ* hybridization for *Chrdl2* in adjacent longitudinal sections of digit III (Figure 8D, S3C and D). Ectopic expression is observed in the digit III of the injected limb. Phalanx condensations are observed, however overall SOX9 staining appears slightly weaker, compared to the contralateral control digit (Figure 8D). Moreover, expanded *Chrdl2* expression in soft tissues around the future skeletal element is observed. However, the endogenous *Chrdl2* expression in the developing joint

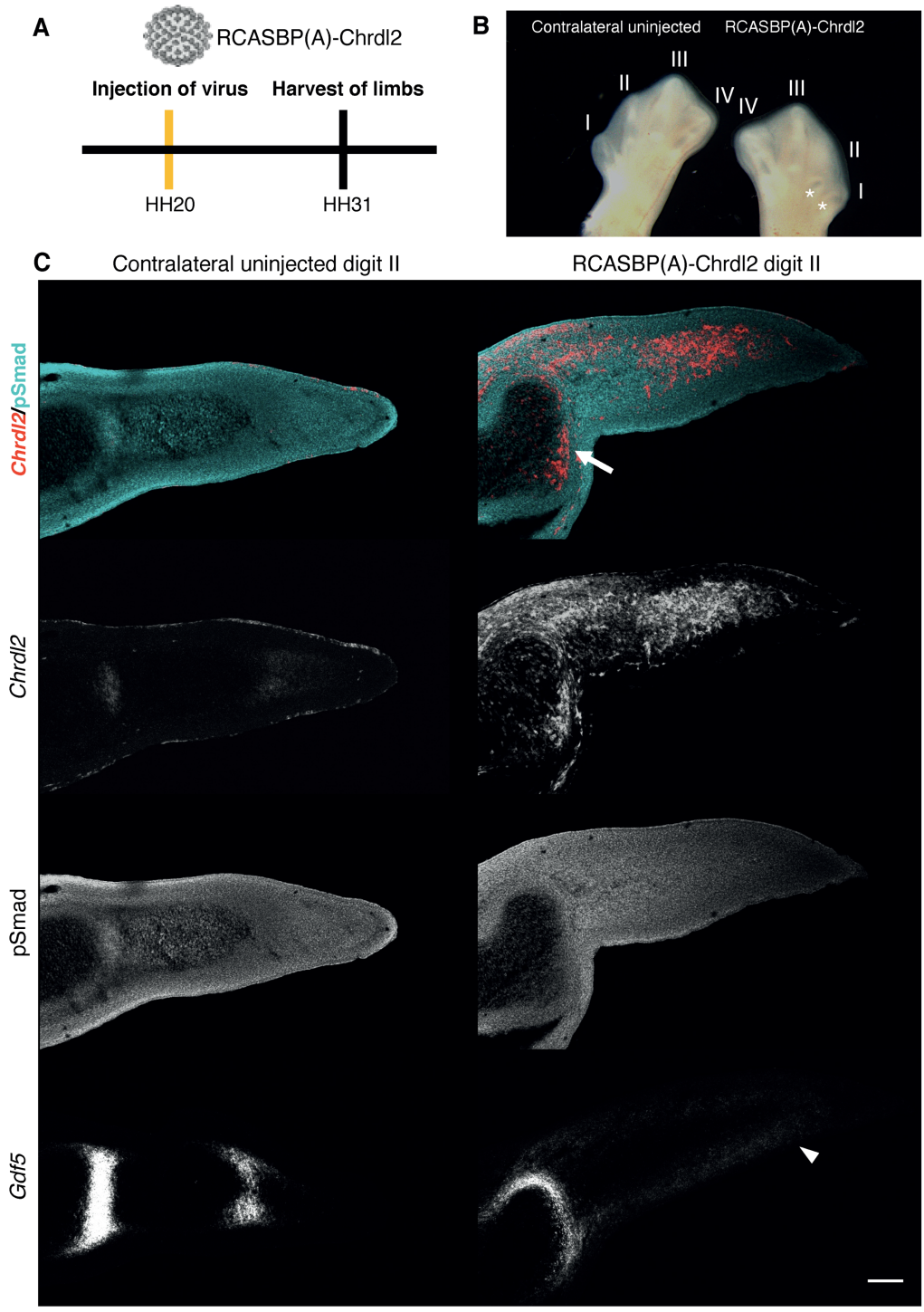

Figure 9. Effect of overexpression of *Chrdl2* on BMP signaling. (**A**) Timeline of the experimental setup of RCASBP(A)-Chrdl2 microinjection into the limb bud. (**B**) RCASBP(A)-Chrdl2 infected limb at HH31 after injection into the limb bud right at HH20 and the contralateral uninjected limb. Digits I and II only show metatarsal condensations (asterisks) (**C**) Fluorescent RNA *in situ* hybridization for *Chrdl2* combined with immunohistochemistry for pSmad1,5,9 in longitudinal digit II sections from limbs in panel B, and fluorescent RNA *in situ* hybridization for *Gdf5* in adjacent longitudinal sections. In infected digits, only metacarpal condensations are visible (arrow), and the distal mesenchyme fails to condense. The *Gdf5* band of the metatarso-phalangeal joint appears expanded, and low ectopic expression of *Gdf5* is visible distally (arrowhead). Scale bar = 100 µm.

seems to be downregulated. Indeed, it seem that *Chrdl2* is not anymore expressed in a band at the level of the developing joint, as is the case in the contralateral limb. Finally, to visualize the developing joints, we performed fluorescent *in situ* hybridization for *Gdf5* (Figure 8D, S3C and D). In digits of RCAS-Chrdl2 injected limb, we can observe that there are less joints (Figure 8D) or even absence of joint (Figure S3C). *Gdf5* is still expressed in bands in the developing proximal joints that are formed. However, its expression domain seems expanded, and more rounded at the distal tip of the digit.

To conclude, *Chrdl2* ectopic expression in the limb bud with the use of RCAS virus, resulted in limb alterations only at the autopod level, with development of truncated digits and the persistence of interdigit tissue.

Next, as *Chrdl2* is a putative inhibitor of BMP pathway (Nakayama et al., 2004), we aimed to analyze the impact of *Chrdl2* ectopic expression on BMP pathway activity. To do so, we decided to collect embryo earlier, at a stage when we know that BMP activity is still dynamic and easy to detect. To do so, RCAS-Chrdl2 virus was injected into the chicken limb bud at stage HH20. Eggs were incubated up to stage HH31, 5 days after injection, and limbs were harvested for analysis (Figure 9A). Injection in the limb bud at stage HH20 with RCAS-GFP virus resulted at HH31 in an infection within digits, and did not induce morphological malformation of the limb (Figure S2A-A'' and D). The area of infection is much more restricted, as expected for the shorter incubation period (Figure S2D). In limbs injected with RCAS-Chrld2 virus, we can sometimes observe that digits I and II are truncated, and only the metatarsal condensations remain visible (asterisks, Figure 9B). This phenotype is consistent with the truncation or absence of digits observed when limbs are incubated longer to develop (Figure 8B). Fluorescent *in situ* hybridization for *Chrdl2* in section of the malformed digit reveal that *Chrdl2* is broadly expressed ectopically in the digit (Figure 9C). We combined *Chrdl2 in situ* hybridization with immunohistochemistry for pSmad1,5,9, as a readout of the BMP pathway activity. In digit of the contralateral uninjected limb, we can localize the presence of pSmad at the tip of the digit corresponding to the PFR. However, in digits of RCAS-Chrdl2 injected limbs no specific pSmad staining was observed, suggesting a loss of the PFR. Moreover, in areas of high ectopic *Chrdl2* expression, skeletal condensations are affected. Distally, the tissue remains mesenchymal, with no signs of condensations. At the metatarsal level, the effects on condensations are more subtle, and seem to involve more shape than overall condensation changes. Then, to see the impact of *Chrdl2* ectopic expression on joint cell fate establishment, we did fluorescent *in situ* hybridization for *Gdf5* in adjacent longitudinal sections of the digit. We observed absence of forming joints, distally to the metatarsophalangeal joint. However, an expanded expression of *Gdf5* is visible in the soft tissue around the expected condensation

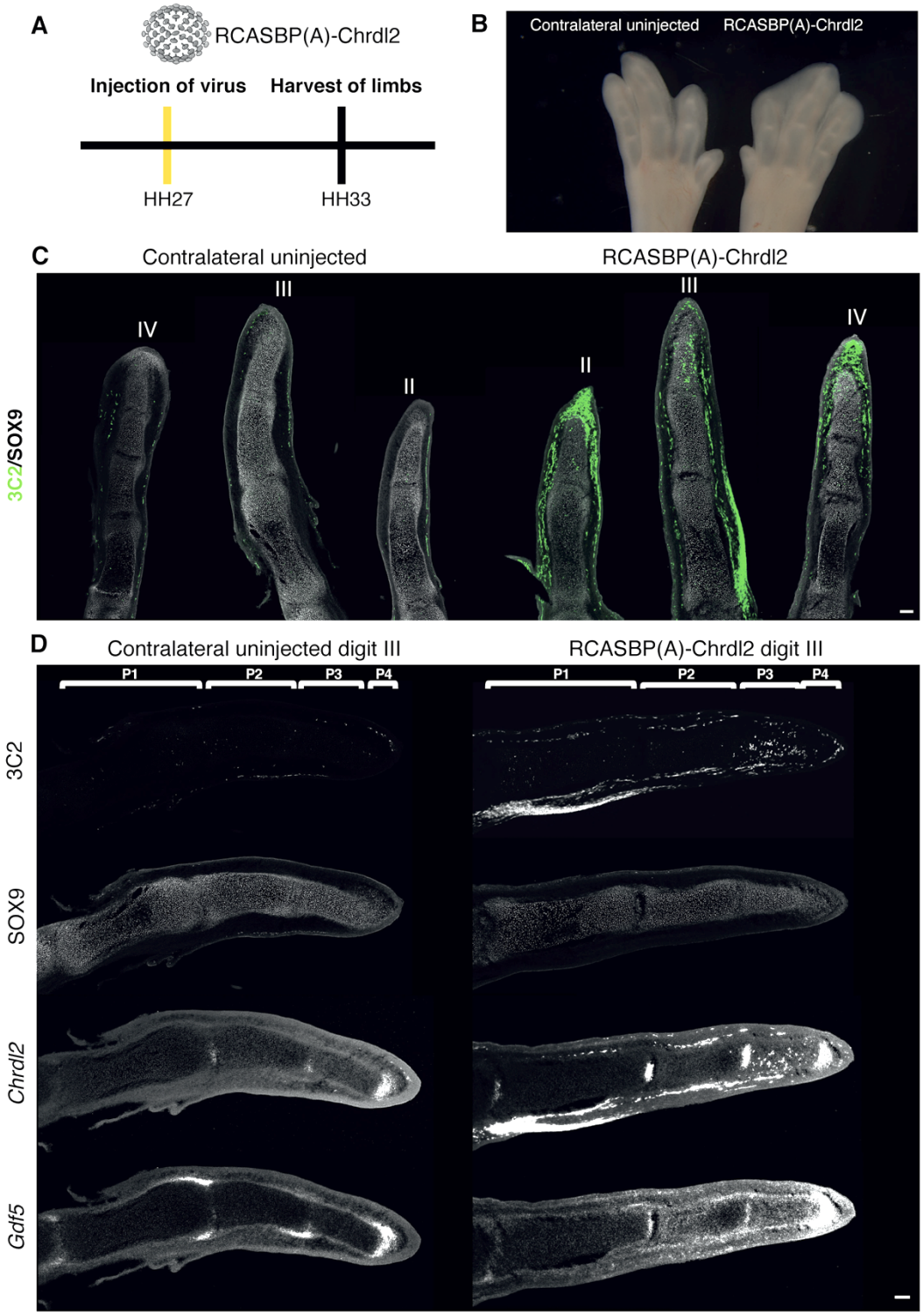

Figure 10. Effect of overexpression of *Chrdl2* in the PFR. (**A**) Timeline of the experimental setup of RCASBP(A)-Chrdl2 microinjection into the PFR. (**B**) RCASBP(A)-Chrdl2 infected limb at HH33 after injection into the PFR of digit III of limb right at HH27 and the contralateral uninjected limb. (**C**) Immunohistochemistry for 3C2 (viral protein) and SOX9 in longitudinal sections of digits from limbs in panel B. (**D**) Fluorescent RNA *in situ* hybridization for *Chrdl2* or *Gdf5* in adjacent longitudinal sections of digit III stained for 3C2/SOX9 in panel C. Scale bars = 100 µm.

that did not form. In conclusion, ectopic expression of *Chrdl2* induces an absence of condensations, with alterations of the BMP pathway activity in the PFR of the developing digit. Because the phenotype was so severe after an early injection of RCAS-Chrdl2 into the limb bud, we decided to inject it in the PFR proper, to ectopically express *Chrdl2* only in digit progenitors and thus potentially disturb the development of only one digit. To do so, RCAS-Chrdl2 virus was injected into the PFR of digit III at stage HH27. Eggs were incubated up to stage HH33, 2 days after injections, and limb were harvested for analysis (Figure 10A). Injection in the PFR at HH27 with RCAS-GFP virus resulted at HH33 in an infection within the injected digit (Figure S2C-C'' and E). In limbs injected with RCAS-Chrld2 virus, we can observe that interdigital tissue was present between digit II and III, compared to the uninjected contralateral limb in which digits are separated (Figure 10B). However, the digit morphology seemed not affected. Immunohistochemistry for 3C2 and for SOX9, in longitudinal sections of these digits, reveals that infected cells are present within the digit III, but also in digit II and IV, but digit III is the one with more infection within the skeletal elements (Figure 10C). Fluorescent *in situ* hybridization for *Chrdl2* in adjacent longitudinal section of digit III shows ectopic expression of *Chrdl2* within the digit and at the digit tip (Figure 10D). To see the impact of ectopic expression of *Chrdl2* on the joint cell lineage, we performed fluorescent *in situ* hybridization for *Gdf5*. Expression of *Gdf5* seems upregulated in RCAS-Chrdl2 injected limb compared to the contralateral uninjected limb. Indeed, *Gdf5* expression is strong at the digit tip and diffuse in the soft tissue around the skeletal elements. Overall, *Chrdl2* ectopic expression in the PFR does not seem to impair the digit morphology, but can induce upregulation of *Gdf5* expression.

Altogether, these data suggest that ectopically overexpressing *Chrdl2* in the developing digit inhibits the formation of phalanx condensations, possibly through an alteration of the BMP pathway, with misregulation of *Gdf5* and loss of the PFR. Collectively, this results in the development of truncated digits, as well as persistence of interdigit tissue.

Discussion

In this study, we describe the transcriptional dynamics of the digit progenitor cells lineage, to identify candidate genes for the establishment of the phalanx versus joint cell fate identity, and used viral overexpression to functionally test one of the emerging candidates.

First, we aimed to trace the descendants of the digit progenitor cell lineage, to figure out the origin of joint and phalanx cells. Our observation gave us good evidence that progenitors of both cell types are coming from the PFR. However, it seems that not all the interzones cell are

coming from the same progenitor population (Shwartz et al., 2016). Indeed, the labeling of Gdf5-positive interzone cells using a knock-in Gdf5-CreERT2 mouse, failed to mark the entire organ. In fact, there is a constant influx of new cells that are integrated into the developing joint. This observation is not incompatible with our model of joint progenitor emergence from the PFR, but it suggest that the PFR may not be the only source of progenitor cells to form the joint structure, and that cells from the vicinity could be integrated, as already suggested by other studies (Koyama et al., 2008; Pacifici et al., 2005).

In order to molecularly identify the cell populations involved in digit development, and mostly to identify the pool of digit progenitor cells forming the PFR, we analyzed the expression patterns of several maker genes and report their transcriptional signatures specific to these different cell populations. Importantly, using combination of fluorescence *in situ* and immunohistochemistry for pSmad, a marker of the PFR, in chicken digit sections, we confirm the expression of *Sox9*, *Bmpr1b* and *Inhba* in the PFR, as was already suggested (Merino et al., 1999b; Suzuki et al., 2008). Moreover, we detail the expression of *Chrdl1*, which was previously only suggested by whole mount *in situ* staining (Allen et al., 2013). Strikingly, expression of *Tcf7l2*, which was observed outside of the PFR in mouse limbs (Witte et al., 2010), colocalizes with the pSmad signal of the PFR in chicken. Consequently, even if there is no marker gene exclusive for the PFR, we provide a non-exhaustive list of genes which combinatorial expression constitutes a transcriptional signature to identify this cell population involved in chicken digit development.

To identify molecular players involved in cell fate decisions made by the digit progenitors coming from the PFR, we used single-cell RNA-sequencing data of the autopod at HH29. We provide a list of candidate genes for the joint cell identity establishment: *Chrdl2*, *Smoc1*, *Dusp1*, *Inhba*, *Rcan1*, *Gas1* and *Creb5*. Additionally, comparing the single-cell RNA-sequencing data of the chicken autopod with bulk RNA-sequencing data from mouse joint and chondrocyte cells suggested that there are molecular similarities in these cell type populations across between chicken and mice. The candidate genes for the joint cell identity thus seem to be conserved across tetrapods. However, the transcriptional mouse data for the joint lineage was produced by isolation of *Gdf5*+ cells, excluding all transcriptional changes that could occur before *Gdf5* expression and thus being implicated in the specification of digit progenitors into joint progenitor cells. In addition, the mouse data was performed with joint cells from the knee/elbow and the ankle/wrist, whereas the chicken data was performed on digit joint cells, which can result in transcriptional differences. Indeed, joints in the autopod have differences in the developmental process compared to joints connecting the stylopod and the zeugopod (Archer et al., 2003).

Because fine temporal variability of gene expression patterns present along the phalanx and joint cell lineages can be lost with cluster-based single-cell RNA-seq analyses, we investigated this temporal variability during digit progenitor cell differentiation using pseudotime analysis. The reconstruction of the transcription dynamic during digit development shows that digit progenitors of the PFR are coming from the distal mesenchyme and can be characterized by the onset of expression of genes previously shown to be part of the transcriptional signature of the PFR. We also reconstructed the differentiation process of these progenitors *in silico*, that can either start to express genes for chondrogenic maturation or start to express joint maker genes, to undergo joint cell differentiation process. This analysis allowed us to identify transcriptional dynamic changes along reconstructed trajectories of the digit progenitor cell fate divergence, and thus helps to identify potential regulator of cell fate decision during digit patterning. Collectively, using RNA sequencing data and pseudotime analysis, we analyzed the transcriptional dynamic of digit patterning along the digit progenitor cells lineage. This provided us with a list of candidate genes for cell fate decision regulation during digit development, whose role needed to be investigated *in vivo*.

We focused our investigation on the role of *Chrdl2*, a gene proposed to be a BMP pathway regulator (Nakayama et al., 2004). Interestingly, *Chrdl2* presented a expression pattern complementary to *Chrdl1*, its paralogous gene, suggesting that they may have distinct role during digit development, despite the similarities in protein sequence we observed between these two genes. Indeed, the ligand-binding domains, allowing the protein to interact with BMP pathway ligand, seem largely conserved. However, studies reveal that cysteine-rich motif composing the ligand binding domain may have multiple roles (Oren et al., 2004; Yu et al., 2004). Thus, *Chrdl1* and *Chrdl2* could still have distinct role during digit development, in agreement with their complementary endogenous expression patterns. *Chrdl1* function in the developing limb was already describe by Allen and colleagues, using viral overexpression studies similar to our approach (Allen et al., 2013). They observed that ectopic expression of *Chrdl1* within the chicken limb induces oligodactyly, with overgrowth of soft tissue and the absence of chondrogenesis needed for digit formation. Their results also showed that the expression of genes downstream of the BMP pathway were impaired by the ectopic expression of *Chrdl1*. The morphological phenotype that we observed in *Chrdl2* overexpressed embryos is surprisingly similar to the one observed in *Chrdl1*. Indeed, to elucidate the function of *Chrdl2 in vivo*, we induced *Chrdl2* ectopic expression in chicken embryos using the RCAS system. We observed that in developing digits ectopic *Chrdl2* expression inhibits the formation of condensations, through alteration of the BMP pathway, with misregulation of *Gdf5* and loss of the PFR. This results in development of truncated digit and persistence of interdigit tissue. Like

for *Chrdl1*, the misexpression of *Chrld2* seems to affect mostly the formation of the distalmost phalanges, as opposed to the stylopod or zeugopod, or the more proximally located metatarsals of the autopod. We hypothesize that, during digit development, *Chrdl2* acts as an inhibitor of BMP signaling and thus prevents the phosphorylation of Smad into the active transcription factor, inducing a downregulation of BMP pathway. However, as for *Bmpr1b* knockout mice, a morphological effect seems only to concern the distally located phalanges (Yi et al., 2000). The upregulation of *Gdf5*, on the other hand, observed when *Chrdl2* is overexpressed, could be explained by the potential absence of a negative feedback of BMP signaling on *Gdf5* transcription to regulate it (see Chapter I). Additionally, the persistence of interdigit tissue in autopod with *Chrdl2* overexpression suggest that *Chrdl2* could inhibit the apoptosis that normally occur there. Further experiment would be needed to assert cell death differences when *Chrdl2* in overexpressed. However, the persistence of soft interdigit tissue suggest a similar impact on BMP inhibition as was reported in the webbed feet of waterbirds (Merino et al., 1999c; Tokita et al., 2020).

Similar phenotypes as the ones observed with *Chrdl2* overexpression were also obtained in models of BMP pathway inhibition. Indeed, ectopic expression of *Noggin* with an RCAS(A)-Noggin virus resulted in shortening of the cartilage elements and loss of some of the digits, as well as repression of programmed cell death in the interdigit (Capdevila and Johnson, 1998). Moreover, overexpression of a dominant negative form of the BMP pathway receptor, *Bmpr1b*, also results in a similar phenotype observed with overexpression of BMP antagonists, supporting the importance of BMP signaling modulation by antagonists during digit development (Zou and Niswander, 1996; Zou et al., 1997). In addition to the impact of *Chrdl2* overexpression within the digit, *Chrdl2* overexpression in interdigit tissue also seemed to result in anteriorization of digit identity (Figure S4). Indeed, we observed that RCAS-Chdl2 injection in the interdigit area posterior to digit II, resulted in a shorter digit II development, with the same digit formula than digit I, similarly to implantation of a soaked bead with NOGGIN into interdigit (Suzuki et al., 2008).

Altogether, this suggest that *Chrdl2* acts as a likely BMP signaling modulator during digit development. Thus, multiple BMP antagonists are required for digit development, and they may act together to regulate BMP pathway, inducing modulation of BMP pathway activity in time and space during digit development to establish the phalanx *versus* joint cell fate decisions (Lorda-Diez et al., 2013b). However, the differences in their temporal and spatial expression patterns, as well as in their expression levels, makes it likely that intricate cross-regulatory mechanisms are at play. Therefore, *in silico* screens for putative regulatory

interactions, between the different molecules (see also Chapter I), should make targeted experimental interventions more feasible.

Overall, by combining RNA-sequencing, modeling and experimental embryology, we aimed to understand the molecular mechanisms underlying the phalanx *versus* joint cell fate decision and how complex BMP regulation of this process results in diverse digit patterns. This will help to identify the molecules implied in joint and cartilage cells specification, and thus potentially help to produce *in vitro* joint/cartilage-induced embryonic stem cells for treatment of diseases like for example osteoarthritis which is a major medical problem.

Contributions

This study was conceived and designed by the author and Patrick Tschopp. Experimental embryology (microinjection experiments, embryo collection and dissection), embryo processing (embedding and cryosectioning), cloning of probe templates, optimization of staining (*in situ* hybridization and immunohistochemistry) and confocal imaging were carried out by the author. RNA sequencing experiments and subsequent data analyses were conducted by Christian Feregrino and Patrick Tschopp. Troubleshooting of virus production was carried out by Sabrina Fischer and the author.

Supplementary figures

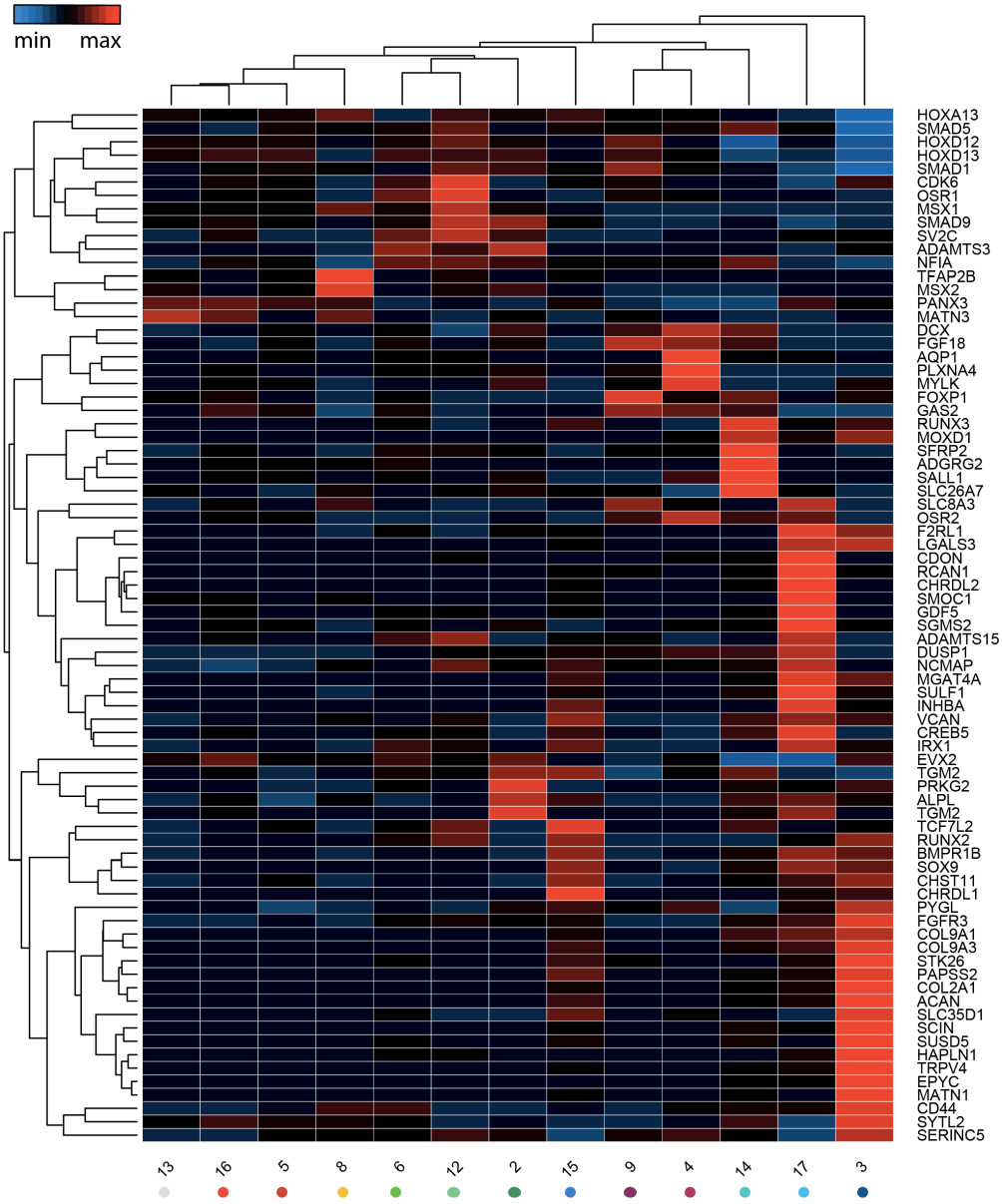

Figure S1. Analysis of chick HH29 hindlimb pseudobulk data. Heatmap visualization of orthologous genes expression across distinct mesenchymal cell sub-cluster in Figure 3C.

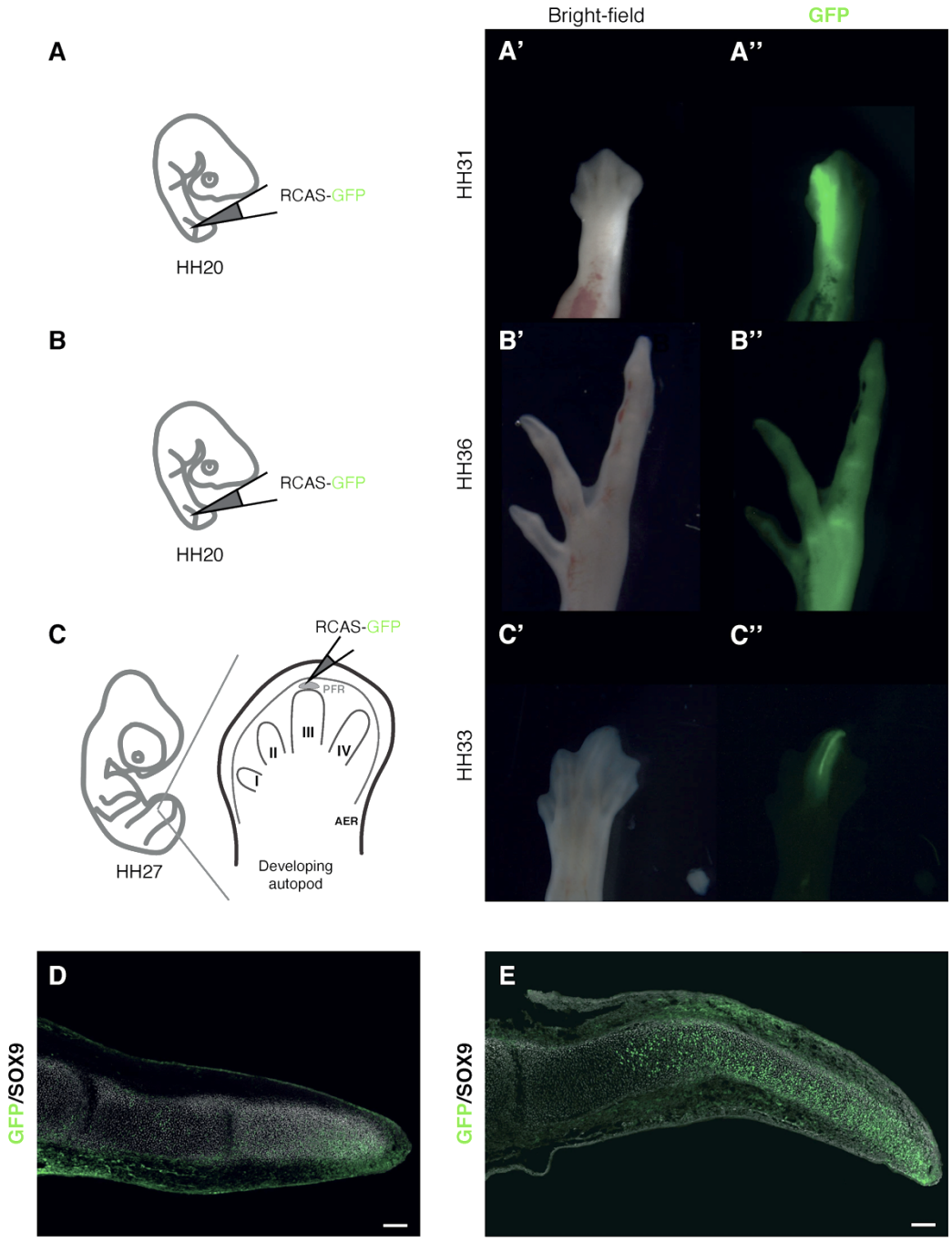

Figure S2. Injection strategies of RCAS viruses. (**A-B**) Scheme of RCAS-GFP injection into limb bud at HH20. (**C**) Scheme of RCAS-GFP injection into PFR at HH27. PFR: Phalanx-forming region. AER: Apical ectodermal ridge. (**A'-A''**) RCAS-GFP infected limb at HH31 after injection into limb bud at HH20. (**B'-B''**) RCAS-GFP infected limb at HH36 after injection into limb bud at HH20. (**C'-C''**) RCAS-GFP infected limb at HH33 after injection into PFR at HH27. (**D**) Immunohistochemistry for GFP and SOX9 in longitudinal digit III sections from limb in panel A'. (**E**) Immunohistochemistry for GFP and SOX9 in longitudinal digit III sections from limb in panel C'. Scale bars = 100 µm.

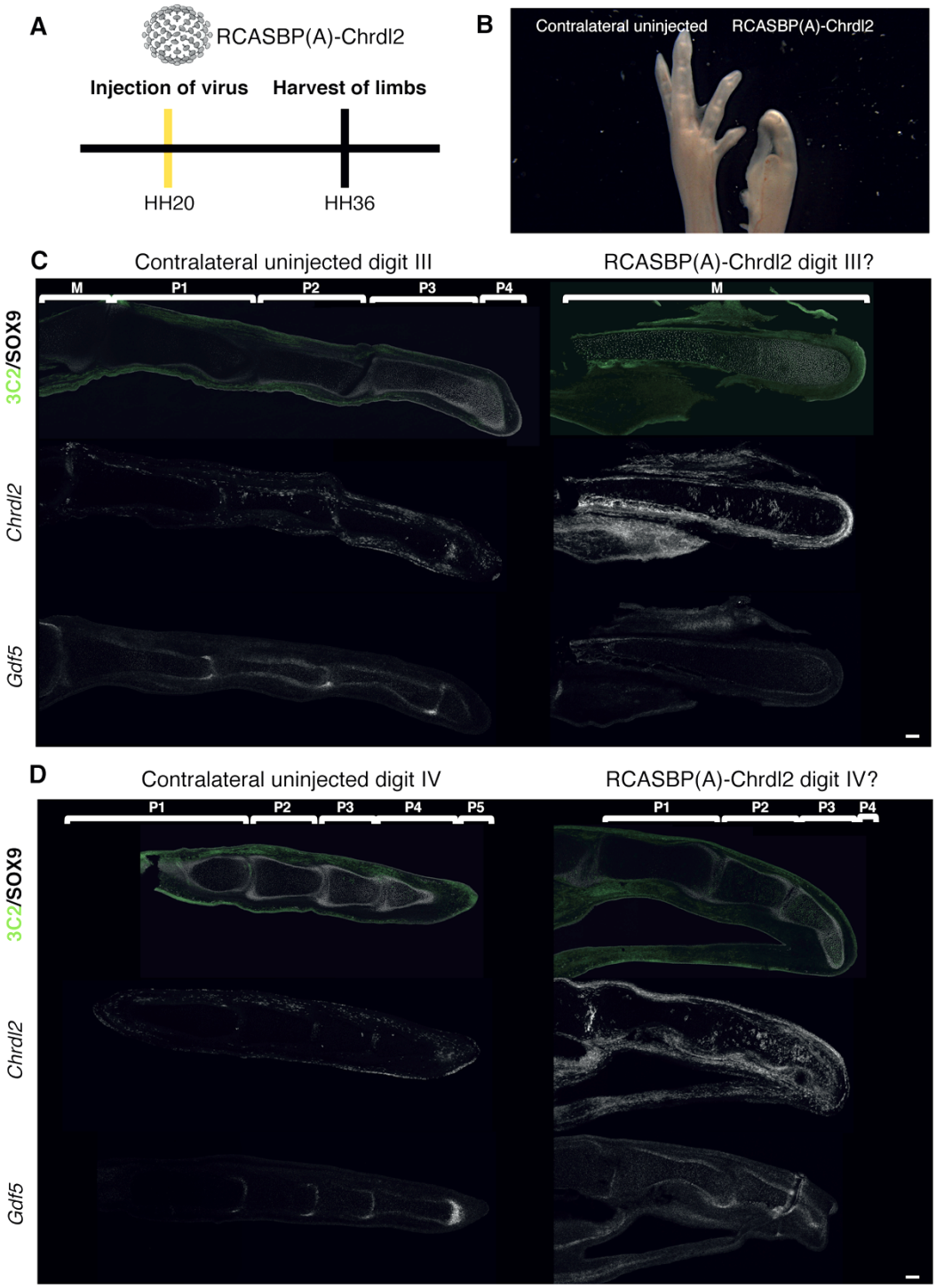

Figure S3. Effect of overexpression of *Chrdl2* on chick leg digit patterning. (**A**) Timeline of the experimental setup of RCASBP(A)-Chrdl2 microinjection into the limb bud. (**B**) RCASBP(A)-Chrdl2 infected limb at HH36 after injection into the limb bud right at HH20 and the contralateral uninjected limb. (**C**) Immunohistochemistry for 3C2 (viral protein) and SOX9 in longitudinal digit III sections from limbs in panel B and fluorescent RNA *in situ* hybridization for *Chrdl2* or *Gdf5* in adjacent longitudinal sections. (**D**) Immunohistochemistry for GFP and SOX9 in longitudinal digit IV sections from limbs in panel B and fluorescent RNA *in situ* hybridization for *Chrdl2* or *Gdf5* in adjacent longitudinal sections. Scale bars = 100 µm.

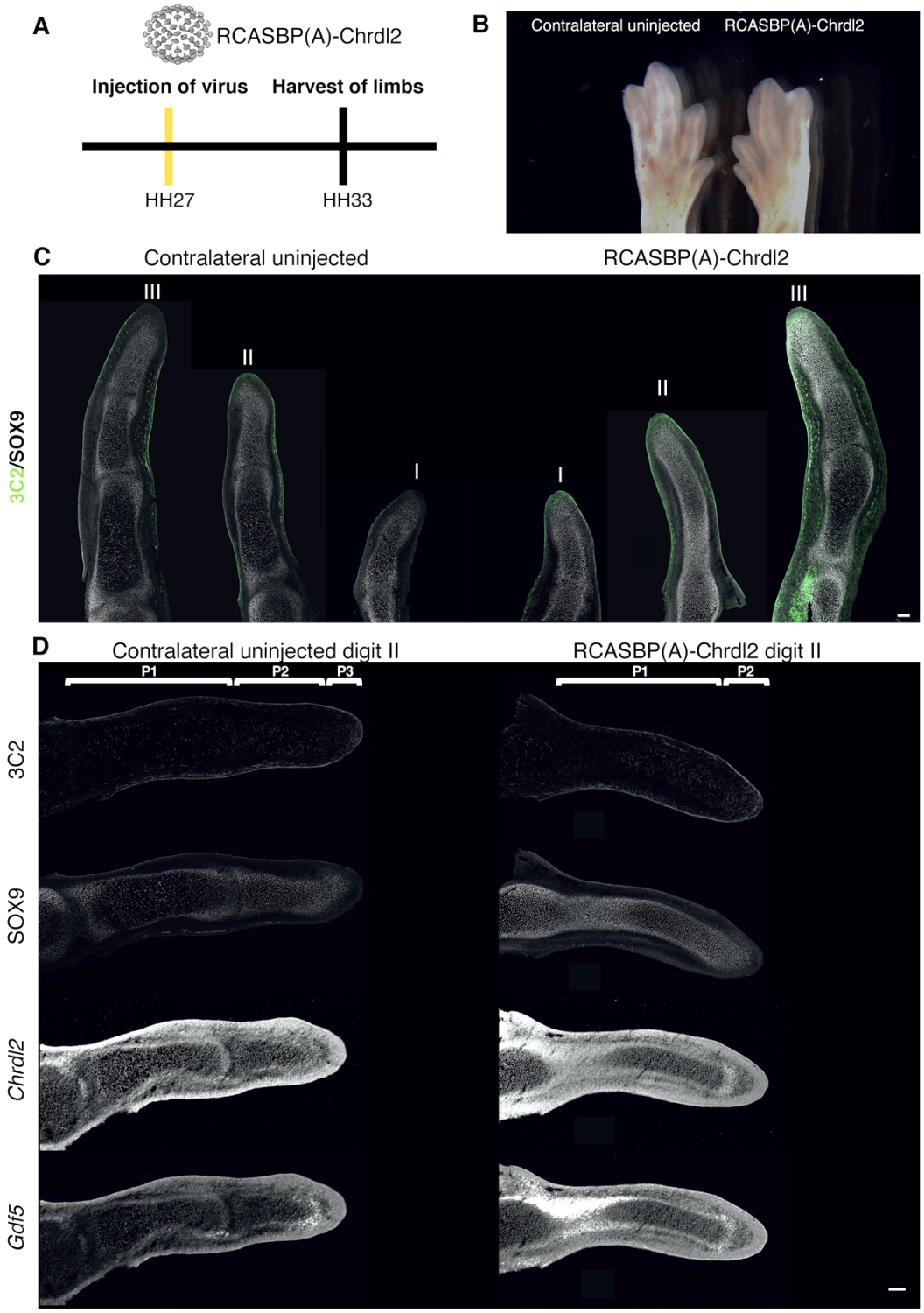

Figure S4. Effect of overexpression of *Chrdl2* in the interdigit. (**A**) Timeline of the experimental setup of RCASBP(A)-Chrdl2 microinjection into the interdigit. (**B**) RCASBP(A)-Chrdl2 infected limb at HH33 after injection into the interdigit between digits II and III of limb right at HH27 and the contralateral uninjected limb. (**C**) Immunohistochemistry for 3C2 (viral protein) and SOX9 in longitudinal sections of digits from limbs in panel B. (**D**) Fluorescent RNA *in situ* hybridization for *Chrdl2* or *Gdf5* in adjacent longitudinal sections of digit II stained for 3C2/SOX9 in panel C. Scale bars = 100 µm.

GENERAL DISCUSSION

Pattern formation is an essential feature of a multicellular organism's development, and variations in patterning mechanisms are thought to contribute substantially to morphological diversification. Throughout nature, repetitive morphological structures are plentiful to be found. For example, tetrapod digits are composed of a series of individual digit bones, the so-called phalanges, connected to each other via synovial joints. Thanks to this modular architecture, morphologically highly distinct digit patterns have emerged over the course of vertebrate evolution. Different numbers of phalanges per digit occur, both within and between species, ranging from a 2-3-4-5-3 phalanx formula in the putative ancestral condition, to a 2-3-4-5 phalanx formula in chicken or a 2-3-3-3-3 in mice (Wagner, 2014; Xu and Mackem, 2013). The TGF-beta superfamily, including signaling through Bone morphogenetic proteins (BMPs), has been implicated in digit segmentation. However, the molecular mechanisms underlying specification and diversification of digit patterns remain unclear. During embryogenesis, at the tip of each growing digit, a delicate balance of cell proliferation and cell type specification in a group of progenitor cells, the phalanx-forming region (PFR), needs to be precisely controlled to ensure proper phalanx patterning.

This thesis work aims at investigating how molecular cues are integrated and interpreted, to orchestrate growth and cell fate decisions at the PFR into either joint or phalanx precursors, and to what extent can these mechanisms be modified on an evolutionary timescale, to generate novel digit morphologies. Accordingly, we aimed to study signaling gradients and self-organization during tetrapod digit pattern formation and evolution. To do so, we reviewed pattern formation and evolution of repetitive morphological structures with a particular focus on the cellular and molecular dynamics necessary for the specification of repetitive patterns of phalanges in the developing digit. To shed light on this pattern formation and diversification, we produced data for growth and signaling dynamics during digit development. Additionally, we explored the establishment of the joint *versus* phalanx cell identity, to understand the patterning relevant cell fate decisions during digit development.

Pattern formation and evolution of repetitive morphological structures

To appreciate the different possible mechanisms involved in digit segmentation, as well as in evolutionary digit pattern diversification, we first investigated general aspects of pattern formation and evolution of repetitive morphological structures. We reviewed experimental and theoretical approaches *in vivo*, *ex vivo*, *in vitro* and *in silico*, to study how positional information might work alongside other mechanisms to assure proper pattern formation and evolution of this repetitive structure. We focused on the formation of repetitive patterns within a directionally growing embryonic field, e.g., phytomers in the plant shoot, somite formation in the elongating

vertebrate primary body axis, and phalanges in the growing tetrapod digit. In all three examples, a proliferating progenitor population at one extremity defines one of the boundaries of the field to be patterned, as well as the directionality of tissue growth. We highlight the role of positional information in defining the temporal and spatial dynamics of such directed growth. Formation of periodic patterns therein appears to rely on a combination of positional information, coming from growth-driven displacements of molecular gradients, with a secondary, putatively self-organizing patterning module. Such combinatorial systems provide overall robustness and evolvability, as the underlying processes are modulated over evolutionary timescales to enable morphological diversification.

Growth and signaling dynamics during digit development: pattern formation and diversification

Several studies have tried to elucidate the underlying mechanisms involved in the specification and patterning of repetitive morphological structures, like phalanges. For example, members of the TGF-beta superfamily, including the Bone morphogenetic proteins (BMP), have been shown to be essential for digit patterning. Several human digit malformation syndromes are caused by mutations in these genes, and studies in animal models have confirmed the importance of a precise regulation of BMP signaling for digit pattern formation (Stricker and Mundlos, 2011). However, the exact roles of the different BMP pathway players, and their regulatory relationship between each other to form a potentially self-organizing process producing periodic phalanx-joint pattern, remains unknown.

Accordingly, we produced quantitative data for growth and signaling dynamics during digit development in the chicken foot and we combined them with *in silico* modelling, in order to understand digit pattern formation and diversification. First, we measured growth dynamics during digit development in chicken. Our results revealed that within a digit, growth rates are different between the phalanges, suggesting a difference in tip proliferation between digits. This difference in tip growth could explain differences in phalanges number. However, to further investigate this hypothesis, additional and more global digit tip proliferation data would be required. Next, we describe transcriptional and signaling dynamics of cell fate decisions during digit patterning at high spatiotemporal resolution. We provide evidence for an alternating pattern of bands of *Noggin* and *Gdf5* expression, which are in phase together, at the future joint region, and pSmad1,5,9 activity, which is out of phase and located inside the presumptive phalanx bone. These spatiotemporal dynamics observed *in vivo* suggested to us a potential role of those genes in a putative self-organizing, Turing-like process controlling phalanges patterning. Accordingly, we proposed a BMP-based Turing model to approximate digit

patterning *in silico* and to recapitulate the spatiotemporal molecular dynamics observed *in vivo*. Simulations support the importance of the model players in the formation of a periodic phalanx-joint pattern. Additionally, the model was able to reproduce different molecular signatures *in silico*, which eventually result in distinct digit morphologies. We thus speculate that the *in silico* model proposed here may help to predict the causative parameter alterations that can transform one species-specific pattern into another, and thus help to identify putative molecular changes underlying digit pattern diversification that occurred during tetrapod evolution.

Despite the success of our model to predict BMP-based Turing model proposed in reproducing digit pattern formation and diversification, the model includes several simplifications, and several points require further attention, e.g. the patterning role of the perichondrium or mechanical cues on PFR formation and maintenance.

Patterning relevant cell fate decisions during digit development: establishment of the joint *versus* phalanx cell identity

The frequency of phalanx-joint patterns within digits relies on the spatiotemporal control of cell fate decisions at the PFR, into either phalanx or joint progenitors that will eventually differentiate into the structures shaping a digit. Several cues may induce periodic specification of these progenitors, however how these cues received by the PFR are interpreted, to allow the phalanx *versus* joint cell fate decisions during digit development, is still not fully known. To identify putative novel regulators of cell fate decisions, we performed single-cell RNA-sequencing, pseudotime analyses and experimental embryology using viral mis-expression.

We first traced the digit progenitor cell lineage, to figure out the origin of joint and phalanx cells. We have evidence that indeed progenitors of both cell types are coming from the PFR. Next, we analyzed the expression patterns of several maker genes and report their transcriptional signatures specific to the different cell populations emanating from the PFR. In addition, we provide a non-exhaustive list of genes whose combinatorial expression constitutes a transcriptional signature to identify this central cell population involved in tetrapod digit development. Then, we used single-cell RNA-sequencing data and pseudotime analysis to analyze the transcriptional dynamics of digit patterning along the digit progenitor cell lineages. Thank to these analyses, we identified candidate genes for cell fate decision regulation during digit development. We focused our investigation on the role of *Chrdl2*, a gene proposed to be a BMP pathway regulator (Nakayama et al., 2004). Ectopically overexpressing *Chrdl2* in the developing digit inhibits the formation of phalanx condensations, possibly through an alteration of the BMP pathway, with mis-regulation of *Gdf5* expression and a loss of the PFR, resulting in the development of truncated digits, as well as persistence of interdigit tissue. These

observations support the importance of BMP signaling modulation by antagonists during digit development. Therefore, it appears that multiple BMP antagonists are required for digit development, and through precise cross-regulation in time and space they regulate the BMP pathway, inducing modulation of BMP pathway activity to establish proper phalanx *versus* joint cell fate decisions (Lorda-Diez et al., 2013b). Moreover, these different pathway modulators might be important in different phases of digit development. Accordingly, it would be interesting to investigate the expression patterns of *Noggin* following ectopic expression of *Chrdl2* within the PFR. Additionally, the BMP pathway activity was only investigated after an early injection of RCAS-Chrdl2 into the limb bud inducing a severe phenotype. Thus, we will investigate the BMP pathway activity after a late injection of RCAS-Chrdl2 into the PFR, followed by whole mount immunohistochemistry for pSmad1,5,9, the readout of the BMP pathway activity, combined with whole mount *in situ* hybridization for *Chrdl2*, a technique that I already optimized in lab.

Conclusion

In this thesis, I presented a combination of *in vivo* and *in silico* data to analyze the developmental dynamics of digit progenitor proliferation and specification into phalanx *versus* joint progenitor cells. I produced quantitative data for *in vivo* growth and spatiotemporal transcriptional dynamics of digit patterning, and combined it with *in silico* modeling, to understand how patterning and cell fate decisions are coordinated to give rise to different digit morphologies. Additionally, using single-cell RNA-sequencing and Pseudotime analyses, we defined potential novel regulators of cell fate decisions of the joint and phalanx precursors shaping a digit. Altogether, our observations suggest that the broad morphological diversity of digits emerged from the spatial re-organization of a heavily conserved self-organizing mechanism involving a cross-regulation of BMP pathway gene members. The different analyses performed for this thesis work complement each other. Given that we now can use *in silico* screens for putative alterations in these regulatory interactions, between different candidate molecules, we can define experimental analyses to test the prediction of the model. Conversely, we can use experimental data and analyses to refine the *in silico* model.

Collectively, by studying pattern formation and evolution in tetrapod digits, this thesis work helps us to shed light on the patterning mechanisms occurring during digit development, and to identify candidate molecules potentially involved in joint and phalanx progenitor specification. This experimental and theoretical combinatory approach may thus contribute to our understanding of the mechanisms underlying tetrapod digit patterns specification and diversification.

MATERIALS AND METHOD

1. Embryo tissue sampling and processing

a. Chicken embryos

Fertilized chicken eggs were incubated at 38°C in a humified incubator to be harvested and staged according to the Hamburger-Hamilton developmental table (Hamburger and Hamilton, 1951). The embryos were harvested in ice-cold PBS and desired samples were dissected and fixed with 4% paraformaldehyde for 2 h on ice.

For whole mount *in situ* hybridization, samples were first dehydrated in a gradient of methanol dilutions in PBS (25%, 50%, 75%) and then stored in 100% methanol at -20°C.

For cryosections, desired samples were equilibrated and dehydrates in sucrose gradient solutions with: 10% sucrose/PBS and 30% sucrose/PBS. For embedding, the desired samples were mounted in OCT and frozen at -80°C. cryosectioning was performed at 18 µm thickness, with a Leica cryostat and transferred onto Superfrost Plus slides, which were then stored at -80°C until staining.

b. Mouse embryos

DupC mouse embryos were provided by Dr. Daniel Ibrahim and Prof. Dr. Stefan Mundlos of the MPI for Molecular Genetics, Berlin, Germany. Genotyping of the DupC mouse was done by performing quantitative PCR (qPCR), to quantify the genomic copy levels of Kcnj2 in DupC mice, to determine their genotype: wild type, heterozygous or homozygous for the DupC allele. All mouse samples were stored in 100% Methanol at -20°C. To prepare the samples for embedding, they were rehydrated in gradient dilutions of methanol in PBS (75%, 50%, 25%), then washed in PBS and equilibrated and dehydrated in gradient solutions with sucrose: 10% sucrose/PBS and 30% sucrose/PBS. For embedding, the desired samples were mounted in OCT and frozen at -80°C. 18 µm cryosections were performed with a Leica cryostat and transferred onto Superfrost Plus slides, which were then stored at -80°C until staining.

2. Microinjections of chicken embryos

Fertilized chicken eggs were incubated at 38°C in a humified incubator. When experiments were performed with viruses, special pathogen-free (SPF) fertilized chicken eggs were used (INRAE, Nouzilly FRANCE). Before injection, 3 mL of albumen was removed with a 18G needle on a syringe. Eggs were opened by cutting a small window in the shell and staged according to the Hamburger-Hamilton developmental table (Hamburger and Hamilton, 1951). The desired solution (DiI or virus solution) was injected with a pulled glass capillary needle into the desired area (limb bud or PFR). After injection, some drops of 1% Penicillin-

Streptomycin/PBS were added on the top of the embryo and the window was sealed with scotch tape. Eggs were put back in incubator at 38°C until the desired stage.

3. BrdU Administration

Fertilized chicken eggs were incubated at 38°C in a humified incubator. Before BrdU administration, 3 mL of albumen was removed with a 18G needle on a syringe. Eggs were opened by cutting a small window in the shell and staged according to the Hamburger-Hamilton developmental table (Hamburger and Hamilton, 1951). 250 µL of undiluted BrdU solution (Cytivia RPN201) was injected with a 30G needle on a syringe into the amniotic cavity of embryos at stage HH29 (day 6). After injection, some drops of 1% Penicillin-Streptomycin/PBS were added on the top of the embryo and the window was sealed with scotch tape. Eggs were put back in incubator at 38°C. 3 h after BrdU application, embryos were harvested in ice-cold PBS and desired samples were dissected and fixed with 4% paraformaldehyde for 2 h on ice. Samples were prepared for cryosection as described above.

4. RCAS virus production and optimization

a. Standard transfection and virus production workflow

A cDNA fragment containing the entire coding region of the chicken *Chrdl2* gene was cloned into the plasmid vector pSlax13 and subcloned into RCASB(A) plasmid. Viruses were produced based in part of previous descriptions (Logan and Tabin, 1998) (Figure 1A). 180 000 cells of the chicken embryo fibroblast cells line DF1 were seeded onto a 6 cm dish in 4 mL of complete growth medium (DMEM complemented with 10% FBS and 1% Penicillin/Streptomycin). 3 days after, cells reached 70-90% confluency and complete growth medium was replaced with 2,6 mL of medium without antibiotics. 6 µg of RCASBP(A)-gChrdl2 or RCASBP(A)-GFP plasmid diluted in 200 µL of Opti-MEM was mixed with 1:80 Lipofectamine/Opti-MEM. After 20 min, the Lipofectamine-DNA mix was added dropwise on all the surface of the plate and mixed gently. Cells were incubated for 4-6 h, then the medium was changed. 2 days after, cells were confluent and were subcultured to two 10 cm dishes. For RCAS-Chrdl2 virus, which not possessed a fluorescent protein, 20 µL of trypsinized cells were seed in a well of a 24-well plate with 350 µL of complete growth medium and a day after, cells were fixed and stained for 3C2 to check the success of the transfection (see Protocol for Titration below). 2 days after, cells were confluent and were subcultured to five 15 cm dishes. 2 days after, when cells were superconfluent, medium was replaced with DMEM complemented with 1% FBS and 1% Penicillin/Streptomycin. The next day, the cell culture

medium containing viral particles was harvested and that for 2 more consecutive days. Viral supernatants were frozen and stored at -80°C.

b. Concentration of virus

Tubes containing viral supernatants were thawed in a water bath at room temperature and inverted during thaw. Once supernatants thawed, they were placed on ice. Supernatant were centrifuged at 750 g for 15 min at 4°C in a JA-12 rotor (Deceleration: 5) and filtered using a 0,48 µm filter to remove cell debris. Filtered supernatants were placed in Ultraclear centrifuge tubes (Beckman-Coulter) (an aliquot was kept for subsequent virus titration). Filtered supernatants were ultracentrifuged at 21 000 rpm for 3 h at 4°C in a SW28 rotor (Acceleration: 3 and Deceleration: 6). After the centrifugation, buckets of the rotor were placed carefully on ice. The supernatants were gently discarded by inversion over a beaker and the remaining medium at the entrance of the tube was aspirated with glass Pasteur pipette placed on a vacuum pump. Then, Ultraclear tubes were dried by inverting them for 1 min. Additionally, the 2/3 of the tube wall were dried with a paper towel wrapped around the finger so that a minimum of solution remains in the tubes. The ultraclear tubes were sealed with parafilm and put on ice. They were shaken at 140 rpm for 2 h at 4°C. After shaking, the viral pellet in each Ultraclear tube was resuspended by pipetting 50 times all around the pellet and then 50 times on the pellet without making bubbles. To avoid repeated freeze/thaw of the stocks, 10 µL aliquots of the concentrated viral suspension were prepared and stored at -80°C.

c. Titration of virus

To know the approximate titer of the concentrated viral solution, DF1 cells were infected with serial dilutions of the concentrated and unconcentrated virus solutions. To do so, 40 000 cells were seeded per well of a 24-well plate in 350 µL of complete growth medium. 2 days after, cells reached 70-90% confluence and complete growth medium was replaced with serial dilutions of supernatants, the unconcentrated virus solution (1, 1:5, 1:10, 1:50 and 1:1000) and dilutions of concentrated virus solution (1:1000, 1:10 000, 1:100 000, 1:1 000 000 and 1:10 000 000). After 2 days, assay for viral infection was performed via FACS, for RCAS-GFP, and *via* immunohistochemistry for 3C2, for RCAS-Chrdl2.

For FACS analyses, cells were trypsinized and fixed in 4% PFA for 8 min at room temperature and the percentage of GFP-positive cells were measured on a BD FACSAria™ III.

For immunohistochemistry for 3C2, cells were fixed in well with 4% PFA for 8 min at room temperature. After fixation, cells were washed with PBS and then permeabilized in 350 µL/well of PBS-Triton (1X PBS with 0,1% Triton) for 10 min. Cells were then washed and blocked in

300 µL/well of 10% HIGS/PBS for 1 h at room temperature. Cells were incubated overnight at 4°C with 3C2 antibody (DSHB AMV-3C2 mouse) diluted 1:50 in 1% HIGS/PBS. The day after, cells were washed in PBS and incubated 1 h at room temperature with secondary antibody, biotinylated anti-mouse diluted in 1% HIGS/PBS. Cells were then washed with PBS and incubated 1 h at room temperature with amplification complex, streptavidin conjugated with alkaline phosphatase, diluted in 1% HIGS/PBS for 1 h at room temperature. After incubation, cells were washed with PBS and then 10 min with 1X TBS (For 1 L of 10X TBS: 80 g NaCl, 2 g KCl in ddH_2O, 250 mL 1 M Tris pH 7,5, Adjust pH to 7,4 with HCl, Complete with ddH_2O). To detect 3C2, and thus infected cells, cells were incubated for 8 min in 450 µL/well of development solution (For 5,1 mL of development solution: 0,5 mL 1 M Tris pH 9.5, 0,1 mL 5 M NaCl, 4,4 mL ddH_2O and 100 µL NBT/BCIP).

d. Optimization of virus production

Before investigation the effects of ectopic *Chrdl2* expression, we needed to troubleshoot virus production, to get more efficient viral transduction. During virus production, the timing to harvest the culture medium containing viral particles is important. In the lab, we tried two different timepoints, to see which one allows to collect culture medium most highly concentrated in viral particles, and thus to get the highest titer of virus at the end of the production. To do so, we produced RCAS-GFP virus, containing the maker gene of the GFP, to be able to visualize the infected cells that can be easily counted by looking in a microscope or with FACS analysis. We first transfected the cells with a plasmid encoding for RCAS-GFP virus and expanded the cells (Figure 1B). Cells were then subcultured in order to have them confluent “early” or “late” after the transfection, meaning to have them covering the surface of the dish early or late after the transfection. The collection of the culture medium containing the viruses, the viral supernatant, is done on 3 consecutives days: day 9 to 11 after the transfection in the “early confluent” condition and day 11 to 13 in the “late confluent” condition. Next, concentration of the supernatant, using an ultracentrifuge, was performed in both conditions to get concentrated solutions of viruses. Then, in order to know with which condition we get the viruses with higher titer, we performed titration of both of the virus solutions. To do so, we infected cells with dilution of the concentrated supernatant or the unconcentrated supernatant, used as a control to check if the virus solution was concentrated after ultracentrifugation (Figure 1C). Then, calculation of infection efficiency was measured by FACS. FACS analysis shows us that in both conditions we managed to concentrate viruses and to get efficient viruses (Figure 1D). Indeed, infecting cells with concentrated solution of viruses diluted at 1 in 1000 allow us to get more than 50% of infection: 67,8% in the “early confluent” condition and 52,3%

in the “late confluent” condition. The FACS analysis indicates also that the “early confluent” condition allows us to get higher titer for viruses. Thus, we decided to follow the “early confluent” condition for the subsequent virus production.

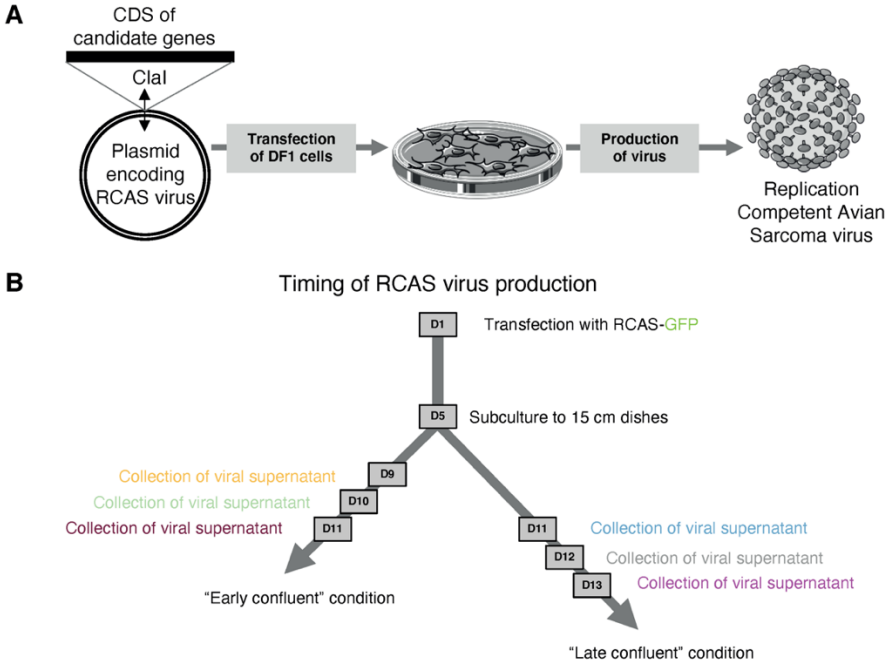

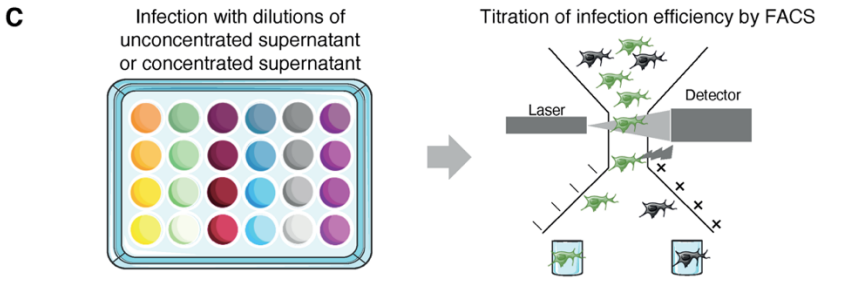

D

Sample	%GFP+
EC unconcentrated day 1 diluted 1:10	82,7
EC unconcentrated day 1 diluted 1:100	20,7
EC unconcentrated day 2 diluted 1:10	91
EC unconcentrated day 2 diluted 1:100	33,1
EC unconcentrated day 3 diluted 1:10	92,3
EC unconcentrated day 3 diluted 1:100	35,7
EC concentrated diluted 1:100	99,7
EC concentrated diluted 1:1 000	98,3
EC concentrated diluted 1:10 000	67,8
EC concentrated diluted 1:100 000	14,2

Sample	%GFP+
LC unconcentrated day 1 diluted 1:10	78,3
LC unconcentrated day 1 diluted 1:100	22,3
LC unconcentrated day 2 diluted 1:10	86,5
LC unconcentrated day 2 diluted 1:100	27,4
LC unconcentrated day 3 diluted 1:10	91
LC unconcentrated day 3 diluted 1:100	34,6
LC concentrated diluted 1:100	99,5
LC concentrated diluted 1:1 000	96
LC concentrated diluted 1:10 000	52,3
LC concentrated diluted 1:100 000	8,4

Figure 1. Standard workflow and optimization of virus production. (**A**) Scheme of RCAS virus production process. (**B**) Timeline of virus production in “early confluent” or “late confluent” conditions. (**C**) Titration of RCAS virus infection efficiency. (**D**) Percent of GFP positive cells in function of the different conditions and concentrations to estimate the RCAS virus titer.

5. Immunohistochemistry on cryosections

Different buffers were used for immunochemistry, depending on the primary antibody used. For GDF5, NOGGIN and pSmad1,5,9, TNT buffer was used (For 1 L of TNT: 100 mL 1 M Tris pH 7,5, 30 mL 5 M NaCl, 870 mL ddH_2O and 0,05% Tween). For 3C2, BrdU, GFP and Sox9, PBST buffer was used (For 1 L of PBST: 1X PBS with 1 mL 100X Triton, 2 g BSA and 1 mL 20% SDS).

Cryosections were first thawed and air dried for 15 min at room temperature. To remove OCT, slides were washed 3 times in TN for the 'TNT buffer protocol' and in PBS for the 'PBST buffer protocol'. For BrdU, GDF5, GFP, NOGGIN, pSmad1,5,9 and SOX9, a step of antigen retrieval was needed. To do so, slides were incubated in 1:5000 Proteinase K in TN for 10 min at room temperature, then rinsed in TN or PBS, post-fixed for 5 min in 4% PFA and rinsed in TN or PBS. For BrdU staining an additional step of DNA denaturation after antigen retrieval was performed. For that, slides were incubated in 2N HCl for 30 min at 37°C. For pSmad1,5,9, a step to inactivate endogen peroxidases was performed with 0,3% H_2O_2 in TN for 1 h at room temperature. Then, all slides were blocked in either 0,5% BR/TNT or PBST for 1 h at room temperature. Primary antibodies were diluted (see Table I) in either 0,5% BR/TNT or PBST and incubated in a humid chamber overnight at 4°C. Slides were washed 3 times in TNT or PBST and incubated with secondary antibodies diluted in either 0,5% BR/TNT or PBST for 1h at room temperature. Slides were washed 3 times in TNT or PBST. For GDF5, pSmad1,5,9 and SOX9, signals were amplified using biotinylated secondary antibodies. For GDF5, detection was done with a streptavidin-conjugated alkaline phosphatase, and revelation was done in 1:100 NBT/BCIP in NTM for 10 min. For pSmad1,5,9, detection was done with streptavidin-conjugated peroxidase and revelation was done with the TSA Plus Cyanine 3 or 5 (Akoya Biosciences). For SOX9, detection was done with streptavidin-conjugated fluorophore. For the other antibodies, direct detection was done with secondary antibodies conjugated with fluorophores. Finally, slides were mounted with Fluoromount aqueous mounting medium (Sigma) and imaged with a confocal microscope (Olympus Fluoview FV3000).

Table I. Antibodies used for immunohistochemistry

Antibody	Reference	Dilution
3C2	DSHB AMV-3C2 mouse	1:30
BrdU	Sigma B8434-25UL mouse	1:200
GDF5	Abcam ab137698 rabbit	1:50
GFP	Abcam ab13970 chicken	1:1000

NOGGIN	Abcam ab16054 rabbit	1:100
pSmad1,5,9	Cell Signaling 13820S rabbit	1:300
SOX9	Millipore AB5535 rabbit	1:1000

6. *In situ* hybridization probe production

Probe templates were cloned into the pGEM-T easy or pSlax13, which contain, respectively, SP6 and T3, or T3 and T7 polymerase binding sites for transcription of antisense probes (see Table II). Template plasmids for the synthesis of *gGdf5*, *gSox9*, *mGdf5* and *mKcnj2* probes come from the collection of the lab.

Probe templates were amplified by PCR. *In vitro* transcription was carried out using T3, T7 or SP6 RNA polymerase (Promega) and digoxigenin or fluorescein labeled nucleotides (Roche). Probes were purified with RNeasy mini kit (QUIAGEN) and stored at -80°C.

Table II. Cloning primers of *in situ* hybridization probes

Probe	Forward primer (5'>3')	Reverse primer
gBmpr1b	GATACAAATGAGGTAGACATCCCTCCAAAC	CTGTATATCCCTGTGTAAACAAGGGCAG
gChrdl1	CATGAGAAGAAAGTGGAGATCGG	AAGAATTCAGCTTAACAGTGACCCTTTTCA
gChrdl2	ATGCTCCCCGGTGCGGGTCC	CTGTTTGCTGATCTTCTTGG
gCreb5	AAGAATTCAGCATGATTTATGAGGAATCAAAGATGAACTTGGAGC	AAGAATTCAGCTTAAAGGATGGGGTTGATGTCTGTTCT
gDusp1	AAGAATTCAGCATGGTGAACCTGCGGGTGTGTGC	AAGAATTCAGCTCAGCAGCTCGGGGAGGTGG
gGas1	ACTCGGGGATCCTAGCGCTG	GAAATCCACCTTCCTTAGCTG
gInhba	CACACGTGTCTATGAACAGC	GAAAACGTTGCACTTTGAG
gNoggin	ATGGATCATTCCCAGTGCC	CTAGCAGGAGCACTTGCACTCC
gRcan1	CATGCATTTTAGAAACTTTAACTACAGTTTTAGTTCTCTGATTGCC	AAGAATTCAGCTCAGCTTAAATGGGAAGGAG
gSmoc1	CATGCCGCCCCGGGCCTGG	AAAAGCTTAGCCTACACCAAGCGGCCTATGAAAGGGTTAAGGCCTTGT
gSprty2	GAATATCTGCTCCAACGATGATGAGGAC	GGAGGGGTGACACTTGTAAGATGC
gTcf7l2	AAAGAGAGTGCAGCCATCAACCAAATCC	AGGATGGCGGCGGCATCATG
mCreb5	AGCTCCACCCTCAGTCAGCTTA	TTCATGGGATATGGATGGACCATAA
mDusp1	GTCATCCCAGTAACAAAATGTCTTCTC	TGGGAGCTGGTCCTTATTTATTTAACAC
mGas1	GGATCCTTAATTCTAAGACAC	CGGTCAAAGAGAACATGGCCC
mInhba	CTTTAGGCACAGCCAGGAAG	GCCACTGTCTTCTCTGGACTCTC
mRcan1	CCAGAAGAGCATATTGTGCTGATTT	TTTCACCCCCATTGAAACGTGAA
mSmoc1	AGGAGACAGGACTGACCGTCAGACA	TCTGAAATCCATGCTGGCCAGCACA

7. *In situ* hybridization (whole mount, non-fluorescent or fluorescent on cryosections)

Whole mount *in situ* hybridization and non-fluorescent *in situ* hybridization on cryosections were performed according to standard protocols (for details, see (McGlinn and Mansfield, 2011)).

For fluorescent *in situ* hybridization on cryosections, hybridization of the probe was performed as for non-fluorescent *in situ* hybridization, as were the post-hybridization washes. Slides were then washed in TNT (For 1 L of TNT: 100 mL 1 M Tris pH 7,5, 30 mL 5 M NaCl, 870 mL ddH_2O and 0,05% Tween). Inactivation of endogen peroxidases was performed with 0,3% H_2O_2 in TN for 1 h at room temperature. Then, slides were blocked in 0,5% BR/TNT for 1 h at room temperature. Incubation with anti-digoxigenin or anti-fluorescein-POD (Roche) diluted 1:300 in 0,5% BR/TNT was performed in a humid chamber overnight at 4°C. Slides were washed 8 times 10 min in TNT. Revelation was done with 1:50 TSA Plus Cyanine 3 or 5 (Akoya Biosciences) for 1 h at room temperature. Slides were then washed 2 times in TNT and 4 times in PBSTT (1X PBS with 0,1% Triton and 0,05% Tween). Finally, slides were mounted with Fluoromount aqueous mounting medium (Sigma) and imaged with a confocal microscope (Olympus Fluoview FV3000).

Multiple fluorescent *in situ* hybridization on cryosections was performed as fluorescent *in situ*, with hybridization at the same time for both probes, one labeled with digoxigenin, the other with fluorescein nucleotides. Then revelation was performed first with anti-digoxigenin-POD (Roche) followed by TSA Plus Cyanine 3 (Akoya Biosciences). Then an inactivation step of the peroxidase was performed in 0,6% H_2O_2/TNT for 1 h at room temperature. The second revelation was performed with anti-fluorecein-POD (Roche) followed by TSA Plus Cyanine 5 (Akoya Biosciences).

Fluorescent *in situ* hybridization combined with immunohistochemistry for pSmad1,5,9 was performed by doing fluorescent *in situ* hybridization followed by immunohistochemistry in TNT buffer as describe above.

8. Measurements of phalanx lengths

Chicken hindlimbs were collected at different time points, along a developmental timecourse: every 4 h from 128 to 204 h and every 8 h from 204 to 336 h. A maximum of 2 embryos were collect per time point and both hindlimbs of each embryo were dissected. Chromogenic or fluorescent *in situ* hybridization for *Gdf5* was performed on early stages, and simple DAPI stain on later stages. Slides were imaged with a confocal microscope (Olympus Fluoview FV3000).

Pictures were stitched with Pairwise-stitching plug-in in Fiji. Measurements of phalanges were performed on pictures with Fiji, by drawing a line going from the middle of a joint to the middle of the following joint, or from the most distal joint, the last joint, to the AER. Plots of the digit and phalanx growths were done in R studio.

9. Measurements of fluorescence profiles in digit

Slides were imaged with a confocal microscope (Olympus Fluoview FV3000). For digit sections stained with pSmad1,5,9, 3 Z-stack pictures were acquired with 8 µm steps between the virtual sections. Pictures were stitched with the Pairwise-stitching plug-in in Fiji. After image processing, measurements of fluorescence in function of the distance from the AER within the digit domain were performed on pictures with Fiji, by measuring pixel intensity along a line with a width of 100 pixels draw along the digit (Analyze>Plot profile). Fluorescence intensity measurements were normalized to rescale the data between 0 and 1 based on the maximum and minimum value (Max=1; Min=0). Finally, plots of normalized fluorescence intensity (NFI), in function of digit domain, and heatmap visualizations were done in R studio.

10. Measurement of non-nuclear versus nuclear fluorescence intensity

To quantify the nuclear signal of our NOGGIN IHC, a DAPI mask inverted signal was subtracted from the fluorescent staining signal with Fiji. To obtain a picture of the non-nuclear signal, the original DAPI mask signal was subtracted from the fluorescent staining signal. Fluorescence intensity measurements were done on about 50 cells at the proximal end and 50 cells at the distal end of the phalanx. To do so, cells were freehand selected and measurements of the mean grey value among cells was obtained with Fiji. Plots of non-nuclear *versus* nuclear fluorescence intensity measured on cells in proximal end and distal end of the phalanx were produced in R studio.

11. Pseudotime analyses

Pseudotime analyses were performed with autopod HH29 single-cell RNA-sequencing data previously published in (Feregrino et al., 2019). Briefly, clustering analyses were performed with the toolkit Seurat v3.1.4 (Stuart et al., 2019), in R studio. Only the chondrocyte clusters were used to analyze the branching points. Using highly variable genes, a diffusion map was calculated with the R package Destiny (Angerer et al., 2016). Calculation of pseudotime trajectories was performed with Slingshot (Street et al., 2018). Finally, differential expression analysis along the pseudotime was done using the MAST package (Finak et al., 2015), and expression heatmaps were visualized in R studio.

12. Bulk RNA-sequencing of mouse chondrocytes and joint progenitors

Gdf5- (Rountree et al., 2004) or Sox9-Cre (Akiyama et al., 2005) mouse strains were crossed with Rosa26-LoxP-tdTomato_STOP-LoxP-GFP reporter mouse. Embryos resulting from these crosses were harvested at E14.5, and dissected in ice-cold PBS. GFP+ fluorescent tissue was microdissected under a stereoscope, and dissociated using a combined Trypsin and Collagenase digest for 30 min at 37 °C. To isolate proximal or distal *Gdf5*+ cells and proximal or distal *Sox9*+ cells, cell suspensions were FACS-sorted using the GFP channel on a BD FACSAria™ II. Between 20'000 and 150'000 cells were collected, and RNA was extracted using the PicoPure™ RNA Isolation Kit (Thermo Fisher). Sequencing libraries were produced using the Arcturus PicoPure RNA Isolation Kit (Life Technologies) and enriched for mRNA fraction using MPG mRNA Purification Kit (PureBiotech). Multiplexed RNA-seq libraries were produced using the SPIA cDNA synthesis kit and the Ovation Ultralow DR Multiplex system (NuGen). Sequencing was performed at the HMS Biopolymers Facility. Reads were aligned and quantified using the the RNA-seq unified mapper (RUM) (Grant et al., 2011). All data analysis and visualization was performed in R, using edgeR (Robinson et al., 2010) GO-seq (Young et al., 2010) and base R graphic packages.

REFERENCES

Abley, K., De Reuille, P.B., Strutt, D., Bangham, A., Prusinkiewicz, P., Marée, A.F.M., Grieneisen, V.A., and Coen, E. (2013). An intracellular partitioning-based framework for tissue cell polarity in plants and animals. Development *140*, 2061–2074.

Aires, R., de Lemos, L., Nóvoa, A., Jurberg, A.D., Mascrez, B., Duboule, D., and Mallo, M. (2019). Tail Bud Progenitor Activity Relies on a Network Comprising Gdf11, Lin28, and Hox13 Genes. Dev Cell *48*, 383-395.e8.

Akam, M. (1995). Hox genes and the evolution of diverse body plans. Philos Trans R Soc Lond, B, Biol Sci *349*, 313–319.

Akiyama, H., Chaboissier, M.-C., Martin, J.F., Schedl, A., and de Crombrugghe, B. (2002). The transcription factor Sox9 has essential roles in successive steps of the chondrocyte differentiation pathway and is required for expression of Sox5 and Sox6. Genes Dev *16*, 2813–2828.

Akiyama, H., Kim, J.-E., Nakashima, K., Balmes, G., Iwai, N., Deng, J.M., Zhang, Z., Martin, J.F., Behringer, R.R., Nakamura, T., et al. (2005). Osteo-chondroprogenitor cells are derived from Sox9 expressing precursors. Proc Natl Acad Sci U S A *102*, 14665–14670.

Allen, J.M., McGlinn, E., Hill, A., and Warman, M.L. (2013). Autopodial development is selectively impaired by misexpression of chordin-like 1 in the chick limb. Dev. Biol. *381*, 159–169.

Angerer, P., Haghverdi, L., Büttner, M., Theis, F.J., Marr, C., and Buettner, F. (2016). destiny: diffusion maps for large-scale single-cell data in R. Bioinformatics *32*, 1241–1243.

Antebi, Y.E., Linton, J.M., Klumpe, H., Bintu, B., Gong, M., Su, C., McCardell, R., and Elowitz, M.B. (2017). Combinatorial Signal Perception in the BMP Pathway. Cell *170*, 1184-1196.e24.

Archer, C.W., Dowthwaite, G.P., and Francis-West, P. (2003). Development of synovial joints. Birth Defects Res. C Embryo Today *69*, 144–155.

Askary, A., Mork, L., Paul, S., He, X., Izuhara, A.K., Gopalakrishnan, S., Ichida, J.K., McMahon, A.P., Dabizljevic, S., Dale, R., et al. (2015). Iroquois Proteins Promote Skeletal Joint Formation by Maintaining Chondrocytes in an Immature State. Dev Cell *35*, 358–365.

Aulehla, A., and Johnson, R.L. (1999). Dynamic expression of lunatic fringe suggests a link between notch signaling and an autonomous cellular oscillator driving somite segmentation. Dev Biol *207*, 49–61.

Aulehla, A., and Pourquié, O. (2010). Signaling gradients during paraxial mesoderm development. Cold Spring Harb Perspect Biol *2*, a000869.

Aulehla, A., Wehrle, C., Brand-Saberi, B., Kemler, R., Gossler, A., Kanzler, B., and Herrmann, B.G. (2003). Wnt3a plays a major role in the segmentation clock controlling somitogenesis. Dev Cell *4*, 395–406.

Aulehla, A., Wiegraebe, W., Baubet, V., Wahl, M.B., Deng, C., Taketo, M., Lewandoski, M., and Pourquié, O. (2008). A beta-catenin gradient links the clock and wavefront systems in mouse embryo segmentation. Nat Cell Biol *10*, 186–193.

Bajard, L., Morelli, L.G., Ares, S., Pécréaux, J., Jülicher, F., and Oates, A.C. (2014). Wnt-regulated dynamics of positional information in zebrafish somitogenesis. Development *141*, 1381–1391.

de Bakker, M.A.G., Fowler, D.A., den Oude, K., Dondorp, E.M., Navas, M.C.G., Horbanczuk, J.O., Sire, J.-Y., Szczerbińska, D., and Richardson, M.K. (2013). Digit loss in archosaur

evolution and the interplay between selection and constraints. Nature *500*, 445–448.

de Bakker, M.A.G., van der Vos, W., de Jager, K., Chung, W.Y., Fowler, D.A., Dondorp, E., Spiekman, S.N.F., Chew, K.Y., Xie, B., Jiménez, R., et al. (2021). Selection on Phalanx Development in the Evolution of the Bird Wing. Mol Biol Evol *38*, 4222–4237.

Bandyopadhyay, A., Kubilus, J.K., Crochiere, M.L., Linsenmayer, T.F., and Tabin, C.J. (2008). Identification of unique molecular subdomains in the perichondrium and periosteum and their role in regulating gene expression in the underlying chondrocytes. Dev Biol *321*, 162–174.

Barna, M., and Niswander, L. (2007). Visualization of cartilage formation: insight into cellular properties of skeletal progenitors and chondrodysplasia syndromes. Dev Cell *12*, 931–941.

Bénazéraf, B., Francois, P., Baker, R.E., Denans, N., Little, C.D., and Pourquié, O. (2010). A random cell motility gradient downstream of FGF controls elongation of an amniote embryo. Nature *466*, 248–252.

Benková, E., Michniewicz, M., Sauer, M., Teichmann, T., Seifertová, D., Jürgens, G., and Friml, J. (2003). Local, efflux-dependent auxin gradients as a common module for plant organ formation. Cell *115*, 591–602.

Besnard, F., Refahi, Y., Morin, V., Marteaux, B., Brunoud, G., Chambrier, P., Rozier, F., Mirabet, V., Legrand, J., Lainé, S., et al. (2014). Cytokinin signalling inhibitory fields provide robustness to phyllotaxis. Nature *505*, 417–421.

Bhatia, N., and Heisler, M.G. (2018). Self-organizing periodicity in development: organ positioning in plants. Development *145*.

Bhatia, N., Bozorg, B., Larsson, A., Ohno, C., Jönsson, H., and Heisler, M.G. (2016). Auxin Acts through MONOPTEROS to Regulate Plant Cell Polarity and Pattern Phyllotaxis. Curr Biol *26*, 3202–3208.

Bi, W., Deng, J.M., Zhang, Z., Behringer, R.R., and de Crombrugghe, B. (1999). Sox9 is required for cartilage formation. Nat Genet *22*, 85–89.

Bolognesi, R., Farzana, L., Fischer, T.D., and Brown, S.J. (2008). Multiple Wnt genes are required for segmentation in the short-germ embryo of Tribolium castaneum. Curr Biol *18*, 1624–1629.

Bowman, J.L., and Eshed, Y. (2000). Formation and maintenance of the shoot apical meristem. Trends Plant Sci *5*, 110–115.

Brena, C., and Akam, M. (2013). An analysis of segmentation dynamics throughout embryogenesis in the centipede Strigamia maritima. BMC Biology *11*, 112.

Brunet, L.J., McMahon, J.A., McMahon, A.P., and Harland, R.M. (1998). Noggin, cartilage morphogenesis, and joint formation in the mammalian skeleton. Science *280*, 1455–1457.

Callos, J.D., and Medford, J.I. (1994). Organ positions and pattern formation in the shoot apex. The Plant Journal *6*, 1–7.

Capdevila, J., and Johnson, R.L. (1998). Endogenous and ectopic expression of noggin suggests a conserved mechanism for regulation of BMP function during limb and somite patterning. Dev Biol *197*, 205–217.

Carapuço, M., Nóvoa, A., Bobola, N., and Mallo, M. (2005). Hox genes specify vertebral types in the presomitic mesoderm. Genes Dev *19*, 2116–2121.

Casanova, J.C., and Sanz-Ezquerro, J.J. (2007). Digit morphogenesis: is the tip different? Dev Growth Differ *49*, 479–491.

Chen, G., Deng, C., and Li, Y.-P. (2012). TGF-β and BMP signaling in osteoblast differentiation

and bone formation. Int J Biol Sci *8*, 272–288.

Chijimatsu, R., and Saito, T. (2019). Mechanisms of synovial joint and articular cartilage development. Cell. Mol. Life Sci. *76*, 3939–3952.

Chimal-Monroy, J., and Díaz de León, L. (1999). Expression of N-cadherin, N-CAM, fibronectin and tenascin is stimulated by TGF-beta1, beta2, beta3 and beta5 during the formation of precartilage condensations. Int J Dev Biol *43*, 59–67.

Chimal-Monroy, J., Rodriguez-Leon, J., Montero, J.A., Gañan, Y., Macias, D., Merino, R., and Hurle, J.M. (2003). Analysis of the molecular cascade responsible for mesodermal limb chondrogenesis: Sox genes and BMP signaling. Dev Biol *257*, 292–301.

Chipman, A.D., Arthur, W., and Akam, M. (2004). A Double Segment Periodicity Underlies Segment Generation in Centipede Development. Current Biology *14*, 1250–1255.

Choe, C.P., Miller, S.C., and Brown, S.J. (2006). A pair-rule gene circuit defines segments sequentially in the short-germ insect Tribolium castaneum. Proc Natl Acad Sci U S A *103*, 6560–6564.

Clack, J.A. (2002). An early tetrapod from “Romer’s Gap.” Nature *418*, 72–76.

Clark, E., and Peel, A.D. (2018). Evidence for the temporal regulation of insect segmentation by a conserved sequence of transcription factors. Development *145*, dev155580.

Cooke, J., and Zeeman, E.C. (1976). A clock and wavefront model for control of the number of repeated structures during animal morphogenesis. J Theor Biol *58*, 455–476.

Cooper, K.L., Hu, J.K.-H., ten Berge, D., Fernandez-Teran, M., Ros, M.A., and Tabin, C.J. (2011). Initiation of proximal-distal patterning in the vertebrate limb by signals and growth. Science *332*, 1083–1086.

Cooper, L.N., Berta, A., Dawson, S.D., and Reidenberg, J.S. (2007). Evolution of hyperphalangy and digit reduction in the cetacean manus. Anat Rec (Hoboken) *290*, 654–672.

Cooper, L.N., Sears, K.E., Armfield, B.A., Kala, B., Hubler, M., and Thewissen, J.G.M. (2018). Review and experimental evaluation of the embryonic development and evolutionary history of flipper development and hyperphalangy in dolphins (Cetacea: Mammalia). Genesis *56*.

Cornwall Scoones, J., and Hiscock, T.W. (2020). A dot-stripe Turing model of joint patterning in the tetrapod limb. Development.

Corson, F., Couturier, L., Rouault, H., Mazouni, K., and Schweisguth, F. (2017). Self-organized Notch dynamics generate stereotyped sensory organ patterns in Drosophila. Science *356*.

Cotterell, J., Robert-Moreno, A., and Sharpe, J. (2015). A Local, Self-Organizing Reaction-Diffusion Model Can Explain Somite Patterning in Embryos. Cell Syst *1*, 257–269.

Dahal, G.R., Pradhan, S.J., and Bates, E.A. (2017). Inwardly rectifying potassium channels influence Drosophila wing morphogenesis by regulating Dpp release. Development *144*, 2771–2783.

Dahn, R.D., and Fallon, J.F. (2000). Interdigital regulation of digit identity and homeotic transformation by modulated BMP signaling. Science *289*, 438–441.

Dale, J.K., Maroto, M., Dequeant, M.-L., Malapert, P., McGrew, M., and Pourquie, O. (2003). Periodic notch inhibition by lunatic fringe underlies the chick segmentation clock. Nature *421*, 275–278.

Decker, R.S. (2017). Articular cartilage and joint development from embryogenesis to adulthood. Semin. Cell Dev. Biol. *62*, 50–56.

Decker, R.S., Koyama, E., and Pacifici, M. (2014). Genesis and morphogenesis of limb synovial

joints and articular cartilage. Matrix Biol. *39*, 5–10.

Deng, Z.-L., Sharff, K.A., Tang, N., Song, W.-X., Luo, J., Luo, X., Chen, J., Bennett, E., Reid, R., Manning, D., et al. (2008). Regulation of osteogenic differentiation during skeletal development. Front. Biosci. *13*, 2001–2021.

Dequéant, M.-L., Glynn, E., Gaudenz, K., Wahl, M., Chen, J., Mushegian, A., and Pourquié, O. (2006). A complex oscillating network of signaling genes underlies the mouse segmentation clock. Science *314*, 1595–1598.

Domagalska, M.A., and Leyser, O. (2011). Signal integration in the control of shoot branching. Nat Rev Mol Cell Biol *12*, 211–221.

Douady, S., and Couder, Y. (1992). Phyllotaxis as a physical self-organized growth process. Phys Rev Lett *68*, 2098–2101.

Driever, W., and Nüsslein-Volhard, C. (1988). The bicoid protein determines position in the Drosophila embryo in a concentration-dependent manner. Cell *54*, 95–104.

Dubrulle, J., and Pourquié, O. (2004a). Coupling segmentation to axis formation. Development *131*, 5783–5793.

Dubrulle, J., and Pourquié, O. (2004b). fgf8 mRNA decay establishes a gradient that couples axial elongation to patterning in the vertebrate embryo. Nature *427*, 419–422.

Dubrulle, J., McGrew, M.J., and Pourquié, O. (2001). FGF signaling controls somite boundary position and regulates segmentation clock control of spatiotemporal Hox gene activation. Cell *106*, 219–232.

Dunty, W.C., Biris, K.K., Chalamalasetty, R.B., Taketo, M.M., Lewandoski, M., and Yamaguchi, T.P. (2008). Wnt3a/beta-catenin signaling controls posterior body development by coordinating mesoderm formation and segmentation. Development *135*, 85–94.

Economou, A.D., Ohazama, A., Porntaveetus, T., Sharpe, P.T., Kondo, S., Basson, M.A., Gritli-Linde, A., Cobourne, M.T., and Green, J.B.A. (2012). Periodic stripe formation by a Turing-mechanism operating at growth zones in the mammalian palate. Nat Genet *44*, 348–351.

Esteve-Altava, B. (2017). In search of morphological modules: a systematic review. Biological Reviews *92*, 1332–1347.

Fallon, J.F., Frederick, J.M., Carrington, J.L., Lanser, M.E., and Simandl, B.K. (1983). Studies on a limbless mutant in the chick embryo. Prog Clin Biol Res *110 Pt A*, 33–43.

Fallon, J.F., López, A., Ros, M.A., Savage, M.P., Olwin, B.B., and Simandl, B.K. (1994). FGF-2: apical ectodermal ridge growth signal for chick limb development. Science *264*, 104–107.

Fedak, T.J., and Hall, B.K. (2004). Perspectives on hyperphalangy: patterns and processes. J. Anat. *204*, 151–163.

Feregrino, C., Sacher, F., Parnas, O., and Tschopp, P. (2019). A single-cell transcriptomic atlas of the developing chicken limb. BMC Genomics *20*, 401.

Finak, G., McDavid, A., Yajima, M., Deng, J., Gersuk, V., Shalek, A.K., Slichter, C.K., Miller, H.W., McElrath, M.J., Prlic, M., et al. (2015). MAST: a flexible statistical framework for assessing transcriptional changes and characterizing heterogeneity in single-cell RNA sequencing data. Genome Biol *16*, 278.

Francis-West, P.H., Parish, J., Lee, K., and Archer, C.W. (1999). BMP/GDF-signalling interactions during synovial joint development. Cell Tissue Res *296*, 111–119.

Franke, M., Ibrahim, D.M., Andrey, G., Schwarzer, W., Heinrich, V., Schöpflin, R., Kraft, K., Kempfer, R., Jerković, I., Chan, W.-L., et al. (2016). Formation of new chromatin domains

determines pathogenicity of genomic duplications. Nature *538*, 265–269.

Gañan, Y., Macias, D., Duterque-Coquillaud, M., Ros, M.A., and Hurle, J.M. (1996). Role of TGF beta s and BMPs as signals controlling the position of the digits and the areas of interdigital cell death in the developing chick limb autopod. Development *122*, 2349–2357.

Genzer, M.A., and Bridgewater, L.C. (2007). A Col9a1 enhancer element activated by two interdependent SOX9 dimers. Nucleic Acids Res *35*, 1178–1186.

Glen, C.M., Kemp, M.L., and Voit, E.O. (2019). Agent-based modeling of morphogenetic systems: Advantages and challenges. PLoS Comput Biol *15*, e1006577.

Gola, E.M., and Banasiak, A. (2016). Diversity of phyllotaxis in land plants in reference to the shoot apical meristem structure. Acta Societatis Botanicorum Poloniae *85*.

Goldstein, R.S., and Kalcheim, C. (1992). Determination of epithelial half-somites in skeletal morphogenesis. Development *116*, 441–445.

Gomez, C., and Pourquié, O. (2009). Developmental control of segment numbers in vertebrates. J Exp Zool B Mol Dev Evol *312*, 533–544.

Gomez, C., Ozbudak, E.M., Wunderlich, J., Baumann, D., Lewis, J., and Pourquié, O. (2008). Control of segment number in vertebrate embryos. Nature *454*, 335–339.

Gómez-Skarmeta, J.L., Campuzano, S., and Modolell, J. (2003). Half a century of neural prepatterning: the story of a few bristles and many genes. Nat. Rev. Neurosci. *4*, 587–598.

Grant, G.R., Farkas, M.H., Pizarro, A.D., Lahens, N.F., Schug, J., Brunk, B.P., Stoeckert, C.J., Hogenesch, J.B., and Pierce, E.A. (2011). Comparative analysis of RNA-Seq alignment algorithms and the RNA-Seq unified mapper (RUM). Bioinformatics *27*, 2518–2528.

Gratzner, H.G. (1982). Monoclonal antibody to 5-bromo- and 5-iododeoxyuridine: A new reagent for detection of DNA replication. Science *218*, 474–475.

Green, J.B.A., and Sharpe, J. (2015). Positional information and reaction-diffusion: two big ideas in developmental biology combine. Development *142*, 1203–1211.

Green, J.B.A., and Smith, J.C. (1990). Graded changes in dose of a Xenopus activin A homologue elicit stepwise transitions in embryonic cell fate. Nature *347*, 391–394.

Gros, J., and Tabin, C.J. (2014). Vertebrate limb bud formation is initiated by localized epithelial-to-mesenchymal transition. Science *343*, 1253–1256.

Gu, J., Lu, Y., Li, F., Qiao, L., Wang, Q., Li, N., Borgia, J.A., Deng, Y., Lei, G., and Zheng, Q. (2014). Identification and characterization of the novel Col10a1 regulatory mechanism during chondrocyte hypertrophic differentiation. Cell Death Dis *5*, e1469.

Guo, X., Day, T.F., Jiang, X., Garrett-Beal, L., Topol, L., and Yang, Y. (2004). Wnt/beta-catenin signaling is sufficient and necessary for synovial joint formation. Genes Dev. *18*, 2404–2417.

Hamburger, V., and Hamilton, H.L. (1951). A series of normal stages in the development of the chick embryo. J. Morphol. *88*, 49–92.

Harfe, B.D., Scherz, P.J., Nissim, S., Tian, H., McMahon, A.P., and Tabin, C.J. (2004). Evidence for an expansion-based temporal Shh gradient in specifying vertebrate digit identities. Cell *118*, 517–528.

Hartmann, C., and Tabin, C.J. (2001). Wnt-14 plays a pivotal role in inducing synovial joint formation in the developing appendicular skeleton. Cell *104*, 341–351.

Haupaix, N., Curantz, C., Bailleul, R., Beck, S., Robic, A., and Manceau, M. (2018). The periodic coloration in birds forms through a prepattern of somite origin. Science *361*.

Healy, C., Uwanogho, D., and Sharpe, P.T. (1999). Regulation and role of Sox9 in cartilage formation. Dev. Dyn. *215*, 69–78.

Hiscock, T.W., and Megason, S.G. (2015). Mathematically guided approaches to distinguish models of periodic patterning. Development *142*, 409–419.

Hiscock, T.W., Tschopp, P., and Tabin, C.J. (2017). On the Formation of Digits and Joints during Limb Development. Dev. Cell *41*, 459–465.

Ho, W.K.W., Freem, L., Zhao, D., Painter, K.J., Woolley, T.E., Gaffney, E.A., McGrew, M.J., Tzika, A., Milinkovitch, M.C., Schneider, P., et al. (2019). Feather arrays are patterned by interacting signalling and cell density waves. PLoS Biol *17*, e3000132.

Holder, N. (1977). An experimental investigation into the early development of the chick elbow joint. J Embryol Exp Morphol *39*, 115–127.

Hu, J., and He, L. (2008). Patterning mechanisms controlling digit development. J Genet Genomics *35*, 517–524.

Huang, B.-L., Trofka, A., Furusawa, A., Norrie, J.L., Rabinowitz, A.H., Vokes, S.A., Mark Taketo, M., Zakany, J., and Mackem, S. (2016). An interdigit signalling centre instructs coordinate phalanx-joint formation governed by 5'Hoxd-Gli3 antagonism. Nat Commun *7*, 12903.

Hubaud, A., Regev, I., Mahadevan, L., and Pourquié, O. (2017). Excitable Dynamics and Yap-Dependent Mechanical Cues Drive the Segmentation Clock. Cell *171*, 668-682.e11.

Iimura, T., and Pourquié, O. (2006). Collinear activation of Hoxb genes during gastrulation is linked to mesoderm cell ingression. Nature *442*, 568–571.

Impagnatiello, M.A., Weitzer, S., Gannon, G., Compagni, A., Cotten, M., and Christofori, G. (2001). Mammalian sprouty-1 and -2 are membrane-anchored phosphoprotein inhibitors of growth factor signaling in endothelial cells. J Cell Biol *152*, 1087–1098.

Ishimatsu, K., Hiscock, T.W., Collins, Z.M., Sari, D.W.K., Lischer, K., Richmond, D.L., Bessho, Y., Matsui, T., and Megason, S.G. (2018). Size-reduced embryos reveal a gradient scaling-based mechanism for zebrafish somite formation. Development *145*.

Jaeger, J. (2011). The gap gene network. Cell Mol Life Sci *68*, 243–274.

Jones, K.E., Benitez, L., Angielczyk, K.D., and Pierce, S.E. (2018). Adaptation and constraint in the evolution of the mammalian backbone. BMC Evol Biol *18*, 172.

Jönsson, H., Heisler, M.G., Shapiro, B.E., Meyerowitz, E.M., and Mjolsness, E. (2006). An auxin-driven polarized transport model for phyllotaxis. Proc Natl Acad Sci U S A *103*, 1633–1638.

Jörg, D.J., Oates, A.C., and Jülicher, F. (2016). Sequential pattern formation governed by signaling gradients. Phys Biol *13*, 05LT03.

Kan, A., and Tabin, C.J. (2013). c-Jun is required for the specification of joint cell fates. Genes Dev. *27*, 514–524.

Kavanagh, K.D., Shoval, O., Winslow, B.B., Alon, U., Leary, B.P., Kan, A., and Tabin, C.J. (2013). Developmental bias in the evolution of phalanges. Proc. Natl. Acad. Sci. U.S.A. *110*, 18190–18195.

Kiani, C., Chen, L., Wu, Y.J., Yee, A.J., and Yang, B.B. (2002). Structure and function of aggrecan. Cell Res *12*, 19–32.

Koyama, E., Shibukawa, Y., Nagayama, M., Sugito, H., Young, B., Yuasa, T., Okabe, T., Ochiai, T., Kamiya, N., Rountree, R.B., et al. (2008). A distinct cohort of progenitor cells participates in synovial joint and articular cartilage formation during mouse limb skeletogenesis. Dev. Biol. *316*, 62–73.

Kozhemyakina, E., Lassar, A.B., and Zelzer, E. (2015). A pathway to bone: signaling molecules and transcription factors involved in chondrocyte development and maturation. Development *142*, 817–831.

Krol, A.J., Roellig, D., Dequéant, M.-L., Tassy, O., Glynn, E., Hattem, G., Mushegian, A., Oates, A.C., and Pourquié, O. (2011). Evolutionary plasticity of segmentation clock networks. Development *138*, 2783–2792.

Kuhlemeier, C. (2017). Phyllotaxis. Curr Biol *27*, R882–R887.

Kumar, S., and Duester, G. (2014). Retinoic acid controls body axis extension by directly repressing Fgf8 transcription. Development *141*, 2972–2977.

Larraín, J., Bachiller, D., Lu, B., Agius, E., Piccolo, S., and De Robertis, E.M. (2000). BMP-binding modules in chordin: a model for signalling regulation in the extracellular space. Development *127*, 821–830.

Lauschke, V.M., Tsiairis, C.D., François, P., and Aulehla, A. (2013). Scaling of embryonic patterning based on phase-gradient encoding. Nature *493*, 101–105.

Lee, C., and Clark, S.E. (2013). Core pathways controlling shoot meristem maintenance. Wiley Interdiscip Rev Dev Biol *2*, 671–684.

Lefebvre, V., and Bhattaram, P. (2010). Vertebrate skeletogenesis. Curr Top Dev Biol *90*, 291–317.

Lefebvre, V., Huang, W., Harley, V.R., Goodfellow, P.N., and de Crombrugghe, B. (1997). SOX9 is a potent activator of the chondrocyte-specific enhancer of the pro alpha1(II) collagen gene. Mol Cell Biol *17*, 2336–2346.

Li, P., and Elowitz, M.B. (2019). Communication codes in developmental signaling pathways. Development *146*.

Liao, B.-K., Jörg, D.J., and Oates, A.C. (2016). Faster embryonic segmentation through elevated Delta-Notch signalling. Nat Commun *7*, 11861.

Logan, M., and Tabin, C. (1998). Targeted gene misexpression in chick limb buds using avian replication-competent retroviruses. Methods *14*, 407–420.

Logan, M., Martin, J.F., Nagy, A., Lobe, C., Olson, E.N., and Tabin, C.J. (2002). Expression of Cre Recombinase in the developing mouse limb bud driven by a Prxl enhancer. Genesis *33*, 77–80.

Long, F., Chung, U., Ohba, S., McMahon, J., Kronenberg, H.M., and McMahon, A.P. (2004). Ihh signaling is directly required for the osteoblast lineage in the endochondral skeleton. Development *131*, 1309–1318.

Loomis, C.A., Kimmel, R.A., Tong, C.X., Michaud, J., and Joyner, A.L. (1998). Analysis of the genetic pathway leading to formation of ectopic apical ectodermal ridges in mouse Engrailed-1 mutant limbs. Development *125*, 1137–1148.

Lopez-Rios, J. (2016). The many lives of SHH in limb development and evolution. Semin Cell Dev Biol *49*, 116–124.

Lorda-Diez, C.I., Montero, J.A., Diaz-Mendoza, M.J., Garcia-Porrero, J.A., and Hurle, J.M. (2013a). βig-h3 potentiates the profibrogenic effect of TGFβ signaling on connective tissue progenitor cells through the negative regulation of master chondrogenic genes. Tissue Eng Part A *19*, 448–457.

Lorda-Diez, C.I., Montero, J.A., Rodriguez-Leon, J., Garcia-Porrero, J.A., and Hurle, J.M. (2013b). Expression and functional study of extracellular BMP antagonists during the morphogenesis of the digits and their associated connective tissues. PLoS ONE *8*, e60423.

Lorda-Diez, C.I., Duarte-Olivenza, C., Hurle, J.M., and Montero, J.A. (2022). Transforming growth factor beta signaling: The master sculptor of fingers. Dev Dyn *251*, 125–136.

Mahalwar, P., Walderich, B., Singh, A.P., and Nüsslein-Volhard, C. (2014). Local reorganization of xanthophores fine-tunes and colors the striped pattern of zebrafish. Science *345*, 1362–1364.

Mallo, M. (2016). Revisiting the involvement of signaling gradients in somitogenesis. FEBS J *283*, 1430–1437.

Mallo, M., Wellik, D.M., and Deschamps, J. (2010). Hox genes and regional patterning of the vertebrate body plan. Dev Biol *344*, 7–15.

Manfrin, A., Tabata, Y., Paquet, E.R., Vuaridel, A.R., Rivest, F.R., Naef, F., and Lutolf, M.P. (2019). Engineered signaling centers for the spatially controlled patterning of human pluripotent stem cells. Nat. Methods *16*, 640–648.

Manukyan, L., Montandon, S.A., Fofonjka, A., Smirnov, S., and Milinkovitch, M.C. (2017). A living mesoscopic cellular automaton made of skin scales. Nature *544*, 173–179.

Mariani, F.V., Fernandez-Teran, M., and Ros, M.A. (2017). Ectoderm-mesoderm crosstalk in the embryonic limb: The role of fibroblast growth factor signaling. Dev Dyn *246*, 208–216.

Marín-Llera, J.C., Garciadiego-Cázares, D., and Chimal-Monroy, J. (2019). Understanding the Cellular and Molecular Mechanisms That Control Early Cell Fate Decisions During Appendicular Skeletogenesis. Front Genet *10*, 977.

Maroto, M., Bone, R.A., and Dale, J.K. (2012). Somitogenesis. Development *139*, 2453–2456.

McGlinn, E., and Mansfield, J.H. (2011). Detection of gene expression in mouse embryos and tissue sections. Methods Mol Biol *770*, 259–292.

McQueen, C., and Towers, M. (2020). Establishing the pattern of the vertebrate limb. Development *147*, dev177956.

Meinhardt, H., Koch, A.-J., and Bernasconi, G. (1998). Models of pattern formation applied to plant development. In Symmetry in Plants, (WORLD SCIENTIFIC), pp. 723–758.

Mentink, R.A., and Tsiantis, M. (2015). From limbs to leaves: common themes in evolutionary diversification of organ form. Front Genet *6*, 284.

Merino, R., Macias, D., Gañan, Y., Economides, A.N., Wang, X., Wu, Q., Stahl, N., Sampath, K.T., Varona, P., and Hurle, J.M. (1999a). Expression and function of Gdf-5 during digit skeletogenesis in the embryonic chick leg bud. Dev. Biol. *206*, 33–45.

Merino, R., Macias, D., Gañan, Y., Rodriguez-Leon, J., Economides, A.N., Rodriguez-Esteban, C., Izpisua-Belmonte, J.C., and Hurle, J.M. (1999b). Control of digit formation by activin signalling. Development *126*, 2161–2170.

Merino, R., Rodriguez-Leon, J., Macias, D., Gañan, Y., Economides, A.N., and Hurle, J.M. (1999c). The BMP antagonist Gremlin regulates outgrowth, chondrogenesis and programmed cell death in the developing limb. Development *126*, 5515–5522.

Mikasa, M., Rokutanda, S., Komori, H., Ito, K., Tsang, Y.S., Date, Y., Yoshida, C.A., and Komori, T. (2011). Regulation of Tcf7 by Runx2 in chondrocyte maturation and proliferation. J Bone Miner Metab *29*, 291–299.

Minina, E., Schneider, S., Rosowski, M., Lauster, R., and Vortkamp, A. (2005). Expression of Fgf and Tgfbeta signaling related genes during embryonic endochondral ossification. Gene Expr. Patterns *6*, 102–109.

Montavon, T., Le Garrec, J.-F., Kerszberg, M., and Duboule, D. (2008). Modeling Hox gene

regulation in digits: reverse collinearity and the molecular origin of thumbness. Genes Dev *22*, 346–359.

Montero, J.A., Lorda-Diez, C.I., Gañan, Y., Macias, D., and Hurle, J.M. (2008). Activin/TGFbeta and BMP crosstalk determines digit chondrogenesis. Dev. Biol. *321*, 343–356.

Moreno, T.A., and Kintner, C. (2004). Regulation of segmental patterning by retinoic acid signaling during Xenopus somitogenesis. Dev Cell *6*, 205–218.

Moreno-Risueno, M.A., Norman, J.M.V., Moreno, A., Zhang, J., Ahnert, S.E., and Benfey, P.N. (2010). Oscillating Gene Expression Determines Competence for Periodic Arabidopsis Root Branching. Science *329*, 1306–1311.

Mori-Akiyama, Y., Akiyama, H., Rowitch, D.H., and de Crombrugghe, B. (2003). Sox9 is required for determination of the chondrogenic cell lineage in the cranial neural crest. Proc Natl Acad Sci U S A *100*, 9360–9365.

Morimoto, M., Takahashi, Y., Endo, M., and Saga, Y. (2005). The Mesp2 transcription factor establishes segmental borders by suppressing Notch activity. Nature *435*, 354–359.

Müller, D., and Leyser, O. (2011). Auxin, cytokinin and the control of shoot branching. Ann Bot *107*, 1203–1212.

Multerer, M.D., Wittwer, L.D., Stopka, A., Barac, D., Lang, C., and Iber, D. (2018). Simulation of Morphogen and Tissue Dynamics. In Morphogen Gradients: Methods and Protocols, J. Dubrulle, ed. (New York, NY: Springer New York), pp. 223–250.

Mundlos, S. (2009). The brachydactylies: a molecular disease family. Clin Genet *76*, 123–136.

Murray, P.J., Maini, P.K., and Baker, R.E. (2011). The clock and wavefront model revisited. J Theor Biol *283*, 227–238.

Nagy, L.M., and Carroll, S. (1994). Conservation of wingless patterning functions in the short-germ embryos of Tribolium castaneum. Nature *367*, 460–463.

Naiche, L.A., Holder, N., and Lewandoski, M. (2011). FGF4 and FGF8 comprise the wavefront activity that controls somitogenesis. PNAS *108*, 4018–4023.

Nakamasu, A., Takahashi, G., Kanbe, A., and Kondo, S. (2009). Interactions between zebrafish pigment cells responsible for the generation of Turing patterns. Proc Natl Acad Sci U S A *106*, 8429–8434.

Nakayama, N., Han, C.E., Scully, S., Nishinakamura, R., He, C., Zeni, L., Yamane, H., Chang, D., Yu, D., Yokota, T., et al. (2001). A novel chordin-like protein inhibitor for bone morphogenetic proteins expressed preferentially in mesenchymal cell lineages. Dev Biol *232*, 372–387.

Nakayama, N., Han, C.E., Cam, L., Lee, J.I., Pretorius, J., Fisher, S., Rosenfeld, R., Scully, S., Nishinakamura, R., Duryea, D., et al. (2004). A novel chordin-like BMP inhibitor, CHL2, expressed preferentially in chondrocytes of developing cartilage and osteoarthritic joint cartilage. Development *131*, 229–240.

Niswander, L., Tickle, C., Vogel, A., Booth, I., and Martin, G.R. (1993). FGF-4 replaces the apical ectodermal ridge and directs outgrowth and patterning of the limb. Cell *75*, 579–587.

Nohno, T., Koyama, E., Myokai, F., Taniguchi, S., Ohuchi, H., Saito, T., and Noji, S. (1993). A chicken homeobox gene related to Drosophila paired is predominantly expressed in the developing limb. Dev Biol *158*, 254–264.

Nolan, K., Kattamuri, C., Rankin, S.A., Read, R.J., Zorn, A.M., and Thompson, T.B. (2016). Structure of Gremlin-2 in Complex with GDF5 Gives Insight into DAN-Family-Mediated BMP Antagonism. Cell Rep *16*, 2077–2086.

Nüsslein-Volhard, C., Frohnhöfer, H.G., and Lehmann, R. (1987). Determination of anteroposterior polarity in Drosophila. Science *238*, 1675–1681.

Oates, A.C., Morelli, L.G., and Ares, S. (2012). Patterning embryos with oscillations: structure, function and dynamics of the vertebrate segmentation clock. Development *139*, 625–639.

Oren, A., Toporik, A., Biton, S., Almogy, N., Eshel, D., Bernstein, J., Savitsky, K., and Rotman, G. (2004). hCHL2, a novel chordin-related gene, displays differential expression and complex alternative splicing in human tissues and during myoblast and osteoblast maturation. Gene *331*, 17–31.

Pacifici, M., Koyama, E., and Iwamoto, M. (2005). Mechanisms of synovial joint and articular cartilage formation: recent advances, but many lingering mysteries. Birth Defects Res. C Embryo Today *75*, 237–248.

Palmeirim, I., Henrique, D., Ish-Horowicz, D., and Pourquié, O. (1997). Avian hairy gene expression identifies a molecular clock linked to vertebrate segmentation and somitogenesis. Cell *91*, 639–648.

Panousopoulou, E., and Green, J.B.A. (2016). Invagination of Ectodermal Placodes Is Driven by Cell Intercalation-Mediated Contraction of the Suprabasal Tissue Canopy. PLoS Biol *14*, e1002405.

Patel, N.H. (1994). The evolution of arthropod segmentation: insights from comparisons of gene expression patterns. Development *1994*, 201–207.

Payne, J.L., and Wagner, A. (2019). The causes of evolvability and their evolution. Nat Rev Genet *20*, 24.

Pearse, R.V., Scherz, P.J., Campbell, J.K., and Tabin, C.J. (2007). A cellular lineage analysis of the chick limb bud. Dev Biol *310*, 388–400.

Pérez-Gómez, R., Haro, E., Fernández-Guerrero, M., Bastida, M.F., and Ros, M.A. (2018). Role of Hox genes in regulating digit patterning. Int J Dev Biol *62*, 797–805.

Peter, I.S., and Davidson, E.H. (2011). A gene regulatory network controlling the embryonic specification of endoderm. Nature *474*, 635–639.

Potuijt, J.W.P., Galjaard, R.-J.H., van der Spek, P.J., van Nieuwenhoven, C.A., Ahituv, N., Oberg, K.C., and Hovius, S.E.R. (2019). A multidisciplinary review of triphalangeal thumb. J Hand Surg Eur Vol *44*, 59–68.

Pourquié, O. (2018). Somite formation in the chicken embryo. Int J Dev Biol *62*, 57–62.

Raspopovic, J., Marcon, L., Russo, L., and Sharpe, J. (2014). Modeling digits. Digit patterning is controlled by a Bmp-Sox9-Wnt Turing network modulated by morphogen gradients. Science *345*, 566–570.

Ray, A., Singh, P.N.P., Sohaskey, M.L., Harland, R.M., and Bandyopadhyay, A. (2015). Precise spatial restriction of BMP signaling is essential for articular cartilage differentiation. Development *142*, 1169–1179.

Reinhardt, D., Mandel, T., and Kuhlemeier, C. (2000). Auxin regulates the initiation and radial position of plant lateral organs. Plant Cell *12*, 507–518.

Remak, R. (1855). Untersuchungen über die Entwickelung der Wirbelthiere.

Richardson, M.K., and Oelschläger, H.H.A. (2002). Time, pattern, and heterochrony: a study of hyperphalangy in the dolphin embryo flipper. Evol. Dev. *4*, 435–444.

Richardson, M.K., Gobes, S.M.H., van Leeuwen, A.C., Polman, J.A.E., Pieau, C., and Sánchez-Villagra, M.R. (2009). Heterochrony in limb evolution: developmental mechanisms and natural

selection. J Exp Zool B Mol Dev Evol *312*, 639–664.

Richmond, D.L., and Oates, A.C. (2012). The segmentation clock: inherited trait or universal design principle? Curr Opin Genet Dev *22*, 600–606.

Riddle, R.D., Johnson, R.L., Laufer, E., and Tabin, C. (1993). Sonic hedgehog mediates the polarizing activity of the ZPA. Cell *75*, 1401–1416.

Robinson, M.D., McCarthy, D.J., and Smyth, G.K. (2010). edgeR: a Bioconductor package for differential expression analysis of digital gene expression data. Bioinformatics *26*, 139–140.

Rockel, J.S., Yu, C., Whetstone, H., Craft, A.M., Reilly, K., Ma, H., Tsushima, H., Puviindran, V., Al-Jazrawe, M., Keller, G.M., et al. (2016). Hedgehog inhibits β-catenin activity in synovial joint development and osteoarthritis. J. Clin. Invest. *126*, 1649–1663.

Roselló-Díez, A., Ros, M.A., and Torres, M. (2011). Diffusible signals, not autonomous mechanisms, determine the main proximodistal limb subdivision. Science *332*, 1086–1088.

Rossi, G., Manfrin, A., and Lutolf, M.P. (2018). Progress and potential in organoid research. Nature Reviews Genetics *19*, 671.

Rountree, R.B., Schoor, M., Chen, H., Marks, M.E., Harley, V., Mishina, Y., and Kingsley, D.M. (2004). BMP receptor signaling is required for postnatal maintenance of articular cartilage. PLoS Biol *2*, e355.

Sacher, F., Feregrino, C., Tschopp, P., and Ewald, C.Y. (2021). Extracellular matrix gene expression signatures as cell type and cell state identifiers. Matrix Biol Plus *10*, 100069.

Sako, K., Pradhan, S.J., Barone, V., Inglés-Prieto, Á., Müller, P., Ruprecht, V., Čapek, D., Galande, S., Janovjak, H., and Heisenberg, C.-P. (2016). Optogenetic Control of Nodal Signaling Reveals a Temporal Pattern of Nodal Signaling Regulating Cell Fate Specification during Gastrulation. Cell Rep *16*, 866–877.

Sanz-Ezquerro, J., and Tickle, C. (2003a). Digital development and morphogenesis. J Anat *202*, 51–58.

Sanz-Ezquerro, J.J., and Tickle, C. (2003b). Fgf signaling controls the number of phalanges and tip formation in developing digits. Curr. Biol. *13*, 1830–1836.

Sarrazin, A.F., Peel, A.D., and Averof, M. (2012). A segmentation clock with two-segment periodicity in insects. Science *336*, 338–341.

Saunders, J.W. (1948). The proximo-distal sequence of origin of the parts of the chick wing and the role of the ectoderm. J Exp Zool *108*, 363–403.

Saunders, J.W., Jr., and Gasseling, M.T. (1968). Ectodermal-mesodermal interactions in the origin of limb symmetry.

Schoppmeier, M., and Schröder, R. (2005). Maternal Torso Signaling Controls Body Axis Elongation in a Short Germ Insect. Curr Biol *15*, 2131–2136.

Schweisguth, F., and Corson, F. (2019). Self-Organization in Pattern Formation. Dev Cell *49*, 659–677.

Searls, R.L., and Janners, M.Y. (1971). The initiation of limb bud outgrowth in the embryonic chick. Dev Biol *24*, 198–213.

Sears, K.E., Behringer, R.R., Rasweiler, J.J., and Niswander, L.A. (2006). Development of bat flight: morphologic and molecular evolution of bat wing digits. Proc. Natl. Acad. Sci. U.S.A. *103*, 6581–6586.

Seemann, P., Schwappacher, R., Kjaer, K.W., Krakow, D., Lehmann, K., Dawson, K., Stricker, S., Pohl, J., Plöger, F., Staub, E., et al. (2005). Activating and deactivating mutations in the

receptor interaction site of GDF5 cause symphalangism or brachydactyly type A2. J Clin Invest *115*, 2373–2381.

Sharpe, J. (2017). Computer modeling in developmental biology: growing today, essential tomorrow. Development *144*, 4214–4225.

Sheeba, C.J., Andrade, R.P., and Palmeirim, I. (2016). Mechanisms of vertebrate embryo segmentation: Common themes in trunk and limb development. Semin Cell Dev Biol *49*, 125–134.

Sheth, R., Marcon, L., Bastida, M.F., Junco, M., Quintana, L., Dahn, R., Kmita, M., Sharpe, J., and Ros, M.A. (2012). Hox genes regulate digit patterning by controlling the wavelength of a Turing-type mechanism. Science *338*, 1476–1480.

Shimoyama, A., Wada, M., Ikeda, F., Hata, K., Matsubara, T., Nifuji, A., Noda, M., Amano, K., Yamaguchi, A., Nishimura, R., et al. (2007). Ihh/Gli2 signaling promotes osteoblast differentiation by regulating Runx2 expression and function. Mol Biol Cell *18*, 2411–2418.

Shwartz, Y., Viukov, S., Krief, S., and Zelzer, E. (2016). Joint Development Involves a Continuous Influx of Gdf5-Positive Cells. Cell Rep *15*, 2577–2587.

Shyer, A.E., Rodrigues, A.R., Schroeder, G.G., Kassianidou, E., Kumar, S., and Harland, R.M. (2017). Emergent cellular self-organization and mechanosensation initiate follicle pattern in the avian skin. Science *357*, 811–815.

Sick, S., Reinker, S., Timmer, J., and Schlake, T. (2006). WNT and DKK determine hair follicle spacing through a reaction-diffusion mechanism. Science *314*, 1447–1450.

Singh, P.N.P., Shea, C.A., Sonker, S.K., Rolfe, R.A., Ray, A., Kumar, S., Gupta, P., Murphy, P., and Bandyopadhyay, A. (2018). Precise spatial restriction of BMP signaling in developing joints is perturbed upon loss of embryo movement. Development *145*.

Smith, R.S., Guyomarc'h, S., Mandel, T., Reinhardt, D., Kuhlemeier, C., and Prusinkiewicz, P. (2006). A plausible model of phyllotaxis. Proc Natl Acad Sci U S A *103*, 1301–1306.

Somssich, M., Je, B.I., Simon, R., and Jackson, D. (2016). CLAVATA-WUSCHEL signaling in the shoot meristem. Development *143*, 3238–3248.

Sonnen, K.F., Lauschke, V.M., Uraji, J., Falk, H.J., Petersen, Y., Funk, M.C., Beaupeux, M., François, P., Merten, C.A., and Aulehla, A. (2018). Modulation of Phase Shift between Wnt and Notch Signaling Oscillations Controls Mesoderm Segmentation. Cell *172*, 1079-1090.e12.

Spagnoli, A., O'Rear, L., Chandler, R.L., Granero-Molto, F., Mortlock, D.P., Gorska, A.E., Weis, J.A., Longobardi, L., Chytil, A., Shimer, K., et al. (2007). TGF-beta signaling is essential for joint morphogenesis. J. Cell Biol. *177*, 1105–1117.

Später, D., Hill, T.P., Gruber, M., and Hartmann, C. (2006). Role of canonical Wnt-signalling in joint formation. Eur Cell Mater *12*, 71–80.

Stewart, T.A., Bhat, R., and Newman, S.A. (2017). The evolutionary origin of digit patterning. Evodevo *8*, 21.

Stewart, T.A., Lemberg, J.B., Taft, N.K., Yoo, I., Daeschler, E.B., and Shubin, N.H. (2020). Fin ray patterns at the fin-to-limb transition. Proc Natl Acad Sci U S A *117*, 1612–1620.

Storm, E.E., and Kingsley, D.M. (1996). Joint patterning defects caused by single and double mutations in members of the bone morphogenetic protein (BMP) family. Development *122*, 3969–3979.

Storm, E.E., and Kingsley, D.M. (1999). GDF5 coordinates bone and joint formation during digit development. Dev. Biol. *209*, 11–27.

Storm, E.E., Huynh, T.V., Copeland, N.G., Jenkins, N.A., Kingsley, D.M., and Lee, S.J. (1994). Limb alterations in brachypodism mice due to mutations in a new member of the TGF beta-superfamily. Nature *368*, 639–643.

Street, K., Risso, D., Fletcher, R.B., Das, D., Ngai, J., Yosef, N., Purdom, E., and Dudoit, S. (2018). Slingshot: cell lineage and pseudotime inference for single-cell transcriptomics. BMC Genomics *19*, 477.

Stricker, S., and Mundlos, S. (2011). Mechanisms of digit formation: Human malformation syndromes tell the story. Dev. Dyn. *240*, 990–1004.

Stuart, T., Butler, A., Hoffman, P., Hafemeister, C., Papalexi, E., Mauck, W.M., Hao, Y., Stoeckius, M., Smibert, P., and Satija, R. (2019). Comprehensive Integration of Single-Cell Data. Cell *177*, 1888-1902.e21.

Su, N., Jin, M., and Chen, L. (2014). Role of FGF/FGFR signaling in skeletal development and homeostasis: learning from mouse models. Bone Res *2*, 14003.

Summerbell, D., Lewis, J.H., and Wolpert, L. (1973). Positional information in chick limb morphogenesis. Nature *244*, 492–496.

Sussex, I.M. (1989). Developmental programming of the shoot meristem. Cell *56*, 225–229.

Suzuki, T., and Fallon, J.F. (2021). The dynamic spatial and temporal relationships between the phalanx-forming region and the interdigits determine digit identity in the chick limb autopod. Dev Dyn *250*, 1318–1329.

Suzuki, T., Hasso, S.M., and Fallon, J.F. (2008). Unique SMAD1/5/8 activity at the phalanx-forming region determines digit identity. Proc. Natl. Acad. Sci. U.S.A. *105*, 4185–4190.

Swinton, J., Ochu, E., and MSI Turing's Sunflower Consortium (2016). Novel Fibonacci and non-Fibonacci structure in the sunflower: results of a citizen science experiment. R Soc Open Sci *3*, 160091.

Tabin, C., and Wolpert, L. (2007). Rethinking the proximodistal axis of the vertebrate limb in the molecular era. Genes Dev. *21*, 1433–1442.

Teichmann, T., and Muhr, M. (2015). Shaping plant architecture. Front Plant Sci *6*, 233.

Ten Tusscher, K. (2018). Of mice and plants: Comparative developmental systems biology. Dev Biol.

Thompson, D.W. (1992). On Growth and Form (Cambridge: Cambridge University Press).

Tickle, C., Summerbell, D., and Wolpert, L. (1975). Positional signalling and specification of digits in chick limb morphogenesis. Nature *254*, 199–202.

Tokita, M., Matsushita, H., and Asakura, Y. (2020). Developmental mechanisms underlying webbed foot morphological diversity in waterbirds. Sci Rep *10*, 8028.

Trapnell, C., Cacchiarelli, D., Grimsby, J., Pokharel, P., Li, S., Morse, M., Lennon, N.J., Livak, K.J., Mikkelsen, T.S., and Rinn, J.L. (2014). The dynamics and regulators of cell fate decisions are revealed by pseudotemporal ordering of single cells. Nat Biotechnol *32*, 381–386.

Troilo, H., Zuk, A.V., Tunnicliffe, R.B., Wohl, A.P., Berry, R., Collins, R.F., Jowitt, T.A., Sengle, G., and Baldock, C. (2014). Nanoscale structure of the BMP antagonist chordin supports cooperative BMP binding. Proc Natl Acad Sci U S A *111*, 13063–13068.

True, J.R., and Haag, E.S. (2001). Developmental system drift and flexibility in evolutionary trajectories. Evol Dev *3*, 109–119.

Tschopp, P., and Duboule, D. (2011). A regulatory 'landscape effect' over the HoxD cluster. Dev Biol *351*, 288–296.

Tsiairis, C.D., and Aulehla, A. (2016). Self-Organization of Embryonic Genetic Oscillators into Spatiotemporal Wave Patterns. Cell *164*, 656–667.

Turing, A.M. (1952). The chemical basis of morphogenesis. Philosophical Transactions of the Royal Society of London. Series B, Biological Sciences *237*, 37–72.

Turner, D.A., Baillie-Johnson, P., and Arias, A.M. (2016). Organoids and the genetically encoded self-assembly of embryonic stem cells. BioEssays *38*, 181–191.

Vanstraelen, M., and Benková, E. (2012). Hormonal interactions in the regulation of plant development. Annu Rev Cell Dev Biol *28*, 463–487.

Vargas, A.O., and Wagner, G.P. (2009). Frame-shifts of digit identity in bird evolution and Cyclopamine-treated wings. Evol Dev *11*, 163–169.

Vargesson, N., Clarke, J.D., Vincent, K., Coles, C., Wolpert, L., and Tickle, C. (1997). Cell fate in the chick limb bud and relationship to gene expression. Development *124*, 1909–1918.

Verd, B., Clark, E., Wotton, K.R., Janssens, H., Jiménez-Guri, E., Crombach, A., and Jaeger, J. (2018). A damped oscillator imposes temporal order on posterior gap gene expression in Drosophila. PLoS Biol *16*, e2003174.

Vermot, J., and Pourquié, O. (2005). Retinoic acid coordinates somitogenesis and left-right patterning in vertebrate embryos. Nature *435*, 215–220.

Vortkamp, A., Lee, K., Lanske, B., Segre, G.V., Kronenberg, H.M., and Tabin, C.J. (1996). Regulation of rate of cartilage differentiation by Indian hedgehog and PTH-related protein. Science *273*, 613–622.

Wagner, G.P. (2014). Homology, Genes, and Evolutionary Innovation.

Wainwright, P.C., and Reilly, S.M. (1994). Ecological Morphology: Integrative Organismal Biology (University of Chicago Press).

Wang, C., and Lehmann, R. (1991). Nanos is the localized posterior determinant in Drosophila. Cell *66*, 637–647.

Wellik, D.M. (2009). Hox genes and vertebrate axial pattern. Curr Top Dev Biol *88*, 257–278.

Witte, F., Chan, D., Economides, A.N., Mundlos, S., and Stricker, S. (2010). Receptor tyrosine kinase-like orphan receptor 2 (ROR2) and Indian hedgehog regulate digit outgrowth mediated by the phalanx-forming region. Proc. Natl. Acad. Sci. U.S.A. *107*, 14211–14216.

Wolpert, L. (1969). Positional information and the spatial pattern of cellular differentiation. J. Theor. Biol. *25*, 1–47.

Wolpert, L. (1989). Positional information revisited. Development *107 Suppl*, 3–12.

Wopat, S., Bagwell, J., Sumigray, K.D., Dickson, A.L., Huitema, L.F.A., Poss, K.D., Schulte-Merker, S., and Bagnat, M. (2018). Spine Patterning Is Guided by Segmentation of the Notochord Sheath. Cell Rep *22*, 2026–2038.

Xu, X., and Mackem, S. (2013). Tracing the evolution of avian wing digits. Curr. Biol. *23*, R538-544.

Yi, S.E., Daluiski, A., Pederson, R., Rosen, V., and Lyons, K.M. (2000). The type I BMP receptor BMPRIB is required for chondrogenesis in the mouse limb. Development *127*, 621–630.

Yonekura, T., Iwamoto, A., Fujita, H., and Sugiyama, M. (2019). Mathematical model studies of the comprehensive generation of major and minor phyllotactic patterns in plants with a predominant focus on orixate phyllotaxis. PLoS Comput Biol *15*, e1007044.

Yoon, B.S., Ovchinnikov, D.A., Yoshii, I., Mishina, Y., Behringer, R.R., and Lyons, K.M. (2005).

Bmpr1a and Bmpr1b have overlapping functions and are essential for chondrogenesis in vivo. Proc Natl Acad Sci U S A *102*, 5062–5067.

Young, M.D., Wakefield, M.J., Smyth, G.K., and Oshlack, A. (2010). Gene ontology analysis for RNA-seq: accounting for selection bias. Genome Biol *11*, R14.

Young, N.M., Winslow, B., Takkellapati, S., and Kavanagh, K. (2015). Shared rules of development predict patterns of evolution in vertebrate segmentation. Nat Commun *6*, 6690.

Young, R.L., Bever, G.S., Wang, Z., and Wagner, G.P. (2011). Identity of the avian wing digits: problems resolved and unsolved. Dev Dyn *240*, 1042–1053.

Yu, K., Kang, K.-H., Heine, P., Pyati, U., Srinivasan, S., Biehs, B., Kimelman, D., and Bier, E. (2004). Cysteine repeat domains and adjacent sequences determine distinct bone morphogenetic protein modulatory activities of the Drosophila Sog protein. Genetics *166*, 1323–1336.

Zeller, R., López-Ríos, J., and Zuniga, A. (2009). Vertebrate limb bud development: moving towards integrative analysis of organogenesis. Nat. Rev. Genet. *10*, 845–858.

Zhu, J., Nakamura, E., Nguyen, M.-T., Bao, X., Akiyama, H., and Mackem, S. (2008). Uncoupling Sonic hedgehog control of pattern and expansion of the developing limb bud. Dev. Cell *14*, 624–632.

Zhu, X., Rudolf, H., Healey, L., François, P., Brown, S.J., Klingler, M., and El-Sherif, E. (2017). Speed regulation of genetic cascades allows for evolvability in the body plan specification of insects. Proc Natl Acad Sci U S A *114*, E8646–E8655.

Zou, H., and Niswander, L. (1996). Requirement for BMP signaling in interdigital apoptosis and scale formation. Science *272*, 738–741.

Zou, H., Wieser, R., Massagué, J., and Niswander, L. (1997). Distinct roles of type I bone morphogenetic protein receptors in the formation and differentiation of cartilage. Genes Dev. *11*, 2191–2203.

Zülch, A., Becker, M.B., and Gruss, P. (2001). Expression pattern of Irx1 and Irx2 during mouse digit development. Mech Dev *106*, 159–162.

Zuniga, A. (2015). Next generation limb development and evolution: old questions, new perspectives. Development *142*, 3810–3820.

APPENDIXES

Published content

Received: 18 July 2019 | Revised: 30 October 2019 | Accepted: 4 November 2019

DOI: 10.1002/dvdy.131

REVIEW

Developmental Dynamics WILEY

A sense of place, many times over - pattern formation and evolution of repetitive morphological structures

Emmanuelle Grall | **Patrick Tschopp**

DUW Zoology, University of Basel, Basel, Switzerland

Correspondence
Patrick Tschopp, DUW Zoology, University of Basel, Vesalgasse 1, CH-4051 Basel, Switzerland.
Email: patrick.tschopp@unibas.ch

Funding information
Swiss National Science Foundation, Grant/Award Number: 31003A_170022

Abstract

Fifty years ago, Lewis Wolpert introduced the concept of "positional information" to explain how patterns form in a multicellular embryonic field. Using morphogen gradients, whose continuous distributions of positional values are discretized via thresholds into distinct cellular states, he provided, at the theoretical level, an elegant solution to the "French Flag problem." In the intervening years, many experimental studies have lent support to Wolpert's ideas. However, the embryonic patterning of highly repetitive morphological structures, as often occurring in nature, can reveal limitations in the strict implementation of his initial theory, given the number of distinct threshold values that would have to be specified. Here, we review how positional information is complemented to circumvent these inadequacies, to accommodate tissue growth and pattern periodicity. In particular, we focus on functional anatomical assemblies composed of such structures, like the vertebrate spine or tetrapod digits, where the resulting segmented architecture is intrinsically linked to periodic pattern formation and unidirectional growth. These systems integrate positional information and growth with additional patterning cues that, we suggest, increase robustness and evolvability. We discuss different experimental and theoretical models to study such patterning systems, and how the underlying processes are modulated over evolutionary timescales to enable morphological diversification.

KEYWORDS

directional growth, morphological diversification, patterning modules, periodic pattern formation, positional information, repetitive morphological structures, self-organization

1 | INTRODUCTION

Repetitive structures are plentiful throughout nature—be it the juxtaposed leaves on the branch of a tree, the body segments of an insect, or the individual bones that make up the vertebrate spine. From an evolutionary perspective, such repetitive patterns can be explained by the adaptive value the repetition of a certain anatomical unit can provide in itself. Moreover, repeatedly re-deploying and modifying a pre-existing developmental patterning module can enable morphological diversification. For example, in case of the vertebrate spinal column, individual vertebrae are attached to one another in a stable yet movable fashion. This repetitive vertebral architecture ensures the overall suppleness of the structure that is required for body movement, while also providing a solid protective encasement of the delicate spinal cord it encloses. At the same time, by exploiting the inherent developmental modularity of these spinal building blocks, the overall number of vertebrae can differ substantially between species, and each individual vertebra along the anterior-posterior axis can be modified in its morphology.[1,2] The

concept of modularity is thus central to our understanding of how repetitive patterns can arise on both developmental and evolutionary timescales.[3-5] How then, however, is a certain patterning module repeatedly specified during embryogenesis, in a reliable and robust manner, while at the same time allowing for slight deviations that eventually can be canalized into evolutionarily novel morphologies?

Fifty years ago, the theoretical biologist Lewis Wolpert introduced his concept of "positional information" that, to this day, continues to influence the way we think about developmental pattern formation.[6] He hypothesized that cells in an embryonic field have their relative position specified through a coordinate system based on three essential features: boundaries, that define the field and to which the relative position of a cell needs to be specified; a scalar to measure the distance from said boundaries; and polarity, emergent from the juxtaposition of differing scalar values, to confer directionality to this measurement. Both scalar and polarity of the system have come to be associated most often with a diffusible substance or "morphogen," a term originally introduced by Alan Turing,[7] even though Wolpert also alluded to other potential mechanisms.[8] To illustrate the concept of positional information, Wolpert first assumed a multicellular field with uniform progenitor identities. Through localized production and subsequent dispersal of a substance, that is, a morphogen, cells in the embryonic field would be exposed to differing concentrations along a gradient, which in turn bestows upon them distinct "positional values." According to distinct "thresholds" of morphogen concentration, this continuous distribution of positional values is then differentially interpreted by the cells in the field and translated into discretized cellular states (Figure 1A). Thus, over the course of development, an initial asymmetry in morphogen production would allow cells to acquire different, concentration-based positional values, categorize these values into a discontinuous distribution of changes in cell-intrinsic parameters, and ultimately result in spatially distinct cell fate decisions. This is famously illustrated in the so-called "French Flag problem," in which Wolpert's model posits the sub-division of a homogeneous population of cells into three discrete "cell type domains" as a result of threshold-based interpretation of a continuous morphogen gradient (Figure 1A). In the decades since its initial proposal, the concept of positional information has accumulated support from a range of experimental observations, beginning with classical embryology approaches,[9,10] and followed by investigations into the underlying cellular, molecular, and biochemical mechanisms.[11-13]

Despite its far-reaching implications and experimental validation, there remain certain common patterning motifs, as well as evolutionary variations therein, that Wolpert's initial theory alone cannot explain satisfactorily. These patterns include, as already Wolpert acknowledged himself, the ones underlying the formation of repetitive morphological structures (Figure 1B,C). He reasoned that for highly repetitive architectures the assumption of a pre-patterning mechanism would provide a more parsimonious explanation than a purely positional information-based system, given the increasingly high number of distinct thresholds that are to be defined in the latter.[8]

In this review, we focus on the repeated deployment of developmental patterning modules, and how positional information might work alongside other mechanisms to assure proper pattern formation and evolution. After a brief overview of repetitive pattern formation in both two- and one-dimensional domains, we will shift our focus to systems where the polarity of the resulting repetitive pattern is inherently linked to the directionality of tissue growth. We will highlight the role of positional information in defining the temporal and spatial dynamics of such directed growth and discuss the challenges of establishing morphogen gradients in non-static embryonic fields with high cellular turnover. At the same time, positional information can define windows of "patterning competency," for proliferating progenitors to respond to additional, often self-organizing mechanisms, which eventually result in segmented architectures made of repetitive morphological structures. We emphasize the apparent ease with which evolutionary variations in segment repetitions can be achieved under such conditions—through modifications of positional information, growth parameters or the additional patterning modules—as evidenced by morphological extremes like the vertebral column of snakes or the number of digit bones in cetacean flippers. Finally, we will review experimental and theoretical approaches to study these processes in vivo, ex vivo, in vitro, and in silico, and how results from such studies continue to contribute to our understanding of developmental pattern formation and evolutionary diversification.

2 | THE FORMATION OF REPETITIVE PATTERNS IN NATURE—POSITIONAL INFORMATION AND SELF-ORGANIZATION

Pattern formation is an essential feature of multicellular organism development, and variations in patterning

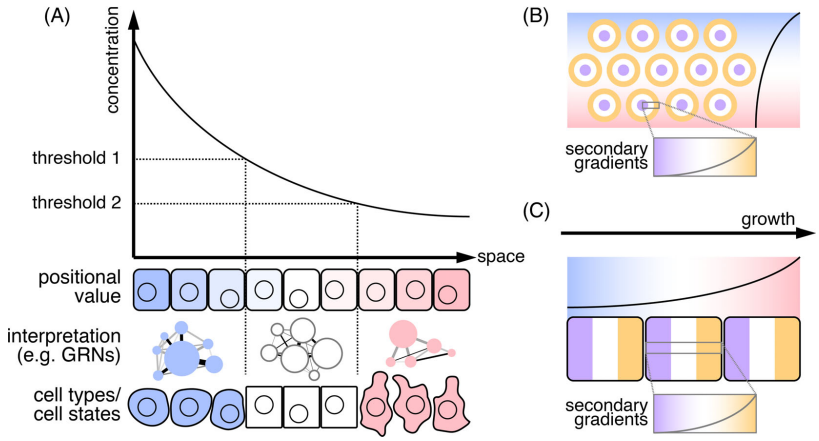

FIGURE 1 "Positional information" and the emergence of repetitive patterns. A, Wolpert's classic illustration of positional information and its relation to the "French Flag problem." A morphogen is locally produced, secreted, and dispersed to establish a molecular gradient over an embryonic field. Cells are exposed to different molecular concentrations along the gradient, endowing them with distinct "positional values." According to distinct "thresholds," these positional values are differentially interpreted by the cells (eg, rewiring of gene regulatory networks [GRNs]) and result in distinct cell fate decisions. B, Positional information in two-dimensional, repetitive patterns. While the formation of many two-dimensional, repetitive patterns can be explained by self-organizing principles, their implementation is often constrained by additional, pre-existing positional information cues (blue to red gradient). Once initiated, repetitive elements may act as secondary morphogen sources and exert their effect on the surrounding tissue in a positional information-like manner (concentric patterns, purple to orange gradients). C, Positional information in one-dimensional, repetitive patterns driven by directional growth. Growth dynamics and their underlying progenitor populations rely on morphogen gradients that determine a field of competency (blue to red gradient). Moreover, previously formed segments may inherit positional information-containing polarity and establish secondary morphogen gradients themselves, to modulate the formation of successive elements (purple to orange gradients)

mechanisms are thought to contribute substantially to morphological diversification. Consequently, pattern formation has fascinated scientists for centuries and, owing to its amenability to abstraction, has stimulated collaborations between experimental and theoretical biologists.[14-16] Formation of periodic patterns, in particular, has attracted mathematicians and computational modelers alike.[17] Two of the most prominent conceptual frameworks in the field of pattern formation are certainly Wolpert's theory on positional information, and Alan Turing's "reaction-diffusion"-based mechanisms. Unlike positional information, Turing models do not explicitly require any polarized molecular asymmetries prior to pattern emergence. Rather, slight spatial imbalances in the initial distribution of a cross-regulatory pair of an "activator" and an "inhibitor" are accentuated over time, due to different diffusibilities of the two substances, and thereby give rise to essentially self-organizing patterns.[6,7,18] While positional information had found plenty of experimental support early on—owing in large part to the rise of molecular genetics that helped to elucidate the segmentation network in *Drosophila* or cell fate specification in the early frog embryo (see below)—Turing systems and other self-organizing models have recently gained renewed interest.[19] Examples include symmetry-breaking events that underlie the emergence of repetitive, two-dimensional patterns (Figure 1B), like the induction of ectodermal appendages in the amniote skin,[20] spacing of stripe-color patterns in fish,[21] bristles placement on the fruit fly thorax,[22] rugae formation in the mammalian palate,[23] or the formation of digits in the tetrapod autopod.[24] Additionally, rather than focusing exclusively on the self-organizing properties of reaction-diffusion-type molecular systems, the role of cellular and/or mechanical mechanisms is increasingly being acknowledged,[25-28] as well as the potential to rely on the inherent periodicity of molecular oscillators to generate repetitive patterns.[29] While the oscillatory nature of these latter systems can be an emergent property at the tissue level, and hence be referred to as self-organizing,[30,31] their impact on the formation of repetitive spatial patterns is less direct. Unlike Turing models, which can reach stable states inside static embryonic fields, the temporal dynamics of a molecular oscillator necessitate its coupling to other variables, for example, polarized growth, to translate wave-like gene activities into a

defined spatial pattern (Figure 1C).[32] Importantly, however, in most of the patterning scenarios investigated thus far, neither self-organizing principles nor positional information seem to function in an entirely isolated fashion. Rather, they frequently co-occur, in parallel or close temporal succession, and similar patterning principles might repeat themselves during the maturation of a particular morphological structure. For example, while the periodicity of a given two-dimensional pattern may rely on self-organizing properties, potential sub-types of the resulting units—for example, different *Drosophila* sensory bristles or tetrapod digit homeotic identities—can be defined by pre-existing morphogen gradients (Figure 1B; blue to red).[22,33,34] Once initiated, these repetitive structures have the potential to act as morphogen sources themselves, to refine the emerging pattern or instruct the fate of neighboring elements (Figure 1B,C; purple to orange).[22,35] Collectively, combining "positional information" with growth and additional patterning modules alleviates many of the problems inherent to the establishment of highly repetitive structures, were they to be specified by "positional information" only (eg, setting up reliable long-range gradients or precisely defining multiple threshold values). Such combinatorial patterning modules can therefore contribute to increase pattering robustness as well as boost the potential for their evolutionary reshuffling.[33,36,37] Hence, it appears that the strict dichotomy often attributed to the deployment of these two distinct patterning concepts during embryogenesis—that is, "positional information" or "self-organization"—is likely artificial and, as previously suggested, a more realistic approximation of development would entail various combinations of the two (Figure 1B,C).[8,18,19]

3 | ARTHROPOD SEGMENTATION—POSITIONAL INFORMATION AND THE SPECIFICATION OF REPETITIVE PATTERNS IN STATIC AND EXPANDING DOMAINS

It can been argued that part of the tremendous evolutionary success of arthropods, both in terms of taxonomic diversity and sheer abundance, is attributable to their segmented, metameric body plan organization. Indeed, functional specializations of different body segments have enabled the exploitation of a wide variety of different ecological niches.[38,39] The study of insect embryogenesis and segment formation, in particular, has substantially contributed to our understanding of how positional information can instruct the formation of repetitive patterns. For one, unlike for the aforementioned combinatorial patterning modes, during the early segmentation of the *Drosophila* embryo Wolpert's concept of positional information manifests itself most explicitly. Accordingly, anterior-posterior patterning in *Drosophila* was amongst the first experimental models to unequivocally prove some of Wolpert's key predictions. During *Drosophila* embryogenesis, all body segments are already contained within the length of the embryo's syncytial blastoderm. Fundamental to establishing positional information in this system, and by extension the specification of primary body axis segmentation and polarity, are two opposing gradients. Their presence had already been inferred from cytoplasmic constriction and transplantation experiments, and was predicted to rely on maternal gene products deposited on either end of the egg.[9] With the identification of *bicoid*, the causative anterior determinant, and subsequently *Nanos*, its posterior counterpart, the first molecules emerged to validate Wolpert's claims.[11,40] Downstream of *bicoid* and *Nanos*, a hierarchically organized gene regulatory network interprets the positional values of the two gradients, to sub-divide the anterior-posterior body axis, specify individual segments and establish segment polarity and identity.[41] Hence, within the static domain of the *Drosophila* embryo, two opposing gradients, with cross-regulatory interactions for increased precision, and their differential cell-intrinsic interpretation suffice to reliably specify the positional values required for the formation of all body segments.

However, while the simultaneous specification of body segments is characteristic for long-germ band insects such as *Drosophila*, in short-germ band insects like the flour beetle *Tribolium casteneum* segments are formed sequentially, from anterior to posterior as the embryo elongates.[42] This mode of segmentation thus intimately links growth-based axis elongation to periodic pattern formation and is, in fact, considered to be the ancestral condition for arthropods in general.[43] The posterior region of short-germ band embryos contains a growth zone of proliferating progenitor cells that drives axis elongation. Positional information, based on a gradient of Wnt/β-catenin activity that delineates a posterior growth zone, and a molecular oscillator, involving the cyclic expression of "Pair rule" genes, are required for axis extension and segmentation in short-germ band insects.[42,44-46] Unlike in *Drosophila*, where Pair-rule genes are concomitantly expressed in a striped pattern demarcating the future segments, dynamic waves of cyclic Pair-rule gene expression propagate along the *Tribolium* growth zone, to sequentially segment the emerging primary body axis. Additionally, *Caudal*, *Dichaete* and *Odd-paired* expression in *Tribolium* form spatiotemporally dynamic wavefronts that travel along the

anterior-posterior axis of the elongating embryo, while in *Drosophila* their sequential activation acts as a timer of Pair-rule gene expression.[47] Hence, although displaying drastically different growth modes for axis elongation, in both long-germ and short-germ insect segmentation similar sets of orthologous genes are essential in anterior-posterior pattern formation. The underlying genetic circuitries thus seem to contain an ability to compute and execute analogous patterning functions, both within static embryonic fields as well as along progressively elongating domains.[47-49] Disparities in their regulatory architectures, though, between long-germ and short-germ insects, emphasize the importance of properly integrating temporally dynamic gene expression programs with positional information in directionally growing domains.[47,49,50] The fact that short-germ band insects do not seem to exploit their mode of axis elongation to increase overall segment number, like for example in the vertebral column of snakes (see below), may hint at an underlying developmental constraint, originating from molecular crosstalk between the two systems in insects.[42,51] Intriguingly, though, primary body axis patterning in other arthropod clades such as the *Myriapoda* clearly is more variable, with overall segment numbers in for example, geophilomorph centipedes ranging from 27 to 191.[52] Hence, how seemingly similar genetic cassettes are cross-regulated in both space and time, and integrated with a particular growth dynamic, is what ultimately appears to determine the resulting segmented pattern and its evolvability.[43,53]

4 | POSITIONAL INFORMATION, DIRECTIONAL GROWTH, AND THE PERIODIC SPECIFICATION OF ONE-DIMENSIONAL PATTERNS

By explicitly decoupling the control of growth dynamics from a self-organizing mechanism, modular variations of periodic pattern formation—and hence segment numbers—can be achieved through evolutionary modifications altering either one or both of the two parameters. For the control of directional growth, morphogen-based positional information often delineates a pool of progenitor cells and, accordingly, gradient dynamics can define the spatial and temporal extent of proliferative axis elongation. Establishing accurate positional information within a directionally growing embryonic field, however, can present several challenges. Rather than cells being located statically within the field, and thus able to interpret a morphogen gradient both spatially and temporally, they dynamically traverse the domain to be patterned, as tissue elongation occurs. The history of positional cues that the cells experience thus directly relates to the directional growth dynamics they themselves help to establish.

There are numerous examples in nature where the creation of repetitive morphological structures depends on growth dynamics that can be approximated along a one-dimensional domain. While for much of the remainder of this review we focus on two iconic 1D-patterns in vertebrates—that of the somite-driven segmentation of the primary body axis and the individualization of phalangeal bones in tetrapod digits—it is worth mentioning that similar periodic patterns, some with striking similarities, have also arisen in the plant kingdom. Given the independent advent of multicellularity in the animal and plant kingdoms, the underlying mechanisms of these patterning systems must have evolved convergently. However, as previously argued by others, certain unifying design principles, as well as conserved molecular and/or cellular features implemented in these patterning systems, can emerge from such distant comparisons.[54-56]

4.1 | Plant shoot segmentation: Repetitive patterns of phytomers

In most plants, above-ground growth relies on cell proliferation at the tip of the elongating shoot. This growth is sustained by a stem cell population that is located inside the so-called "shoot apical meristem" (SAM).[57] The basic structure of the SAM can be roughly subdivided into a central zone—the reservoir containing the stem cells—a rib zone which forms the bulk of the plant stem, and a peripheral zone from which lateral organs such as leaves develop.[58] Importantly, shoot elongation occurs in a segmented fashion, through the successive addition of repetitive structures known as "phytomers." Each phytomer is composed of a node carrying a leaf, an internode region and an axillary bud that allows for branching (Figure 2A).

Inside the SAM, stem cell proliferation vs differentiation needs to be tightly balanced. Genetic analyses in *Arabidopsis*, as well as comparative studies across species, have revealed the presence of multi-faceted regulatory cascades centered on the CLAVATA-WUSCHEL axis that maintain the undifferentiated state of the SAM stem cells.[59,60] SAM stem cells provide the cellular building blocks to the different components of the phytomer, including the axillary buds. Axillary buds can act as meristems, just like the SAM, and give rise to secondary shoots that are either vegetative (eg, lateral branches) or reproductive (ie, flowers) in nature. They can thus be considered as several secondary 1D-growing fields connected to one major 1D-growing domain whose

directionality is determined by the location of the SAM. By extension, spatiotemporal modulation of the patterning and positioning of these axillary buds along the apical-basal axis of the main shoot allows plants to diversify their overall architectures.[61]

Inside the main shoot, the repetitive deployment of the segmental phytomers depends on "phyllotaxis," the process of periodic placement of plant lateral organs in regular intervals both around the central and apical-basal axes of the shoot.[62] Subsequent elongation of the phytomer then leads to the species-specific spacing patterns observed between the individual segments. For the radial patterns circumscribing the shoot, lateral organ placement can occur in whorled, distichous (alternate), decussate (opposite) as well as spiral arrangements—the latter invoking the famous Fibonacci sequence.[63-65] Auxin, a phytohormone produced in the SAM, has been shown to have a central role in lateral organ formation and thus phyllotaxis. Indeed, micro-manipulations of auxin concentration reveal that when auxin levels decrease, stem cells start to differentiate.[66,67] Thus, gradients of auxin concentration provide positional information along the apical-basal axis, and critically contribute to control the balance between cell proliferation and differentiation (Figure 2A).[66] During phyllotaxis, PIN proteins, a family of membrane bound efflux carriers, control the generation of new auxin maxima and polar transport of auxin by PIN proteins allows for periodic pattern formation of organ initiation on the plant shoot.[66,68,69] Several studies have suggested the presence of additional feedback mechanisms to ensure proper organ placement, both at the level of auxin transport or via inhibition from previously formed organ primordia.[70,71] In parallel to these mostly auxin-based inhibitory functions, cytokinin, another phytohormone, plays important roles in phyllotactic patterning.[72] Cytokinin is mainly produced in roots and is transported up the shoot, thus forming a basal-to-apical gradient of cytokinin and, in association with auxin, defining robust positional information along the shoot (Figure 2A). Cross-regulatory effects between the two hormones, at the level of their respective syntheses or transport modes, as well as intercellular movement of additional inhibitors seem to define this interaction at a molecular and cellular level.[71,73,74] Moreover, the fact that the eventual basal-to-apical 1D-pattern of the shoot involves—in its inception—a two-dimensional component, namely the circumferential positioning of lateral branches, has led to the consideration of different self-organizing properties involved in the process. For example, inhibitory fields of leaf primordia have been proposed to affect spacing during phyllotactic patterning,[64] and already Turing himself, and others, have argued that activator-inhibitor pairs might underlie the patterning phenomenon of phyllotaxis.[7,62,75,76] How exactly such interplay of positional information and self-organizing principles is realized, however, and in which way the rate of apical-basal growth as

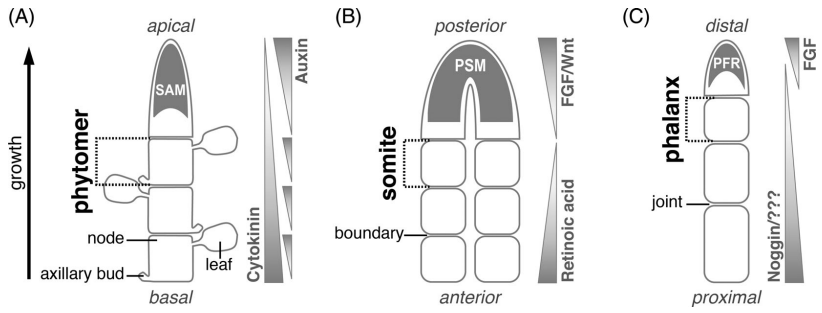

FIGURE 2 Formation of repetitive morphological structures across kingdoms. A, In plants, apical-basal growth depends on a proliferative zone at the apex of the shoot called the "shoot apical meristem" (SAM). The elongating shoot is segmented into repetitive structures known as "phytomers," which are composed of a node carrying the leaf, an internode region and an axillary bud. The integration of two opposing gradient systems of phytohormones—auxin, mainly synthetized in the meristems, and cytokinin, mainly synthetized in roots—provides positional information along the apical-basal axis, and helps to define a balance of proliferation and differentiation. B, Vertebrate axial elongation depends on the successive formation of "somites," which originate from progenitors within the presomitic mesoderm (PSM). Posterior-to-anterior gradients of FGF and Wnt and an anterior-to-posterior gradient of Retinoic acid (RA) provide positional information along the primary body axis. These gradients delineate a "determination front," at which progenitors respond to molecular oscillators to initiate segmentation. C, Tetrapod digits grow proximal-distally due to progenitor proliferation within the phalanx forming region (PFR), which relies on a distal FGFs. Once progenitors leave the PFR, cell fate decision into either joint- or cartilage-forming cells instruct the digit segmentation pattern into individual "phalanges," potentially modulated by BMP inhibitors released from previously formed elements

determined by the SAM affects this balance, is an area of active investigation using both theoretical and experimental approaches.[62,67,77]

4.2 | Vertebrate primary body axis segmentation: Repetitive patterns of somites

During vertebrate embryogenesis, the paraxial mesoderm, localized on both sides of the developing neural tube, is segmented into a series of repetitive structures that are known as "somites." Cells inside these somites give rise to a variety of tissues in the adult body, such as for example, muscle, dermis, tendons, or the progenitors of the axial skeleton.[78] Most somite-derived tissues lose their segmented appearance as they mature. Notably, although somite number determines vertebral count, even the separation into individual vertebrae is secondary to the original somite boundaries. Vertebrae form from the repeated fusion of the caudal and rostral halves of two consecutive somites, with additional patterning cues emanating from the notochord.[79-81] From an evolutionary perspective, overall somite number, and by extension vertebral count, can vary substantially between different vertebrate species.[1] Moreover, these skeletal somite derivatives appear highly regionalized along the anterior–posterior axis, with characteristic vertebral morphologies that reflect their distinct functions along the spine.[82,83]

Somitogenesis initiates anteriorly, adjacent to the head mesoderm, and progresses along the primary body axis as the embryo elongates at its posterior end. Segmentation occurs periodically, with a species-specific temporal rhythm, with somites progressively forming from the paraxial mesoderm with a remarkably regular rate of segmentation.[29] The maintenance of this process critically depends on a posterior progenitor population, which in its unsegmented state is known as the "presomitic mesoderm" (PSM) and acts as a unidirectional growth zone (Figure 2B).[84] As these mesenchymal cells approach the anterior margin of the PSM, an epithelium surrounding a mesenchymal core begins to form, thereby defining the individual somites. Hence, by controlling the elongation rate inside the PSM, as well as the temporal rhythmicity with which new boundaries are initiated, the basic pattern of somitogenesis is controlled.[85] Several models have been suggested to conceptualize the temporal and spatial aspects of this somitogenic process, most notably the "clock and wavefront" model.[86] This model proposes two distinct mechanisms that, in combination, provide an explanation for the sequential formation of somites. First, a molecular oscillator, or "segmentation clock," instructs the temporal periodicity with which new somites are formed. And second, a hypothetical gradient provides positional information in form of a "wavefront," to define an anterior-posterior position inside the PSM where cells become responsive to the segmentation signals of the clock. This particular location is often referred to as the "determination front." Indeed, the clock and wavefront model has been supported by numerous experimental observations. For example, cyclic expression of *Notch* target genes was reported in the PSM of chick embryos.[87,88] Moreover, mutations therein, as well as experimental perturbations in *Notch* modulators, were shown to affect the molecular clock and somitogenesis in various vertebrate species.[89-91] Following studies have revealed a substantially expanded oscillatory regime inside the PSM. Besides the *Notch* pathway, this includes members of the *Wnt* and *Fgf* signaling cascades,[92,93] both of which have also been implicated in the second major constituent of the model, the "wavefront" (see below). Intriguingly, while the overall pathways of the oscillator seem conserved amongst vertebrates, the actual gene members that show cyclic behavior can vary considerably between species.[94] This argues for substantial stability when determining the net output of the respective signaling network, potentially conferred by multiple feedback loops, which in turn can explain the apparent drift in the developmental system at the molecular level.[95,96] The second major prediction in the model of Cooke and Zeeman is the presence of a wavefront at the anterior margin of the PSM, which acts as a traveling frontier of somite formation competency that moves posteriorly as the embryo elongates.[86] It was suggested that positional information by morphogen signaling gradients emanating from the PSM instructs the positioning of the wavefront. Indeed, posterior-to-anterior gradients of FGF and Wnt as well as an anterior-to-posterior gradient of Retinoic acid (RA) have been reported (Figure 2B). FGF signaling has been shown to determine wavefront position along the axis of the PSM and to be involved in the onset of the segmentation program.[97] High levels of FGF activity maintain an undifferentiated state and confer elevated levels of mobility in posterior cells.[98] As FGF production is restricted to the posterior end of the PSM, FGF levels decrease as the cells travel along to the PSM, allowing anteriorly located progenitors to start their segmentation program while at the same time contributing to axis elongation.[99,100] Additionally, graded *Wnt* activity contributes to the positioning of the wavefront, as well as providing a molecular link to the segmentation clock itself and the proliferative control of axial progenitors.[92,101-103] From the anterior end, a gradient of RA refines this boundary, while at the same time buffering for left-right asymmetries in the formation of somites on either side of the neural tube.[104-106] Hence, integrating the spatial and

temporal dynamics of these gradients with the oscillations of a molecular clock, determines overall elongation and segmentation rate of the PSM, and provides a conceptual framework to contextualize somite size control.[85,107]

The development of models that are able to approximate important aspects of somite segmentation ex vivo, in vitro and/or in silico have empowered experimental and theoretical approaches to study the process at a more quantitative level. Many of them focus on some of the apparent self-organizing properties of the process, in particular for size scaling and the emergence of the molecular oscillator.[30,31,108-111] Some iterations abandon the notion of the importance of global positional information via gradients altogether, in favor of an oscillatory reaction–diffusion mechanism.[112] Importantly, however, only by explicitly including termination of elongation and patterning in these models will the true evolutionary diversity in vertebral formulas be accounted for.[113] This would further entail the control to balance segmentation speed and progenitor pool size,[114] as well as incorporating the temporal and spatial effects of an axial *Hox* code on progenitor proliferation and somite identity.[115-118] Intriguingly, either modulations in the speed of the segmentation clock or, alternatively, changing the duration of progenitor pool persistence have been shown to alter the eventual number of segments in the vertebral column of different species.[114,115]

4.3 | Tetrapod digit segmentation: Repetitive patterns of phalanges

Another striking example of repetitive pattern formation along a single axis of embryonic growth is the development of tetrapod digits. Tetrapod digits are segmented into individual digit bones called phalanges, which in adult hands and feet are connected to each other by synovial joints. Analogous to the somite-derived vertebral column, different numbers of phalanges per digit occur, both within and between species. According to the fossil record, early tetrapods already showed differences in phalanges count in their digits.[119] Once the pentadactyl "ground state" of the autopod had been established, the ancestral phalanx numbers per digit are believed to be 2-3-4-5-3, for digits I to V.[4,120] However, these numbers have changed considerably in different tetrapod clades. For example, the majority of mammalian autopods display a 2-3-3-3-3 phalanx formula for their five digits,[4,120] while certain cetacean species have drastically increased the overall number of bones per digit. This resulted in an extreme variation of the ancestral phalanges pattern known as "hyperphalangy."[121] Moreover, phalanges in a given digit vary not only in number, but also differ markedly in individual size, both length- and girth-wise. As a consequence, within a given species, the number, size and shape of the phalanges are reflective of each digit's homeotic identity.[4,33]

At the onset of digit development the autopod plate is composed of alternating interdigit areas and digital rays, as previously specified by a Turing-like patterning mechanism.[24,34,122] While in the more proximal parts the metacarpals and metatarsals already start to condense, at the very distal tip of the autopod the actual outgrowth of the digits starts. Interestingly, the underlying molecular mechanisms for building these distal autopod elements are likely distinct from the more proximal ones, as demonstrated by the loss of phalange development in *Bmpr1b* knockout mice while metacarpals remain relatively unaffected.[123] Proliferation of a distal progenitor population, known as the "phalanx-forming region" (PFR), or "digital cresent" (DC),[124-126] allows for the growth of the digit to occur unidirectionally along its proximal-distal axis (Figure 2C). The PFR itself is thought to originate from the distal mesenchyme, localized just beneath a specialized epithelial structure called the apical ectodermal ridge (AER). Epithelial cells inside the AER are known to mediate overall limb growth, by secreting FGF signals that promote proliferation in the underlying mesenchyme.[127] Consequently, a FGF gradient specifies a distal domain of growth competency, which is translated into digit elongation at the PFR (Figure 2C).[122,124,125,128] FGF signaling from the AER seems to have a role not only in the control of digit length, but also phalanx numbers. By examining *Fgf8* expression in the developing chicken foot—in which each digit is morphologically different, both length- and phalanx number-wise—a correlation of the duration of *Fgf8* expression at the digit tip and the resulting number of phalanges was observed.[129] Experimentally prolonging *Fgf8* expression at the digit tip induces the formation of an additional phalanx, while use of an FGF receptor inhibitor prevents formation of the most distal phalanx.[129] Temporal variations in AER persistence, and by extension duration of FGF signaling, have therefore the potential to explain even extreme deviations from an ancestral phalanx formula, such as for example seen in the hyperphalangy of cetacean flippers.[130] However, while the effect of FGF on cell proliferation suggests an obvious mechanism to control digit length, how can the segmentation into individual phalanges occur at the cellular and molecular level?

It is also within the PFR population that distinct cell fate decisions are thought to occur during digit elongation, instructing digit segmentation along its proximal-distal axis. In contrast to somite formation, where a change of tissue organization (ie, mesenchymal-to-

epithelial) drives segmentation, the partitioning of digits into individual phalanges involves the specification of two distinct cell types. Once proliferation of the PFR progenitor cells has displaced the source of the FGF gradient distally, the proximally located cells lose their progenitor state and undergo a divergent cell type specification. They differentiate accordingly into either chondrocytes—the cellular building blocks of the phalanges themselves—or prospective interzone cells that eventually form the synovial joints to connect the digit bones.[122,131] Hence, by controlling the temporal aspects of this divergent cell fate decision with respect to the overall growth rate, the digit segmentation pattern into individual phalanges can be determined. To faithfully execute this process, the PFR assimilates various signaling inputs that confer positional information and modulate additional, possibly self-organizing mechanisms, to result in correct digit segmentation patterns and thus homeotic identity. Most notably, it has been demonstrated in chicken embryos that the forming digits have their segmentation pattern specified by the interdigit mesenchyme that is located immediately posterior to them.[33] Interdigit mesenchyme "cut-and-swap" experiments result in homeotic transformations that corroborate the idea that the interdigit mesenchyme is involved in digit identity specification. Multiple lines of evidence implicate gradients of BMP signaling, originating from the interdigit tissue, to establish this positional information system at the molecular level. For example, implantation of a bead soaked with the BMP antagonist NOGGIN within the interdigit induces an anteriorization of digit identity.[33] Moreover, the PFRs of different digits were found to carry distinct levels of SMAD1/5/8 activity that correlate well with the eventual differences in their segmentation patterns.[125]

While the role of BMP signaling in determining phalanx numbers in each digit is well accepted, there is mounting evidence that it could also influence phalanx size. Within each digit the phalanges sizes do not vary randomly, but rather seem to change as an integral developmental module, separate from the rest of the autopod.[122,132] Capitalizing on a broad phylogenetic sampling covering multiple vertebrate clades, it was demonstrated that the ratios of measured areas of successive phalanges change in a predictable manner. Namely, the size of a proximally located phalanx is prognostic for the size of more distal phalanges, with the largest phalanges usually found at the proximal end of the digit.[132] Thus, despite the complexity and diversity of phalangeal morphology across digits and species, there appear certain remarkably conserved relationships amongst the distinct elements that point to the presence of conserved developmental modules. Moreover, the periodicity of the eventual pattern may hint at an underlying self-organizing property of the process, potentially Turing-like in nature, that acts concomitantly as digit elongation occurs. Indeed, individualized phalanges sizes are not merely the result of post-patterning events like, for example, growth plate-mediated long bone elongation. Rather, they represent an integral part of the patterning process itself, as size differences are already apparent at early stages of phalanx specification. This corresponds to a timepoint when synovial joint interzones separating the successive phalanges are being initiated.[132,133] Barrier insertion and viral overexpression experiments in chicken, as well as genetic manipulations in mice, suggest that one or more diffusible cues from the previously formed phalanx and/or interzone may be instrumental in this process.[132,133] Several experimental observations also imply the presence of additional, partially self-organizing principles that may help to refine digit pattern periodicity.[122] For example, the ectopic induction of an interzone using retroviral overexpression of *Wnt9a* has been shown to inhibit formation of subsequent joint sites at a distance.[134] Likewise, insertion of a barrier into a proximal phalanx leads to an increased segment sizes in subsequently forming phalanges.[132] Based on its expression in maturing phalanges, as well as the lack of phalangeal joint formation in mutant embryos, *Noggin* has been proposed as the putative diffusible cue underlying these effects (Figure 2C).[135] A progressive build-up of NOGGIN protein, caused by the increasing phalanx expression domain, could instruct subsequent joint specification, once a critical threshold of BMP inhibition has been reached.[133] Using an allelic series in mice, NOGGIN-modulated BMP activity itself has been shown to lie downstream of a 5′Hoxd-Gli3 antagonism. Since both 5′Hoxd genes and Gli3 show quantitative differences in their expression levels along the pinky-to-thumb axis of the developing autopod, this model provides an elegant explanation of how anterior-posterior positional information could be translated into distinct digit identities.[129,133] However, based on the apparent dynamics of BMP signaling in the forming phalanges, across both space and time, additional modulators might be involved in the exact determination of digit-specific phalanx-joint patterns (Grall and Tschopp, unpublished observations).

5 | CONCLUSIONS AND FUTURE DIRECTIONS

As highlighted in the examples above, the three key components of a positional information-based coordinate

system—boundaries, scalar, and polarity—face distinct challenges when we consider their implementation in a directionally growing domain. As for the non-expanding condition proposed in Wolpert's original model, morphogen gradients play an essential role in determining all three parameters. How they are established, however, can be quite different from their static counterparts. For phytomers, somites, and phalanges, the position of a proliferating progenitor population defines one of the boundaries of the field to be patterned, as well as the directionality of tissue growth (Figure 2A-C). Localized production of a morphogen within (SAM, PSM) or nearby (AER) this progenitor population provides the source for establishing a molecular gradient. The time required for a cell to traverse the resulting gradient field, that is, the interval a cell is displaced from the gradient's range of influence by the proliferation of more distally located cells, thus becomes central to the temporal integration of the signal.[8,136] Moreover, the distal production of the morphogen in phytomer and somite progenitors themselves, and the control of its polarized transport or stability, as the cells journey through the field, are essential to define the scalar of the gradient.[67,99] For the PFR, responsiveness to the FGF signals emanating from the overlaying AER alters proliferation rates and, by extension, the time the progenitors spend inside the gradient. The unidirectional nature of the growth, resulting from the distal location of the proliferating progenitor populations, inherently defines the polarity of these gradients. To ensure robustness in establishing and interpreting all of these primary gradients, secondary and opposing gradients act in conjunction (Figure 2A-C). In case of cytokinins (phytomers) and retinoic acid (somites), they function by directly counteracting the distal gradients,[72,105] whereas *Noggin* (phalanges) has been suggested to spatially modulate the induction of the following segments.[133,135] These proximally located gradients are also key to control secondary patterning events in the prospective segments, be it for a graded size control of the forming phalangeal segments,[132] to balance left-right asymmetries in somites,[106] or to control the spacing and orientation of subsequently forming secondary organs in plant shoots.[73,74] Importantly, in all three cases the production of these secondary gradients initiates in an already formed segment, that is, in cells that have been removed from the embryonic field to be patterned. As such, they help to determine and refine the proximal boundaries of the field, while at the same time contribute to segment size control.[5,74,107]

Combining growth-driven displacement of molecular gradients, to establish positional information, with a secondary, self-organizing patterning module appears to be a common design principle in the establishment of periodic patterns.[32] In somitogenesis, the location of segment boundary formation famously depends on the combination of a gradient-dependent, moving "determination front" and cell-intrinsic molecular oscillators.[29,30] Likewise, for root growth in plants—which relies on a SAM-like arrangement of its proliferating progenitors, the root apical meristem (RAM)—oscillating gene expression networks have been reported to control the periodicity of lateral branching.[137] Above ground, however, phyllotaxis has been successfully approximated in silico by activator/inhibitor- and transport-based models.[67,75,138] While molecular similarities to the oscillator-based segmentation of the primary body axis have been proposed for overall tetrapod limb patterning,[139] self-organizing mechanisms in general await further experimental validation and quantitative data, in particular for the patterning of individual phalanges in the distal limb.[122,133] Clearly, however, it appears that the combination of positional information-based directional growth with additional patterning modules, often self-organizing in nature, might generally underlie the periodicity of repetitive morphological structures (see eg, palate growth and Turing mechanisms during mammalian rugae formation[23]).

Indeed, by combining Wolpert's positional information with further patterning systems, either temporally or spatially, the overall robustness of the system might increase, and could thus be buffered against slight developmental deviations that eventually might transition into evolutionary novel patterns.[96,140] While variations in segment numbers are easily explained by alterations in the size or the temporal persistence of the progenitor pool, results from morphological extremes, like vertebral count in snakes or cetacean phalanges, suggest that different sub-modules of the system—for example the speed of an oscillator or proliferation-dependent feedback into the segmentation module—can be affected as well.[114,130] Moreover, size control between individual elements might be internally constrained by the molecular and/or cellular architecture of the ancestral segmentation process, thus restricting the exploration of the entire theoretically available morphospace.[5] And lastly, post-pattering processes, like discretized growth control of individual segments, may provide an additional layer of evolutionary diversification.[141,142] Importantly, all of these observations highlight the fact that rarely, if ever, a certain pattering module might function in a truly isolated fashion. It is therefore more likely that these tight interconnections, between positional information and additional systems hint at the existence of largely context-dependent patterning outputs.

While providing pattering robustness and evolvability, such combinatorial systems can render the acquisition of

quantitative data cumbersome, as well as severely impede the design of clearly interpretable experimental perturbations in order to test certain hypotheses. Here, the development of dedicated ex vivo and/or in vitro models might prove invaluable to study a given patterning module in true isolation. This has already successfully been realized for important aspects of somitogenesis, or in different organoid systems.[31,109,143,144] In combination with microfluidic or optogenetic approaches controlling morphogen signaling, such ex vivo/in vitro methods are likely to contribute to a more quantitative understanding of the underlying molecular and cellular processes.[133,145,146] Furthermore, emerging techniques to measure and perturb various intrinsic parameters with cellular resolution will help to disentangle how virtually homogenous, extracellular positional information can be interpreted differentially cell-intrinsically, to result in discretized cellular states.[128,147] Quantitative data from these newly available technologies should in turn result in the continuing refinement of mathematical and computational models, to approximate periodic pattering of repetitive morphological structures in silico.[17,19]

Finally, implementing these experimental and theoretical methods within the context of an evolutionary-comparative framework might turn out to be mutually beneficial. For example, in silico models may help to predict the causative parameter alterations that can transform one species-specific pattern into another, whereas contrasting repetitive pattern formation over different evolutionary timescales can instruct the design of improved models and experimental approaches alike. Here, studies at the micro-evolutionary level will reveal the degree of plasticity associated with a certain patterning process, while macro-evolutionary comparisons can inform us about potential development constraint. Indeed, embracing the power of comparative approaches may bring us full circle with Wolpert's initial proposition of "positional information," where he discusses the problem in the context of species as diverse as hydra, *Drosophila* or chicken.[6] Such efforts have certainly contributed to our appreciation of two of the major underlying design principles in the patterning systems of highly repetitive structures: the fact that positional information seems to work preferentially in conjunction with additional, often self-organizing patterning modules, and that a decoupling of growth and segmentation control allows for modular alterations in segment numbers.

ACKNOWLEDGMENTS

Work in the Tschopp lab is supported by the University of Basel and the Swiss National Science Foundation (Grant Number: 31003A_170022). The authors would like to thank Nandan Nerurkar and two anonymous reviewers for their helpful comments on the article, as well as apologize to colleagues whose relevant work could not be cited due to space limitations.

ORCID

Patrick Tschopp https://orcid.org/0000-0001-7339-3990

REFERENCES

1. Gomez C, Pourquié O. Developmental control of segment numbers in vertebrates. *J Exp Zool B Mol Dev Evol*. 2009;312(6):533-544.
2. Mallo M, Wellik DM, Deschamps J. Hox genes and regional patterning of the vertebrate body plan. *Dev Biol*. 2010;344(1):7-15.
3. Esteve-Altava B. In search of morphological modules: a systematic review. *Biol Rev*. 2017;92(3):1332-1347.
4. Wagner G. *Homology, Genes, and Evolutionary Innovation*. Princeton; Oxford: Princeton University Press; 2014.
5. Young NM, Winslow B, Takkellapati S, Kavanagh K. Shared rules of development predict patterns of evolution in vertebrate segmentation. *Nat Commun*. 2015;6:6690.
6. Wolpert L. Positional information and the spatial pattern of cellular differentiation. *J Theor Biol*. 1969;25(1):1-47.
7. Turing. The chemical basis of morphogenesis. *Philos Trans R Soc Lond B Biol Sci*. 1952;237(641):37-72.
8. Wolpert L. Positional information revisited. *Development*. 1989;107(Suppl):3-12.
9. Nüsslein-Volhard C, Frohnhöfer HG, Lehmann R. Determination of anteroposterior polarity in Drosophila. *Science*. 1987;238(4834):1675-1681.
10. Tickle C, Summerbell D, Wolpert L. Positional signalling and specification of digits in chick limb morphogenesis. *Nature*. 1975;254(5497):199-202.
11. Driever W, Nüsslein-Volhard C. The bicoid protein determines position in the Drosophila embryo in a concentration-dependent manner. *Cell*. 1988;54(1):95-104.
12. Riddle RD, Johnson RL, Laufer E, Tabin C. Sonic hedgehog mediates the polarizing activity of the ZPA. *Cell*. 1993;75(7):1401-1416.
13. Green JBA, Smith JC. Graded changes in dose of a Xenopus activin A homologue elicit stepwise transitions in embryonic cell fate. *Nature*. 1990;347(6291):391-394.
14. Glen CM, Kemp ML, Voit EO. Agent-based modeling of morphogenetic systems: advantages and challenges. *PLoS Comput Biol*. 2019;15(3):e1006577.
15. Multerer MD, Wittwer LD, Stopka A, Barac D, Lang C, Iber D. Simulation of morphogen and tissue dynamics. In: Dubrulle J, ed. *Morphogen Gradients: Methods and Protocols. Methods in Molecular Biology*. New York, NY: Springer New York; 2018:223-250.
16. Sharpe J. Computer modeling in developmental biology: growing today, essential tomorrow. *Development*. 2017;144(23):4214-4225.
17. Hiscock TW, Megason SG. Mathematically guided approaches to distinguish models of periodic patterning. *Development*. 2015;142(3):409-419.
18. Green JBA, Sharpe J. Positional information and reaction-diffusion: two big ideas in developmental biology combine. *Development*. 2015;142(7):1203-1211.

19. Schweisguth F, Corson F. Self-Organization in Pattern Formation. *Dev Cell*. 2019;49(5):659-677.
20. Sick S, Reinker S, Timmer J, Schlake T. WNT and DKK determine hair follicle spacing through a reaction-diffusion mechanism. *Science*. 2006;314(5804):1447-1450.
21. Nakamasu A, Takahashi G, Kanbe A, Kondo S. Interactions between zebrafish pigment cells responsible for the generation of Turing patterns. *Proc Natl Acad Sci U S A*. 2009;106 (21):8429-8434.
22. Corson F, Couturier L, Rouault H, Mazouni K, Schweisguth F. Self-organized notch dynamics generate stereotyped sensory organ patterns in Drosophila. *Science*. 2017; 356(6337):eaai7407.
23. Economou AD, Ohazama A, Porntaveetus T, et al. Periodic stripe formation by a Turing-mechanism operating at growth zones in the mammalian palate. *Nat Genet*. 2012;44(3): 348-351.
24. Sheth R, Marcon L, Bastida MF, et al. Hox genes regulate digit patterning by controlling the wavelength of a Turing-type mechanism. *Science*. 2012;338(6113):1476-1480.
25. Ho WKW, Freem L, Zhao D, et al. Feather arrays are patterned by interacting signalling and cell density waves. *PLoS Biol*. 2019;17(2):e3000132.
26. Mahalwar P, Walderich B, Singh AP, Nüsslein-Volhard C. Local reorganization of xanthophores fine-tunes and colors the striped pattern of zebrafish. *Science*. 2014;345(6202):1362-1364.
27. Panousopoulou E, Green JBA. Invagination of ectodermal placodes is driven by cell intercalation-mediated contraction of the suprabasal tissue canopy. *PLoS Biol*. 2016;14(3): e1002405.
28. Shyer AE, Rodrigues AR, Schroeder GG, Kassianidou E, Kumar S, Harland RM. Emergent cellular self-organization and mechanosensation initiate follicle pattern in the avian skin. *Science*. 2017;357(6353):811-815.
29. Oates AC, Morelli LG, Ares S. Patterning embryos with oscillations: structure, function and dynamics of the vertebrate segmentation clock. *Development*. 2012;139(4):625-639.
30. Tsiairis CD, Aulehla A. Self-organization of embryonic genetic oscillators into spatiotemporal wave patterns. *Cell*. 2016;164 (4):656-667.
31. Hubaud A, Regev I, Mahadevan L, Pourquié O. Excitable dynamics and yap-dependent mechanical cues drive the segmentation clock. *Cell*. 2017;171(3):668-682.e11.
32. Richmond DL, Oates AC. The segmentation clock: inherited trait or universal design principle? *Curr Opin Genet Dev*. 2012; 22(6):600-606.
33. Dahn RD, Fallon JF. Interdigital regulation of digit identity and homeotic transformation by modulated BMP signaling. *Science*. 2000;289(5478):438-441.
34. Raspopovic J, Marcon L, Russo L, Sharpe J. Digit patterning is controlled by a Bmp-Sox9-Wnt Turing network modulated by morphogen gradients. *Science*. 2014;345(6196):566-570.
35. Manukyan L, Montandon SA, Fofonjka A, Smirnov S, Milinkovitch MC. A living mesoscopic cellular automaton made of skin scales. *Nature*. 2017;544(7649):173-179.
36. Gómez-Skarmeta JL, Campuzano S, Modolell J. Half a century of neural prepatterning: the story of a few bristles and many genes. *Nat Rev Neurosci*. 2003;4(7):587-598.
37. Haupaix N, Curantz C, Bailleul R, Beck S, Robic A, Manceau M. The periodic coloration in birds forms through a prepattern of somite origin. *Science*. 2018;361(6408):eaar4777.
38. Akam M. Hox genes and the evolution of diverse body plans. *Philos Trans R Soc Lond B Biol Sci*. 1995;349(1329):313-319.
39. Wainwright PC, Reilly SM. *Ecological Morphology: Integrative Organismal Biology*. Chicago: University of Chicago Press; 1994.
40. Wang C, Lehmann R. Nanos is the localized posterior determinant in drosophila. *Cell*. 1991;66(4):637-647.
41. Jaeger J. The gap gene network. *Cell Mol Life Sci*. 2011;68(2): 243-274.
42. Choe CP, Miller SC, Brown SJ. A pair-rule gene circuit defines segments sequentially in the short-germ insect *Tribolium castaneum*. *Proc Natl Acad Sci U S A*. 2006;103(17):6560-6564.
43. Patel NH. The evolution of arthropod segmentation: insights from comparisons of gene expression patterns. *Development*. 1994;1994(Supplement):201-207.
44. Bolognesi R, Farzana L, Fischer TD, Brown SJ. Multiple Wnt genes are required for segmentation in the short-germ embryo of *Tribolium castaneum*. *Curr Biol*. 2008;18(20):1624-1629.
45. Nagy LM, Carroll S. Conservation of wingless patterning functions in the short-germ embryos of *Tribolium castaneum*. *Nature*. 1994;367(6462):460-463.
46. Sarrazin AF, Peel AD, Averof M. A segmentation clock with two-segment periodicity in insects. *Science*. 2012;336(6079): 338-341.
47. Clark E, Peel AD. Evidence for the temporal regulation of insect segmentation by a conserved sequence of transcription factors. *Development*. 2018;145(10):dev155580.
48. Verd B, Clark E, Wotton KR, et al. A damped oscillator imposes temporal order on posterior gap gene expression in Drosophila. *PLoS Biol*. 2018;16(2):e2003174.
49. Zhu X, Rudolf H, Healey L, et al. Speed regulation of genetic cascades allows for evolvability in the body plan specification of insects. *Proc Natl Acad Sci U S A*. 2017;114(41):E8646-E8655.
50. Peter IS, Davidson EH. A gene regulatory network controlling the embryonic specification of endoderm. *Nature*. 2011;474 (7353):635-639.
51. Schoppmeier M, Schröder R. Maternal torso signaling controls body axis elongation in a short germ insect. *Curr Biol*. 2005;15 (23):2131-2136.
52. Chipman AD, Arthur W, Akam M. A double segment periodicity underlies segment generation in centipede development. *Curr Biol*. 2004;14(14):1250-1255.
53. Brena C, Akam M. An analysis of segmentation dynamics throughout embryogenesis in the centipede Strigamia maritima. *BMC Biol*. 2013;11(1):112.
54. Abley K, De Reuille PB, Strutt D, et al. An intracellular partitioning-based framework for tissue cell polarity in plants and animals. *Development*. 2013;140(10):2061-2074.
55. Mentink RA, Tsiantis M. From limbs to leaves: common themes in evolutionary diversification of organ form. *Front Genet*. 2015;6:284.
56. Ten Tusscher K. Of mice and plants: comparative developmental systems biology. *Dev Biol*. 2018. https://doi.org/10.1016/j.ydbio.2018.10.024.
57. Sussex IM. Developmental programming of the shoot meristem. *Cell*. 1989;56(2):225-229.

58. Bowman JL, Eshed Y. Formation and maintenance of the shoot apical meristem. *Trends Plant Sci*. 2000;5(3):110-115.
59. Lee C, Clark SE. Core pathways controlling shoot meristem maintenance. *Wiley Interdiscip Rev Dev Biol*. 2013;2(5): 671-684.
60. Somssich M, Je BI, Simon R, Jackson D. CLAVATA-WUSCHEL signaling in the shoot meristem. *Development*. 2016;143(18):3238-3248.
61. Teichmann T, Muhr M. Shaping plant architecture. *Front Plant Sci*. 2015;6:233.
62. Bhatia N, Heisler MG. Self-organizing periodicity in development: organ positioning in plants. *Development*. 2018;145(3): dev149336.
63. Callos JD, Medford JI. Organ positions and pattern formation in the shoot apex. *Plant J*. 1994;6(1):1-7.
64. Douady S, Couder Y. Phyllotaxis as a physical self-organized growth process. *Phys Rev Lett*. 1992;68(13):2098-2101.
65. Gola EM, Banasiak A. Diversity of phyllotaxis in land plants in reference to the shoot apical meristem structure. *Acta Soc Bot Pol*. 2016;85(4):3529.
66. Reinhardt D, Mandel T, Kuhlemeier C. Auxin regulates the initiation and radial position of plant lateral organs. *Plant Cell*. 2000;12(4):507-518.
67. Smith RS, Guyomarc'h S, Mandel T, Reinhardt D, Kuhlemeier C, Prusinkiewicz P. A plausible model of phyllotaxis. *Proc Natl Acad Sci U S A*. 2006;103(5):1301-1306.
68. Benková E, Michniewicz M, Sauer M, et al. Local, efflux-dependent auxin gradients as a common module for plant organ formation. *Cell*. 2003;115(5):591-602.
69. Kuhlemeier C. Phyllotaxis. *Curr Biol*. 2017;27(17):R882-R887.
70. Bhatia N, Bozorg B, Larsson A, Ohno C, Jönsson H, Heisler MG. Auxin acts through MONOPTEROS to regulate plant cell polarity and pattern phyllotaxis. *Curr Biol*. 2016;26 (23):3202-3208.
71. Domagalska MA, Leyser O. Signal integration in the control of shoot branching. *Nat Rev Mol Cell Biol*. 2011;12(4):211-221.
72. Vanstraelen M, Benková E. Hormonal interactions in the regulation of plant development. *Annu Rev Cell Dev Biol*. 2012; 28:463-487.
73. Besnard F, Refahi Y, Morin V, et al. Cytokinin signalling inhibitory fields provide robustness to phyllotaxis. *Nature*. 2014;505(7483):417-421.
74. Müller D, Leyser O. Auxin, cytokinin and the control of shoot branching. *Ann Bot*. 2011;107(7):1203-1212.
75. Meinhardt H, Koch A-J, Bernasconi G. Models of pattern formation applied to plant development. In: *Symmetry in Plants*. Volume 4. Series in Mathematical Biology and Medicine. Singapore: WORLD SCIENTIFIC; 1998: pp. 723-758.
76. Swinton J, Ochu E. MSI Turing's sunflower consortium. Novel Fibonacci and non-Fibonacci structure in the sunflower: results of a citizen science experiment. *R Soc Open Sci*. 2016;3 (5):160091.
77. Yonekura T, Iwamoto A, Fujita H, Sugiyama M. Mathematical model studies of the comprehensive generation of major and minor phyllotactic patterns in plants with a predominant focus on orixate phyllotaxis. *PLoS Comput Biol*. 2019;15(6):e1007044.
78. Pourquié O. Somite formation in the chicken embryo. *Int J Dev Biol*. 2018;62(1–2-3):57-62.
79. Goldstein RS, Kalcheim C. Determination of epithelial half-somites in skeletal morphogenesis. *Development*. 1992;116(2): 441-445.
80. Remak R. *Untersuchungen Über Die Entwickelung Der Wirbelthiere*. books.google.com; Berlin: G. Reimer, 1855.
81. Wopat S, Bagwell J, Sumigray KD, et al. Spine patterning is guided by segmentation of the notochord sheath. *Cell Rep*. 2018;22(8):2026-2038.
82. Jones KE, Benitez L, Angielczyk KD, Pierce SE. Adaptation and constraint in the evolution of the mammalian backbone. *BMC Evol Biol*. 2018;18(1):172.
83. Wellik DM. Hox genes and vertebrate axial pattern. *Curr Top Dev Biol*. 2009;88:257-278.
84. Dubrulle J, Pourquié O. Coupling segmentation to axis formation. *Development*. 2004;131(23):5783-5793.
85. Mallo M. Revisiting the involvement of signaling gradients in somitogenesis. *FEBS J*. 2016;283(8):1430-1437.
86. Cooke J, Zeeman EC. A clock and wavefront model for control of the number of repeated structures during animal morphogenesis. *J Theor Biol*. 1976;58(2):455-476.
87. Aulehla A, Johnson RL. Dynamic expression of lunatic fringe suggests a link between notch signaling and an autonomous cellular oscillator driving somite segmentation. *Dev Biol*. 1999; 207(1):49-61.
88. Palmeirim I, Henrique D, Ish-Horowicz D, Pourquié O. Avian hairy gene expression identifies a molecular clock linked to vertebrate segmentation and somitogenesis. *Cell*. 1997;91(5): 639-648.
89. Dale JK, Maroto M, Dequeant M-L, Malapert P, McGrew M, Pourquie O. Periodic notch inhibition by lunatic fringe underlies the chick segmentation clock. *Nature*. 2003;421(6920): 275-278.
90. Liao B-K, Jörg DJ, Oates AC. Faster embryonic segmentation through elevated Delta-notch signalling. *Nat Commun*. 2016; 7:11861.
91. Morimoto M, Takahashi Y, Endo M, Saga Y. The Mesp2 transcription factor establishes segmental borders by suppressing notch activity. *Nature*. 2005;435(7040):354-359.
92. Aulehla A, Wehrle C, Brand-Saberi B, et al. Wnt3a plays a major role in the segmentation clock controlling somitogenesis. *Dev Cell*. 2003;4(3):395-406.
93. Dequéant M-L, Glynn E, Gaudenz K, et al. A complex oscillating network of signaling genes underlies the mouse segmentation clock. *Science*. 2006;314(5805):1595-1598.
94. Krol AJ, Roellig D, Dequéant M-L, et al. Evolutionary plasticity of segmentation clock networks. *Development*. 2011;138 (13):2783-2792.
95. Maroto M, Bone RA, Dale JK. Somitogenesis. *Development*. 2012;139(14):2453-2456.
96. True JR, Haag ES. Developmental system drift and flexibility in evolutionary trajectories. *Evol Dev*. 2001;3(2):109-119.
97. Dubrulle J, McGrew MJ, Pourquié O. FGF signaling controls somite boundary position and regulates segmentation clock control of spatiotemporal Hox gene activation. *Cell*. 2001;106 (2):219-232.
98. Bénazéraf B, Francois P, Baker RE, Denans N, Little CD, Pourquié O. A random cell motility gradient downstream of FGF controls elongation of an amniote embryo. *Nature*. 2010; 466(7303):248-252.

99. Dubrulle J, Pourquié O. fgf8 mRNA decay establishes a gradient that couples axial elongation to patterning in the vertebrate embryo. *Nature*. 2004;427(6973):419-422.
100. Naiche LA, Holder N, Lewandoski M. FGF4 and FGF8 comprise the wavefront activity that controls somitogenesis. *Proc Natl Acad Sci*. 2011;108(10):4018-4023.
101. Aulehla A, Wiegraebe W, Baubet V, et al. A beta-catenin gradient links the clock and wavefront systems in mouse embryo segmentation. *Nat Cell Biol*. 2008;10(2):186-193.
102. Bajard L, Morelli LG, Ares S, Pécréaux J, Jülicher F, Oates AC. Wnt-regulated dynamics of positional information in zebrafish somitogenesis. *Development*. 2014;141(6):1381-1391.
103. Dunty WC, Biris KK, Chalamalasetty RB, Taketo MM, Lewandoski M, Yamaguchi TP. Wnt3a/beta-catenin signaling controls posterior body development by coordinating mesoderm formation and segmentation. *Development*. 2008;135(1):85-94.
104. Kumar S, Duester G. Retinoic acid controls body axis extension by directly repressing Fgf8 transcription. *Development*. 2014;141(15):2972-2977.
105. Moreno TA, Kintner C. Regulation of segmental patterning by retinoic acid signaling during Xenopus somitogenesis. *Dev Cell*. 2004;6(2):205-218.
106. Vermot J, Pourquié O. Retinoic acid coordinates somitogenesis and left-right patterning in vertebrate embryos. *Nature*. 2005;435(7039):215-220.
107. Aulehla A, Pourquié O. Signaling gradients during paraxial mesoderm development. *Cold Spring Harb Perspect Biol*. 2010;2(2):a000869.
108. Ishimatsu K, Hiscock TW, Collins ZM, et al. Size-reduced embryos reveal a gradient scaling-based mechanism for zebrafish somite formation. *Development*. 2018;145(11):dev161257.
109. Lauschke VM, Tsiairis CD, François P, Aulehla A. Scaling of embryonic patterning based on phase-gradient encoding. *Nature*. 2013;493(7430):101-105.
110. Murray PJ, Maini PK, Baker RE. The clock and wavefront model revisited. *J Theor Biol*. 2011;283(1):227-238.
111. Sonnen KF, Lauschke VM, Uraji J, et al. Modulation of phase shift between Wnt and notch Signaling oscillations controls mesoderm segmentation. *Cell*. 2018;172(5):1079-1090.e12.
112. Cotterell J, Robert-Moreno A, Sharpe J. A local, self-organizing reaction-diffusion model can explain somite patterning in embryos. *Cell Syst*. 2015;1(4):257-269.
113. Jörg DJ, Oates AC, Jülicher F. Sequential pattern formation governed by signaling gradients. *Phys Biol*. 2016;13(5):05LT03.
114. Gomez C, Ozbudak EM, Wunderlich J, Baumann D, Lewis J, Pourquié O. Control of segment number in vertebrate embryos. *Nature*. 2008;454(7202):335-339.
115. Aires R, de Lemos L, Nóvoa A, et al. Tail bud progenitor activity relies on a network comprising Gdf11, Lin28, and Hox13 genes. *Dev Cell*. 2019;48(3):383-395.e8.
116. Carapuço M, Nóvoa A, Bobola N, Mallo M. Hox genes specify vertebral types in the presomitic mesoderm. *Genes Dev*. 2005;19(18):2116-2121.
117. Iimura T, Pourquié O. Collinear activation of Hoxb genes during gastrulation is linked to mesoderm cell ingression. *Nature*. 2006;442(7102):568-571.
118. Tschopp P, Duboule D. A regulatory 'landscape effect' over the HoxD cluster. *Dev Biol*. 2011;351(2):288-296.
119. Clack JA. An early tetrapod from "Romer's gap". *Nature*. 2002;418(6893):72-76.
120. Xu X, Mackem S. Tracing the evolution of avian wing digits. *Curr Biol*. 2013;23(12):R538-R544.
121. Cooper LN, Berta A, Dawson SD, Reidenberg JS. Evolution of hyperphalangy and digit reduction in the cetacean Manus. *Anat Rec*. 2007;290(6):654-672.
122. Hiscock TW, Tschopp P, Tabin CJ. On the formation of digits and joints during limb development. *Dev Cell*. 2017;41(5):459-465.
123. Yi SE, Daluiski A, Pederson R, Rosen V, Lyons KM. The type I BMP receptor BMPRIB is required for chondrogenesis in the mouse limb. *Development*. 2000;127(3):621-630.
124. Montero JA, Lorda-Diez CI, Gañan Y, Macias D, Hurle JM. Activin/TGFbeta and BMP crosstalk determines digit chondrogenesis. *Dev Biol*. 2008;321(2):343-356.
125. Suzuki T, Hasso SM, Fallon JF. Unique SMAD1/5/8 activity at the phalanx-forming region determines digit identity. *Proc Natl Acad Sci U S A*. 2008;105(11):4185-4190.
126. Witte F, Chan D, Economides AN, Mundlos S, Stricker S. Receptor tyrosine kinase-like orphan receptor 2 (ROR2) and Indian hedgehog regulate digit outgrowth mediated by the phalanx-forming region. *Proc Natl Acad Sci U S A*. 2010;107(32):14211-14216.
127. Mariani FV, Fernandez-Teran M, Ros MA. Ectoderm-mesoderm crosstalk in the embryonic limb: the role of fibroblast growth factor signaling. *Dev Dyn*. 2017;246(4):208-216.
128. Feregrino C, Sacher F, Parnas O, Tschopp P. A single-cell transcriptomic atlas of the developing chicken limb. *BMC Genomics*. 2019;20(1):401.
129. Sanz-Ezquerro JJ, Tickle C. Fgf signaling controls the number of phalanges and tip formation in developing digits. *Curr Biol*. 2003;13(20):1830-1836.
130. Richardson MK, Oelschläger HHA. Time, pattern, and heterochrony: a study of hyperphalangy in the dolphin embryo flipper. *Evol Dev*. 2002;4(6):435-444.
131. Shwartz Y, Viukov S, Krief S, Zelzer E. Joint development involves a continuous influx of Gdf5-positive cells. *Cell Rep*. 2016;15(12):2577-2587.
132. Kavanagh KD, Shoval O, Winslow BB, et al. Developmental bias in the evolution of phalanges. *Proc Natl Acad Sci U S A*. 2013;110(45):18190-18195.
133. Huang B-L, Trofka A, Furusawa A, et al. An interdigit signalling Centre instructs coordinate phalanx-joint formation governed by 5′Hoxd-Gli3 antagonism. *Nat Commun*. 2016;7:12903.
134. Hartmann C, Tabin CJ. Wnt-14 plays a pivotal role in inducing synovial joint formation in the developing appendicular skeleton. *Cell*. 2001;104(3):341-351.
135. Brunet LJ, McMahon JA, McMahon AP, Harland RM. Noggin, cartilage morphogenesis, and joint formation in the mammalian skeleton. *Science*. 1998;280(5368):1455-1457.
136. Harfe BD, Scherz PJ, Nissim S, Tian H, McMahon AP, Tabin CJ. Evidence for an expansion-based temporal Shh gradient in specifying vertebrate digit identities. *Cell*. 2004;118(4):517-528.
137. Moreno-Risueno MA, Norman JMV, Moreno A, Zhang J, Ahnert SE, Benfey PN. Oscillating gene expression determines

competence for periodic Arabidopsis root branching. *Science*. 2010;329(5997):1306-1311.
138. Jönsson H, Heisler MG, Shapiro BE, Meyerowitz EM, Mjolsness E. An auxin-driven polarized transport model for phyllotaxis. *Proc Natl Acad Sci U S A*. 2006;103(5):1633-1638.
139. Sheeba CJ, Andrade RP, Palmeirim I. Mechanisms of vertebrate embryo segmentation: common themes in trunk and limb development. *Semin Cell Dev Biol*. 2016;49:125-134.
140. Payne JL, Wagner A. The causes of evolvability and their evolution. *Nat Rev Genet*. 2019;20(1):24-38.
141. Sears KE, Behringer RR, Rasweiler JJ, Niswander LA. Development of bat flight: morphologic and molecular evolution of bat wing digits. *Proc Natl Acad Sci U S A*. 2006;103(17):6581-6586.
142. Thompson DW. *On Growth and Form*. Cambridge: University Press; 1917.
143. Rossi G, Manfrin A, Lutolf MP. Progress and potential in organoid research. *Nat Rev Genet*. 2018;19(11):671-687.
144. Turner DA, Baillie-Johnson P, Arias AM. Organoids and the genetically encoded self-assembly of embryonic stem cells. *Bioessays*. 2016;38(2):181-191.
145. Manfrin A, Tabata Y, Paquet ER, et al. Engineered signaling centers for the spatially controlled patterning of human pluripotent stem cells. *Nat Methods*. 2019;16(7):640-648.
146. Sako K, Pradhan SJ, Barone V, et al. Optogenetic control of nodal signaling reveals a temporal pattern of nodal signaling regulating cell fate specification during gastrulation. *Cell Rep*. 2016;16(3):866-877.
147. Li P, Elowitz MB. Communication codes in developmental signaling pathways. *Development*. 2019;146(12):1-2. https://doi.org/10.1242/dev.170977.

How to cite this article: Grall E, Tschopp P. A sense of place, many times over - pattern formation and evolution of repetitive morphological structures. *Developmental Dynamics*. 2020;249:313–327. https://doi.org/10.1002/dvdy.131